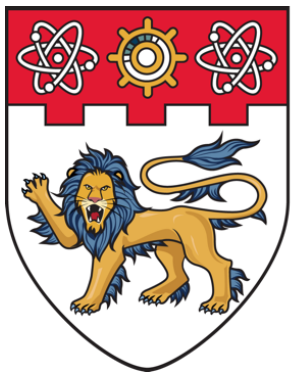

NANYANG TECHNOLOGICAL UNIVERSITY
SINGAPORE

SIZE DISTRIBUTION MEASUREMENT OF POLYDISPERSE MACROMOLECULAR SAMPLES USING NANOPARTICLE TRACKING ANALYSIS

KIM AHRAM

SCHOOL OF MATERIALS SCIENCE AND ENGINEERING

2019

SIZE DISTRIBUTION MEASUREMENT OF POLYDISPERSE MACROMOLECULAR SAMPLES USING NANOPARTICLE TRACKING ANALYSIS

KIM AHRAM

SCHOOL OF MATERIALS SCIENCE AND ENGINEERING

A thesis submitted to the Nanyang Technological University
in partial fulfilment of the requirement for the degree of
Doctor of Philosophy

2019

Statement of Originality

I hereby certify that the work embodied in this thesis is the result of original research, is free of plagiarised materials, and has not been submitted for a higher degree to any other University or Institution.

July 24th, 2019

. . . . . .
Date

. . . . . .
KIM Ahram

Supervisor Declaration Statement

I have reviewed the content and presentation style of this thesis and declare it is free of plagiarism and of sufficient grammatical clarity to be examined. To the best of my knowledge, the research and writing are those of the candidate except as acknowledged in the Author Attribution Statement. I confirm that the investigations were conducted in accord with the ethics policies and integrity standards of Nanyang Technological University and that the research data are presented honestly and without prejudice.

July 24th, 2019

. . . . . .
Date

Nam-Joon Cho

Authorship Attribution Statement

This thesis contains material from 2 papers published in the following peer-reviewed journals in which I am listed as an author.

Chapter 4 is published as A. Kim, W. B. Ng, W. Berndt, and N. J. Cho. Validation of Size Estimation of Nanoparticle Tracking Analysis on Polydisperse Macromolecule Assembly. *Scientific Reports* **9**, 2639 (2019). DOI: 10.1038/s41598-019-38915-x.

The contributions of the co-authors are as follows:

- Prof. Cho made the initial conceptual idea and edited the manuscript.
- I prepared the manuscript drafts.
- I designed the study with Prof. Cho, analyzed the data, and produced the figures.
- All DLS measurements including sample preparation were conducted by Dr. Ng. All NTA measurements were conducted by Dr. Ng and Mr. Berndt.

Chapter 5 is published as A. Kim, W. Berndt, and N. J. Cho. Improved Size Determination by Nanoparticle Tracking Analysis: Influence of Recognition Radius. *Analytical Chemistry* **91**, 9508 (2019). DOI: 10.1021/acs.analchem.9b00454.

The contributions of the co-authors are as follows:

- I and Prof. Cho made the initial conceptual idea and edited the manuscript.
- I prepared the drafts of the manuscript.
- I designed the study with Prof. Cho, derived the modified displacement probability, wrote the simulation codes, analyzed the data, and produced the figures.
- All NTA measurements on polystyrene standard samples were conducted by Mr. Berndt.

July 24th, 2019

. . . . . .

Date

. . . . . .

KIM Ahram

Abstract

The standard technique used to measure the size distribution of nanometer-sized particles in suspension is dynamic light scattering (DLS). Recently, nanoparticle tracking analysis (NTA) has been introduced to measure the diffusion coefficient of particles in a sample to determine their size distribution in relation to DLS results. Because DLS and NTA use identical physical characteristics to determine particle size but differ in the weighting of the distribution, NTA can be a good verification tool for DLS and vice versa. In this study, two NTA data analysis methods based on maximum-likelihood estimation were evaluated, namely finite track length adjustment and an iterative method, on monodisperse polystyrene beads and polydisperse vesicles by comparing the results with DLS. The NTA results from both methods agreed well with the mean size and relative variance values from DLS for monodisperse polystyrene standards. However, for the lipid vesicles prepared in various polydispersity conditions, the iterative method resulted in a better match with DLS. Further, it was found that it is better to compare the native number-weighted NTA distribution with DLS, rather than its converted distribution weighted by intensity. Nanoparticle tracking analysis is a size measurement technique that determines the size distribution of particles in suspension by tracking individual particles undergoing Brownian motion. A key element in the measurement analysis is the recognition radius, which distinguishes the individual, tracked particles from one another. However, by defining a finite radius, the displacement of tracked particles is effectively restricted, translating into an overestimation of particle size. A modified probability model that describes the restricted displacement of a tracked particle is introduced to achieve more accurate size distribution determination. Through virtual NTA measurement by computer simulations and real NTA experiments, the analytical performance of the modified displacement probability was tested in comparison to the conventional probability. Whereas the conventional displacement probability results in an overestimation of the particle size, the modified displacement probability mitigates the effect of the overestimation and provides more accurate mean size within an error of less than 6% the nominal size.

Lay Summary

Dynamic light scattering (DLS) and nanoparticle tracking analysis (NTA) are size measurement techniques for particles in suspension in the nanometer scale. They both acquire size information by measuring the diffusion coefficient of particles, or the random movements of particles, while their respective detection principles are different. This makes the two techniques a complimentary technique to each other, which improves the accuracy of the measured size distribution. In this thesis, the two techniques are compared to find an optimal condition that results from the two technique is well compared. To do so, the analysis methods used for interpreting data from DLS and NTA were reviewed, from which optimal methods were chosen for the comparison of the two techniques on polydisperse biological samples. The comparison suggested that DLS and NTA provide very consistent results. It also showed that the results from the two techniques are better compared when the results are presented in their respective native representation than when one of the results are converted into the representation of the other.

The evaluation was further extended to the influence of a parameter, or the recognition radius, used in NTA in analyzing results from NTA. The recognition radius is a virtual boundary that a particle can be recognized as the same particle during its movement. In NTA, the recognition radius is essential to acquire data of particle tracks. However, the recognition radius excludes the longest movements of particles and effectively decreases the magnitude of the particle movements, resulting in an overestimation of the particle size. To resolve the influence of the recognition radius, a modified model to compensate the recognition radius was suggested and tested by simulations and experiments. The simulations and experiments confirmed that the modified model provides better size accuracy. It suggested a lower limit for the recognition radius. If the recognition radius is set to below the lower limit, the acquired measurements deviate from the true value. On the other hand, the simulation also suggested that an upper limit for the recognition radius should be given if the particle concentration is high. If the concentration is high, the distance between particles gets closer, which makes the recognition process fail for a long

recognition radius. To reduce such a situation, the recognition radius should be chosen to be smaller than a certain limit. These findings suggest that the recognition radius for NTA should be carefully chosen to have accurate size measurements.

Acknowledgements

I would like to express my gratitude to Nanyang Technological University (NTU) for providing me a great opportunity for the doctoral studies in Singapore. The life in Singapore has been so wonderful that I could enjoy the life during the doctoral course.

I also like to thank my supervisor, Professor Nam-Joon Cho for all the support and guidance he has provided during my doctoral period. It was the greatest opportunities I've had to have his encouragement on continuing the period. His passion and knowledge have led me well in exploring this uncharted territory of research. He also gave me great insights whenever I faced difficulties in finding ways to solve the problems. I cannot imagine how I go through the period without his support and guidance, and without him it would have been not possible to complete the course.

For my tough experiments, Mr. William Bernt helped me to acquire some of the important data and gave me insights to understand. Without his help, my experiments would have been much tougher.

During the days in Singapore, I met so many precious colleagues that I've never expected before arriving here, in the Engineering in Translational Science (ETS) group. Each of them was so passionate and energetic, and it was so encouraging to me to do my studies here. Firstly, I would like to thank Dr. Wei Beng Ng, who has helped me in getting acquainted with all the instruments that I've used for my study. His help was indispensable in conducting my works. I also give thanks to my colleagues, Dr. Joonhui Kim, Dr. Jae Park, Hogyun Jinn and Soohyun Park. They have given me so much energy in the laboratory.

And, finally, I really appreciate the support from my wife and my family. Eunsun has shown me her support from Day 1 until now and encouraged me to have faith in me to complete this work. Seohyun, my daughter, has been a great supporter as well. I really

thank Seohyun for the love she has shown. Thank my mom and dad for your great love. Without their love it would have been very tough for me to navigate this journey.

This work relied heavily on the computer code/database developed by Dr. Sssss who helped me install this software on our supercomputer cluster.

Table of Contents

Table Captions

Figure Captions

Figure 3.3 The process flow of the size determination methods based on maximum likelihood estimation. (a) By assuming a size distribution described by adjustable parameters, the FTLA method looks for the parameter values that maximize the likelihood of the given NTA tracks. (b) The iterative correction method refines the size distribution that approaches to the maximum likelihood over each iteration.

Figure 4.1 In NTA, particles suspended in liquid are illuminated by a laser beam. Scattered light by the particles is monitored by the microscope, from which the position of the particles is identified by the software. The software tracks the trajectory of the particles and constructs particle tracks, from which the average squared displacement is calculated and converted into the corresponding hydrodynamic diameter.

Figure 4.2 Schematic representation of the size determination methods based on maximum likelihood estimation. By assuming a size distribution described by adjustable parameters, the FTLA method looks for the parameter values that maximize the likelihood of the given NTA tracks. The iterative correction method refines the size distribution that approaches to the maximum likelihood over each iteration.

Figure 4.3 (a) Mean and (b) relative variance of the size distributions of PS latex nanoparticle samples measured by DLS and NTA. Mean size is displayed as a value relative to its respective nominal sample size. The size information from DLS was acquired using the cumulant method, while the results from NTA were acquired by applying three different methods, i.e., direct conversion of acquired tracks (DC), FTLA and the iterative method (IC).

Figure 4.4 The size distributions of monodisperse PS latex standard samples of a nominal size of (a) 92, (b) 269 and (c) 343 nm measured by DLS and NTA. The size distribution from DLS assumes a log-normal distribution acquired from the cumulant method, while those from NTA are from the three different analysis methods, i.e., direct conversion (DC), FTLA and the iterative method (IC).

Figure 4.5 (a) Mean and relative variance of the size distributions of the POPC vesicle samples measured by DLS and NTA and (b) relative mean size from NTA with respect to their corresponding mean size from DLS. DLS values are derived from the cumulant method, while the NTA results are obtained by applying the three different analysis methods, i.e., direct conversion (DC), FTLA and the iterative method (IC).

Figure 4.6 Comparison of the size distributions of the POPC vesicle samples analyzed by the different size distribution estimation methods for NTA measurements. The direct conversion (black), FTLA (green) and the iterative (blue) methods were applied for the size distribution estimations. The vesicle samples were prepared by extrusion through (a) 50-nm, (b) 100-nm, (c) 200-nm and (d) 400-nm pore filter or by freeze-thaw treatment (e-l) of 3 to 17 cycles before extrusion through a 400-nm pore filter. The bin width of the size distributions is in 2 nm.

Figure 4.7 Size distribution of the POPC vesicle samples prepared in various polydispersity conditions measured by DLS and NTA. DLS results (solid red line) are from the cumulant method while NTA results (solid blue line) are acquired by applying the iterative method. For comparison, the size distribution of NTA is reconstructed into an intensity-weighted distribution (dotted black line) by introducing the thin-shell sphere model for the conversion. The vesicle samples were prepared by extrusion through (a) 50-nm, (b) 100-nm, (c) 200-nm and (d) 400-nm pore filters or by freeze-thaw treatment of (e-l) 3 to 17 cycles before extrusion through a 400-nm pore filter.

Figure 4.8 (a) Mean size and (b) relative variance of the POPC vesicle samples measured by NTA compared with DLS (open red square). NTA results were analyzed by the iterative method (solid black triangle) and reconstructed into an intensity-weighted distribution (open black triangle) using the thin-shell sphere model for the conversion.

Figure 5.1 Illustrative description of the NTA tracking process. The particle locations at $t_0 + \Delta t$ are evaluated with respect to the particle locations at t_0 to identify particles'

trajectory and construct a track. Scenario 1: Only one particle at $t_0 + \Delta t$ is found within the recognition radius from a particle at t_0, which identifies the two particles as the same particle, and the tracking process continues to $t_0 + \Delta t$. Scenario 2: No particle at $t_0 + \Delta t$ is found within the recognition radius, which terminates the tracking process at t_0. Scenario 3: More than two particles at $t_0 + \Delta t$ are found within the recognition range, which interferes and terminates the tracking process at t_0.

Figure 5.2 Results from computer simulations. The distribution of tracks used in Figures 5.3 and 5.4 at a recognition range of 1, 1.5, 2 and 5 μm. The tracks were acquired from the simulations used in (a) Figure 5.3, whose size is 100 nm at a concentration of 1×10^9 particles/ml, and in (b) Figure 5.4, whose size distribution consists of an 'ideal' set of a normal distribution with a mean of 100 nm and and relative variance 0.05 at a concentration of 1×10^9 particles/ml. A total of 21605, 9855, 9078 and 8855 tracks were collected from the 100-nm-sized particles simulation, among which 8310, 5329, 4616 and 3585 tracks whose track length is more than 4 were chosen for the analysis at a recognition range of 1, 1.5, 2 and 5 μm, respectively. A total of 21420, 10270, 9123 and 8730 tracks were collected from the particles simulation of the normal distribution, among which 7677, 5357, 4607 and 3564 tracks whose track length is more than 4 were chosen for the analysis at a recognition range of 1, 1.5, 2 and 5 μm, respectively.

Figure 5.3 Simulated NTA measurements of ideally monodisperse, 100-nm diameter nanoparticles. Different recognition radius values, *L*, of 1, 1.5, 2 and 5 μm were tested based on a total of 8310, 5329, 4616 and 3585 tracks, respectively. Acquired tracks were processed to determine the size distribution using the iteration-based MLE method with the (a) conventional displacement probability or (b) modified displacement probability. The nanoparticle concentration was 1×10^9 particles/ml. The computed mean diameter and relative variation (RV) for each size distribution are reported.

Figure 5.4 Simulated NTA measurements of 100 ± 5 nm diameter nanoparticles. Different recognition radius values, *L*, of 1, 1.5, 2 and 5 μm were tested based on a total of 7677, 5357, 4607 and 3564 tracks, respectively. Acquired tracks were processed to determine the

size distribution using the iteration-based MLE method with the (a) conventional displacement probability or (b) modified displacement probability. The nanoparticle concentration was 1×10^9 particles/ml. The computed mean diameter and relative variation (RV) for each size distribution are reported.

Figure 5.5 Results from a computer simulation. Mean size and relative variance of the size distributions determined from the simulated Brownian movements of particles, where the tracks of the particles are recognized at a various recognition radius from 1 to 5 μm. For each simulation, an 'ideal' set of particles whose size distribution follows a normal distribution of a mean size of (a) 20, (b) 50, (c) 100 and (d) 200 nm with relative variance of 0 (black circle), 0.01 (red open square) and 0.05 (blue triangle) at a concentration of 1×10^9 particles/ml was used. For each combination of a mean size and relative variance, 25 runs of simulated NTA measurements were produced. From the recognized tracks of the simulated measurements on a various recognition radius, the size distribution was estimated by the iterative MLE method with the conventional displacement probability (left) and the modified displacement probability (right). The acquired mean size is displayed with respect to the nominal mean size of the respective simulated particle sets. Dashed guidelines show the expected overestimated mean size due to the use of the conventional probability. Note that the size distributions on the simulations of a mean size condition of 20 and 50 nm estimated with the modified displacement probability do not converge well when the recognition radius is 1.5 and 1 μm, respectively, and their corresponding mean size and relative variance are not displayed in (a) and (b).

Figure 5.6 Results from a computer simulation. Mean size and relative variance of the size distributions determined from the simulated Brownian movements of particles, where the tracks of the particles are recognized at a various recognition range from 1 to 5 μm. For each simulation, a set of particles with a bi-modal distribution whose mean size is (a) 20, (b) 50, (c) 100 and (d) 200 nm with relative variance of 0 (black circle), 0.01 (red open square) and 0.05 (blue triangle) at a concentration of 1×10^9 particles/ml was used. The corresponding size pairs for 20-, 50-, 100- and 200-nm mean size are 18 and 22, 45 and 50, 90 and 110, and 180 and 220 nm, respectively, for relative variance of 0.01, and 15.5 and

24.5, 39 and 61, 78 and 122, and 155 and 245 nm, respectively, for relative variance of 0.05. For each combination of a mean size and relative variance, 25 runs of simulated NTA measurements were produced. From the recognized tracks of the simulated measurements on a various recognition range, the size distribution was estimated by the iterative MLE method with the conventional displacement probability (left) and the modified displacement probability (right). The acquired mean size is displayed with respect to the nominal mean size of the respective simulated particle sets. Dashed guidelines show the expected overestimated mean size due to the use of the conventional probability. Note that the estimated size distributions on the simulations with a mean size condition of 20 and 50 nm do not converge well when the recognition range is 1.5 and 1 μm, respectively, and their corresponding mean size and relative variance are not displayed in (a) and (b).

Figure 5.7 Reanalyzed results of the computer simulation shown in Figure 5.5. Mean size and relative variance of the size distributions determined from the simulated Brownian movements of particles, where those false tracks are excluded from the analysis. For each simulation, an 'ideal' set of particles whose size distribution follows a normal distribution of a mean size of (a) 20, (b) 50, (c) 100 and (d) 200 nm with relative variance of 0 (black circle), 0.01 (red open square) and 0.05 (blue triangle) at a concentration of 1×10^9 particles/ml was used. For each combination of a mean size and relative variance, 25 runs of simulated NTA measurements were produced. From the recognized tracks of the simulated measurements on a various recognition range, the size distribution was estimated by the iterative MLE method with the conventional displacement probability (left) and the modified displacement probability (right). The acquired mean size is displayed with respect to the nominal mean size of the respective simulated particle sets. Dashed guidelines show the expected overestimated mean size due to the use of the conventional probability. Note that the estimated size distributions on the simulations with a mean size condition of 20 and 50 nm do not converge well when the recognition range is 1.5 and 1 μm, respectively, and their corresponding mean size and relative variance is not displayed in (a) and (b).

Figure 5.8 Reanalyzed results of the computer simulation shown in Figure 5.6. Mean size and relative variance of the size distributions determined from the simulated Brownian

movements of particles, where those false tracks are excluded from the analysis. For each simulation, monomodal particles with a size of (a) 20, (b) 50, (c) 100, and (d) 200 nm at a concentration of 1×10^8 (black circle), 1×10^9 (red open square) and 1×10^{10} particles/ml (blue triangle) were generated. For each combination of mean size and concentration, 25 runs of simulated NTA measurements were produced. From the recognized tracks of the simulated measurements on a various recognition range, the size distribution was estimated by the iterative MLE method with the conventional displacement probability (left) and the modified displacement probability (right). The acquired mean size is displayed with respect to the nominal mean size of the respective simulated particle sets. Dashed guidelines show the expected overestimated mean size due to the use of the conventional probability. Note that the size distributions from the simulations of a mean size condition of 20 and 50 nm estimated by the modified displacement probability do not converge well when the recognition range is below 1.5 and 1 μm, respectively, and their corresponding relative variance is not displayed.

Figure 5.9 Results from a computer simulation. The position of the peaks identified from the size distributions determined from the simulated Brownian movements of particles, where the tracks of the particles are recognized at a various recognition radius from 1 to 5 μm. For each simulation, a set of particles with a bi-modal distribution whose mean size is (a) 20, (b) 50, (c) 100 and (d) 200 nm with relative variance of 0.05 at a concentration of 1×10^9/ml was used. The corresponding position of the nominal peaks for a mean size of 20, 50, 100 and 200 nm are 16 and 25, 39 and 61, 78 and 122, and 155 and 245 nm, respectively. For each mean size condition, 25 runs of simulated NTA measurements were produced. From the recognized tracks of the simulated measurements on a various recognition radius, the size distribution was estimated by the iterative MLE method with the conventional displacement probability (left) and the modified displacement probability (right). Dashed guidelines show the respective nominal peak positions.

Figure 5.10 Results from a computer simulation. Mean size and relative variance of the size distributions determined from the simulated Brownian movements of particles, where the tracks of the particles are recognized at a various recognition radius from 1 to 5 μm.

For each simulation, monomodal particles with a size of (a) 20, (b) 50, (c) 100, and (d) 200 nm at a concentration of 1×10^8 (black circle), 1×10^9 (red open square) and 1×10^{10} particles/ml (blue triangle) were generated. For each combination of mean size and concentration, 25 runs of simulated NTA measurements were produced. From the recognized tracks of the simulated measurements on a various recognition radius, the size distribution was estimated by the iterative MLE method with the conventional displacement probability (left) and the modified displacement probability (right). The acquired mean size is displayed with respect to the nominal mean size of the respective simulated particle sets. Dashed guidelines show the expected overestimated mean size due to the use of the conventional probability. Note that the size distributions from the simulations of a mean size condition of 20 and 50 nm estimated by the modified displacement probability do not converge well when the recognition radius is below 1.5 and 1 μm, respectively, and their corresponding relative variance is not displayed in (a) and (b).

Figure 5.11 Reanalyzed results of the computer simulation shown in Figure 5.10. Mean size and relative variance of the size distributions determined from the simulated Brownian movements of particles, where those false tracks are excluded from the analysis. For each simulation, monomodal particles with a size of (a) 20, (b) 50, (c) 100, and (d) 200 nm at a concentration of 1×10^8 (black circle), 1×10^9 (red open square) and 1×10^{10} particles/ml (blue triangle) were generated. For each combination of mean size and concentration, 25 runs of simulated NTA measurements were produced. From the recognized tracks of the simulated measurements on a various recognition range, the size distribution was estimated by the iterative MLE method with the conventional displacement probability (left) and the modified displacement probability (right). The acquired mean size is displayed with respect to the nominal mean size of the respective simulated particle sets. Dashed guidelines show the expected overestimated mean size due to the use of the conventional probability. Note that the size distributions from the simulations of a mean size condition of 20 and 50 nm estimated by the modified displacement probability do not converge well when the recognition range is below 1.5 and 1 μm, respectively, and their corresponding relative variance is not displayed.

Figure 5.12 Results from a computer simulation. The average track length of the particles tracks used for the size distribution determination from the simulated Brownian movements of particles, where the tracks of the particles are recognized at a various recognition range from 1 to 5 μm. For each simulation, monomodal particles with a size of (a) 20, (b) 50, (c) 100, and (d) 200 nm at a concentration of 1×10^8 (black circle), 1×10^9 (red open square) and 1×10^{10} particles/ml (blue triangle) were generated. For each combination of mean size and concentration, 25 runs of simulated NTA measurements were produced.

Figure 5.13 Mean size and relative variance of the size distributions determined from NTA measurements of PS latex nanoparticles with a nominal size of (a) 51.6 and (b) 181.6 nm using a various recognition radius from 1.1 to 5.4 μm at two different concentrations of 1×10^8 (left) and 1×10^9 particles/ml (right). Three runs of measurements were conducted for each combination of nominal sample size and concentration. From the tracks acquired from the NTA measurements at a various recognition radius, the size distribution was estimated by the iterative estimation method with the conventional (black square) and the modified (red open circle) displacement probabilities. With the modified displacement probability, it was not possible to achieve a good convergence of the size estimation when the recognition radius is small, i.e. up to 1.6 μm for the 51.6-nm standard and not displayed in (a) and (b).

Figure 5.14 Size distributions determined from NTA measurements of PS latex nanoparticles with a nominal size of (a, b) 51.6 and (c, d) 181.6 nm at a recognition range L from 1.1 to 5.4 μm. For each nominal size, two different concentration levels, (a, c) 1×10^9 and (b, d) 1×10^8 particles/ml, were prepared for each particle size. Three runs of measurements were conducted for each combination of nominal sample size and concentration, where the distributions above are the average of the three runs each. The size distributions are estimated with the conventional displacement probability (left) and the modified displacement probability (right) on the tracks recognized at a various recognition range from 1.1 μm (top) to 5.4 μm (bottom). Those tracks with a minimum track length of 5 was used for the analysis. The bin width of the size distributions is 2 nm,

and each distribution is normalized with respect to its respective maximum. With the modified displacement probability, it was not possible to achieve a good convergence of the size estimation on the 51.6-nm standard at a recognition range of 1.1 µm.

Abbreviations

AF4	Asymmetrical Flow Field-Flow Fractionation
AFM	Atomic Force Microscopy
AUC	Analytical Ultracentrifugation
DC	Direct Conversion
DDS	Drug Delivery System
DLS	Dynamic Light Scattering
FFF	Field Flow Fractionation
FTLA	Finite Track Length Adjustment
IC	Iterative Correction
MALS	Multi-Angle Light Scattering
MJD	Max Jump Distance
MLE	Maximum Likelihood Estimation
NTA	Nanoparticle Tracking Analysis
PC	Phosphatidylcholine
PDI	Polydispersity Index
PI	Polydispersity Index
POPC	1-palmitoyl-2-oleoyl-sn-glycero-3-phosphocholine
PS	Polystyrene
RGD	Rayleigh-Ganz-Debye
RV	Relative Variance
SEC	Size Exclusion Chromatography
SEM	Scanning Electron Microscopy
SOP	Standard Operating Procedures
TEM	Transmission Electron Microscopy

Chapter 1

Introduction

In evaluating the physicochemical properties of drug delivery systems, characterization of the particle size is critical. Although many size measurement techniques can be employed for such a purpose, results from each technique requires validation since each technique has its own definition on the particle size and the quantity of particles. DLS and NTA are popular techniques for particles in suspension in the nanometer scale, where they measure the same physical property to determine the size but differ in the quantity of particles each provides. In this thesis, the two techniques were evaluated and compared to find a proper method to interpret the results for polydisperse biological samples. In particular, the parameters for NTA analysis were investigated to find their influences on the results. To achieve this goal, simulations and theoretical analysis were combined to identify critical parameters in analyzing results from DLS and NTA. This chapter introduces a background of the research field and presents the problem statement and specific objectives addressed in this research as well as the hypotheses.

1.1 Hypothesis

In characterizing and evaluating the physicochemical properties of drug delivery systems, it is critical to determine the size information with nanometer scale precision since not only their material properties but also their size govern the properties [1-10]. The determination of size of biological nanoparticles is also important in academic studies of various biochemical processes occurring on lipid membranes, e.g., on suspended or attached vesicles or on supported lipid bilayers [11]. While there are various size measurement techniques that can be employed, proper interpretation of the results acquired by a technique should be made since the physical meaning that each technique delivers differs from one another [12]. For example, microscopy-based techniques such as transmission electron microscopy and atomic force microscopy capture an image of particles, whose size is extracted by measuring the topographical length from the captured image [12-17]. Whereas, size exclusion chromatography (SEC) observes the time of elution, which is related to the volume of particles [18, 19]. To compare the results from the two techniques, it is necessary to assume that the two definitions of size are identical or convertible into the other form. However, such an assumption is often very far from the reality and could result in wrong information.

Moreover, the quantity of particles each technique provides also varies, such as number, volume or even an arbitrary unit like light intensity [12]. Difference in the quantity makes comparisons of results from various techniques more difficult, since the difference not only requires conversion of a quantity into another but also results in a biased sensitivity that depends on the size of particles [12, 20, 21]. For example, dynamic light scattering (DLS) detects the intensity of scattered light by particles in suspension that are illuminated by laser [20, 22]. Roughly, the intensity is proportional to the square of the particle volume, and it is well known that presence of large particles overshadows the signal from smaller particles in DLS measurements. In addition, the intensity of DLS is also dependent on the material properties of the measured particles like the refractive index, making the interpretation of results even more complex.

Due to the different characteristics of each size measurement technique, a single measurement technique is not sufficient to determine the size distribution of particles [12, 23]. This becomes more significant if a sample is polydisperse. Hence, any technique that is newly introduced for size characterization requires an evaluation to verify if its results could be interpreted without producing misleading information.

Nanoparticle tracking analysis (NTA) is a size measurement technique introduced in 2006 [24, 25]. NTA measures the diffusion coefficient of particles in suspension to determine their size, which is the same physical property that DLS measures for size measurements. An advantage of NTA is its number-weighted size distribution of measured particles, which is less sensitive to the variation of particle size in the distribution [13, 24, 26]. Since NTA is a relatively new technique and measures the same physical properties as DLS, many studies have evaluated if NTA could complement DLS that has a bias toward a larger size due to its intensity-weighted sensitivity [15, 24, 27-31]. Those studies found that NTA is very comparable to DLS in the accuracy of size determination. On the other hand, they also found that NTA produces a broader size distribution than the nominal distribution even for very monodisperse samples compared with other techniques including DLS and TEM [24]. In these studies, the broader size distribution was attributed to the stochastic uncertainty of the particle tracks obtained in NTA, whose degree can be reduced by applying the maximum likelihood estimation (MLE) principle [32, 33]. However, comparative studies on NTA after the introduction of the MLE principle to NTA analysis has been mainly focused on the evaluation of the MLE principle and not extended toward realistic biological samples, which are polydisperse.

In this regard, this thesis addresses the necessity of evaluations on NTA on polydisperse biological samples while applying the MLE principle. A benefit of NTA is its number-weighted size distribution on providing the quantity, which is advantageous on polydisperse samples. Application of the MLE principle on NTA analysis improves the size resolution of NTA by reducing the stochastic uncertainty and makes NTA more useful in analyzing polydisperse samples [34]. In particular, the

physical quantity that NTA measures, or the diffusion coefficient of particles, is the same to DLS, which makes it a very good comparative technique to each other. Hence, the comparison of DLS and NTA has an advantage in interpreting the definition of the size that each measures. On the other hand, the quantity each technique produces is light intensity and number for DLS and NTA, respectively, which requires an adequate conversion for a proper comparison [12, 20, 35]. The conversion of a number-weighted size distribution into an intensity-weighted distribution requires a model for the scattering factor, which is described by the Mie theory. Considering the refractive index of biological samples is close to that of medium, the Rayleigh-Ganz-Debye (RGD) approximation could be used for the scattering factor [36-39]. This conversion would provide insights on how results from DLS and NTA would compare and what is a better way to compare the two results while the improved NTA analysis method is used. In short, key questions on the evaluation of NTA would include:

- Does the size accuracy of NTA improve if the MLE principle is employed? Is there any limitation in applying the MLE principle for polydisperse biological samples?
- How do the different quantities of the size distribution that DLS and NTA compare? Does the conversion of a size distribution from NTA into the quantity of DLS, or the intensity, compare better?
- What kind of factors in NTA affect the accuracy of NTA in determining the size distribution? Is there any factor that results in a systematic deviation?

To address these key questions, this thesis starts from the known analysis method to evaluate NTA and finds factors that can be modified to improve the analysis. Specifically, it aims to identify and reflect the influence of the recognition range, which is directly related with the determination of particle size in NTA. This leads to the following specific hypotheses in this thesis:

- Size distribution determined by NTA is improved by adopting the MLE principle for polydisperse samples and shows a better comparison with DLS.

- The conversion of a number-weighted size distribution acquired with NTA provides a better comparison when it is compared with an intensity-weighted size distribution acquired with DLS.
- A finite recognition radius used in NTA effectively limits the average squared displacement of tracks acquired by NTA, resulting in an overestimation of the determined particle size. Hence, incorporation of the influence of the recognition radius in NTA size determination is critical for an accurate size determination of NTA.

1.2 Objectives and Scope

DLS is a popular size measurement technique for nanometer-scale particles in suspension. It produces size information in a short time, which makes it a routine measurement technique for a quick size determination though it is also well known for its sensitivity bias toward larger particles in polydisperse samples [12, 20, 22, 40]. This bias often misleads the size information of polydisperse samples and requires measurements with other techniques for validation. For such a purpose, NTA can be a good comparative technique since it measures the same physical property, or the diffusion coefficient of particles, to determine the size [24, 25]. In this thesis, the two techniques are evaluated to find a proper method to compare results from the two on polydisperse samples, while the MLE method are applied for the analysis of NTA results. In doing so, the influence of the recognition radius, or the upper limit for a distance by which a particle is tracked in NTA, is identified and reflected into the analysis method of NTA.

Within this scope, the main objective of the thesis is to develop methodologies to evaluate NTA and DLS and identify the influence of the recognition radius in analyzing NTA results. To accomplish the objective, the following studies were conducted to establish the method to interpret results from DLS and NTA as well as assess the influence of the recognition radius.

- Methodologies to interpret results from DLS and NTA was established to properly reflect the nature of polydisperse biological particles. For NTA

analysis, three different approaches to analyze particle tracks, namely direct conversion, parameter-optimization MLE and iteration-based MLE methods, were evaluated to determine the optimal method for the analysis. Since the two technique gives different quantity for the particle size distribution, a model based on the RGD approximation was used to convert the number-weighted size distribution of NTA into an intensity-weighted distribution of DLS.

- Influences of the recognition radius used for NTA particle tracking was identified by employing computer simulations while varying the particle size and the particle concentration. The simulation provided an ideal measurement condition, revealing false tracks where two different particles are recognized as the same particle. If false tracks are excluded from the NTA analysis, the determined size distribution showed expected results where the determined particle size changes according to a chosen recognition radius. When false tracks are included, which is the case of real measurements, a spurious peak was found in the acquired size distribution on an increasing recognition radius since false tracks were more created.
- A various recognition radius was used for the track recognition of NTA analysis on the simulation, which revealed the influence of the recognition radius in determining the particle size. For the determination, a modified displacement probability that reflects the finite recognition radius was introduced to improve the accuracy of size distribution determination. Results using the modified displacement probability as well as the conventional displacement probability were compared with the nominal value used for the simulation. The results showed that the conventional probability resulted in overestimation on the particle size as expected by the theoretical calculation while the modified probability minimized the overestimation and produced a good match with the nominal value.
- In applying a various recognition radius, the nominal size distribution for the simulation was chosen to have an ‘ideal’ size distribution that follows a normal distribution that have a various standard deviation. From the simulated

results, determined size distribution using the conventional and modified displacement probabilities was compared to test if the two probabilities determine the standard deviation as the nominal value. The two probabilities did not show much difference on a long recognition radius while they produced a deviation from the nominal value on a short recognition radius with respect to the diffusion scale of the nominal particle size. However, the deviation generated by the modified displacement probability is less apparent compared to the conventional probability.

- A various particle concentration was also applied in the simulation. An increased particle concentration was expected to produce more false tracks since the average distance between two particles would decrease. This setting suggested to reduce the value for a recognition radius to minimize probable false tracks, while a small recognition radius may result in an overestimation in the particle size and an abnormal standard deviation for the size distribution. This can be used as a basis to find a proper recognition radius to acquire more accurate size distribution in NTA.

1.3 Dissertation Overview

The thesis is organized into the following chapters.

Chapter 1 provides the background of the study for the necessity of accurate size characterization of nanometer-scale particles and outlines the rationale motivating the research topic, including key goals, objectives and project scope.

Chapter 2 reviews the literature, introduces various size measurement techniques used for particles in suspension and highlights some important factors in determining appropriate techniques for the size characterization, including classifications and characteristics of those techniques. It also introduces the principles of the two chosen size measurement techniques in this study, DLS and NTA, where their respective methodologies to analyze acquired data are presented. Since NTA is a main subject for this study, it focuses on how

each factor of NTA influences the results in NTA measurements.

Chapter 3 provides a description of materials, experimental techniques, computer simulations and analysis methods in analyzing the results along with physical principles of the used techniques.

Chapter 4 describes how results of DLS and NTA compare on monodisperse and polydisperse samples in suspension. Since biological particles in the nanometer scale generally has a polydisperse size distribution, both techniques require careful interpretation on the results. This chapter uses an improved method to analyze NTA results, and compares the results by converting the number-weighted size distribution of NTA into an intensity-weighted distribution.

Chapter 5 describes the influence of the recognition radius in determining the size distribution of NTA. The recognition range limits a probable particle displacement larger than the range, resulting in effective overestimation of the size. To consider the effect in the size determination of NTA, a modified displacement probability that describes the particle movement observed by NTA is introduced and incorporated with the iteration-based MLE method. The modified method was applied to simulations and real experiments and finds a better size accuracy and resolution than the conventional displacement probability. Moreover, it was evaluated to find the effect of particle concentration on the choice of the recognition range based on simulation results.

Chapter 6 summarizes key findings of the work in measuring the size of polydisperse biological particles in the nanometer scale with DLS and NTA. Particular attention is made to the influence of the recognition radius in determining the concentration of the particles, especially on a polydisperse condition, which effectively counts smaller particles less than larger particles in acquiring particle tracks in NTA.

1.4 Findings and Outcomes/Originality

The findings achieved in this work led to several novel outcomes on how to evaluate and analyze results from NTA. The key findings of this thesis can be summarized as follows:

1. NTA was evaluated by comparing with DLS, where monodisperse and polydisperse samples were used to represent ideal and practical examples of sample measurements. In doing so, improved methods to analyze the results from NTA was introduced, which use the MLE principle. The comparison showed that an iteration-based MLE was more useful for NTA analysis since the method does not require an assumption for the size distribution analysis.
2. Since the quantities that NTA and DLS provide differ from each other, i.e. number and light intensity, respectively, the comparison of results from the two techniques is not straightforward. To reflect the difference, a conversion of the number-weighted size distribution of NTA into an intensity-weighted distribution was evaluated. As a polydisperse biological samples, measurement results on vesicle samples prepared in a various condition were tested for the conversion. The comparison indicated that their respective native quantity, i.e. number for NTA and intensity for DLS, compares better than when the number-weighted size distribution of NTA was converted into an intensity-weighted distribution.
3. In analyzing NTA results, the influence of the recognition radius was identified. The recognition range set to distinguish tracked particles from their respective neighboring particles excludes probable long displacements of those tracked particles and effectively underestimates the average squared displacement of particle tracks. This is translated into an overestimation of particle size. To take the finite recognition radius into the size estimation of NTA, a modified displacement probability was introduced and incorporated into the iteration-based MLE method. The modified probability showed a better size accuracy than the conventional probability for particle displacements in simulations and real experiments. In the simulations, it also resulted in a better size resolution which distinguish two separate particle sizes from each other.
4. The simulation also suggested that when the recognition radius is too large, it would

result in spurious peaks in the analyzed size distribution. It was identified that the spurious peaks were due to false particle tracks, where two different particles are recognized as the same particle. Since false tracks happen when two different particles are near to each other, the chance to have false tracks would change depending on the particle concentration, i.e. a higher chance of false tracks on a higher concentration. It indicates that a smaller recognition radius would be more appropriate to minimize false tracks in NTA detection for a higher particle concentration. Whereas, the simulation also showed that a small recognition radius fails to determine a proper size distribution from acquired tracks, where a lower bound for a proper size distribution is approximately two times the diffusion scale of the measured particle size. These factors highlight that a proper choice of the recognition radius is very critical in determining a size distribution with NTA.

References

[1] Shi, J., et al., Nanotechnology in drug delivery and tissue engineering: from discovery to applications. *Nano Lett*, 2010. **10**(9): p. 3223-30.

[2] Parveezn, S., R. Misra, and S.K. Sahoo, Nanoparticles: a boon to drug delivery, therapeutics, diagnostics and imaging. *Nanomedicine*, 2012. **8**(2): p. 147-66.

[3] Blanco, E., H. Shen, and M. Ferrari, Principles of nanoparticle design for overcoming biological barriers to drug delivery. *Nat Biotechnol*, 2015. **33**(9): p. 941-51.

[4] Chang, H.I. and M.K. Yeh, Clinical development of liposome-based drugs: formulation, characterization, and therapeutic efficacy. *Int J Nanomedicine*, 2012. **7**: p. 49-60.

[5] Tan, M.L., P.F. Choong, and C.R. Dass, Recent developments in liposomes, microparticles and nanoparticles for protein and peptide drug delivery. *Peptides*, 2010. **31**(1): p. 184-93.

[6] Bamrungsap, S., et al., Nanotechnology in therapeutics: a focus on nanoparticles as a drug delivery system. *Nanomedicine (Lond)*, 2012. **7**(8): p. 1253-71.

[7] Warne, N.W., Development of high concentration protein biopharmaceuticals: the use of platform approaches in formulation development. *Eur J Pharm Biopharm*, 2011. **78**(2): p. 208-12.

[8] Tsuchikama, K. and Z. An, Antibody-drug conjugates: recent advances in conjugation and linker chemistries. *Protein Cell*, 2018. **9**(1): p. 33-46.

[9] Li, B.L., et al., Directing Assembly and Disassembly of 2D MoS2 Nanosheets with DNA for Drug Delivery. *ACS Appl Mater Interfaces*, 2017. **9**(18): p. 15286-15296.

[10] Komiyama, M., et al., Chemistry Can Make Strict and Fuzzy Controls for Bio-Systems: DNA Nanoarchitectonics and Cell-Macromolecular Nanoarchitectonics. *Bull Chem Soc Jpn*, 2017. **90**(9): p. 967-1004.

[11] Jackman, J.A., et al., Vesicle adhesion and rupture on silicon oxide: influence of freeze-thaw pretreatment. *Langmuir*, 2014. **30**(8): p. 2152-60.

[12] Merkus, H.G., *Particle size measurements: fundamentals, practice, quality*. Particle Technology Series. 2009, New York: Springer. xii, 533 pp.

[13] de Temmerman, P.J., et al., Size measurement uncertainties of near-monodisperse, near-spherical nanoparticles using transmission electron microscopy and particle-tracking analysis. *Journal of Nanoparticle Research*, 2014. **16**(10): p. 17.

[14] Troiber, C., et al., Comparison of four different particle sizing methods for siRNA polyplex characterization. *European Journal of Pharmaceutics and Biopharmaceutics*, 2013. **84**(2): p. 255-264.

[15] Sokolova, V., et al., Characterisation of exosomes derived from human cells by nanoparticle tracking analysis and scanning electron microscopy. *Colloids Surf B Biointerfaces*, 2011. **87**(1): p. 146-50.

[16] Anderson, W., et al., A comparative study of submicron particle sizing platforms: accuracy, precision and resolution analysis of polydisperse particle size distributions. *J Colloid Interface Sci*, 2013. **405**: p. 322-30.

[17] Bootz, A., et al., Comparison of scanning electron microscopy, dynamic light scattering and analytical ultracentrifugation for the sizing of poly(butyl cyanoacrylate) nanoparticles. *Eur J Pharm Biopharm*, 2004. **57**(2): p. 369-75.

[18] Fraunhofer, W., G. Winter, and C. Coester, Asymmetrical flow field-flow fractionation and multiangle light scattering for analysis of gelatin nanoparticle drug carrier systems. *Anal Chem*, 2004. **76**(7): p. 1909-20.

[19] Liu, J., J.D. Andya, and S.J. Shire, A critical review of analytical ultracentrifugation and field flow fractionation methods for measuring protein aggregation. *AAPS J*, 2006.

8(3): p. E580-E589.

[20] Hassan, P.A., S. Rana, and G. Verma, Making sense of Brownian motion: colloid characterization by dynamic light scattering. *Langmuir*, 2015. **31**(1): p. 3-12.

[21] Panchal, J., et al., Analyzing subvisible particles in protein drug products: a comparison of dynamic light scattering (DLS) and resonant mass measurement (RMM). *AAPS Journal*, 2014. **16**(3): p. 440-51.

[22] Pecora, R., Dynamic light scattering: applications of photon correlation spectroscopy. 2013: Springer Science & Business Media.

[23] Sediq, A.S., et al., Protein–polyelectrolyte interactions: Monitoring particle formation and growth by nanoparticle tracking analysis and flow imaging microscopy. *European Journal of Pharmaceutics and Biopharmaceutics*, 2015. **93**: p. 339-345.

[24] Filipe, V., A. Hawe, and W. Jiskoot, Critical evaluation of nanoparticle tracking analysis (NTA) by NanoSight for the measurement of nanoparticles and protein aggregates. *Pharmaceutical Research*, 2010. **27**(5): p. 796-810.

[25] Malloy, A. and B. Carr, NanoParticle tracking analysis - The Halo™ system. *Particle & Particle Systems Characterization*, 2006. **23**(2): p. 197-204.

[26] Bartlett, T.R., et al., Bi2O3 Nanoparticle Clusters: Reversible Agglomeration Revealed by Imaging and Nano-Impact Experiments. *Chemistry–A European Journal*, 2016. **22**(22): p. 7408-7414.

[27] Chan, M.Y., et al., Particle sizing of nanoparticle adjuvant formulations by dynamic light scattering (DLS) and nanoparticle tracking analysis (NTA), in Vaccine Adjuvants. 2017, Springer. p. 239-252.

[28] Mehn, D., et al., Larger or more? Nanoparticle characterisation methods for recognition of dimers. *RSC Advances*, 2017. **7**(44): p. 27747-27754.

[29] Boyd, R.D., S.K. Pichaimuthu, and A. Cuenat, New approach to inter-technique comparisons for nanoparticle size measurements: using atomic force microscopy, nanoparticle tracking analysis and dynamic light scattering. *Colloids and Surfaces A: Physicochemical and Engineering Aspects*, 2011. **387**(1-3): p. 35-42.

[30] Montes-Burgos, I., et al., Characterisation of nanoparticle size and state prior to nanotoxicological studies. *Journal of Nanoparticle Research*, 2010. **12**(1): p. 47-53.

[31] Hou, J., et al., Nanoparticle tracking analysis versus dynamic light scattering: Case

study on the effect of Ca2+ and alginate on the aggregation of cerium oxide nanoparticles. *Journal of hazardous materials*, 2018. **360**: p. 319-328.

[32] Walker, J.G., Improved nano-particle tracking analysis. *Measurement Science and Technology*, 2012. **23**(6): p. 065605.

[33] Saveyn, H., et al., Accurate particle size distribution determination by nanoparticle tracking analysis based on 2-D Brownian dynamics simulation. *Journal of Colloid and Interface Science*, 2010. **352**(2): p. 593-600.

[34] Kestens, V., et al., Validation of a particle tracking analysis method for the size determination of nano- and microparticles. *Journal of Nanoparticle Research*, 2017. **19**(8): p. 271.

[35] Rasteiro, M.G., C.C. Lemos, and A. Vasquez, Nanoparticle characterization by PCS: The analysis of bimodal distributions. *Particulate Science and Technology*, 2008. **26**(5): p. 413-437.

[36] Maulucci, G., et al., Particle size distribution in DMPC vesicles solutions undergoing different sonication times. *Biophys J*, 2005. **88**(5): p. 3545-50.

[37] Lawrie, A.S., et al., Microparticle sizing by dynamic light scattering in fresh-frozen plasma. *Vox Sang*, 2009. **96**(3): p. 206-12.

[38] Hinna, A., et al., Filter-extruded liposomes revisited: a study into size distributions and morphologies in relation to lipid-composition and process parameters. *J Liposome Res*, 2015: p. 1-10.

[39] Pencer, J. and F.R. Hallett, Effects of vesicle size and shape on static and dynamic light scattering measurements. *Langmuir*, 2003. **19**(18): p. 7488-7497.

[40] Berne, B.J. and R. Pecora, *Dynamic light scattering: with applications to chemistry, biology, and physics*. Dover ed. 2000, Mineola, N.Y.: Dover Publications. vii, 376 pp.

Chapter 2

Literature Review

Nanoparticle Tracking Analysis is a size measurement technique for particles in suspension that measures individual particles and produces a number-weighted size distribution. Due to its individual tracking, it is advantageous in measuring polydisperse samples while it shows a broad size distribution even for monodisperse samples. This is due to the stochastic nature of Brownian motion of particles that NTA observes, creating uncertainties in determining the size. By recognizing the uncertainty is related with the track length, NTA could improve measurement results by reducing the effect of the uncertainty. Yet, there have been scant studies that validated the improved size estimation method for NTA for polydisperse samples. Moreover, the recognition range set for the tracking of particles excludes a probable displacement of particles under tracking. It effectively reduces the average of squared displacement of acquired tracks, which is converted into a smaller diffusion coefficient of a particle, hence a larger size. This effect could be avoided by selecting a long enough recognition range for the tracking, while such a choice is not always available especially on a high concentration where a particle under track should be isolated from neighboring particles by more than the chosen recognition range. For a more accurate size determination of NTA, the finite recognition range should be incorporated with the size determination method of NTA.

2.1 Size Measurement Techniques for Particles in Suspension

2.1.1 Overview

To measure a size of particles in suspension, various principles can be used to measure certain physical properties of such particles and translate into a corresponding size [1-6]. Those principles include visualization of particles [7, 8], light scattering [9, 10], physical separation [11, 12], Brownian motion [13-15], mechanical or electrical changes on surrounding mechanism [2] and so on. The size information produced by each technique typically represents a characteristic size that corresponds to equivalent spheres, where the relation between the size and measured properties depends on the principle of a used technique [1, 11, 12].

Since principles of measurement techniques vary, and so does the definition of the measured size by each technique, the results from different techniques may not produce the same values. Hence, a single technique alone cannot fully determine size information. For example, microscopy-based techniques, such as scanning electron microscopy (SEM) and atomic force microscopy (AFM), are some of the most popular methods to obtain the topographical size of particles, as well as their shape and texture [1, 8, 16-18]. Imaging has been preferred due to its intuitive high-resolution visualization of particles and the minimal influence of artifacts in size determination [1]. However, microscopy-based techniques require laborious sample preparation steps, and the sample must be removed from its native or working environment, often resulting in a deformation to the samples. In addition, throughput is limited and sampling may result in biased information [1].

Another strategy is to separate the particles in the sample, creating a spatial macromolecular redistribution in a medium, in which the degree of separation is determined by the mass or volume of the macromolecules and can be converted into their size [1]. This approach is a feature of various techniques, including size exclusion chromatography (SEC), asymmetrical flow field-flow fractionation (AF4) and analytical ultracentrifugation (AUC), which measure differences in the elution, sedimentation or

diffusion of particles [12, 19, 20]. As the particles in the sample are spatially separated depending on their differences in the course of measurement, these techniques can be combined with other size measurement techniques, such as multi-angle light scattering (MALS), to improve the size resolution or measure additional properties, such as molecular weight [21, 22]. As the techniques involve separation of the measured sample, they provide more useful size measurements of polydisperse samples but introduce distortion of the sample condition due to the medium used [1].

Among non-destructive measurement techniques, dynamic light scattering (DLS) is the most widely used due to its simplicity. Upon laser illumination, the intensity of the light scattered by the particles in suspension changes both temporally and spatially depending on the size and weight of the particles and can be converted into size information [1, 9]. Despite being a powerful and accessible tool, DLS has several drawbacks due to the inherent limitation of intensity-biased detection [9, 14]. DLS determines a particle's size from fluctuations of the scattered light resulted from the Brownian motion of the particles. The intensity of the scattered light is proportional to the square of the volume of the particle, which makes DLS very sensitive to the presence of large particles [14, 23]. Small amounts of large aggregates or dust particles can disturb the size determination if the main population is significantly smaller in size.

To address this problem, other techniques including AFM, SEM, TEM, RPS, AF4 and AUC can be used to verify the size determined by DLS [17, 24-27]. However, the definition of size measured by one technique can be different from that of the others, which makes the comparison complicated as it requires careful interpretation of the data obtained. In particular, DLS measures the hydrodynamic diameter from the diffusion coefficient of particles in suspension, and this diffusion coefficient is converted into the diameter of an assumed hypothetical sphere that has the same diffusion coefficient [9]. In contrast, SEM, for instance, can obtain a geometric size of particles given by measuring the width of individual particles from the image [1, 28]. Recently, a size characterization tool called nanoparticle tracking analysis (NTA) was introduced to acquire the size of particles by determining their diffusion coefficient, meaning that the definition of the size measured by

NTA is identical to that of DLS. NTA can be a good method to verify the results of DLS because they measure the same physical property [15, 29]. Whereas DLS reads the intensity change of scattered light to find the diffusion coefficient of particles, NTA calculates the diffusion coefficient based on the movements of individual particles in successive optical video images [15, 29]. This difference in the detection principles of DLS and NTA results in a difference in the way that the size is reported, i.e., the quantities of the particles measured by DLS and NTA are weighted by intensity and number, respectively, which makes NTA an excellent technique for verifying DLS results.

This implies that comparisons among the techniques are not straightforward and requires proper interpretation of results from one technique to be compared with those from another.

Table 2.1 Overview of particle size measurement techniques. Sample types: A = aerosol; E = emulsion; P = powder; Pa = powder dispersion in air; Sp = spray; Su = suspension [14].

	Size range, µm	Type of size	Type of quant.	Sample type	Sample size	Meas. time, min	Quality	Invest costs, kE	In-/on-line
Chord length	0.5-3,000	Chord length	Number	A,E,Pa,Su	small	<1	-	10-50	yes
DLS		Hydro-dynamic	Scatter Intensity	A,E,Pa,Sp,Su	small	1	-	10-50	
- normal	0.005-1								no
- opt. fiber	0.005-1								yes
Electro-acoustics	0.005-1,000	Hydro-dynamic	Volume	Su	small	10	++	50	no
Electrical mobility	0.0025-1	Electrical mobility	Number	A	small/medium	~1	++	50-80	yes
ESZ	0.5-1000	Volume	Number	Su	small	2	++	10-50	no
Flow cytometry	0.5-400	Volume/Others	Number	E,Su	small	10	++	>50	no
Hegman gage	2-250	Thickness	Number	Su	small	<1	+	<3	no
Hydrodynamic chromatography	0.01-20	Hydro-dynamic	Mass	Su	small	2	+/-	>10	no
Image analysis	500-10^5	Area/Length/Shape	Number	Pa,Sp,Su	small/medium	10	+(+)	3-50	yes
Impaction	0.01-50	Aero-dynamic	Mass	A,Pa	small	10	+/-	1-25	no
Laser diffraction	0.1-10^4	Scatter diameter	Volume	A,E,Pa,Sp,Su	small/medium	<1	++	>10	yes
Microscopy		Length/Shape/	Number		very small	10	+		
- optical	0.3-500	Structure		E,Sp,Su				<10	yes
- SEM	0.01-500			E,Su				>10	no
- TEM	0.001-5			E,Su				>10	no
NMR	0.3-20	Volume	Model	E	medium	10	+/-	>50	(yes)
Opt. part. counters	0.1-200	Cross section	Number	A,E,Pa,Sp,Su	small/medium	3	+	3-35	yes
Phase Doppler	1-1,000	Cross section	Number	A,E,Pa,Sp,Su	small	1	+(+)	>50	yes
Sedimentation		Stokes' diameter		Su					
- gravity	0.3-200	+ diffusion	Mass		small/medium	>30	++	3-50	no
- centrifugal	0.02-10		Mass/opt.		small/medium	15	++	10-50	no
- SFFF	0.02-50		Optical		small	30	++	50	no
Sieving	5-10^5	Sieve	Mass	P,Su	large	20	+	1-20	no
SEC/GPC	0.01-1	Volume	Optical	Su	small	3	+/-	10-50	no
SAXS	0.003-0.3	Cross section	Model	E,P,Su	small	1	-	>50	no
Time of flight	0.5-200	Aerodynamic	Number	A,Pa	small/medium	<1	+	30-40	no
Ultrasound attenuation	0.01-3,000	US-attenuation	Volume	E,Su	medium/large	5	+	>50	yes

2.1.2 Classifications

Size measurement techniques can be classified by whether (i) they measure individual particles in a sample and accumulate the results to represent the size distribution of the measured sample or (ii) they measure the particles in the sample as a whole [1, 30]. The detection principle of the former techniques allows a superposition of acquired results. These techniques include flow cytometry, microscopy-based techniques such as scanning electron microscopy and atomic force microscopy, and light scattering particle counter [30, 31]. These are especially efficient in displaying a size distribution as the quantity of particles are accumulative. However, these techniques usually require a low concentration to avoid interference of overlapped particles [1, 3]. On top of this, collection of information for individual particles require more time than other techniques, resulting in lower throughput.

Some of the techniques collect a set of signals from the particles as a whole or an ensemble. In this case, the acquired signal from an instrument is analyzed by a model to convert into a size distribution [30]. In a most cases, the superposition of acquired results does not apply and interference among the particles would produce distortion on the acquired size distribution. These techniques include dynamic light scattering [14, 32], nuclear magnetic resonance [33, 34] and small angle X-ray scattering [35, 36]. In these techniques, the size and the quantity of particles are acquired from the same signals. Application of theoretical models for the analysis of the results from these techniques often requires constraints to acquire a size distribution, by which the details of the size distribution can be limited [1, 30].

Yet another group of techniques separates particles by the size through their respective principles and determine the size of particles by the degree of separation. For the separation, various principles can be used such as electric charge [37], mass [38], volume [39] and cross section [40]. Those techniques, including size exclusion chromatography, sedimentation, impaction and filed flow fractionation, have an advantage that the analyzed particles are physically separated, which produces an amount of the particles while the size

can be quantified easily. Also, separated particles through the techniques can be used for other analysis [1, 41]. Because of the separation, however, measured samples by the techniques are made different from their original state, which makes the techniques not favored when the amount of sample is limited.

As a different classification of the size measurement techniques, the method to report the quantity of particles can be used: namely, number, volume, mass, cross-section and arbitrary amount [1, 30, 42]. Since the individual particle measurement techniques literally counts the measured particles, the quantity of the measured particles is reported by the number. Whereas those techniques based on separation generally give the quantity based on mass-related information as the separation is related with the mass. On the other hand, the quantity information from the ensemble measurement techniques takes various forms depending on the used principle.

2.1.3 Comparison of Acquired Size Distribution by Different Techniques

As above, each size measurement technique generates size information according to its respective unique principle, where the uniqueness is not only the physical meaning of the size but the quantity of particle and the way each particle is treated by the technique. This makes the comparison of measured size by different techniques complicated. A simple method to compare size information by different technique is to use a characteristic size of acquired size distributions such as mean size and variance [24, 29, 43]. However, this is not enough to compare polydisperse samples as the method does not provide a detailed indication of the difference in the acquired size distribution [3-5]. Another method is to use a cumulative size distribution, which can be presented in the same scale [30, 44]. However, such a comparison is difficult to get quantitative information about the differences from two different measurement techniques. A third method is to use various characteristic sizes from one technique to be set against corresponding sizes from another measurement technique [30]. The method allows a direct quantitative comparison between two different techniques. However, such comparison should be applied with care for size measurement

techniques of similar principles since differences in the principle may result in huge differences in the results.

2.2 Dynamic Light Scattering

2.2.1 Principle

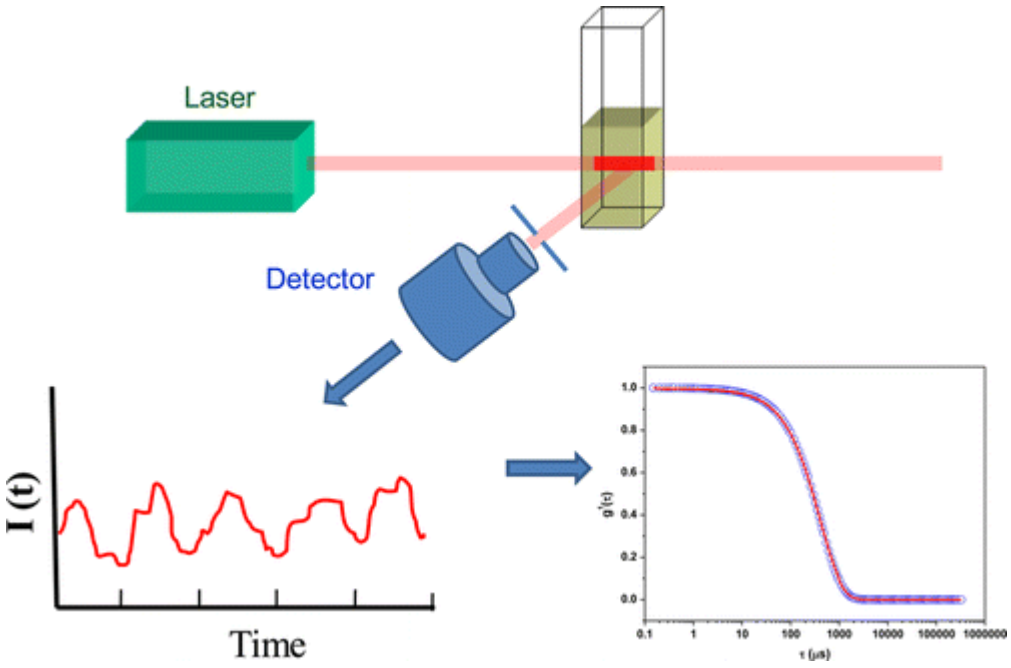

Figure 2.1 Schematic diagram of dynamic light scattering and its autocorrelation graph from the detected scattered light.

DLS extracts the size distribution of particles in suspension from their Brownian motion, whose displacement is related to their diffusion coefficient [9, 14, 23]. The intensity of the light scattered by particles in suspension upon laser illumination changes due to the particles' Brownian motion, and the intensity fluctuation is processed to acquire its auto-correlation function whereby the decay time is related to the particles' diffusion coefficient as follows

$$g^{(1)}(\tau) = A \cdot e^{-Dq^2\tau} + B \quad (2.1)$$

where $g^{(1)}(\tau)$ is the first-order correlation function of the electric field, τ is a delay time, D is the diffusion coefficient, q is the scattering vector and A and B are the amplitude and

the baseline of the correlation function, respectively. For monodisperse spherical particles, the hydrodynamic radius R_h can be related to the diffusion coefficient using the Stokes-Einstein equation

$$D = \frac{k_B T}{6\pi\eta R_h} \quad (2.2)$$

where k_B is the Boltzmann constant, T is the absolute temperature and η is the viscosity of the medium.

For polydisperse samples, the auto-correlation function can be expressed as the integral form

$$g^{(1)}(\tau) = \int G(\Gamma)\exp(-\Gamma\tau)d\Gamma \quad (2.3)$$

where $\Gamma = Dq^2$ is the decay rate for a given size with diffusion coefficient D and $G(\Gamma)$ is the intensity-weighted size distribution. Although a Laplace inversion of the integration produces the size distribution $G(\Gamma)$, it is well known that the inversion is not a well-conditioned problem [1, 9, 14]. Many strategies have been suggested to recover the size distribution from the integration, among which only the cumulant analysis method is recommended by the International Standards Organization [45].

The cumulant analysis method is applied for polydisperse samples of a relatively narrow size distribution [46]. The auto-correlation function can be expanded by the moments about the mean when $\exp(-\Gamma\tau)$ is rewritten in terms of $\bar{\Gamma}$, so that

$$\exp(-\Gamma\tau) = \exp(-\bar{\Gamma}\tau)\exp(-(\Gamma - \bar{\Gamma})\tau) \quad (2.4)$$

where

$$\bar{\Gamma} = \int G(\Gamma)d\Gamma \quad (2.5)$$

By rewriting $\exp(-\Gamma\tau)$ around the mean $\bar{\Gamma}$,

$$g^{(1)}(\tau) = \exp(-\bar{\Gamma}\tau)\int G(\Gamma)\exp(-(\Gamma - \bar{\Gamma})\tau)\,d\Gamma \quad (2.6)$$

where the integral term can be expanded as a series:

$$g^{(1)}(\tau) = \exp(-\bar{\Gamma}\tau)\int G(\Gamma)\left[1-(\Gamma-\bar{\Gamma})\tau+\frac{(\Gamma-\bar{\Gamma})^2}{2!}\tau^2-\frac{(\Gamma-\bar{\Gamma})^3}{3!}\tau^3+\cdots\right]d\Gamma$$

$$= \exp(-\bar{\Gamma}\tau)\left[\int G(\Gamma)d\Gamma-\int G(\Gamma)(\Gamma-\bar{\Gamma})d\Gamma\cdot\tau+\frac{\tau^2}{2!}\int G(\Gamma)(\Gamma-\bar{\Gamma})^2d\Gamma\right.$$

$$\left.-\frac{\tau^3}{3!}\int G(\Gamma)(\Gamma-\bar{\Gamma})^3d\Gamma+\cdots\right]$$

$$= \exp(-\bar{\Gamma}\tau)\left[1+\frac{\tau^2}{2!}\mu_2-\frac{\tau^3}{3!}\mu_3+\cdots\right] \quad (2.7)$$

where μ_m is the moments about the mean, defined as

$$\mu_m = \int G(\Gamma)(\Gamma-\bar{\Gamma})^m d\Gamma \quad (2.8)$$

By taking logarithm on each side of Eq. 2.7,

$$\ln\left(g^1(\tau)\right) = \ln B - \bar{\Gamma}\tau+\frac{\mu_2}{2!}\tau^2-\frac{\mu_3}{3!}\tau^3+\cdots \quad (2.9)$$

where

$$\bar{\Gamma} = \int G(\Gamma)d\Gamma \quad (2.10)$$

$$\mu_2 = \int G(\Gamma)(\Gamma-\bar{\Gamma})^2 d\Gamma \quad (2.11)$$

$$\mu_3 = \int G(\Gamma)(\Gamma-\bar{\Gamma})^3 d\Gamma \quad (2.12)$$

By fitting $\ln\left(g^1(\tau)\right)$, $\bar{\Gamma}$ and μ_2 can be acquired, and then converted to the mean size R_Z and the polydipersity index PI as

$$R_Z = \frac{k_B T}{6\pi\eta\bar{D}} = \frac{k_B T}{6\pi\eta}\cdot\frac{1}{\bar{\Gamma}/q^2} \quad (2.13)$$

$$\text{PI} = \frac{\mu_2}{\bar{\Gamma}^2} \quad (2.14)$$

Although it is only valid for polydisperse samples that meet the criterion $\mu_2\tau^2 \ll 1$ [14, 46], the cumulant method was applied to both PS latex nanoparticle samples and vesicle samples in this study for the comparison with NTA.

2.2.2 Conversion of Size Distribution

The quantity of the size distribution reported by DLS is expressed by the intensity of scattered light detected by the detector, or the sum of the scattered light intensity by the measured particles. Hence, the size R_Z measured by DLS is

$$R_Z = \frac{\sum_i N_i M_i^2 P(R_i) R_i}{\sum_i N_i M_i^2 P(R_i)} \quad (2.15)$$

where N_i is the proportion of particles with a size of R_i and mass of M_i and $P(R_i)$ is the scattering factor of a single particle with the size and mass. When it is compared to the size measured another technique, it needs to be converted into a different form that corresponds to the size defined by the other technique. When it is compared with the size measured by microscopy-based techniques, for example, the size acquired by the techniques is a number-averaged size. Then a number-averaged size is defined as

$$R_N = \frac{\sum_i N_i R_i}{\sum_i N_i} \quad (2.16)$$

When the particles are assumed as point scatters, $P(R_i) = 1$ for all R_i. For more general cases, the scattering factor should be considered. In biological samples, the Rayleigh-Gans-Debye approximation is useful in describing the scattering factor, since the approximation assumes the refractive index of the particles is close to the medium and their size is small enough compared to the wavelength of the illuminated laser divided by $|n - 1|$ where n is the refractive index [13, 25, 47].

In comparing results from DLS with those from other techniques such as NTA or TEM, it is difficult to convert the former into a corresponding dimension of other techniques. In converting the results, the information about N_i is essential. However, DLS is well known for being difficult in resolving the size distribution, which should be acquired from a Laplace inversion of the autocorrelation function measured by DLS. Although many analytical approaches could be used to extract a size distribution from DLS results, only the cumulant analysis method has been recommended as a proper interpretation of DLS results [45]. In the cumulant analysis, only the average size and the polydipersity index, or

the broadness of the size distribution, can be acquired while the detail of the size distribution is mostly neglected. Due to the difficulty in conversion of DLS results, it is more efficient to convert results from other techniques into the form of DLS results.

.

2.3 Nanoparticle Tracking Analysis

2.3.1 Principle

Nanoparticle tracking analysis is a size measurement technique that measures the size of particles in suspension by monitoring the Brownian movement of the particles in the range of 20 to 2000 nm [15, 29, 48]. Particles in suspension undergo Brownian motion, which is described by a random movement whose displacement follows a Gaussian distribution for each axis in the three dimensional space. The standard deviation of the Gaussian distribution is related to the diffusion coefficient of the particle and the time scale at which the displacement is measured. Hence, the information about the particle's movement, i.e. the standard deviation, can be translated into the diffusion scale, and therefore the size according to the Stokes-Einstein equation [15, 29].

To observe the movement of particles in suspension in NTA, a suspended sample is inserted into a chamber, where a narrow laser beam illuminates a part of the chamber. Those particles in the beam path scatter light, which is captured by a CCD camera through an objective lens [15, 29]. In each image of the captured video, the center of particles is recognized and compared with the centers in the previous image to find the displacement of the particles. The comparison is extended to following images until a next particle cannot be recognized, which constructs a track for the recognized particle. From such a track, the average of the displacements of each segment in the track is translated into the diffusion scale of the tracked particle [49].

In determining the diffusion scale, the length of a track, or the number of image frames, in which a particle is recognized, is related with the uncertainty of the determined diffusion scale. Ideally the track length should be long enough to decrease the uncertainty, which is

not always achievable [44, 50]. Due to the finite track length, the uncertainty shows up as a broad size distribution even for very monodisperse samples [29, 44, 50]. To mitigate the effect of track length in broadening an acquired size distribution, there have been many studies to adjust the measurement conditions of the instrument as well as the sample [29, 49, 51].

For the measurement conditions for NTA, interlaboratory comparative studies on the repeatability of NTA measurement showed that consistency is not always guaranteed by practicing even best in-house standard operating procedures (SOPs) that individual laboratories built [52, 53]. In particular, the process for particle recognition from acquired video images is highly dependent on the parameters such as gain, blur, detection threshold and minimum expected particle size. In this regard, the interlaboratory comparative studies found a common SOP could achieve very repeatable results.

On the other hand, der Meeren et al. [49] pointed out that such measurement conditions could not be applied as a general rule since it may require a different measurement condition depending on the sample condition such as the particle concentration and the particle size. In particular, maximum jump distance (MJD), the parameter used as a range that a particle is recognized as the same particle in the next image frame, significantly affects measurement result on a high concentration, while the effect is not significant at a low concentration.

2.3.2 Validation of NTA Results

Since an advantage of NTA over other techniques, especially DLS, is its strength on polydisperse samples, many studies focused on its application on such samples including exosomes and protein aggregation [29, 54-56]. Due to its relative short history, many of the studies verified the technique by comparing with other techniques such as DLS, TEM, AFM, flow cytometry and so on [3-7, 16, 24, 29, 41, 43, 55-61]. Also, those studies started their investigation from well-defined, monodisperse nanoparticle samples and extended the comparison to polydisperse samples.

DLS and NTA reads the same properties of particles for the size characterization, and many studies compared NTA with DLS and showed the size resolution of NTA was comparable to that of DLS [16, 29]. Moreover, the presence of large particles did not compromise the accuracy of NTA, and mixtures of standard nanoparticles of different particle size could be easily detected without affecting the size accuracy [29].

Other studies compared NTA with AFM and TEM as those techniques give the quantity of particles by the number of particles [7, 24, 61]. In the study, the mean size acquired by the two techniques was very close with a small standard deviation of less than 1 nm, while the broadness of acquired size distribution was sharper with AFM. Especially the distribution acquired by NTA, compared with that of AFM, showed a weighted distribution toward a larger size, which was attributed to NTA's ability to measure agglomerates in suspension.

Yet other studies compared various techniques on nanoparticle samples, and found that not a single technique could sufficiently resolve the size distribution and those tested techniques provided complimentary results to one another [4, 62].

More recent comparative studies focused on aggregate analysis on proteins, where DLS was chosen for comparison [55-57]. In those studies, both techniques could find similar results, while the particle concentration required for NTA was lower than for DLS. This suggests that aggregates may hinder proper measurement for DLS, while NTA could distinguish smaller particles from aggregates.

On those verification studies, results from NTA were produced by inverting the acquired average squared displacement [15, 29, 48]. This direct inversion method neglects the track length, which introduces uncertainty in determining the diffusion coefficient. By recognizing the track length of particle tracks measured by NTA, there were a few analysis methods to refine acquired size distributions [44, 50]. Since a method suggested by Walker [50] does not require a prior knowledge about samples, it was introduced to a commercial software. Kestens et al. [63] tested the direct inversion method and the improved method

for NTA size distribution measurements and found that the improved method has much higher sensitivity in the size resolution. Yet, the study pointed out that the uncertainty, or the broadness of the size distribution, is inferior compared to DLS and TEM even with the improved method.

All in all, these comparisons suggest that each technique has certain strengths and NTA is best suited to measurements on polydisperse samples where both large and small ends of the size distribution are of interest.

2.3.3 Improvements on Size Distribution Determination by NTA

NTA relies on the Stokes-Einstein equation to relate the measured displacement of particle tracks into a corresponding size [15, 29], where the Stokes-Einstein equation describes the relation between the diffusion coefficient and the size of a particle as expressed in Eq. 2.2. At the time when NTA was introduced, the diffusion coefficient was acquired by averaging squared displacement of particle tracks.

$$D = \frac{1}{4\Delta t} \cdot \frac{1}{n} \sum_{i=1}^{n} r_i^2 \quad (2.17)$$

where r_i is the two-dimensional displacement of ith track segment of a track whose length is n. An accurate determination of the diffusion coefficient requires the track length n to be long enough, since each displacement of a track is a random process described as Brownian motion [15, 29, 44, 50]. Hence, those initial evaluations on NTA made remarks about the uncertainty due to the finite track length [29, 49]. In order to minimize the stochastic uncertainty in those studies, a minimum track length is used by which those tracks with lengths less than the minimum track length are excluded from the size determination. As the uncertainty due to the track length is inversely proportional to the square root of the track length, most of those studies used a value ranging from 10 to 20 as a minimum track length [29, 44, 49]. However, the method could not achieve high enough accuracy as even a minimum track length of 100, which still allows 10% error in determining the size. Also, a long track length is not always achievable, since a small particle tends to move faster and go out of the tracking region so that tracks of such a

particle terminate earlier compared to a larger particle [49, 50]. In polydisperse samples, especially, a long track length effectively excludes tracks of smaller particles compared to those of larger particles, which may result in inaccurate size measurements on the samples. Recognizing the finite track length in NTA and its effect of the stochastic uncertainty, a few studies tried to improve results by using the maximum likelihood estimation (MLE) principle, which finds an optimal solution that maximizes the likelihood of an estimated size distribution with respect to a set of acquired NTA tracks [44, 50].

One of the studies assumed an arbitrary size distribution with a few adjustable parameters, e.g. log-normal distribution with its mean and standard deviation made adjustable and tried to find a maximum value by varying the adjustable parameters. The method significantly improved the accuracy of size measurements by NTA as the stochastic uncertainty could be highly reduced, and was eventually introduced to one of the commercial software for NTA [63].

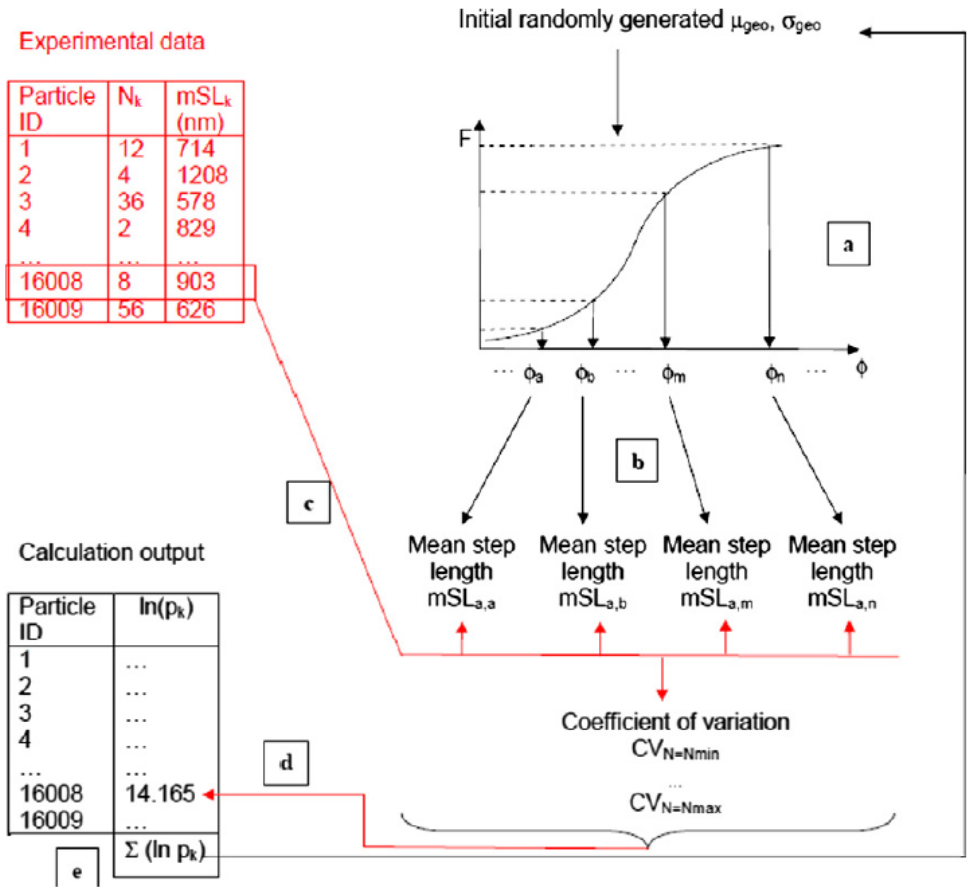

Figure 2.2 Schematic description of computing likelihood from an assumed size distribution with respect to a set of acquired tracks [44].

After the introduction, many studies could benefit from the improvement, by which a higher size resolution could be achieved. Since the method assumed an arbitrary size distribution for the maximization, it was especially useful to identify the size of well-defined size distribution such as a mixture of monodisperse particles of different sizes [60, 64, 65]. However, the requirement for the method limits its application on polydisperse samples of an unknown size distribution. Since the calculation of likelihood requires an assumption on the size distribution of the sample to be analyzed, it often misleads and produces a different result than the real distribution [63].

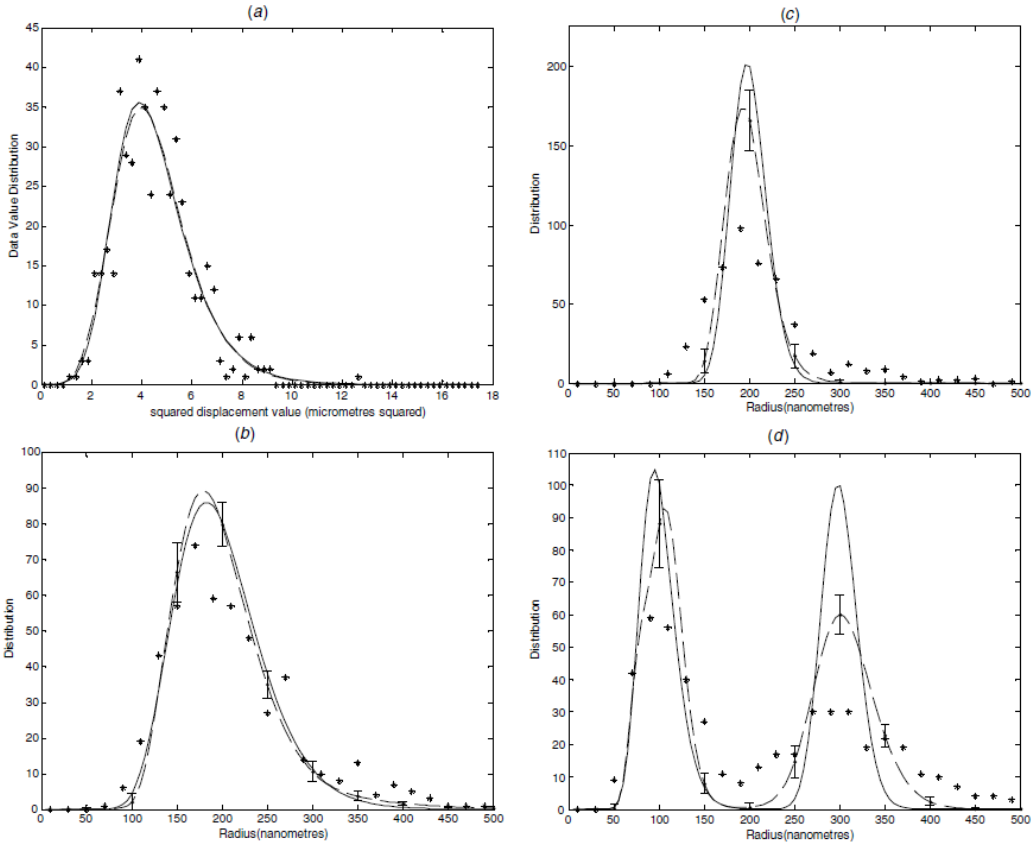

Figure 2.3 Examples of an iteration based MLE method in determining a size distribution of acquired tracks.

As a different approach to apply the MLE principle, an iterative method was suggested that does not require an assumption on the size distribution [50]. An advantage of not guessing a size distribution to determine a size distribution by NTA is beneficial as it is more general in analyzing samples of an unknown size distribution, especially polydisperse samples. Due to the advantage, this method has been incorporated into a commercial software as well and employed for various comparative studies [52, 53].

2.3.4 Particle Concentration Determination by NTA

Advantages of NTA include its ability to measure a particle concentration [6, 41, 60, 66]. Although many techniques such as scanning electron microscopy and atomic force microscopy can provide a particle concentration, NTA has drawn a particular attention since the technique is applied to samples in suspension. NTA identifies the size of

individual particles while the volume it observes is predetermined, translating the particle counts into a particle concentration. On the other hand, other techniques like DLS which does not provide the quantity of particles in a number-based distribution requires a conversion into a number-based distribution. However, such conversions only produce a relative size distribution and most of the time they require calibration to make the distribution absolute. This characteristic of NTA is beneficial for pharmaceutical applications, and many studies evaluated NTA's performance on concentration measurements [39, 67-69]. Those studies mainly targeted polydisperse samples such as protein and vesicles, and monitored their change upon different conditions.

While the conversion of particle counts in NTA into a concentration is straightforward, the identification of particles in NTA is not so. Since NTA identifies particles by analyzing captured images of scattered light, it recognizes the center of bright spots in the images as particles [15]. This makes the identification of particles arbitrary since the parameters to recognize those bright spots as particles can dramatically alter the results of particle identification [29, 70]. The significance of the parameter adjustment was evaluated by an international team, where an application of identical parameters on NTA analysis produced consistent readings across NTA instruments in many laboratories [53]. In doing so, a calibration of the instruments were required since a proper parameter setting should be determined according to the instrumentational configuration. However, an application of such a calibration could be limited since the instrumentational configuration includes the condition of a measured sample, which may not be the same as the sample used for the calibration. This limitation is more pronounced when a sample is polydisperse [70, 71].

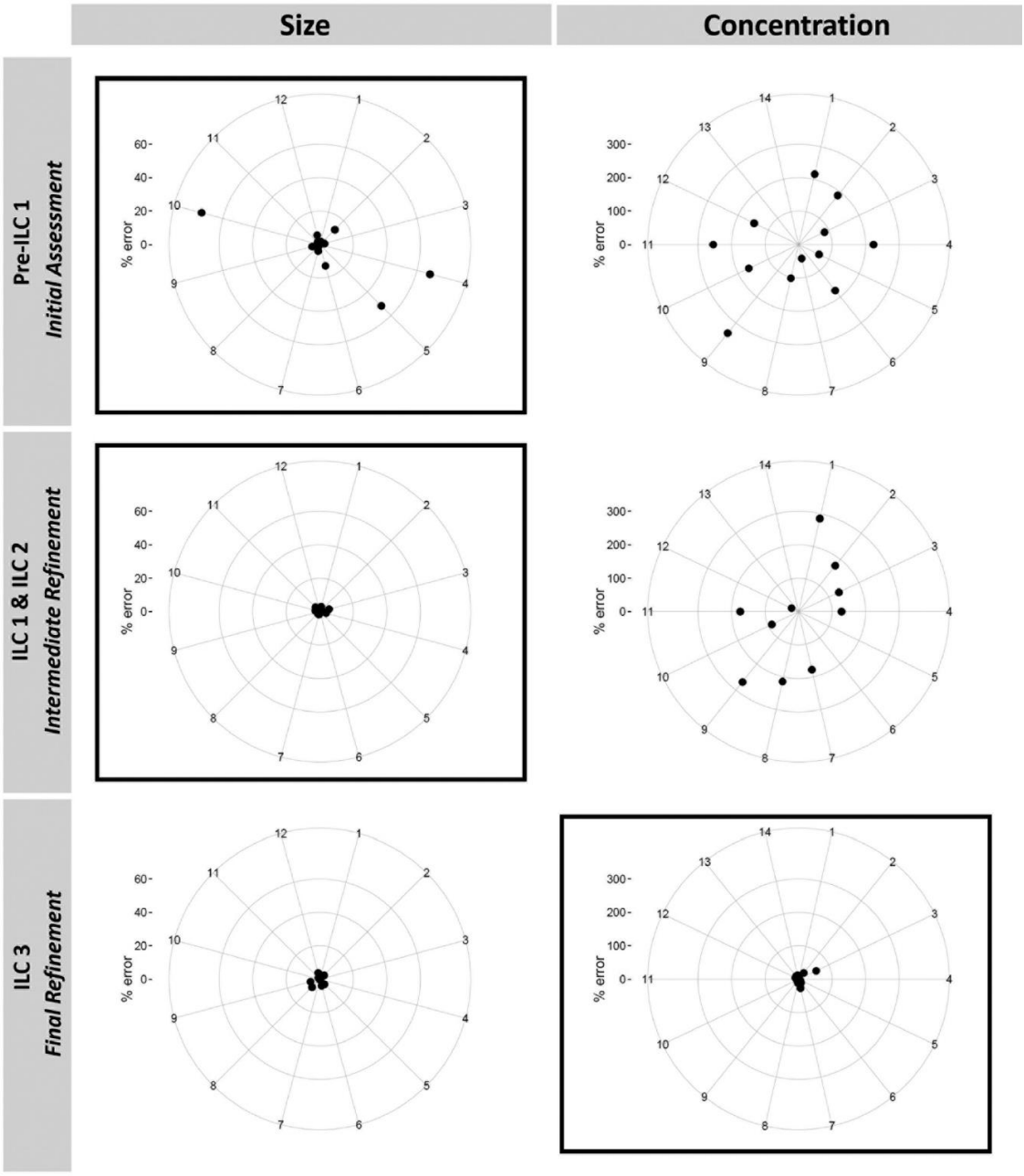

Figure 2.4 Refinements on the size and concentration measurement of NTA through three rounds of inter-laboratory comparison with 100-nm PS latex particles. (Top) Without a proper common protocol, each laboratory used respective method to measure the size and concentration and produced inconsistent results. (Middle) After adopting a common protocol, the measurement on the mean size showed consistent results. (Bottom) The calibration for concentration measurement added consistency on the particle concentration measurement as well as the mean size measurement.

2.4 Outstanding Questions

2.4.1 Evaluation of NTA on polydisperse samples

NTA has an advantage of measuring polydisperse samples in suspension, where its number-weighted size distribution compliments the results of other techniques provided in other quantities such as the volume or an arbitrary unit like light intensity. As NTA is a relatively new technique, many studies have focused on its validation. Since NTA's introduction, many studies evaluated the technique for various types of samples and conditions, which includes reference samples like polystyrene latex nanoparticles of mono- and multimodal size distribution and diverse biological samples such as exosomes and proteins [72-76]. Although those studies agreed that the NTA technique is accurate compared with other well-established techniques like DLS and TEM, they also pointed out that the size distribution produced by NTA is rather broad even for very monodisperse samples [29]. This is attributed to the stochastic nature of the displacement that each tracked particle moves.

To reduce the effect of the stochastic uncertainty in determining the particle size in NTA, a few studies have suggested improved size distribution determination methods based on the MLE principle [44, 50]. Those methods have shown better size resolution in determining the size distribution of monodisperse nanoparticles and their mixtures. Among the methods, an iteration-based MLE method was preferred since it does not require an assumption on the size distribution while the other method assumes an arbitrary size distribution for optimization. The iteration-based method has been introduced to the commercial software of NTA instruments and widely used in many studies [63].

Although many studies focused on evaluation of NTA on various sample types, evaluations on the new estimation method for NTA have been limited to reference particle samples, which are very monodisperse or mixtures of monodisperse particles. As an advantage of NTA over other techniques is its good performance on polydisperse samples, it is essential to evaluate the improved method on such polydisperse samples. The evaluation also invites

the need to address comparisons with other techniques that also includes conversion of the number-weighted size distribution into a corresponding quantity of other techniques.

2.4.2 Influence of the recognition radius

In determining the particle size in NTA, NTA measures the diffusion coefficient of each tracked particle and relates it to the size according to the Stokes-Einstein equation. Conventionally, the diffusion coefficient of tracked particles is acquired by averaging squared displacement of track segments of each particle track. This approach is correct since the Brownian motion of suspended particle is expressed by a Gaussian distribution in each direction [15, 29, 48]. Many evaluation studies on NTA have validated the size accuracy of NTA, where the size, or the diffusion coefficient, is determined by averaging the squared displacements.

However, the detection principle of NTA defines a certain limit on each displacement, by which a particle is recognized as the same particle in the following image. The limit, or the recognition radius, is called as the Max Jump Distance in the commercial software of NTA instruments [49]. Due to the recognition radius, the average of squared displacement would be smaller than the expected value acquired if there is no limit for the displacement, resulting in an overestimation of the particle size. If the recognition radius is long enough compared to the diffusion scale of the measured particles, then the reduction in the average squared displacement would be negligible. An experimental study on the influence of the recognition radius proposed a certain lower limit for a proper determination of the particle size measured by NTA [49]. However, the requirement for the recognition range cannot be always met since the lower limit is dependent on the particle concentration. On a high particle concentration, the recognition range should be chosen small so that neighboring particles near a tracked particle are apart from the tracked particle by more than the recognition range. If the recognition range is set too long, a tracked particle would not be isolated from neighboring particles, resulting in a quick termination of particle tracks.

Given an inevitable situation of a short recognition range, it is very probable to have an overestimation of a particle size due to the limited displacement of particle tracks. This indicates that accurate measurement of the diffusion coefficient is important that include the effect of the recognition range. Since the displacement probability of a particle can be modified by reflecting the recognition range, it could be incorporated with the iteration-based MLE method to have a better size estimation.

References

[1] Merkus, H.G., *Particle size measurements: fundamentals, practice, quality*. Particle Technology Series. 2009, New York: Springer. xii, 533 pp.

[2] Van Der Pol, E., et al., Refractive index determination of nanoparticles in suspension using nanoparticle tracking analysis. *Nano Letters*, 2014. **14**(11): p. 6195-6201.

[3] Akers, J.C., et al., Comparative analysis of technologies for quantifying extracellular vesicles (EVs) in clinical cerebrospinal fluids (CSF). *PloS one*, 2016. **11**(2): p. e0149866.

[4] Bartlett, T.R., et al., Bi2O3 Nanoparticle Clusters: Reversible Agglomeration Revealed by Imaging and Nano-Impact Experiments. *Chemistry–A European Journal*, 2016. **22**(22): p. 7408-7414.

[5] Mehn, D., et al., Larger or more? Nanoparticle characterisation methods for recognition of dimers. *RSC Advances*, 2017. **7**(44): p. 27747-27754.

[6] Lee, H., et al., Evaluation of concentration measurement techniques of colloidal nanoparticles for microfiltration and ultrafiltration applications: Inductively coupled plasma-mass spectrometry, nanoparticle tracking analysis and electrospray-scanning mobility particle sizer. *Separation and Purification Technology*, 2017. **184**: p. 34-42.

[7] de Temmerman, P.J., et al., Size measurement uncertainties of near-monodisperse, near-spherical nanoparticles using transmission electron microscopy and particle-tracking analysis. *Journal of Nanoparticle Research*, 2014. **16**(10): p. 17.

[8] Troiber, C., et al., Comparison of four different particle sizing methods for siRNA polyplex characterization. *European Journal of Pharmaceutics and Biopharmaceutics*, 2013. **84**(2): p. 255-264.

[9] Berne, B.J. and R. Pecora, *Dynamic light scattering: with applications to chemistry, biology, and physics*. Dover ed. 2000, Mineola, N.Y.: Dover Publications. vii, 376 pp.

[10] Maulucci, G., et al., Particle size distribution in DMPC vesicles solutions undergoing different sonication times. *Biophys J*, 2005. **88**(5): p. 3545-50.

[11] Fraunhofer, W., G. Winter, and C. Coester, Asymmetrical flow field-flow fractionation and multiangle light scattering for analysis of gelatin nanoparticle drug carrier systems. *Anal Chem*, 2004. **76**(7): p. 1909-20.

[12] Liu, J., J.D. Andya, and S.J. Shire, A critical review of analytical ultracentrifugation and field flow fractionation methods for measuring protein aggregation. *AAPS J*, 2006. **8**(3): p. E580-E589.

[13] Pecora, R. and S.R. Aragon, Theory of light scattering from hollow spheres. *Chem Phys Lipids*, 1974. **13**(1): p. 1-10.

[14] Hassan, P.A., S. Rana, and G. Verma, Making sense of Brownian motion: colloid characterization by dynamic light scattering. *Langmuir*, 2015. **31**(1): p. 3-12.

[15] Malloy, A. and B. Carr, NanoParticle tracking analysis - The Halo™ system. *Particle & Particle Systems Characterization*, 2006. **23**(2): p. 197-204.

[16] Sokolova, V., et al., Characterisation of exosomes derived from human cells by nanoparticle tracking analysis and scanning electron microscopy. *Colloids Surf B Biointerfaces*, 2011. **87**(1): p. 146-50.

[17] Anderson, W., et al., A comparative study of submicron particle sizing platforms: accuracy, precision and resolution analysis of polydisperse particle size distributions. *J Colloid Interface Sci*, 2013. **405**: p. 322-30.

[18] Bootz, A., et al., Comparison of scanning electron microscopy, dynamic light scattering and analytical ultracentrifugation for the sizing of poly(butyl cyanoacrylate) nanoparticles. *Eur J Pharm Biopharm*, 2004. **57**(2): p. 369-75.

[19] Striegel, A.M., Modern size-exclusion liquid chromatography : practice of gel permeation and gel filtration chromatography. 2nd ed. 2009: Hoboken, N.J.: Wiley.

[20] Yohannes, G., et al., Asymmetrical flow field-flow fractionation technique for separation and characterization of biopolymers and bioparticles. *J Chromatogr A*, 2011. **1218**(27): p. 4104-4116.

[21] Wyatt, P.J., Light scattering and the absolute characterization of macromolecules.

Anal Chim Acta, 1993. **272**(1): p. 1-40.

[22] Podzimek, S., Light scattering, size exclusion chromatography, and asymmetric flow field flow fractionation : powerful tools for the characterization of polymers, proteins, and nanoparticles. 2011: Hoboken, N.J.: Wiley.

[23] Stetefeld, J., S.A. McKenna, and T.R. Patel, Dynamic light scattering: a practical guide and applications in biomedical sciences. *Biophysical Reviews*, 2016. **8**(4): p. 409-427.

[24] Boyd, R.D., S.K. Pichaimuthu, and A. Cuenat, New approach to inter-technique comparisons for nanoparticle size measurements: using atomic force microscopy, nanoparticle tracking analysis and dynamic light scattering. *Colloids and Surfaces A: Physicochemical and Engineering Aspects*, 2011. **387**(1-3): p. 35-42.

[25] Hallett, F.R., J. Watton, and P. Krygsman, Vesicle sizing: Number distributions by dynamic light scattering. *Biophys J*, 1991. **59**(2): p. 357-362.

[26] Bell, N.C., et al., Emerging techniques for submicrometer particle sizing applied to Stober silica. *Langmuir*, 2012. **28**(29): p. 10860-72.

[27] Bayley, H. and C.R. Martin, Resistive-Pulse Sensing-From Microbes to Molecules. *Chem Rev*, 2000. **100**(7): p. 2575-2594.

[28] Amini, R., et al., Intertechnique comparisons for nanoparticle size measurements and shape distribution. *J Hazard Toxic Radioact Waste*, 2016. **20**(1): p. B4015004.

[29] Filipe, V., A. Hawe, and W. Jiskoot, Critical evaluation of nanoparticle tracking analysis (NTA) by NanoSight for the measurement of nanoparticles and protein aggregates. *Pharmaceutical Research*, 2010. **27**(5): p. 796-810.

[30] Ehara, K. and H. Sakurai, Metrology of airborne and liquid-borne nanoparticles: current status and future needs. *Metrologia*, 2010. **47**(2): p. S83-S90.

[31] Gollwitzer, C., et al., A comparison of techniques for size measurement of nanoparticles in cell culture medium. *Analytical Methods*, 2016. **8**(26): p. 5272-5282.

[32] Pecora, R., Dynamic light scattering: applications of photon correlation spectroscopy. 2013: Springer Science & Business Media.

[33] Szoka Jr, F. and D. Papahadjopoulos, Comparative properties and methods of preparation of lipid vesicles (liposomes). *Annual review of biophysics and bioengineering*, 1980. **9**(1): p. 467-508.

[34] Liu, Y., et al., A supramolecular Janus hyperbranched polymer and its photoresponsive self-assembly of vesicles with narrow size distribution. *Journal of the American Chemical Society*, 2013. **135**(12): p. 4765-4770.

[35] Hammouda, B., SANS from polymers—review of the recent literature. *Journal of Macromolecular Science®, Part C: Polymer Reviews*, 2010. **50**(1): p. 14-39.

[36] van der Pol, E., et al., Innovation in detection of microparticles and exosomes. *J Thromb Haemost*, 2013. **11 Suppl 1**: p. 36-45.

[37] Chernyshev, V.S., et al., Size and shape characterization of hydrated and desiccated exosomes. *Analytical and bioanalytical chemistry*, 2015. **407**(12): p. 3285-3301.

[38] Böing, A.N., et al., Single-step isolation of extracellular vesicles by size-exclusion chromatography. *Journal of extracellular vesicles*, 2014. **3**(1): p. 23430.

[39] Dragovic, R.A., et al., Sizing and phenotyping of cellular vesicles using nanoparticle tracking analysis. *Nanomedicine*, 2011. **7**(6): p. 780-8.

[40] Grabarek, A.D., et al., Critical Evaluation of Microfluidic Resistive Pulse Sensing for Quantification and Sizing of Nanometer-and Micrometer-Sized Particles in Biopharmaceutical Products. *Journal of pharmaceutical sciences*, 2019. **108**(1): p. 563-573.

[41] Steppert, P., et al., Quantification and characterization of virus-like particles by size-exclusion chromatography and nanoparticle tracking analysis. *Journal of Chromatography A*, 2017. **1487**: p. 89-99.

[42] Shang, J. and X. Gao, Nanoparticle counting: towards accurate determination of the molar concentration. *Chem Soc Rev*, 2014. **43**(21): p. 7267-78.

[43] Van der Pol, E., et al., Particle size distribution of exosomes and microvesicles determined by transmission electron microscopy, flow cytometry, nanoparticle tracking analysis, and resistive pulse sensing. *Journal of Thrombosis and Haemostasis*, 2014. **12**(7): p. 1182-1192.

[44] Saveyn, H., et al., Accurate particle size distribution determination by nanoparticle tracking analysis based on 2-D Brownian dynamics simulation. *Journal of Colloid and Interface Science*, 2010. **352**(2): p. 593-600.

[45] *Particle size analysis: Dynamic light scattering (DLS)*, in *ISO 22412:2017*. 2017, International Standard Organization: Geneva, Switzerland.

[46] Koppel, D.E., Analysis of macromolecular polydispersity in intensity correlation spectroscopy: the method of cumulants. *J Chem Phys*, 1972. **57**(11): p. 4814-4820.

[47] Pencer, J. and F.R. Hallett, Effects of vesicle size and shape on static and dynamic light scattering measurements. *Langmuir*, 2003. **19**(18): p. 7488-7497.

[48] Bob Carr, P.H., Andrew Malloy, Philip Nelson, Matthew Wright, Jonathan Smith, Applications of nanoparticle tracking analysis in nanoparticle research - a mini-review. *European Journal of Parenteral & Pharmaceutical Sciences*, 2009. **14**: p. 35-40.

[49] Van Der Meeren, P., M. Kasinos, and H. Saveyn, Relevance of two-dimensional brownian motion dynamics in applying nanoparticle tracking analysis, in Methods in Molecular Biology. 2012. p. 525-534.

[50] Walker, J.G., Improved nano-particle tracking analysis. *Measurement Science and Technology*, 2012. **23**(6): p. 065605.

[51] Zhou, C., et al., Characterization of Nanoparticle Tracking Analysis for Quantification and Sizing of Submicron Particles of Therapeutic Proteins. *Journal of Pharmaceutical Sciences*, 2015. **104**(8): p. 2441-2450.

[52] Hole, P., et al., Interlaboratory comparison of size measurements on nanoparticles using nanoparticle tracking analysis (NTA). *Journal of Nanoparticle Research*, 2013. **15**: p. 2101.

[53] Maguire, C.M., et al., Benchmark of Nanoparticle Tracking Analysis on Measuring Nanoparticle Sizing and Concentration. *Journal of Micro and Nano-Manufacturing*, 2017. **5**(4): p. 10.

[54] Lawler, D.F., et al., Comprehensive understanding of nano-sized particle separation processes using nanoparticle tracking analysis. *Water Science and Technology*, 2015. **72**(12): p. 2318-2324.

[55] Hou, J., et al., Nanoparticle tracking analysis versus dynamic light scattering: Case study on the effect of Ca2+ and alginate on the aggregation of cerium oxide nanoparticles. *Journal of hazardous materials*, 2018. **360**: p. 319-328.

[56] Wang, C., et al., Quantitative measurement of aggregation kinetics process of nanoparticles using nanoparticle tracking analysis and dynamic light scattering. *Journal of Nanoparticle Research*, 2019. **21**(5): p. 87.

[57] McComiskey, K.P. and L. Tajber, Comparison of particle size methodology and

assessment of nanoparticle tracking analysis (NTA) as a tool for live monitoring of crystallisation pathways. *European Journal of Pharmaceutics and Biopharmaceutics*, 2018. **130**: p. 314-326.

[58] Terejánszky, P., et al., Resistive Pulse Sensing as a High-Resolution Nanoparticle Sizing Method: A Comparative Study. *Particle & Particle Systems Characterization*, 2019: p. 1800543.

[59] Enjeti, A.K., et al., Correlative analysis of nanoparticle tracking, flow cytometric and functional measurements for circulating microvesicles in normal subjects. *Thrombosis research*, 2016. **145**: p. 18-23.

[60] Chan, M.Y., et al., Particle sizing of nanoparticle adjuvant formulations by dynamic light scattering (DLS) and nanoparticle tracking analysis (NTA), in Vaccine Adjuvants. 2017, Springer. p. 239-252.

[61] Arancon, R.A.D., et al., Nanoparticle tracking analysis of gold nanomaterials stabilized by various capping agents. *RSC Advances*, 2014. **4**(33): p. 17114-17119.

[62] Tatischeff, I., et al., Fast characterisation of cell-derived extracellular vesicles by nanoparticles tracking analysis, cryo-electron microscopy, and Raman tweezers microspectroscopy. *Journal of extracellular vesicles*, 2012. **1**(1): p. 19179.

[63] Kestens, V., et al., Validation of a particle tracking analysis method for the size determination of nano- and microparticles. *Journal of Nanoparticle Research*, 2017. **19**(8): p. 271.

[64] Hannon, J.C., et al., Human exposure assessment of silver and copper migrating from an antimicrobial nanocoated packaging material into an acidic food simulant. *Food and Chemical Toxicology*, 2016. **95**: p. 128-136.

[65] Varga, Z., et al., Hollow organosilica beads as reference particles for optical detection of extracellular vesicles. *Journal of Thrombosis and Haemostasis*, 2018. **16**(8): p. 1646-1655.

[66] Gross, J., et al., Nanoparticle tracking analysis of particle size and concentration detection in suspensions of polymer and protein samples: Influence of experimental and data evaluation parameters. *European Journal of Pharmaceutics and Biopharmaceutics*, 2016. **104**: p. 30-41.

[67] Yang, D.T., et al., Evaluation of Nanoparticle Tracking for Characterization of

Fibrillar Protein Aggregates. *AIChE J*, 2014. **60**(4): p. 1236-1244.

[68] Roding, M., et al., Measuring absolute nanoparticle number concentrations from particle count time series. *J Microsc*, 2013. **251**(1): p. 19-26.

[69] Vestad, B., et al., Size and concentration analyses of extracellular vesicles by nanoparticle tracking analysis: a variation study. *J Extracell Vesicles*, 2017. **6**(1): p. 1344087.

[70] Gallego-Urrea, J.A., J. Tuoriniemi, and M. Hassellöv, Applications of particle-tracking analysis to the determination of size distributions and concentrations of nanoparticles in environmental, biological and food samples. *TrAC - Trends in Analytical Chemistry*, 2011. **30**(3): p. 473-483.

[71] Sauvain, J.J., et al., Method validation of nanoparticle tracking analysis to measure pulmonary nanoparticle content: the size distribution in exhaled breath condensate depends on occupational exposure. *J Breath Res*, 2017. **11**(1): p. 016010.

[72] Vasudev, R., S. Mathew, and N. Afonina, Characterization of submicron (0.1-1 μm) particles in therapeutic proteins by nanoparticle tracking analysis. *Journal of Pharmaceutical Sciences*, 2015. **104**(5): p. 1622-1631.

[73] McNicholas, K. and M.Z. Michael, Immuno-characterization of exosomes using nanoparticle tracking analysis, in Exosomes and Microvesicles. 2017, Springer. p. 35-42.

[74] Baldwin, S., et al., Analyzing the miRNA content of extracellular vesicles by fluorescence nanoparticle tracking. *Nanomedicine: Nanotechnology, Biology and Medicine*, 2017. **13**(2): p. 765-770.

[75] Livshits, M.A., et al., Isolation of exosomes by differential centrifugation: theoretical analysis of a commonly used protocol. *Scientific Reports*, 2015. **5**: p. 17319.

[76] Kashid, S.B., R.D. Tak, and R.W. Raut, Antibody tagged gold nanoparticles as scattering probes for the pico molar detection of the proteins in blood serum using nanoparticle tracking analyzer. *Colloids and Surfaces B: Biointerfaces*, 2015. **133**: p. 208-213.

Chapter 3

Experimental Methodology

The materials and their preparation and instrumental settings are described in this chapter. For the evaluation of size measurement techniques, polystyrene latex nanoparticles and 1-palmitoyl-2-oleoyl-sn-glycero-3-phosphocholine vesicle samples were chosen as reference samples for monodisperse and polydisperse samples, respectively. The principles and protocols of the size measurement techniques evaluated in this study, that is, Dynamic Light Scattering (DLS) and Nanoparticle Tracking Analysis (NTA), are designed, followed by the methodology for a computer simulation to theoretically evaluate NTA. A conversion theory from a number-weighted size distribution of NTA to an intensity-weighted size distribution of DLS is introduced and used for the comparison of the results acquired from the two techniques.

3.1 Rationale for selection

Size measurement on nanoparticles in suspension can be achieved in many ways. Among those techniques, DLS has been widely used due to its quick data acquisition [1, 2]. On the other hand, DLS is also well known for its intensity-weighted size information, which often leads to results biased toward a larger size for polydisperse samples.

Most nanometer sized particles originating from biological entities does not have a uniform size but takes a polydisperse size distribution [3-9]. Due to the polydisperse nature of those biologically originated particles, DLS is not a proper tool to measure the size of those samples. Although many researchers have known the drawback of DLS in size characterization, the technique has been widely employed to measure the size of those polydisperse particles due to its simple and quick measurement process [2, 10]. Reviews on DLS also point out the drawback and recommend having a comparative measurement by another technique to complement the information [1]. In this study, NTA was chosen for a comparative technique to DLS. For the comparison, two types of samples were employed: one is PS latex nanoparticle standards and the other is lipid vesicle samples prepared in various conditions.

In comparing the two techniques, NTA sometimes produced a bigger mean size compared to DLS on the same samples. Since the recognition range set for tracking particles in NTA effectively limits the probable displacement of particles up to the recognition range, it is probable that the acquired tracks have a smaller squared average displacement, which translates into a larger particle size. To verify the influence of the recognition radius, a computer simulation was used to produce virtual particle movements and acquire particle tracks from the movements. During the tracking process, a variable recognition radius was applied to recognize particle tracks.

In analyzing acquired tracks from NTA tracking, three different methodologies were compared. One is a direct conversion method, which is a simple inversion of the acquired average squared displacement according to the Stokes-Einstein equation [11, 12]. The other

two relies on the maximum likelihood estimation principle, while the maximization strategy is different from each other [13, 14].

To verify the theoretical findings from the simulations, NIST-traceable PS latex nanoparticle standards were measured by NTA.

3.2 Materials

3.2.1. PS latex nanoparticle standards

Polystyrene (PS) latex nanoparticles are known as an adequate standards as they are spherical in shape and monodisperse in the size distribution, which is good for calibration of size and validation of size resolution [15, 16].

For the comparison of DLS and NTA, polystyrene (PS) latex standards were purchased from Thermo Scientific (Rockford, IL., USA), whose particle size is 92 ± 3, 269 ± 7 and 343 ± 9 nm. The standards were measured with DLS and NTA without dilution.

For the verification of the influence of the recognition radius in NTA, two aliquots of NIST-traceable concentrated (~10wt%) polystyrene latex microspheres (51.6 ± 3 nm and 181.6 ± 9 nm) in liquid suspension were obtained from Colloidal Metrics Corporation (Mountain View, CA). These microspheres were diluted into 0.1-µm-filtered 10 mM KCl (potassium chloride) until the NanoSight gave a concentration of 1×10^9 particles/ml for each sample. These suspensions were then further diluted 1:10 into 0.1-µm-filtered 10 mM KCl to give a measured concentration of 1×10^8 particles/ml.

3.2.2. POPC vesicle

As polydisperse samples for DLS and NTA comparison, 1-palmitoyl-2-oleoyl-sn-glycero-3-phosphocholine (POPC) was purchased from Avanti Polar Lipids Inc., (Alabaster, AL, USA). Vesicles composed of POPC (Avanti Polar Lipids Inc., Alabaster, AL) were

prepared at a lipid concentration of ~5 mg/mL and then diluted before the experiment. Briefly, dried lipid films were hydrated with 10 mM Tris (pH 7.5) buffer solution with 150 mM NaCl, and the sample was then vortexed periodically for 5 min. Vesicle samples were extruded through polycarbonate membranes with either 50, 100, 200 or 400 nm pores sized by a miniextruder (Avanti Polar Lipids). For those samples pretreated with a range of freeze-thaw cycles, freeze-thaw treatment was performed before extrusion on newly hydrated lipid films by using a previously described methodology based on freeze-thaw pretreatment and then extrusion [17]. Specifically, in each treatment cycle, the vesicle suspension was frozen in liquid nitrogen for 30 s, before thawing in an 80 °C water bath for 90 s, and then finally being vortexed to complete each cycle. After the freeze-thaw cycles of 3, 5, 7, 9, 11, 13, 15 or 17 repetitions, vesicles were sized by an extruder (Avanti Polar Lipids) through 400 nm polycarbonate membrane pores. All aqueous solutions and buffers were prepared in Milli-Q water with a minimum resistivity of 18.2 MΩ·cm (Millipore, Billerica, MA).

3.3 Experimental Techniques

3.3.1. Dynamic Light Scattering

DLS extracts the size distribution of particles in suspension from their Brownian motion, whose displacement is related to their diffusion coefficient [1, 18, 19]. The intensity of the light scattered by particles in suspension upon laser illumination changes due to the particles' Brownian motion, and the intensity fluctuation is processed to acquire its auto-correlation function whereby the decay time is related to the particles' diffusion coefficient as described in Eq. 2.1.

For monodisperse spherical particles, the hydrodynamic radius R_h can be related to the diffusion coefficient using the Stokes-Einstein equation in Eq. 2.2.

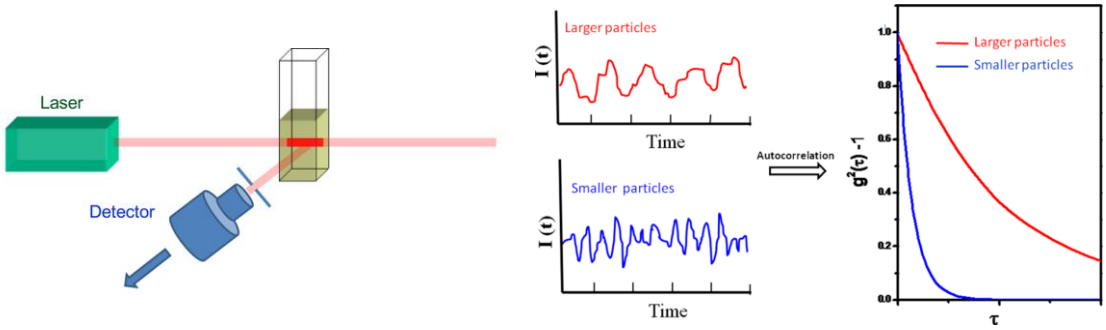

Figure 3.1 Schematic representation of Dynamic Light Scattering. Particles in suspension are illuminated by a laser, where the scattered light from the particles are monitored by the detector. The detected light intensity over time oscillates due to the Brownian motion of the particles, whose auto-correlation curve shows the diffusion coefficient of the particles, and hence the particle size.

For polydisperse samples, the auto-correlation function can be expressed as an integral form as described in Eq. 2.3.

Although a Laplace inversion of the integration produces the size distribution $G(\Gamma)$, it is well known that the inversion is not a well-conditioned problem [1, 18, 20]. Many strategies have been suggested to recover the size distribution from the integration, among which the cumulant analysis method is only method recommended by the International Standards Organization [15].

The cumulant analysis method is applied for relatively narrow polydisperse samples [21]. The mean $\bar{\Gamma}$ and the variance μ_2 of the distribution $G(\Gamma)$ are acquired from the expansion of the logarithm of the auto-correlation function as

$$\ln\left(g^1(\tau)\right) = \ln B - \bar{\Gamma}\tau + \frac{\mu_2}{2!}\tau^2 - \frac{\mu_3}{3!}\tau^3 + \cdots \quad (3.1)$$

where

$$\bar{\Gamma} = \int G(\Gamma)d\Gamma \quad (3.2)$$

$$\mu_2 = \int G(\Gamma)(\Gamma - \bar{\Gamma})^2 d\Gamma \quad (3.3)$$

$$\mu_3 = \int G(\Gamma)(\Gamma - \bar{\Gamma})^3 d\Gamma \quad (3.4)$$

By fitting $\ln\left(g^1(\tau)\right)$, $\bar{\Gamma}$ and μ_2 can be acquired, and then converted to the mean size R_Z and the polydipersity index PI as summarized in Eqs. 2.13 and 2.14.

Although valid for polydisperse samples that meet the criterion $\mu_2\tau^2 \ll 1$ [1, 21], in this study, the cumulant method was applied to both PS latex nanoparticle samples and vesicle samples for the comparison with NTA.

Experimental Protocol

For the DLS measurements, a ZetaPals particle size analyzer (Brookhaven Instruments, Holtsville, NY) with a 658.0 nm monochromatic laser was used. For each sample, three independent runs of 1 min were performed. To avoid unnecessary reflection, all measurements were taken at a scattering angle of 90°, and the measured intensity autocorrelation function was fitted to yield the intensity-weighted size distribution of particles in solution. The deconvolution of the autocorrelation function was done using the cumulants method, which was applied to calculate the intensity-weighted log-normal profile of the size distribution expressed by the average effective diameter and its polydispersity.

3.3.2 Nanoparticle Tracking Analysis

Similar to DLS, NTA extracts the size information of particles in suspension by measuring their diffusion coefficient [11]. As illustrated in Figure 3.2, by taking sequential images of illuminated particles in suspension on a periodic time interval, the displacement of a particle can be identified from successive images and constructed into a track. To determine the displacement of particles, NTA compares the two-dimensional location of particles in an image frame with the subsequent frame. In doing so, NTA sets a certain threshold distance, also known as the maximum jump distance, to properly identify if the two particles in the two adjacent frames are the same particle. If any single particle is found in the successive frame within the threshold distance from the location of the particle in the previous image, the two particles are recognized as the same particle and make a track segment. In the same manner, this recognition process is performed for subsequent frames

and track segments are combined to construct a particle's track. The track terminates if there is no particle in the following frame or if there are more than two particles within the threshold distance. Because of the nature of the tracking process, the track segment length, and the number of track segments, are finite and variable.

For a track of a track segment length n, the mean squared displacement of the track z, expressed as

$$z = \frac{1}{n}\sum_{i=1}^{n} r_i^2 \quad (3.5)$$

where r_i is the two-dimensional displacement of ith track segment of the track, is translated into the diffusion coefficient assuming a 2D Brownian motion, which is related by

$$z = 4D\Delta t \quad (3.6)$$

where D is the diffusion coefficient of the tracked particle and Δt is the time interval of the image frames [11-14]. Then the acquired diffusion coefficient D of the track is converted to the hydrodynamic diameter relying on the Stokes-Einstein equation.

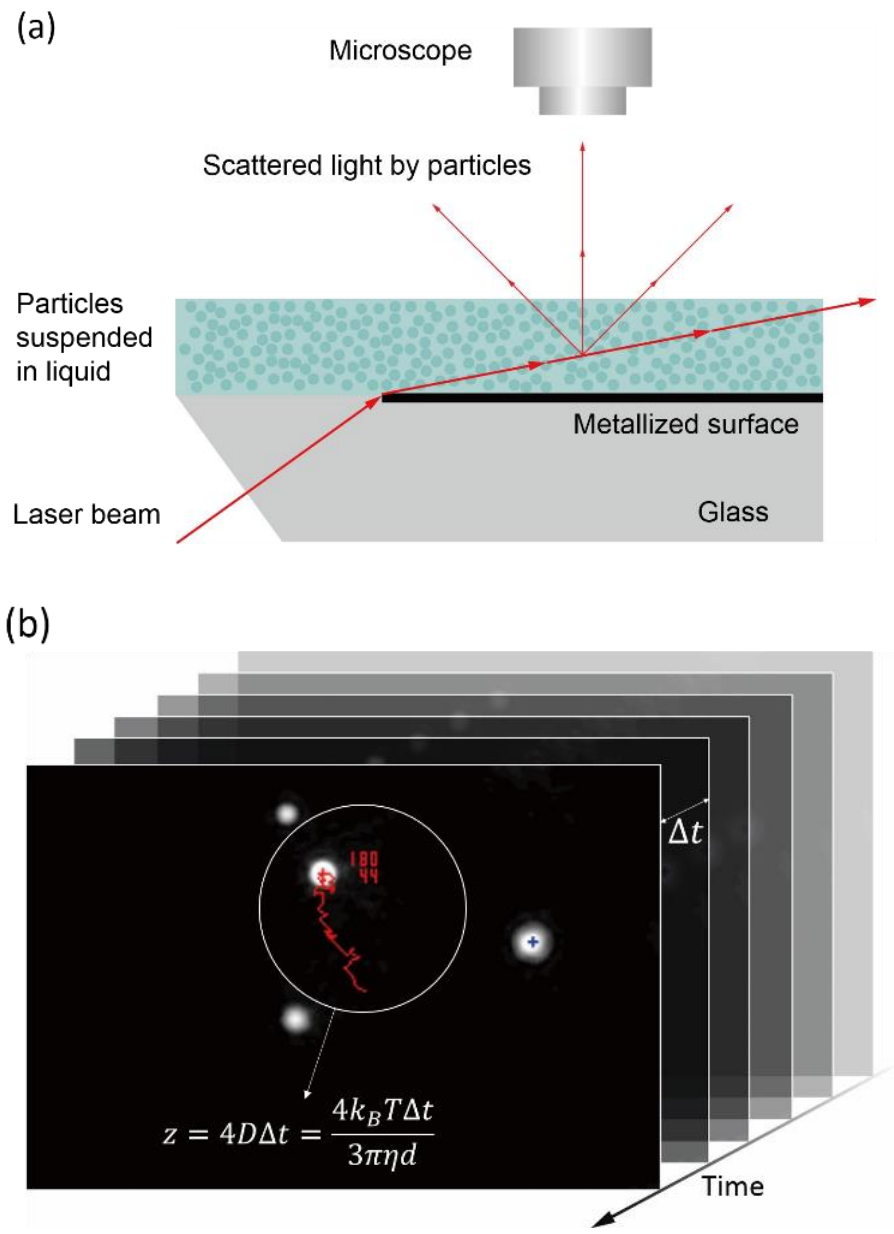

Figure 3.2 (a) Instrumental schematics of NTA detection. The particles suspended in liquid are illuminated by laser beam. Scattered light by the particles is monitored by the microscope, from which the position of the particles is identified by the software. (b) The software tracks the trajectory of the particles and constructs particle tracks. The average squared displacement z of each track is then converted into the corresponding hydrodynamic diameter d according to the Stokes-Einstein equation.

Experimental Protocol

For the comparative study with DLS, NTA measurements were made with an LM10HS (Nanosight Limited, Amesbury, UK) equipped with a scientific CMOS camera, a 20x objective lens, a blue laser module (405 nm, LM12 version C) and NTA software version 3.1. A 1-ml disposable syringe was used to inject the samples into the instrument chamber. The video data for NTA measurements were collected for 30 seconds, repeated three times for each sample. The detection threshold of the NTA software was set to 5 and the maximum jump distance and the minimum track segment length were both set to auto.

Detected tracks were then translated into a size distribution using three different methods, i.e., direct conversion of the detected particle tracks, maximum likelihood estimation with an assumed distribution (the FTLA method) and maximum likelihood estimation by iterative correction. For the conversion, valid tracks were acquired from the detected tracks by the software, with small track segments excluded from the selection.

For the study on the effect of the recognition radius on NTA measurements, the instrument used for the analysis was the Malvern NanoSight LM10 (Amesbury, UK) equipped with a 20× objective, a 405 nm 50 mW laser and a Scientific CMOS detector and software version NTA 2.3 Beta 7. A syringe pump was utilized to flow the samples through the laser viewing module at a rate of 5 ± 2 μm/s. The video data for the NTA measurements were collected for 60 seconds, which was repeated three times for each sample. Acquired video data was processed by the NTA software version 3.1.46 to acquire tracks. During the process, the detection threshold was set to an optimal value depending on the nominal particle size and the concentration, while the value was used for the three runs of each sample condition. The recognition radius, or the max jump distance in the NTA software, varied from 6 to 30 pixels, corresponding to a range of 1.1 to 5.4 μm. The recognized tracks produced by the NTA software were used for the determination of the particle size distribution.

3.4 Simulation

To test the conventional and modified displacement probabilities for the size distribution determination by NTA, Brownian motion of particles were simulated and tracked according to the NTA detection principle by Python 2.7 along with the NumPy package. For the particle placements and movements, a three-dimensional space was created with its width and height corresponding to the field-of-view of the CMOS camera, i.e., 640 and 480 pixels, respectively, with the pixel size set to 179 nm, and the depth to the focal depth of the objective lens, i.e. 7.16 μm [22, 23]. To allow fluctuations in the number of particles detected within the field-of-view over time, an additional space that extends in each of the three dimensions was given. The extension in each direction was six times the diffusion length of the mean particle size of the simulations or at least 2 μm, and the boundary of the space was made periodic in each direction [24].

The number of generated particles was determined by the volume of the created space and the nominal particle concentration. For instance, the average number of particles observed in a frame is about 70 when the concentration is set to 1×10^9 particles/ml. The initial position of the generated particles was given randomly in the three-dimensional space, and the movement of each particle in each direction at the subsequent frames was randomly generated to follow a normal distribution with a standard deviation of $\sqrt{2D_i\Delta t}$ [25], where D_i is the diffusion coefficient of the ith particle and Δt is the time interval between the frames set as 30.74 milliseconds. The time duration of each simulation was 60 seconds, corresponding to 1952 frames including the initial frame. The simulation did not consider either the effect of measurement errors in determining the position of the particles or the drift in the solution [14].

For the recognition of tracks, the position of a particle generated by the simulation in one frame is evaluated with the position of the particles in the following frame. If the distance to the nearest particle in the following frame is less than an arbitrary chosen recognition radius, the particle in the following frame is considered as the same particle in the previous frame and becomes a segment of the constructed track [26]. If either the distance to the

nearest particle is larger than the recognition radius or the distance to the second nearest particle is less than the recognition radius, the particle in the previous frame is regarded as not present in the following frame, resulting in a termination of the track. Since this process evaluates only the distance for the track recognition, two different particles can be recognized as the same particle to produce an abnormal track [27].

3.5 Size Distribution Determination Methods for NTA

NTA determines the size of tracked particles from their diffusion coefficient acquired from the average squared displacements of the tracks. A simple method to obtain the particle size distribution from the acquired tracks is to form a histogram of the particle sizes by directly converting the average squared displacements of the tracks using Eq. 2.17 [11-14, 26]. However, the determined particle size by the direct conversion has an inherent stochastic uncertainty due to the nature of Brownian motion, which necessitates particles to be tracked over many frames to reduce the uncertainty which depends on the track length [13, 14, 28]. Since the availability of tracks of long length depends on the measurement conditions, an accurate size determination by direct conversion is not always achievable even for very monodisperse samples [13, 14, 26, 29].

To minimize the influence of the uncertainty in determining the size distribution, other approaches based on the maximum likelihood estimation (MLE) principle have been suggested that find a size distribution that maximizes the likelihood of the obtained tracks [13, 14]. In this study, two strategies based on the MLE principle were tested. One is to assume an arbitrary size distribution defined by a few parameters and try to optimize the parameters that maximize the likelihood of the size distribution with respect to the acquired tracks. The other is to employ an iterative approach that refines the size distribution to have a larger likelihood over each iteration.

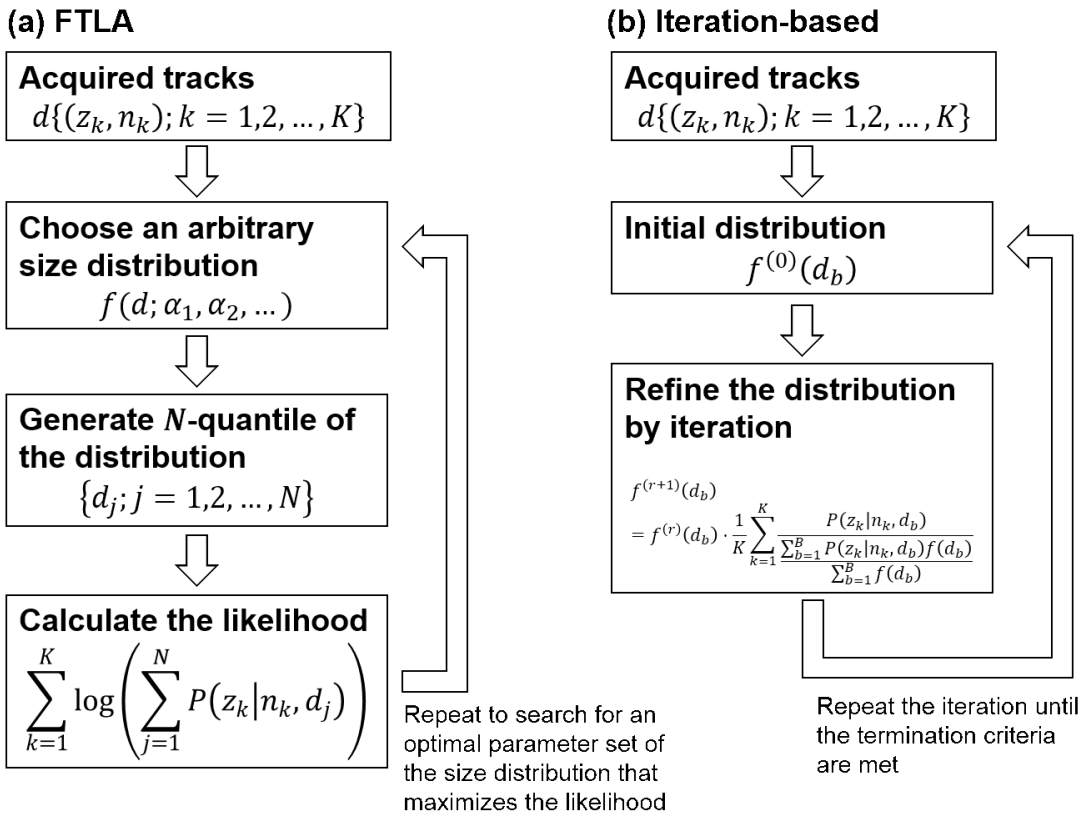

Figure 3.3 The process flow of the size determination methods based on maximum likelihood estimation. (a) By assuming a size distribution described by adjustable parameters, the FTLA method looks for the parameter values that maximize the likelihood of the given NTA tracks. (b) The iterative correction method refines the size distribution that approaches to the maximum likelihood over each iteration.

Maximum Likelihood Estimation with an Assumed Arbitrary Distribution with Parameters

As particles observed by NTA undergo Brownian motion, the probability distribution of the mean squared displacement z of a tracked particle whose size is d with a track segment length n can be described by a gamma distribution as follows [14]:

$$P(z|n,d) = \frac{(ns)^n}{(n-1)!} z^{n-1} e^{-nsz} \quad (3.7)$$

where s is defined as $1/4D\Delta t = 3\pi\eta d/4\Delta t k_B T$. An observed set of tracks Φ of a sample measured by NTA can be related to a particle size distribution $f(d)$ by the integration

$$\Phi = \int_0^\infty f(x) P(z|n,x) dx \quad (3.8)$$

Although the inversion of the integration would enable recovery of $f(d)$ by finding $Q(d|n,z)$ that satisfies

$$f(d) = \sum_{\Phi} \Phi \cdot Q(d|n,z) \quad (3.9)$$

the inversion relation cannot be used because $Q(d|n,z)$ depends on $f(d)$ [30].

Due to the difficulty of finding Q for the inversion, finite track length adjustment (FTLA) can be used to determine $f(d)$ by maximizing the likelihood of the observed list of tracks Φ with an assumed size distribution for $f(d)$ as illustrated in Figure 7 [13]. For an assumed size distribution with a few parameters, for example a log-normal distribution with its geometric mean and geometric standard deviation set as parameters, an "ideal" set of particles d_i (with j = 1–999) is drawn, which comprises 1000-quantiles of the size distribution, i.e., those of particle size d_i that satisfy $C(d_j) = j/1000$ (j = 1–999) for the cumulative size distribution $C(d)$ of $f(d)$. For each particle size d_j, the likelihood of producing a track whose mean squared displacement z and track segment length n is given by

$$L(z,n;d_j) = P(z|n,d_j) \quad (3.10)$$

Hence, the likelihood of producing such a track with a given particle set d_j (j = 1–999) is given as

$$L(z, n; \{d\}) = \sum_{j=1}^{999} P\left(z \middle| n, d_j\right) \quad (3.11)$$

Likewise, the likelihood for all the observed list of tracks Φ becomes

$$L(\Phi; \{d\}) = \prod_{k=1}^{K} \left(\sum_{j=1}^{999} P\left(z_k \middle| n_k, d_j\right) \right) \quad (3.12)$$

where z_k and n_k are the mean squared displacement and the track segment length of the kth track of Φ, respectively, and K is the total number of the observed tracks. For practical reasons, the maximization is performed on the logarithm of the likelihood, as maximizing a positive function also maximizes its logarithm [14]:

$$LL(\Phi; \{d\}) = \log(L) = \sum_{k=1}^{K} \log \left(\sum_{j=1}^{999} P\left(z_k \middle| n_k, d_j\right) \right) \quad (3.13)$$

With the log-likelihood, an optimal parameter set for the size distribution is sought for its maximum value, which determines the size distribution for the observed tracks. As this approach assumes an arbitrary size distribution, a decrease in the likelihood can be expected for the benefit of a simpler solution [30].

Maximum Likelihood Estimation by Iterative Correction

For a size distribution $f(d)$, the log-likelihood of producing the observed list of tracks Φ can be expressed as

$$LL(\Phi) = \sum_{k=1}^{K} \log \left(\frac{1}{\sum_{b=1}^{B} f(d_b)} \sum_{b=1}^{B} P(z_k | n_k, d_b) f(d_b) \right) \quad (3.14)$$

where b is the bin number for the segmented range of particle size d [14].

Then its differentiation with respect to the size distribution is given as

$$\frac{\partial LL}{\partial f} = \sum_{k=1}^{K} \frac{P(z_k|n_k, d_b)}{\sum_{b=1}^{B} P(z_k|n_k, d_b) f(d_b)} - \frac{K}{\sum_{b=1}^{B} f(d_b)} \quad (3.15)$$

At the maximum of the likelihood, the differential becomes zero, leading to

$$\sum_{k=1}^{K} \frac{P(z_k|n_k, d_b)}{\sum_{b=1}^{B} P(z_k|n_k, d_b) f(d_b)} = \frac{K}{\sum_{b=1}^{B} f(d_b)} \quad (3.16)$$

From this relation, it is possible to find the size distribution by an iterative procedure, given as

$$f^{(r+1)}(d_b) = f^{(r)}(d_b) \cdot \frac{1}{K} \sum_{k=1}^{K} \frac{P(z_k|n_k, d_b)}{\sum_{b=1}^{B} P(z_k|n_k, d_b) f(d_b) / \sum_{b=1}^{B} f(d_b)} \quad (3.17)$$

where $f^{(r)}(d)$ is the rth estimate of the size distribution from the iterations as illustrated in Figure 7 [30]. For the initial size distribution $f^{(0)}(d)$, a uniform distribution is chosen [14, 31, 32].

For the termination criteria of the iteration, the chi-squared statistic of the error between a histogram of the mean squared displacement H_z and that calculated from the rth iteration solution $H^{(r)}$ can be used, where

$$\chi^2 = \sum_{m=1}^{M} \frac{\left(H_z(z_m) - H^{(r)}(z_m)\right)^2}{H^{(r)}(z_m)} \quad (3.18)$$

$$H^{(r)}(z_m) = \sum_{n=N_{min}}^{N_{max}} N_n \sum_{b=1}^{B} \frac{P(z_m|n, d_b) f^{(r)}(d_b) \Delta z_m}{\sum_{b=1}^{B} f^{(r)}(d_b)} \quad (3.19)$$

where m is the bin number for the mean squared displacement and N_n is the number of tracks with track segment length n, and in this study the iteration terminates when the change in χ^2 becomes smaller than 1% of the previous value [14].

References

[1] Hassan, P.A., S. Rana, and G. Verma, Making sense of Brownian motion: colloid characterization by dynamic light scattering. *Langmuir*, 2015. **31**(1): p. 3-12.

[2] Pecora, R., Dynamic light scattering: applications of photon correlation spectroscopy. 2013: Springer Science & Business Media.

[3] Vestad, B., et al., Size and concentration analyses of extracellular vesicles by nanoparticle tracking analysis: a variation study. *J Extracell Vesicles*, 2017. **6**(1): p. 1344087.

[4] Gross, J., et al., Nanoparticle tracking analysis of particle size and concentration detection in suspensions of polymer and protein samples: Influence of experimental and data evaluation parameters. *European Journal of Pharmaceutics and Biopharmaceutics*, 2016. **104**: p. 30-41.

[5] Vasudev, R., S. Mathew, and N. Afonina, Characterization of submicron (0.1-1 μm) particles in therapeutic proteins by nanoparticle tracking analysis. *Journal of Pharmaceutical Sciences*, 2015. **104**(5): p. 1622-1631.

[6] Sediq, A.S., et al., Protein–polyelectrolyte interactions: Monitoring particle formation and growth by nanoparticle tracking analysis and flow imaging microscopy. *European Journal of Pharmaceutics and Biopharmaceutics*, 2015. **93**: p. 339-345.

[7] McNicholas, K. and M.Z. Michael, Immuno-characterization of exosomes using nanoparticle tracking analysis, in Exosomes and Microvesicles. 2017, Springer. p. 35-42.

[8] Baldwin, S., et al., Analyzing the miRNA content of extracellular vesicles by fluorescence nanoparticle tracking. *Nanomedicine: Nanotechnology, Biology and Medicine*, 2017. **13**(2): p. 765-770.

[9] Livshits, M.A., et al., Isolation of exosomes by differential centrifugation: theoretical analysis of a commonly used protocol. *Scientific Reports*, 2015. **5**: p. 17319.

[10] Weinbuch, D., et al., Nanoparticulate impurities in pharmaceutical-grade sugars and their interference with light scattering-based analysis of protein formulations. *Pharmaceutical research*, 2015. **32**(7): p. 2419-2427.

[11] Malloy, A. and B. Carr, NanoParticle tracking analysis - The Halo™ system.

Particle & Particle Systems Characterization, 2006. **23**(2): p. 197-204.

[12] Filipe, V., A. Hawe, and W. Jiskoot, Critical evaluation of nanoparticle tracking analysis (NTA) by NanoSight for the measurement of nanoparticles and protein aggregates. *Pharmaceutical Research*, 2010. **27**(5): p. 796-810.

[13] Saveyn, H., et al., Accurate particle size distribution determination by nanoparticle tracking analysis based on 2-D Brownian dynamics simulation. *Journal of Colloid and Interface Science*, 2010. **352**(2): p. 593-600.

[14] Walker, J.G., Improved nano-particle tracking analysis. *Measurement Science and Technology*, 2012. **23**(6): p. 065605.

[15] *Particle size analysis: Dynamic light scattering (DLS)*, in *ISO 22412:2017*. 2017, International Standard Organization: Geneva, Switzerland.

[16] Ehara, K. and H. Sakurai, Metrology of airborne and liquid-borne nanoparticles: current status and future needs. *Metrologia*, 2010. **47**(2): p. S83-S90.

[17] Mayer, L.D., et al., Solute distributions and trapping efficiencies observed in freeze-thawed multilamellar vesicles. *Biochim Biophys Acta*, 1985. **817**(1): p. 193-6.

[18] Berne, B.J. and R. Pecora, *Dynamic light scattering: with applications to chemistry, biology, and physics*. Dover ed. 2000, Mineola, N.Y.: Dover Publications. vii, 376 pp.

[19] Stetefeld, J., S.A. McKenna, and T.R. Patel, Dynamic light scattering: a practical guide and applications in biomedical sciences. *Biophysical Reviews*, 2016. **8**(4): p. 409-427.

[20] Merkus, H.G., *Particle size measurements: fundamentals, practice, quality*. Particle Technology Series. 2009, New York: Springer. xii, 533 pp.

[21] Koppel, D.E., Analysis of macromolecular polydispersity in intensity correlation spectroscopy: the method of cumulants. *J Chem Phys*, 1972. **57**(11): p. 4814-4820.

[22] Zhou, C., et al., Characterization of Nanoparticle Tracking Analysis for Quantification and Sizing of Submicron Particles of Therapeutic Proteins. *Journal of Pharmaceutical Sciences*, 2015. **104**(8): p. 2441-2450.

[23] Hole, P., et al., Interlaboratory comparison of size measurements on nanoparticles using nanoparticle tracking analysis (NTA). *Journal of Nanoparticle Research*, 2013. **15**: p. 2101.

[24] Ladd, A.J., Short-time motion of colloidal particles: Numerical simulation via a

fluctuating lattice-Boltzmann equation. *Physical Review Letters*, 1993. **70**(9): p. 1339.

[25] Michalet, X., Mean square displacement analysis of single-particle trajectories with localization error: Brownian motion in an isotropic medium. *Physical Review E: Statistical Physics, Plasmas, Fluids, and Related Interdisciplinary Topics*, 2010. **82**(4): p. 041914.

[26] Wagner, T., H.G. Lipinski, and M. Wiemann, Dark field nanoparticle tracking analysis for size characterization of plasmonic and non-plasmonic particles. *Journal of Nanoparticle Research*, 2014. **16**: p. 2419.

[27] Van Der Meeren, P., M. Kasinos, and H. Saveyn, Relevance of two-dimensional brownian motion dynamics in applying nanoparticle tracking analysis, in Methods in Molecular Biology. 2012. p. 525-534.

[28] Boyd, R.D., S.K. Pichaimuthu, and A. Cuenat, New approach to inter-technique comparisons for nanoparticle size measurements: using atomic force microscopy, nanoparticle tracking analysis and dynamic light scattering. *Colloids and Surfaces A: Physicochemical and Engineering Aspects*, 2011. **387**(1-3): p. 35-42.

[29] Kestens, V., et al., Validation of a particle tracking analysis method for the size determination of nano- and microparticles. *Journal of Nanoparticle Research*, 2017. **19**(8): p. 271.

[30] Lucy, L.B., Iterative technique for rectification of observed distributions. *Astronomical Journal*, 1974. **79**(6): p. 745-754.

[31] Veklerov, E. and J. Llacer, Stopping rule for the MLE algorithm based on statistical hypothesis testing. *IEEE Trans Med Imag*, 1987. **6**(4): p. 313-319.

[32] Hebert, T.J., Statistical stopping criteria for iterative maximum-likelihood reconstruction of emission images. *Phys Med Biol*, 1990. **35**(9): p. 1221-1232.

Chapter 4*

Validation of Size Estimation of Nanoparticle Tracking Analysis on Polydisperse Macromolecule Assembly

The standard technique used to measure the size distribution of nanometer-sized particles in suspension is dynamic light scattering (DLS). Recently, nanoparticle tracking analysis (NTA) has been introduced to measure the diffusion coefficient of particles in a sample to determine their size distribution in relation to DLS results. Because DLS and NTA use identical physical characteristics to determine particle size but differ in the weighting of the distribution, NTA can be a good verification tool for DLS and vice versa. In this study, two NTA data analysis methods based on maximum-likelihood estimation were evaluated, namely finite track length adjustment (FTLA) and an iterative method, on monodisperse polystyrene beads and polydisperse vesicles by comparing the results with DLS. The NTA results from both methods agreed well with the mean size and relative variance values from DLS for monodisperse polystyrene standards. However, for the lipid vesicles prepared in various polydispersity conditions, the iterative method resulted in a better match with DLS. Further, it was found that it is better to compare the native number-weighted NTA distribution with DLS, rather than its converted distribution weighted by intensity.

---

* This chapter is published as A. Kim, W.B. Ng, W. Bernt, and N.J. Cho. Validation of Size Estimation of Nanoparticle Tracking Analysis on Polydisperse Macromolecule Assembly. *Scientific Reports* 9, 2639 (2019). DOI: 10.1038/s41598-019-38915-x.

4.1 Introduction

Efforts to develop new drugs are not limited to the physicochemical properties of pharmaceuticals. They also include explorations of effective ways to deliver those drugs without compromising efficacy or safety [1-10]. Despite advances in molecular biology research, many drugs still have serious side effects due to the lack of a specific target and correct control release profile, and these side effects limit our ability to design optimal medications for many diseases, including cancer, neurodegenerative diseases and infectious diseases [11-15]. To address this issue, researchers have developed several new modes of drug delivery system (DDS) that have entered clinical practice, including nanoparticles based on polymers, noble metals and lipid based carriers [3, 16-19]. The interactions and stability of such materials are strongly dependent on carrier size, whose characterization is crucial in assessing the quality and determining the efficiency of the DDS [20-22]. In particular, chemical modification of nanoparticles is necessary to make them suitable for physiological conditions, and accurate measurement of their size is necessary for quality control [23-25]. This requirement has become more significant as nanoparticles, and their chemical modifications, have been developed for more specific purposes [1, 26, 27]. Likewise, lipid vesicles, due to their versatile engineering capabilities, have been combined with various therapeutic agents to achieve desired pharmaceutical properties [28, 29]. Due to the inherent self-assembly of lipids, validation of their size and distribution is essential to understand the physical properties that directly correlate with drug efficacy. All of these factors highlight the importance of using accurate and precise measurement techniques to characterize the size distribution of biological and synthetic nanoparticle suspensions.

In the analysis of macromolecular assemblies, various techniques are used to measure the physical properties of samples, including imaging [30, 31], separation of particles [32, 33], scattered light [34, 35] and those measurements are related to the size by conversions relying on various physical principles [36]. Direct imaging techniques, including scanning electron microscopy (SEM), transmission electron microscopy (TEM) and atomic force microscopy (AFM), are some of the most popular methods to obtain the topographical size

of particles, as well as their shape and texture [31, 36-39]. Imaging has been preferred due to its intuitive high-resolution visualization of particles and the minimal influence of artifacts in size determination [36]. However, imaging methods require laborious sample preparation steps, and the sample must be removed from its native or working environment, often resulting in a deformation to the samples. In addition, throughput is limited and limited sampling may result in biased information [36].

Another strategy is to separate the particles in the sample, creating a spatial macromolecular redistribution in a medium, in which the degree of separation is determined by the mass or volume of the macromolecules and can be converted into their size [36]. This approach is a feature of various techniques, including size exclusion chromatography (SEC), asymmetrical flow field-flow fractionation (AF4) and analytical ultracentrifugation (AUC), which measure differences in the elution, sedimentation or diffusion of particles [33, 40, 41]. As the particles in the sample are spatially separated depending on their differences in the course of measurement, these techniques can be combined with other size measurement techniques, such as multi-angle light scattering (MALS), to improve the size resolution or measure additional properties, such as molecular weight [42, 43]. As the techniques involve separation of the measured sample, they provide more useful size measurements of polydisperse samples but introduce distortion of the sample condition due to the medium used [36].

Among non-destructive measurement techniques [44], dynamic light scattering (DLS) is the most widely used due to its simplicity. Upon laser illumination, the intensity of the light scattered by the particles in suspension changes both temporally and spatially depending on the size and weight of the particles and can be converted into size information [34, 36]. Despite being a powerful and accessible tool, DLS has several drawbacks due to the inherent limitation of intensity-biased detection [34, 45]. DLS determines a particle's size from fluctuations of the scattered light resulted from the Brownian motion of the particles. The intensity of the scattered light is proportional to the square of the volume of the particle, which makes DLS very sensitive to the presence of large particles [45, 46]. Small amounts

of large aggregates or dust particles can disturb the size determination if the main population is significantly smaller in size.

To address this problem, other techniques including AFM, SEM, TEM, AF4 and AUC can be used to verify the size determined by DLS [38, 47-49]. However, the definition of size measured by one technique can be different from that of the others, which makes the comparison complicated as it requires careful interpretation of the data obtained. In particular, DLS measures the hydrodynamic diameter from the diffusion coefficient of particles in suspension, and this diffusion coefficient is converted into the diameter of an assumed hypothetical sphere that has the same diffusion coefficient [34]. In contrast, SEM, for instance, can obtain a geometric size of particles given by measuring the width of individual particles from the image [36, 50]. Recently, a size characterization tool called nanoparticle tracking analysis (NTA) was introduced to acquire the size of particles by determining their diffusion coefficient, meaning that the definition of the size measured by NTA is identical to that of DLS. NTA can be a good method to verify the results of DLS because they measure the same physical property [51, 52]. Whereas DLS reads the intensity change of scattered light to find the diffusion coefficient of particles, NTA calculates the diffusion coefficient based on the movements of individual particles in successive optical video images [51, 52]. This difference in the detection principles of DLS and NTA results in a difference in the way that the size is given, i.e., the quantities of the particles measured by DLS and NTA are weighted by intensity and number, respectively, which makes NTA an excellent technique for verifying DLS results.

Initial studies on NTA focused on the validation of NTA measurements of mono- and multimodal nanoparticle samples and compared the results with DLS [47, 49, 52, 53]. These studies confirmed that NTA provides comparable results in determining the size of mono- and multimodal nanoparticles compared with DLS. The validation was extended to comparisons with AFM [47], TEM [38] and AUC [49] techniques, where the distribution given by NTA was a good match for those from the techniques on monomodal samples. When the comparison was extended to polydisperse samples such as proteins and vesicles [52, 54-56], the results showed better size resolution in NTA compared with DLS.

While NTA showed better size resolution than DLS on polydisperse samples, the studies did not observe a narrow distribution from NTA on monodisperse samples. The analysis software for NTA used in the previous studies acquired the size distribution by directly converting the displacement of tracks into the size, which is prone to a stochastic error in determining the size from the particle tracking. Although the studies recognized the uncertainty resulting from the stochastic error [47, 49, 56], they used the size distributions from the direct conversion due to the lack of methods to mitigate the stochastic error. To solve this issue, Saveyn et al. [57] and Walker [58] suggested size estimation methods based on the maximum likelihood estimation (MLE) principle. These methods search a narrower distribution that maximizes the likelihood on the acquired track data either by assuming a certain size distribution with a few adjustable parameters or by taking iterative steps, and can successfully recover a narrower size distribution of monomodal samples from NTA track data. Using this strategy to recover a better size distribution from NTA, monomodal reference samples were measured to compare the results with TEM [30]. Further, Kestens et al. [59] compared versions 2.3 and 3.0 of NTA software, which use the direct conversion and the iterative approach, respectively, and found that the iterative approach has a better size resolution on mono- and multi-modal reference samples.

Inspired by previous studies [52, 57-59], this study aimed to evaluate NTA results with respect to the size estimation methods for NTA. First, monodisperse reference standards of known size values were measured using NTA and compared with DLS. The size analysis of acquired particle tracks of NTA was processed by direct conversion of the tracks and with the two MLE-based methods, namely finite track length adjustment (FTLA) and the iterative method. The comparison confirmed that both of the two MLE-based methods can recover a narrow size distribution of the monodisperse reference standards. The estimation methods were also applied to estimate the size distribution of polydisperse vesicle samples prepared in various polydispersity conditions to verify if FTLA and the iterative method are applicable for polydisperse samples of unknown size distribution. While the iterative method achieved results comparable with DLS, the results from FTLA deviated from those of DLS as it assumes an arbitrary size distribution that may not be appropriate for polydisperse samples. In addition, the size distribution of NTA acquired with the estimation

methods was converted into an intensity-weighted size distribution from its number-weighted distribution to investigate if the conversion gives a better comparison with the DLS results.

4.2 Theory

4.2.1 Dynamic Light Scattering

DLS extracts the size distribution of particles in suspension from their Brownian motion, whose displacement is related to their diffusion coefficient [34, 45, 46]. The intensity of the light scattered by particles in suspension upon laser illumination changes due to the particles' Brownian motion, and the intensity fluctuation is processed to acquire its auto-correlation function whereby the decay time is related to the particles' diffusion coefficient as expressed in Eq. 2.1.

For monodisperse spherical particles, the hydrodynamic radius R_h can be related to the diffusion coefficient using the Stokes-Einstein equation as described in Eq. 2.2. For polydisperse samples, the auto-correlation function can be expressed as the integral form as in Eq. 2.3. Although a Laplace inversion of the integration produces the size distribution $G(\Gamma)$, it is well known that the inversion is not a well-conditioned problem [34, 36, 45]. Many strategies have been suggested to recover the size distribution from the integration, among which the cumulant analysis method is only method recommended by the International Standards Organization [60].

The cumulant analysis method is applied for relatively narrow polydisperse samples [61]. The mean $\bar{\Gamma}$ and the variance μ_2 of the distribution $G(\Gamma)$ are acquired from the expansion of the logarithm of the auto-correlation function as in Eq. 2.9. By fitting $\ln\left(g^1(\tau)\right)$, the mean size R_Z and the polydipersity index PI are given as in Eqs. 2.13 and 2.14.

Although valid for polydisperse samples that meet the criterion $\mu_2\tau^2 \ll 1$ [45, 61], in this study, the cumulant method was applied to both PS latex nanoparticle samples and vesicle samples for the comparison with NTA.

4.2.2 Nanoparticle Tracking Analysis

4.2.2.1 Detection Principle of NTA

Similar to DLS, NTA extracts the size information of particles in suspension by measuring their diffusion coefficient [51]. By taking sequential images of illuminated particles in suspension on a periodic time interval, the displacement of a particle can be identified from successive images and constructed into a track. To determine the displacement of particles, NTA compares the two-dimensional location of particles in an image frame with the subsequent frame. In doing so, NTA sets a certain threshold distance, also known as the maximum jump distance, to properly identify if the two particles in the two adjacent frames are the same particle. If any single particle is found in the successive frame within the threshold distance from the location of the particle in the previous image, the two particles are recognized as the same particle and make a track segment. In the same manner, this recognition process is performed for subsequent frames and track segments are combined to construct a particle's track. The track terminates if there is no particle in the following frame or if there are more than two particles within the threshold distance. Because of the nature of the tracking process, the track segment length, and the number of track segments, are finite and variable.

For a track of a track segment length n, the mean squared displacement of the track z, expressed as

$$z = \frac{1}{n}\sum_{i=1}^{n} r_i^2 \quad (4.1)$$

where r_i is the two-dimensional displacement of ith track segment of the track, is translated into the diffusion coefficient assuming a 2D Brownian motion, which is related by the Stokes-Einstein relation as expressed in Eq. 3.6 [51, 52, 57, 58]. Then the acquired

diffusion coefficient D of the track is converted to the hydrodynamic diameter relying on the Stokes-Einstein equation, and comprises the size distribution of the measured sample.

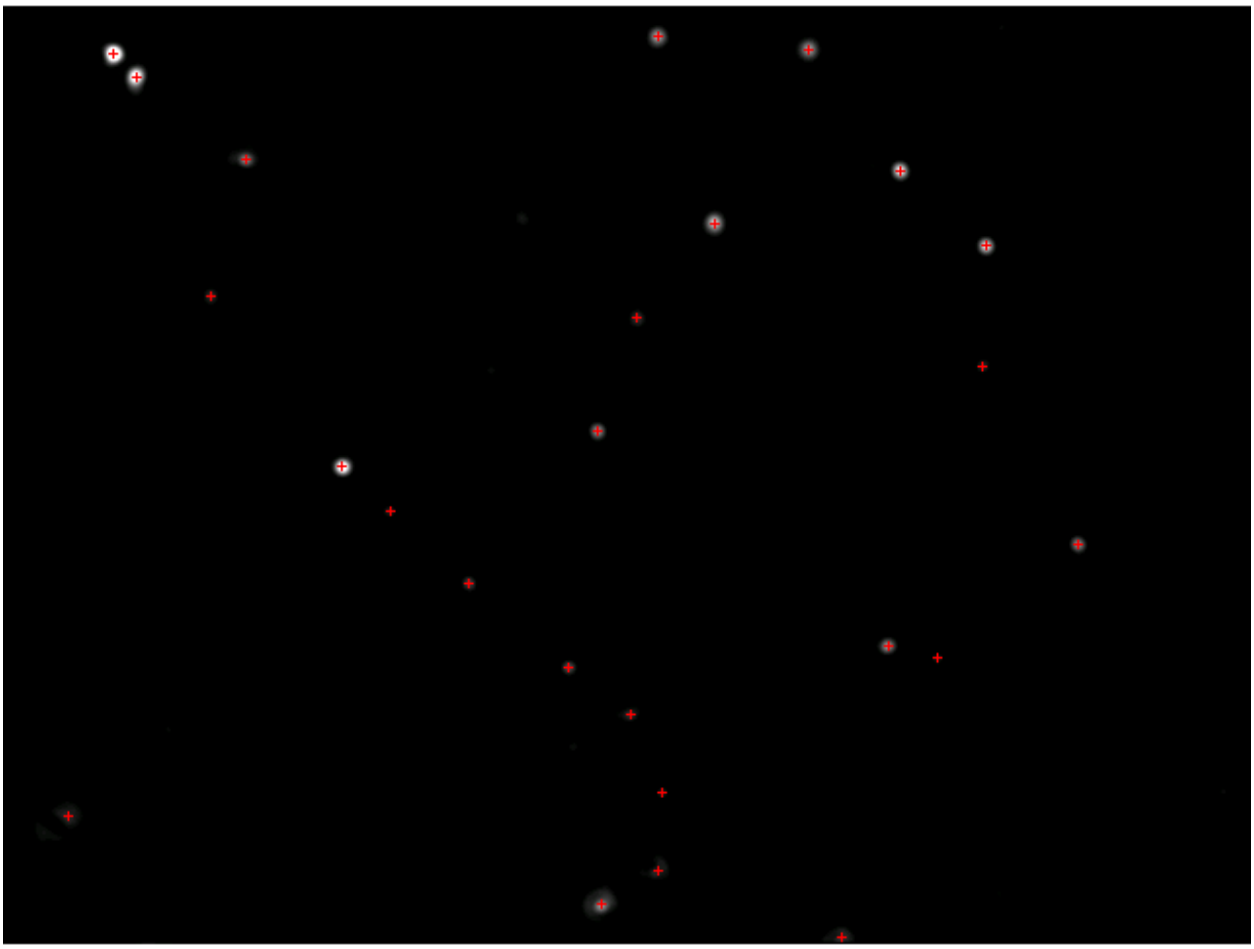

Figure 4.1 In NTA, particles suspended in liquid are illuminated by a laser beam. Scattered light by the particles is monitored by the microscope, from which the position of the particles is identified by the software. The software tracks the trajectory of the particles and constructs particle tracks, from which the average squared displacement is calculated and converted into the corresponding hydrodynamic diameter.

4.2.2.2 Size Distribution Estimation Methods for NTA

Uncertainty in the Mean Squared Displacement Measurement in NTA

Measurement of the mean squared displacement z in NTA assumes that a particle is tracked for long enough that the measured mean squared displacement is close enough to the ideal mean squared displacement. However, as the track segment length is finite, the acquired mean squared displacement z of a track has statistical uncertainty that is inversely proportional to the square root of the track segment length n [54, 62]. Therefore, small track segment lengths would make the measured size distribution significantly broader than its true size distribution and they should be excluded to have a narrower size distribution.

Maximum Likelihood Estimation (MLE) with an Assumed Arbitrary Distribution with Parameters

As particles observed by NTA undergo Brownian motion, the probability distribution of the mean squared displacement z of a tracked particle whose size is d with a track segment length n can be described by a gamma distribution as follows: [58]

$$P(z|n,d) = \frac{(ns)^n}{(n-1)!} z^{n-1} e^{-nsz} \quad (4.2)$$

where s is defined as $1/4D\Delta t = 3\pi\eta d/4\Delta t k_B T$. An observed set of tracks Φ of a sample measured by NTA can be related to a particle size distribution $f(d)$ by the integration

$$\Phi = \int_0^\infty f(x) P(z|n,x) dx \quad (4.3)$$

Although the inversion of the integration would enable recovery of $f(d)$ by finding $Q(d|n,z)$ that satisfies

$$f(d) = \sum_{\Phi} \Phi \cdot Q(d|n,z) \quad (4.4)$$

the inversion relation cannot be used because $Q(d|n,z)$ depends on $f(d)$ [63].

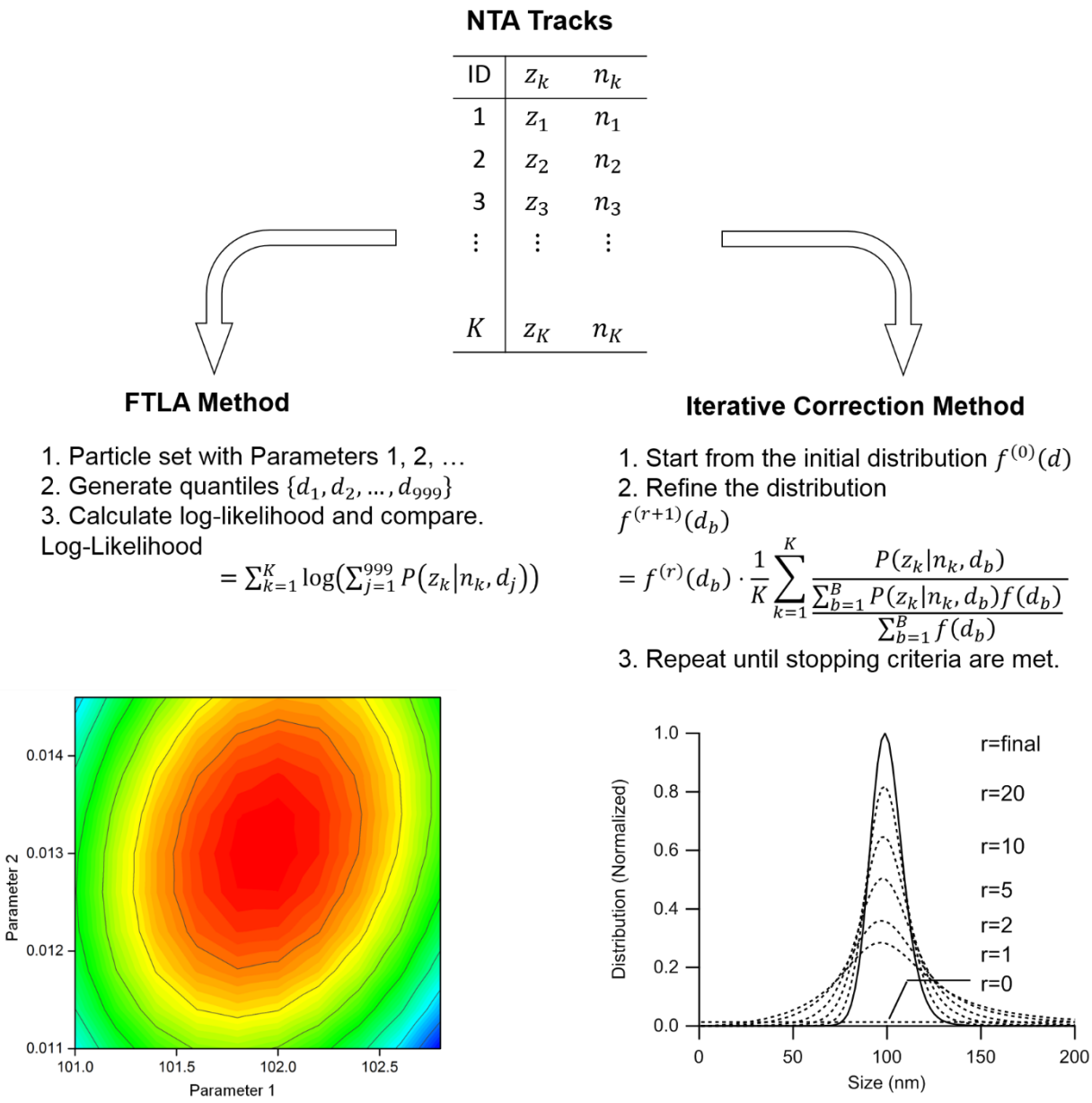

Figure 4.2 Schematic representation of the size determination methods based on maximum likelihood estimation. By assuming a size distribution described by adjustable parameters, the FTLA method looks for the parameter values that maximize the likelihood of the given NTA tracks. The iterative correction method refines the size distribution that approaches to the maximum likelihood over each iteration.

Due to the difficulty of finding Q for the inversion, finite track length adjustment (FTLA) can be used to determine $f(d)$ by maximizing the likelihood of the observed list of tracks Φ with an assumed size distribution for $f(d)$ as illustrated in Figure 4.2 [57]. For an assumed size distribution with a few parameters, for example a log-normal distribution with its geometric mean and geometric standard deviation set as parameters, an "ideal" set of particles d_j (with j = 1–999) is drawn, which comprises 1000-quantiles of the size distribution, i.e., those of particle size d_j that satisfy $C(d_j) = j/1000$ (j = 1–999) for the cumulative size distribution $C(d)$ of $f(d)$. For each particle size d_j, the likelihood of producing a track whose mean squared displacement z and track segment length n is given by

$$L(z, n; d_j) = P(z|n, d_j) \quad (4.5)$$

Hence, the likelihood of producing such a track with a given particle set d_j (j = 1–999) is given as

$$L(z, n; \{d\}) = \sum_{j=1}^{999} P(z|n, d_j) \quad (4.6)$$

Likewise, the likelihood for all the observed list of tracks Φ becomes

$$L(\Phi; \{d\}) = \prod_{k=1}^{K} \left(\sum_{j=1}^{999} P(z_k|n_k, d_j) \right) \quad (4.7)$$

where z_k and n_k are the mean squared displacement and the track segment length of the kth track of Φ, respectively, and K is the total number of the observed tracks. For practical reasons, the maximization is performed on the logarithm of the likelihood, as maximizing a positive function also maximizes its logarithm [58]:

$$LL(\Phi; \{d\}) = \log(L) = \sum_{k=1}^{K} \log \left(\sum_{j=1}^{999} P(z_k|n_k, d_j) \right) \quad (4.8)$$

With the log-likelihood, an optimal parameter set for the size distribution is sought for its maximum value, which determines the size distribution for the observed tracks. As this

approach assumes an arbitrary size distribution, a decrease in the likelihood can be expected for the benefit of a simpler solution [63].

Maximum Likelihood Estimation by Iterative Correction

For a size distribution $f(d)$, the log-likelihood of producing the observed list of tracks Φ can be expressed as

$$LL(\Phi) = \sum_{k=1}^{K} \log\left(\frac{1}{\sum_{b=1}^{B} f(d_b)} \sum_{b=1}^{B} P(z_k|n_k, d_b) f(d_b)\right) \quad (4.9)$$

where b is the bin number for the segmented range of particle size d [58].

Then its differentiation with respect to the size distribution is given as

$$\frac{\partial LL}{\partial f} = \sum_{k=1}^{K} \frac{P(z_k|n_k, d_b)}{\sum_{b=1}^{B} P(z_k|n_k, d_b) f(d_b)} - \frac{K}{\sum_{b=1}^{B} f(d_b)} \quad (4.10)$$

At the maximum of the likelihood, the differential becomes zero, leading to

$$\sum_{k=1}^{K} \frac{P(z_k|n_k, d_b)}{\sum_{b=1}^{B} P(z_k|n_k, d_b) f(d_b)} = \frac{K}{\sum_{b=1}^{B} f(d_b)} \quad (4.11)$$

From this relation, it is possible to find the size distribution by an iterative procedure, given as

$$f^{(r+1)}(d_b) = f^{(r)}(d_b) \cdot \frac{1}{K} \sum_{k=1}^{K} \frac{P(z_k|n_k, d_b)}{\sum_{b=1}^{B} P(z_k|n_k, d_b) f(d_b) / \sum_{b=1}^{B} f(d_b)} \quad (4.12)$$

where $f^{(r)}(d)$ is the rth estimate of the size distribution from the iterations as illustrated in Figure 4.2 [63]. For the initial size distribution $f^{(0)}(d)$, a uniform distribution is chosen [58, 64, 65].

For the termination criteria of the iteration, the chi-squared statistic of the error between a histogram of the mean squared displacement H_z and that calculated from the rth iteration solution $H^{(r)}$ can be used, where

$$\chi^2 = \sum_{m=1}^{M} \frac{\left(H_z(z_m) - H^{(r)}(z_m)\right)^2}{H^{(r)}(z_m)} \quad (4.13)$$

$$H^{(r)}(z_m) = \sum_{n=N_{min}}^{N_{max}} N_n \sum_{b=1}^{B} \frac{P(z_m|n, d_b) f^{(r)}(d_b) \Delta z_m}{\sum_{b=1}^{B} f^{(r)}(d_b)} \quad (4.14)$$

where m is the bin number for the mean squared displacement and N_n is the number of tracks with track segment length n, and in this study the iteration terminates when the change in χ^2 becomes smaller than 1% of the previous value [58].

4.2.3 Conversion of Number-Weighted Distribution of NTA

The size distribution measured by DLS is weighted by the intensity of the scattered light, which is dependent on the particle size, whereas that from NTA is weighted by the number. In comparing the two quantities, one must be converted to match the weighting of the other.

The number-weighted size distribution $f(d)$ from NTA can be converted into an intensity-weighted distribution $f_I(d)$ given by

$$f_I(d) = \frac{f(d)I(q,d)}{\int_0^\infty f(d)I(q,d)dd} \quad (4.15)$$

where q is the scattering vector and $I(q,d)$ is the form factor of the measured particles[66, 67] For vesicles, a thin-shell hollow sphere model is assumed [48, 68, 69], so that

$$I(q,d) = (\pi d^2 t)^2 P(q,d) \quad (4.16)$$

where $P(q,d)$ is the structural factor for the vesicle approximated by the Rayleigh-Gans-Debye (RGD) approximation given by

$$P(q,d) = \left(\frac{\sin(q \cdot d/2)}{q \cdot d/2}\right)^2 \quad (4.17)$$

4.3 Experimental Methods

4.3.1 Materials

Polystyrene latex standards (92 ± 3, 269 ± 7 and 343 ± 9 nm) were purchased from Thermo Scientific (Rockford, IL., USA). 1-palmitoyl-2-oleoyl-sn-glycero-3-phosphocholine (POPC) was purchased from Avanti Polar Lipids Inc., (Alabaster, AL, USA).

4.3.2 Preparation of POPC Vesicles

Vesicles composed of POPC (Avanti Polar Lipids Inc., Alabaster, AL) were prepared at a lipid concentration of ~5 mg/mL and then diluted before the experiment. Briefly, dried lipid films were hydrated with 10 mM Tris (pH 7.5) buffer solution with 150 mM NaCl, and the sample was then vortexed periodically for 5 min. Vesicle samples were extruded through polycarbonate membranes with either 50, 100, 200 or 400 nm pores sized by a miniextruder (Avanti Polar Lipids). For those samples pretreated with a range of freeze-thaw cycles, freeze-thaw treatment was performed before extrusion on newly hydrated lipid films by using a previously described methodology based on freeze-thaw pretreatment and then extrusion [70]. Specifically, in each treatment cycle, the vesicle suspension was frozen in liquid nitrogen for 30 s, before thawing in an 80 °C water bath for 90 s, and then finally being vortexed to complete each cycle. After the freeze-thaw cycles of 3, 5, 7, 9, 11, 13, 15 or 17 repetitions, vesicles were sized by an extruder (Avanti Polar Lipids) through 400 nm polycarbonate membrane pores. All aqueous solutions and buffers were prepared in Milli-Q water with a minimum resistivity of 18.2 MΩ·cm (Millipore, Billerica, MA).

4.3.3 Dynamic Light Scattering

For the DLS measurements, a ZetaPals particle size analyzer (Brookhaven Instruments, Holtsville, NY) with a 658.0 nm monochromatic laser was used. For each sample,

three independent runs of 1 min were performed. To avoid unnecessary reflection, all measurements were taken at a scattering angle of 90°, and the measured intensity autocorrelation function was fitted to yield the intensity-weighted size distribution of particles in solution. The deconvolution of the autocorrelation function was done using the cumulants method, which was applied to calculate the intensity-weighted log-normal profile of the size distribution expressed by the average effective diameter and its polydispersity.

4.3.4 Nanoparticle Tracking Analysis

NTA measurements were made with an LM10HS (Nanosight Limited, Amesbury, UK) equipped with a scientific CMOS camera, a 20x objective lens, a blue laser module (405 nm, LM12 version C) and NTA software version 3.1. A 1-ml disposable syringe was used to inject the samples into the instrument chamber. The video data for NTA measurements were collected for 30 seconds, repeated three times for each sample. The detection threshold of the NTA software was set to 5 and the maximum jump distance and the minimum track segment length were both set to auto.

Detected tracks were then translated into a size distribution using three different methods, i.e., direct conversion of the detected particle tracks, maximum likelihood estimation with an assumed distribution (the FTLA method) and maximum likelihood estimation by iterative correction. For the conversion, valid tracks were acquired from the detected tracks by the software, with tracks of a small track segment length excluded from the selection.

FTLA assumes a certain shape for the size distribution to maximize likelihood, and a log-normal distribution was assumed in this study so that the mean and standard deviation parameters could be optimized to produce maximum likelihood [57]. For the calculation, 1000-quantiles are generated from a log-normal distribution while varying its mean size and standard deviation, which represent an “ideal” set of particles for the assumed size distribution [57].

In the iterative method, the size distribution $f(d)$ is refined by the iteration

$$f^{(j+1)}(d_i) = f^{(j)}(d_i) \cdot \frac{1}{N} \sum_k \frac{P(z_k; n_k, d_i)}{Q^{(j)}} \quad (4.18)$$

$$Q^{(j)} = \sum_i P(z_k; n_k, d_i) f^{(j)}(d_i) \quad (4.19)$$

where $f^{(j)}(d_i)$ is a normalized fraction of those particles in the size distribution of the jth iteration whose size is between d_i and d_{i+1}, and N is the number of tracks in the given set of tracks. The initial size distribution $f^{(0)}(d)$ is set to a uniform distribution so that $f^{(0)}(d_i) = 1/M$, where M is the number of bins for the size distribution. The iterations are performed until the change in the chi-squared value between the histogram of the displacement of the observed tracks and that of the estimated size distribution from the iteration is less than 1% of the previous value [58].

In comparing the results from DLS and NTA, the mean size of NTA from the acquired size distribution is compared with the mean hydrodynamic size R_Z of DLS while the relative variance (RV, the variance divided by the square of the mean size) of NTA is compared with the PI of DLS.

4.4 Results and Discussion

4.4.1 Size Measurements of Polystyrene Latex Nanoparticle Standards

To validate NTA and its size distribution analysis methods, monodisperse polystyrene (PS) latex standards were measured by DLS and NTA. The mean size and the polydispersity index (PI) of the DLS results were acquired by cumulant analysis of the measured auto-correlation function and are shown in Figure 4.3. The mean size obtained by DLS is in good agreement with the nominal values, with 91 ± 1, 278 ± 1 and 352 ± 3 nm acquired for the 92, 269 and 343 nm particle size standards, respectively. The PIs of the samples were 0.037 ± 0.029, 0.016 ± 0.009 and 0.035 ± 0.018, respectively, indicating that the samples were monodisperse.

Size information from NTA, shown in Figure 4.3, was extracted from the track data with segment length greater than 5, and processed by the direct conversion method. The mean sizes of the 92, 269 and 343 nm PS standards were 94 ± 4, 261 ± 3 and 320 ± 3 nm, respectively, close to their respective nominal values. The RVs of the 92, 269 and 343 nm PS standards were 0.075 ± 0.009, 0.033 ± 0.007 and 0.044 ± 0.001, confirming that the size distributions were monodisperse.

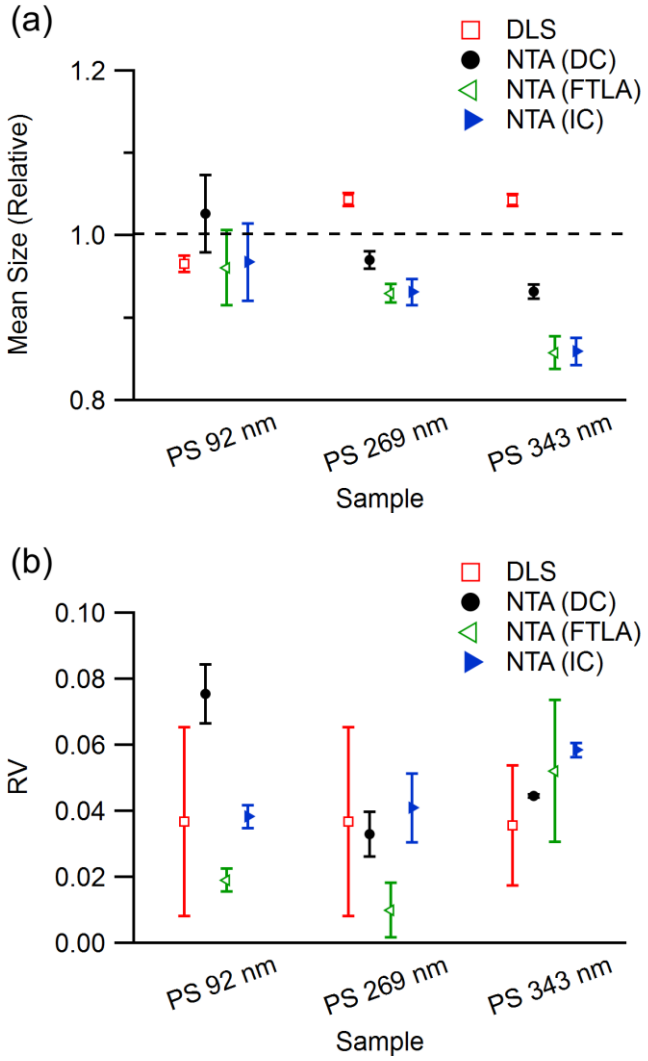

Figure 4.3 (a) Mean and (b) relative variance of the size distributions of PS latex nanoparticle samples measured by DLS and NTA. Mean size is displayed as a value relative to its respective nominal sample size. The size information from DLS was acquired using the cumulant method, while the results from NTA were acquired by applying three different methods, i.e., direct conversion of acquired tracks (DC), FTLA and the iterative method (IC).

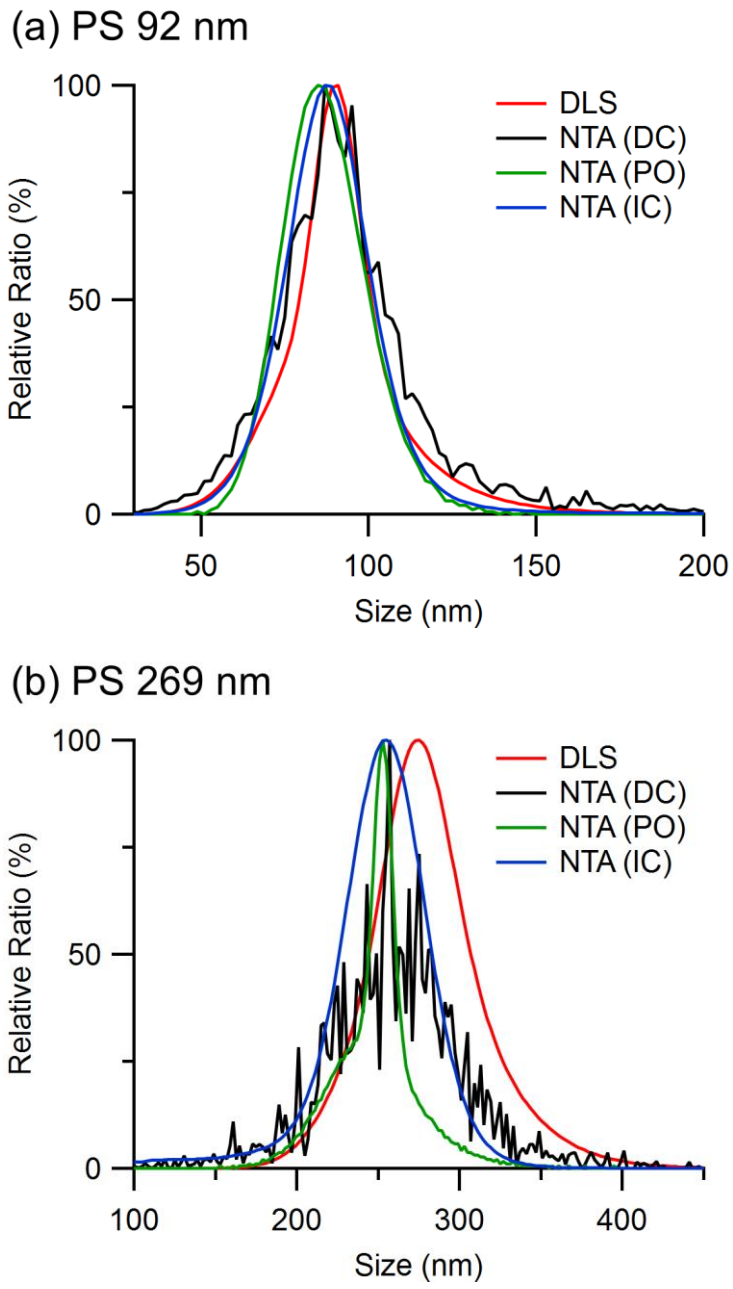
(a) PS 92 nm
Relative Ratio (%)
100
50
0
50
100
150
200
Size (nm)
DLS
NTA (DC)
NTA (PO)
NTA (IC)
(b) PS 269 nm
Relative Ratio (%)
100
50
0
100
200
300
400
Size (nm)
DLS
NTA (DC)
NTA (PO)
NTA (IC)

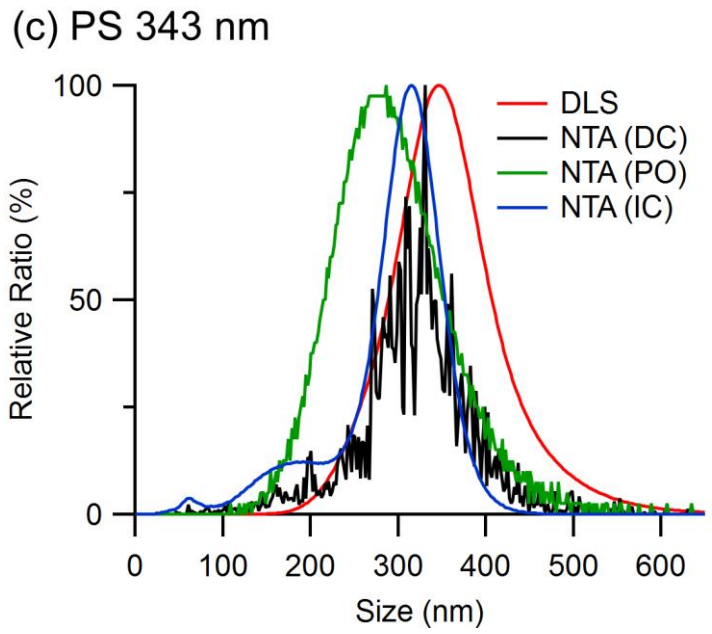

Figure 4.4 The size distributions of monodisperse PS latex standard samples of a nominal size of (a) 92, (b) 269 and (c) 343 nm measured by DLS and NTA. The size distribution from DLS assumes a log-normal distribution acquired from the cumulant method, while those from NTA are from the three different analysis methods, i.e., direct conversion (DC), FTLA and the iterative method (IC).

When the mean size results from DLS and NTA are compared, it is observed that the value measured by DLS is larger than its corresponding result from NTA although both values are close to the corresponding nominal value. The difference of the results from the two techniques gets larger on a larger nominal size of the standard, which was observed in past studies [47, 52]. In particular, Boyd et al. [47] attributed the difference to the different quantities reported by DLS and NTA, i.e. intensity and number, respectively. Although the authors showed that the conversion of number-weighted distribution into intensity explained the difference, application of such conversion cannot be a valid method to be applied to monodisperse samples.

To determine if the RV of the NTA results from the direct conversion could be reduced by considering a limited track segment length, the two MLE-based size estimation

methods, i.e., FTLA and the iterative method, were applied to the particle tracks acquired from the standard samples. The size distributions of the 92 nm standard sample acquired by direct conversion, FTLA and the iterative method are shown in Figure 4.4 as well as the distributions of the other standard samples. As shown in Figure 4.3, mean sizes of 88 ± 4, 250 ± 3 and 294 ± 7 nm acquired by FTLA and 89 ± 4, 250 ± 4 and 295 ± 6 nm acquired by the iterative method were determined for the 92, 269 and 343 nm standard samples, respectively. RVs of 0.019 ± 0.003, 0.010 ± 0.008 and 0.052 ± 0.022 by FTLA and 0.038 ± 0.003, 0.041 ± 0.010 and 0.058 ± 0.002 by the iterative method were acquired for the 92, 269 and 343 nm standard samples, respectively. The RVs of the 256 and 343 nm standards acquired by the FTLA and iterative methods are not very different from those derived by direct conversion, whereas that of the 92 nm standard is significantly reduced. This suggests that the MLE-based methods are effective for size distribution estimation especially when the particle size is small, which tends to result in a limitation in acquiring tracks of high enough track segment length due to the large diffusion coefficient. For small particle samples, the error in size estimation by direct conversion is enlarged as the error is inversely proportional to the square root of the track segment length, making the observed size distribution broad [57]. For large particle samples, the particles in the sample are tracked for long enough that the error in size estimation by direct conversion is as small as that of the MLE-based methods.

In the comparison, the mean sizes of the standard samples determined by the FTLA and iterative methods match each other well despite their different approaches to finding the maximum likelihood. However, the RVs from FTLA are smaller than the corresponding values from the iterative method. The assumed size distribution of FTLA has the advantage of a smoother size distribution but at the expense of reduced likelihood [63], resulting in the smaller RVs of these PS standard sample measurements. Given that the samples are monodisperse, assuming a log-normal distribution for the size distribution estimation does not decrease the likelihood compared with the corresponding result from the iterative method as shown in Table 4.1.

Table 4.1 Log-likelihood of the size distributions of PS latex nanoparticles standards estimated by FTLA and iterative methods with respect to the log-likelihood of the size distribution acquired by the direct conversion of the observed tracks of the PS latex standards.

Sample	Δ log-likelihood		Sample	Δ log-likelihood		Sample	Δ log-likelihood	
	FTLA	Iteration		FTLA	Iteration		FTLA	Iteration
PS92	32.94	35.12	PS269	-4.36	9.78	PS343	-37.66	15.94
	41.99	39.66		4.56	7.31		-1.03	22.75
	15.30	26.76		6.75	4.87		-3.07	9.62

4.4.2 Size Measurement of POPC Vesicles

POPC vesicles prepared in various polydispersity conditions were measured by DLS. The results are presented in Figure 4.5. The mean size of the vesicle samples increased with increasing pore size of the extrusion filter. For vesicle samples extruded through filters with pore sizes of 50 nm (V50), 100 nm (V100), 200 nm (V200) and 400 nm (V400), DLS revealed mean sizes of 91 ± 4, 132 ± 3, 213 ± 4 and 458 ± 13 nm, respectively, and PIs of 0.089 ± 0.032, 0.064 ± 0.035, 0.077 ± 0.048 and 0.291 ± 0.013, respectively. Despite the increase in mean size, the PI does not vary much for pore sizes of 50, 100 and 200 nm, indicating that these samples are relatively monodisperse. However, it jumps to about 0.3 for the 400 nm pore size, showing that the vesicle sample extruded through 400 nm pores is highly polydisperse.

For the vesicles processed by freeze and thaw (FT) treatment before being extruded through a 400-nm pore filter, the mean size shows a gradual decrease with increasing number of cycles. As shown in Figure 4.5, for 3, 5, 7, 9, 11, 13, 15 and 17 FT cycles (FT3 to FT17), the mean sizes were 282 ± 4, 223 ± 2, 185 ± 2, 161 ± 1, 148 ± 1, 131 ± 1, 117 ± 2 and 109 ± 1 nm, respectively. The PI results were 0.273 ± 0.021, 0.224 ± 0.022, 0.197 ± 0.029, 0.149 ± 0.023, 0.181 ± 0.024, 0.168 ± 0.015, 0.189 ± 0.025 and 0.197 ± 0.021, respectively, indicating that the polydispersity of the samples reduced

upon successive FT cycles but did not decrease enough for the sample to be regarded as monodisperse.

The NTA measurements of the same samples were analyzed by using direct conversion, which determined mean sizes of 100 ± 2, 119 ± 9, 211 ± 6 and 329 ± 17 nm and RVs of 0.149 ± 0.059, 0.151 ± 0.082, 0.097 ± 0.002 and 0.136 ± 0.037 for the vesicle samples extruded through pores of 50, 100, 200 and 400 nm, respectively, and mean sizes of 243 ± 12, 225 ± 9, 201 ± 7, 184 ± 8, 171 ± 13, 158 ± 15, 135 ± 4 and 137 ± 1 nm and RVs of 0.171 ± 0.024, 0.288 ± 0.029, 0.223 ± 0.016, 0.206 ± 0.009, 0.273 ± 0.024, 0.305 ± 0.059, 0.245 ± 0.010 and 0.274 ± 0.019 for the vesicle samples treated by 3, 5, 7, 9, 11, 13, 15 and 17 FT cycles, respectively, before being extruded through a 400 nm filter, as shown in Figure 4.5 and Table 4.2.

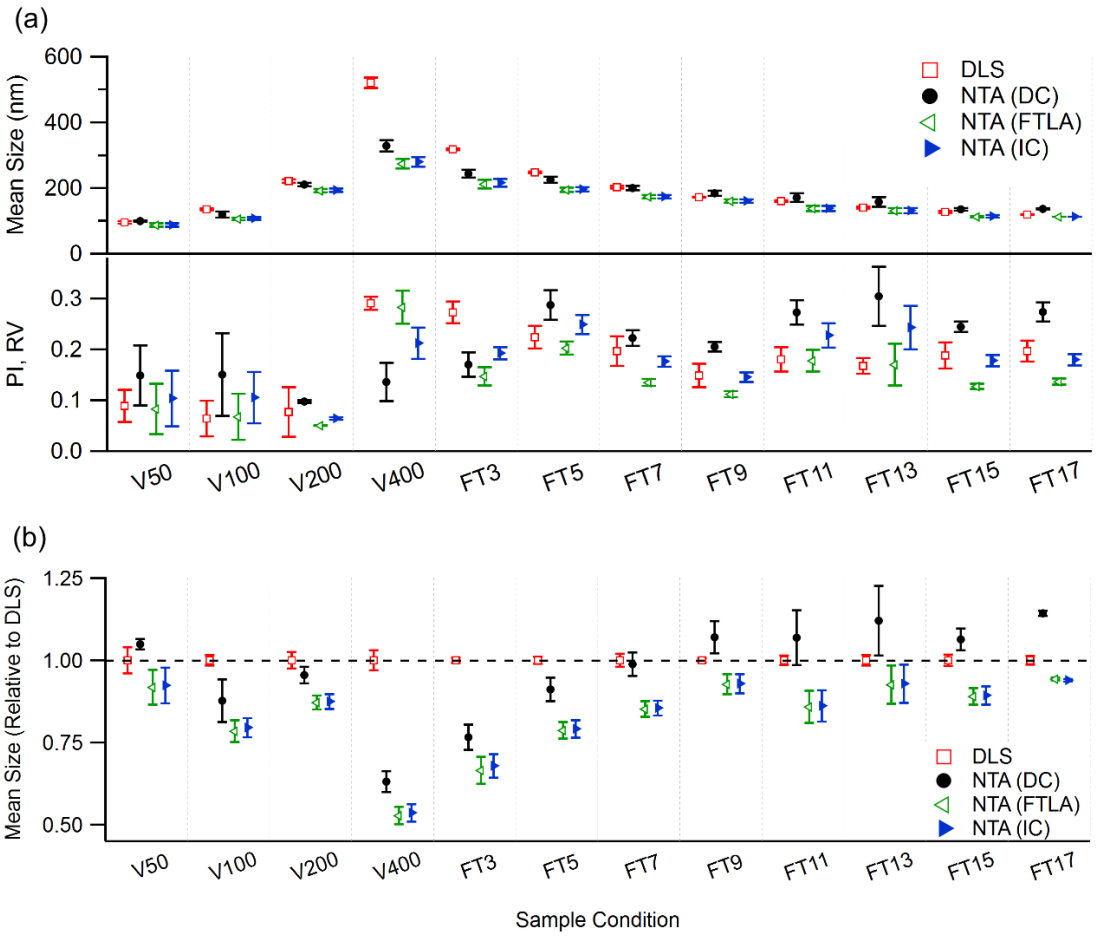

Figure 4.5 (a) Mean and relative variance of the size distributions of the POPC vesicle samples measured by DLS and NTA and (b) relative mean size from NTA with respect to their corresponding mean size from DLS. DLS values are derived from the cumulant method, while the NTA results are obtained by applying the three different analysis methods, i.e., direct conversion (DC), FTLA and the iterative method (IC).

Table 4.2 Mean size and standard deviation of the size distributions of the POPC vesicle samples from DLS and NTA. DLS results were analyzed by the cumulant method, and NTA results were analyzed by the three different estimation methods, i.e., direct conversion, FTLA and the iterative method.

	DLS		NTA					
			DC		FTLA		Iteration	
Sample	Z-avg	PI	Mean	SD	Mean	SD	Mean	SD
50 nm	91 ± 4	0.089 ± 0.032	100 ± 2	38 ± 7	87 ± 5	24 ± 5	88 ± 5	27 ± 5
100 nm	132 ± 3	0.064 ± 0.035	119 ± 9	45 ± 16	106 ± 5	27 ± 10	108 ± 4	34 ± 10
200 nm	213 ± 4	0.077 ± 0.048	211 ± 6	66 ± 2	193 ± 5	43 ± 2	193 ± 5	49 ± 2
400 nm	458 ± 13	0.291 ± 0.013	329 ± 17	119 ± 13	275 ± 14	146 ± 8	279 ± 14	128 ± 5
FT3	282 ± 4	0.273 ± 0.021	243 ± 12	101 ± 12	212 ± 13	81 ± 8	216 ± 11	95 ± 6
FT5	223 ± 2	0.224 ± 0.022	225 ± 9	121 ± 7	195 ± 6	88 ± 6	196 ± 6	98 ± 6
FT7	185 ± 2	0.197 ± 0.029	201 ± 7	94 ± 2	173 ± 5	64 ± 1	173 ± 5	73 ± 1
FT9	161 ± 1	0.149 ± 0.023	184 ± 8	84 ± 6	160 ± 5	54 ± 3	160 ± 5	61 ± 4
FT11	148 ± 1	0.181 ± 0.024	171 ± 13	90 ± 11	138 ± 8	58 ± 6	138 ± 8	66 ± 7
FT13	131 ± 2	0.168 ± 0.015	158 ± 15	87 ± 14	131 ± 8	54 ± 9	131 ± 8	65 ± 8
FT15	117 ± 2	0.189 ± 0.025	135 ± 4	67 ± 3	113 ± 3	40 ± 2	113 ± 4	48 ± 3
FT17	109 ± 1	0.197 ± 0.021	137 ± 1	72 ± 3	113 ± 1	42 ± 1	112 ± 1	48 ± 2

For the different extrusion filter pore sizes, the mean sizes measured by NTA were similar to those from DLS, increasing with increasing filter pore size. However, the RVs acquired from NTA indicated that the samples were polydisperse and did not significantly vary with filter pore size, unlike the PI values obtained by DLS. Especially, the huge difference found from the vesicle sample extruded through 400-nm pore highlights the importance of comparative validation of one measurement to the other. As shown in Figure 4.6(d), the acquired size distribution from NTA indicates a broad distribution with multiple sub-populations, which is difficult to recognize before the measurement. Even the FTLA method for NTA produced a very different size distribution from those acquired with the other NTA analysis methods, since it assumes a normal size distribution for the parameter optimization in this analysis. Like the FTLA analysis for NTA, analysis methods for DLS also assumes certain requirements. Therefore, NTA measurements on polydisperse samples can be useful to validate the application of DLS analysis methods with certain assumptions.

For the various numbers of FT cycles, the trend of mean size measured by NTA also matched that obtained by DLS, decreasing gradually as the number of cycles increased. However, the RVs of the samples from NTA show a gradual increase as the number of FT cycles increases, which is opposite to the trend of the PI measured by DLS, probably because the FT treatment led to homogenization of the vesicle samples [70]. Remarkably, for some of the samples the mean size acquired from NTA was larger than its corresponding mean size from DLS, in contrast to the belief that the mean size of an intensity-weighted distribution is larger than that of its corresponding number-weighted distribution [45, 48]. As the polydispersity of the samples is very large, it is more unlikely that a larger mean size will be obtained from NTA.

As direct conversion is not appropriate in determining standard deviation in the measurements of the PS latex standards, the two MLE-based methods were applied for comparison. The results are presented in Figure 4.5. Using the FTLA method, NTA obtained mean sizes of 87 ± 5, 106 ± 5, 193 ± 5 and 275 ± 14 nm and RVs of 0.083 ± 0.049, 0.068 ± 0.045, 0.051 ± 0.001 and 0.283 ± 0.033 for the filter pore sizes of 50, 100, 200 and 400 nm, respectively, and mean sizes of 212 ± 13, 195 ± 6, 173 ± 5, 160 ± 5, 138 ± 8, 131 ± 8, 113 ± 3 and 113 ± 1 nm and RVs of 0.147 ± 0.018, 0.203 ± 0.013, 0.135 ± 0.007, 0.112 ± 0.006, 0.178 ± 0.021, 0.170 ± 0.040, 0.128 ± 0.005 and 0.137 ± 0.006 for 3, 5, 7, 9, 11, 13, 15 and 17 FT cycles, respectively. The iterative method determined mean sizes of 88 ± 5, 108 ± 4, 193 ± 5 and 279 ± 14 nm and RVs of 0.103 ± 0.055, 0.105 ± 0.050, 0.064 ± 0.002 and 0.212 ± 0.031 for the filter pore size of 50, 100, 200 and 400 nm, respectively, and mean sizes of 216 ± 11, 196 ± 6, 173 ± 5, 160 ± 5, 138 ± 8, 131 ± 8, 113 ± 4 and 112 ± 1 nm and RVs of 0.193 ± 0.012, 0.249 ± 0.019, 0.176 ± 0.010, 0.145 ± 0.009, 0.228 ± 0.024, 0.243 ± 0.043, 0.178 ± 0.011 and 0.180 ± 0.011 for 3, 5, 7, 9, 11, 13, 15 and 17 FT cycles, respectively. The size distribution profiles of the vesicle samples analyzed by the different methods for NTA measurements are presented in Figure 4.6.

Regardless of the condition of the vesicle samples, the mean sizes of the standard sample measurements estimated by the two MLE-based methods match very well despite the different approaches of the two methods. However, the RVs from the two

methods are different, with the RVs from the FTLA method being smaller than those from the iterative method except for the 400-nm filter pore size condition. Although FTLA finds a smaller RV than the iterative method, as noted above, it is at the cost of allowing a smaller likelihood value by assuming a certain shape for the size distribution, i.e., a log-normal distribution, for parameter optimization [63]. In fact, the likelihood value of the size distribution acquired through FTLA is smaller than that from the iterative method except in one case. Moreover, some of the likelihood values are even smaller than their corresponding values from the direct conversion, i.e., without any statistical processing. This implies that FTLA is inappropriate for the estimation of size distributions of NTA measurements on polydisperse samples without a proper assumption of the sample size distribution and that the iterative method is preferable to FTLA for such samples [54].

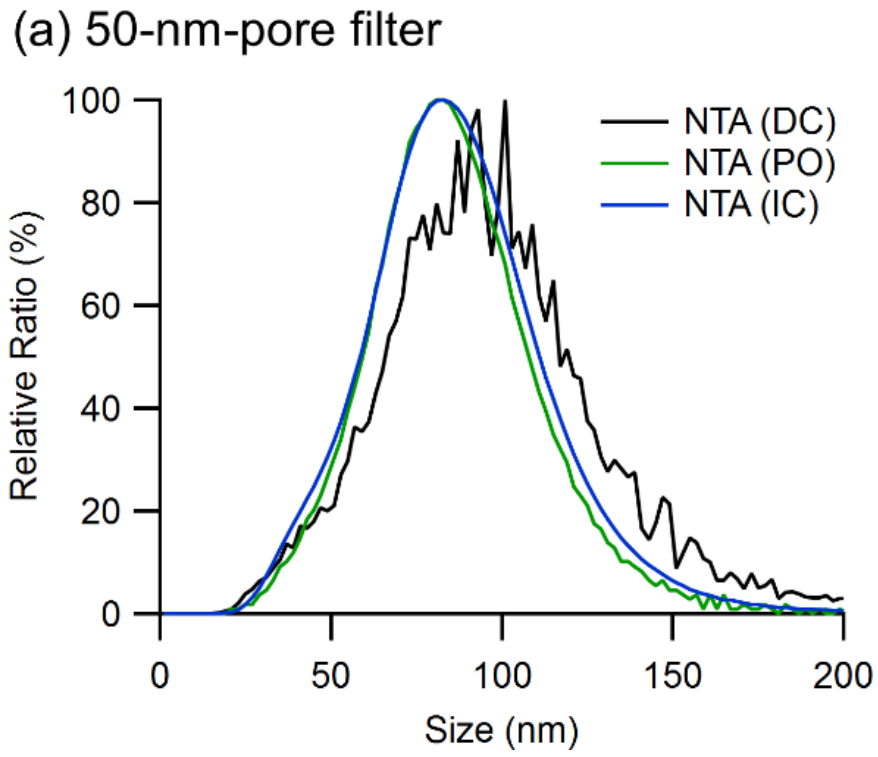

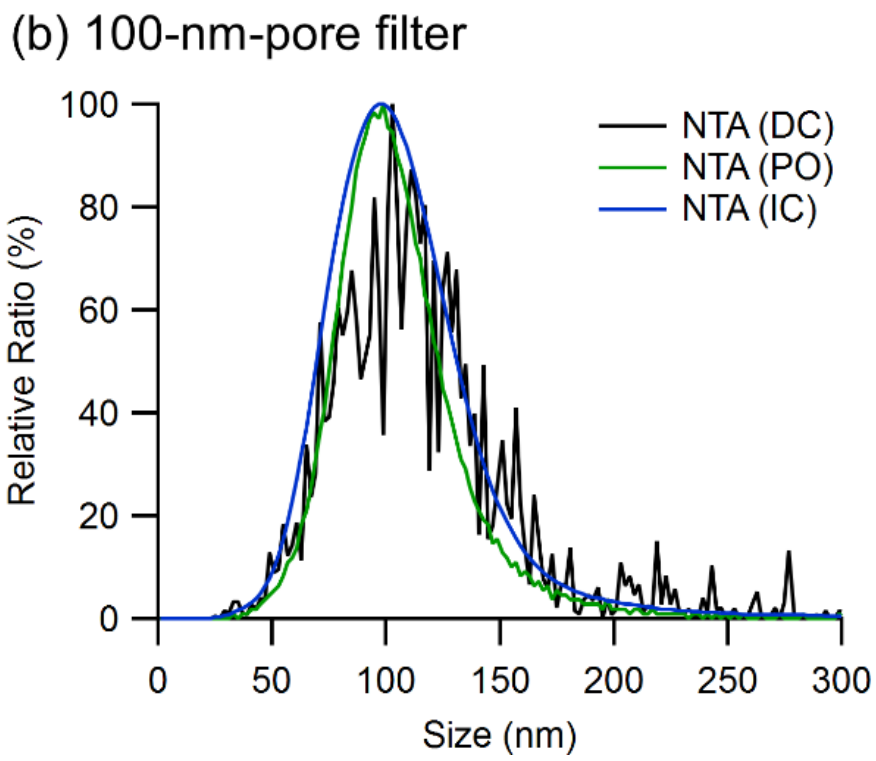
(b) 100-nm-pore filter
Relative Ratio (%)
Size (nm)
NTA (DC)
NTA (PO)
NTA (IC)
0
20
40
60
80
100
0
50
100
150
200
250
300

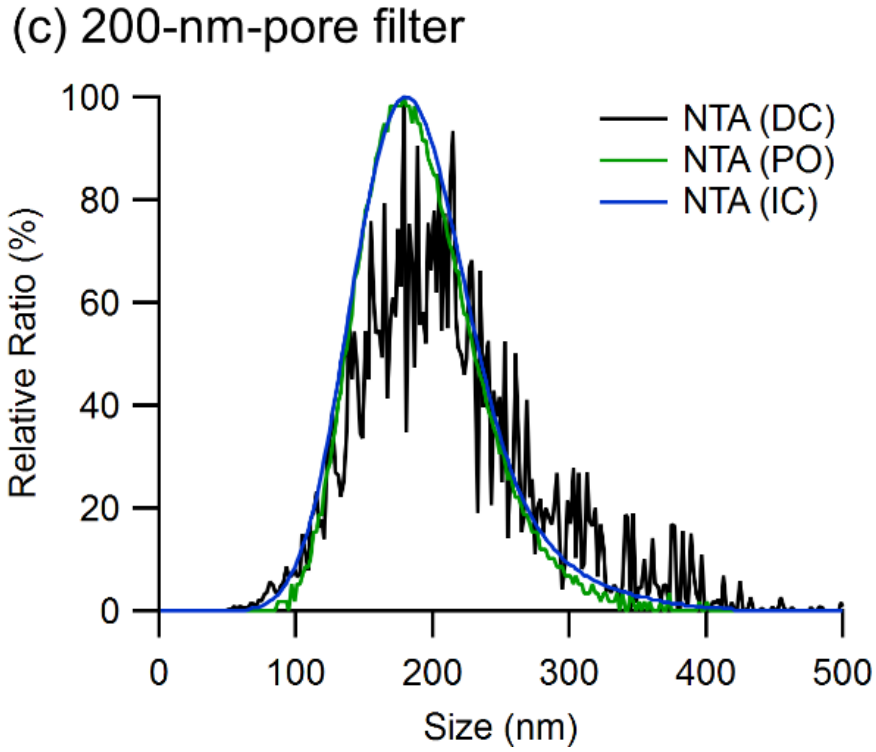
(c) 200-nm-pore filter
Relative Ratio (%)
Size (nm)
NTA (DC)
NTA (PO)
NTA (IC)
0
20
40
60
80
100
0
100
200
300
400
500

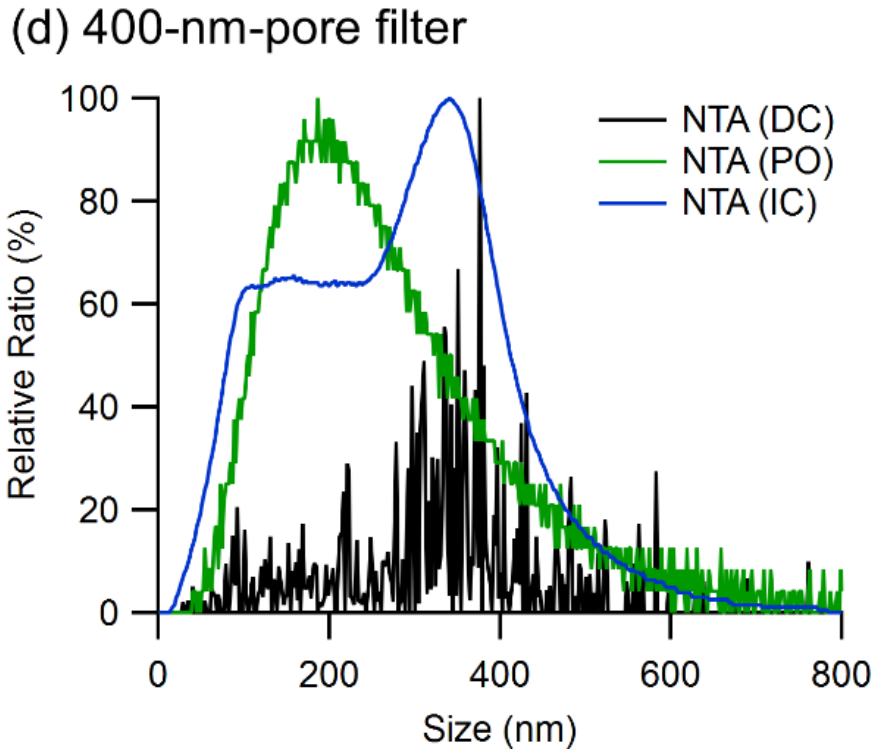
(d) 400-nm-pore filter
Relative Ratio (%)
Size (nm)
NTA (DC)
NTA (PO)
NTA (IC)
0
20
40
60
80
100
0
200
400
600
800

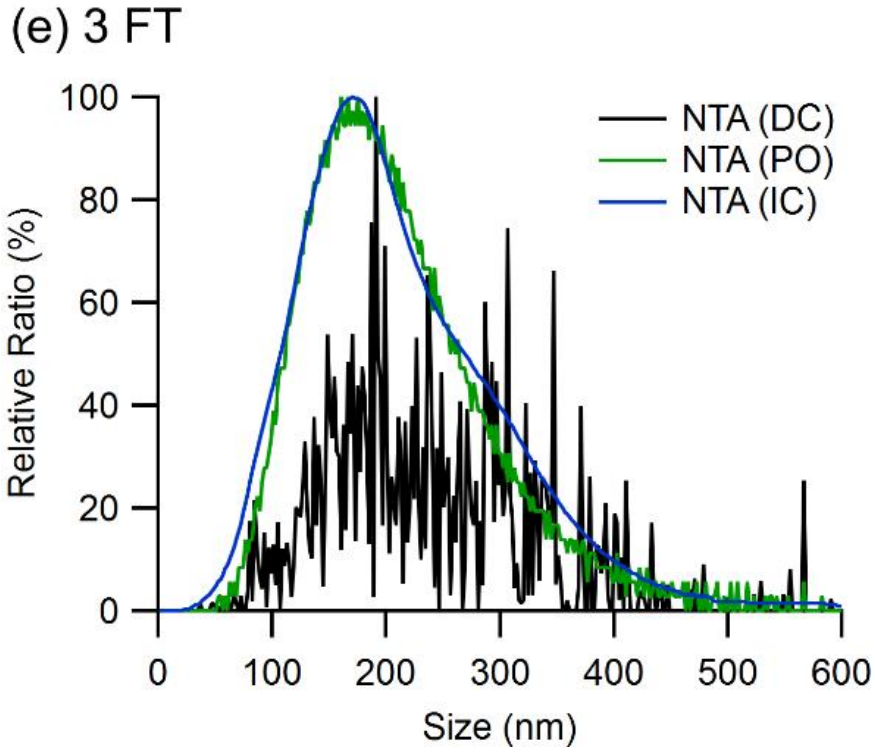
(e) 3 FT
Relative Ratio (%)
Size (nm)
NTA (DC)
NTA (PO)
NTA (IC)
0
20
40
60
80
100
0
100
200
300
400
500
600

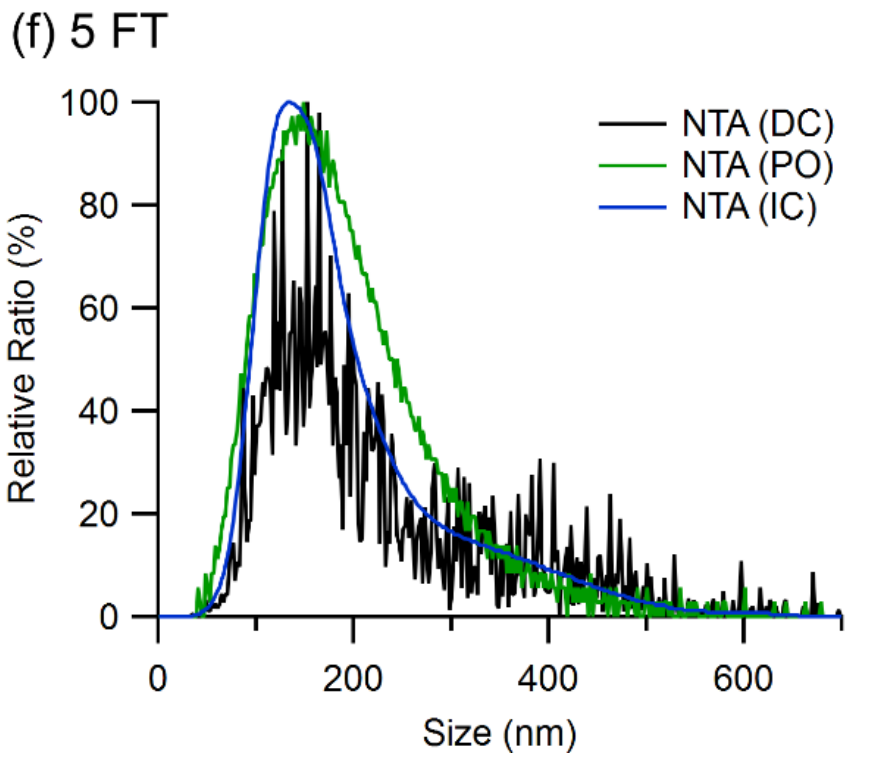
(f) 5 FT
Relative Ratio (%)
100
80
60
40
20
0
0
200
400
600
Size (nm)
NTA (DC)
NTA (PO)
NTA (IC)

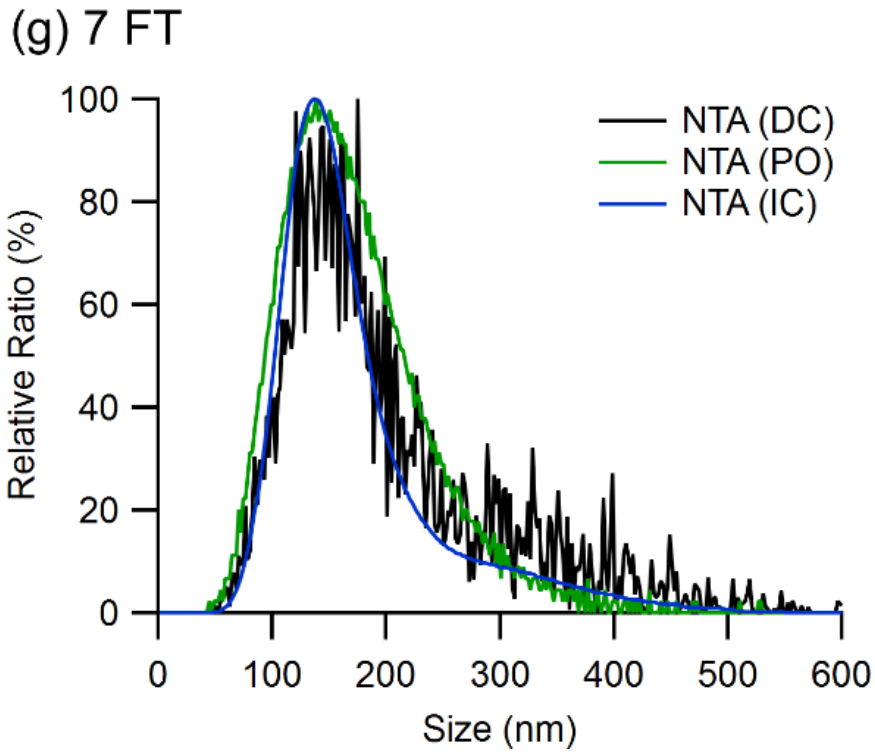
(g) 7 FT
Relative Ratio (%)
100
80
60
40
20
0
0
100
200
300
400
500
600
Size (nm)
NTA (DC)
NTA (PO)
NTA (IC)

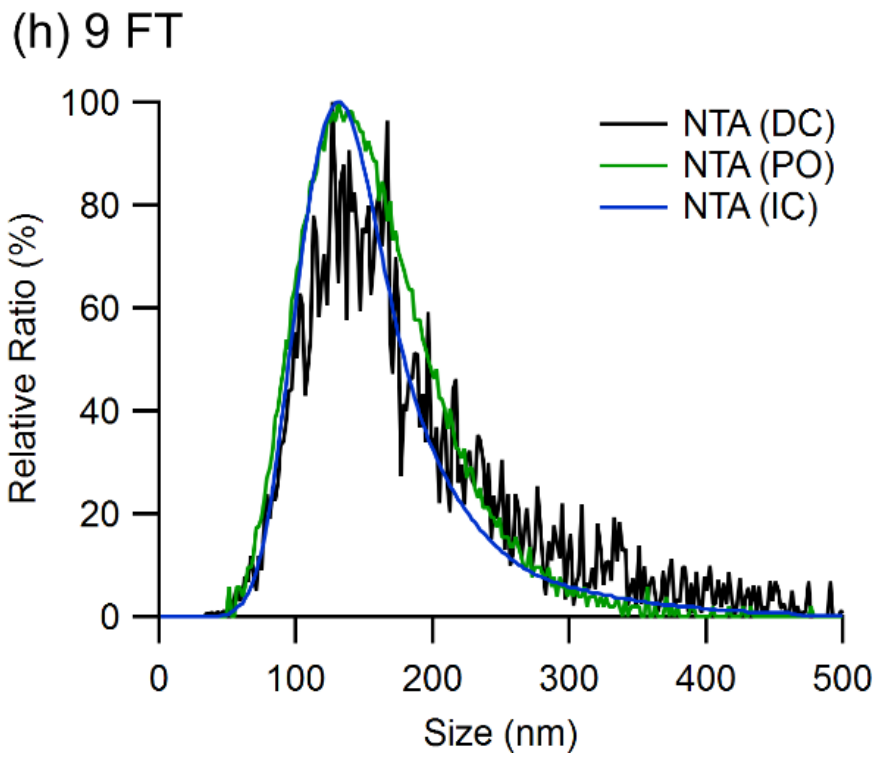
(h) 9 FT
Relative Ratio (%)
100
80
60
40
20
0
0
100
200
300
400
500
Size (nm)
NTA (DC)
NTA (PO)
NTA (IC)

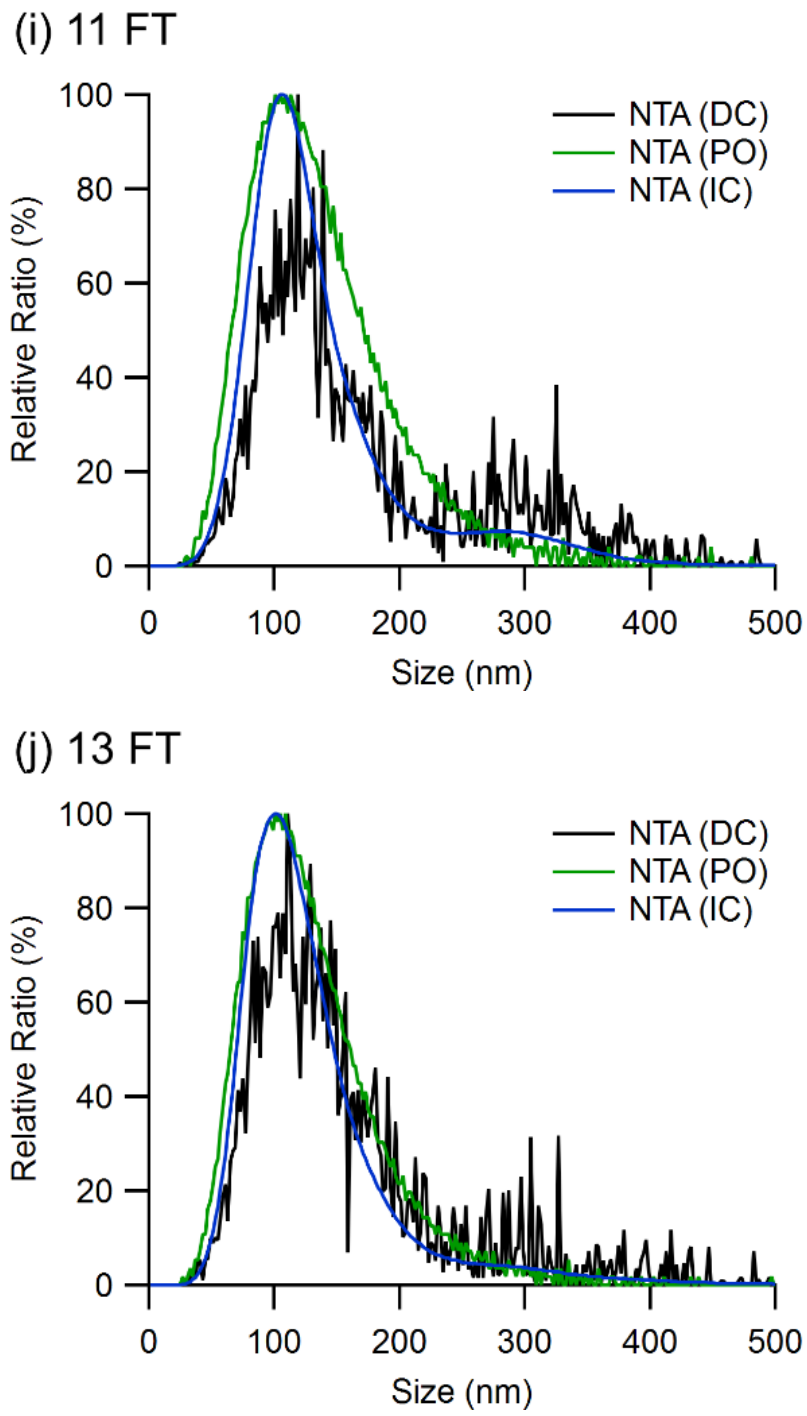

Figure 4.6 Comparison of the size distributions of the POPC vesicle samples analyzed by the different size distribution estimation methods for NTA measurements. The direct conversion (black), FTLA (green) and the iterative (blue) methods were applied for the size distribution estimations. The vesicle samples were prepared by extrusion through (a) 50-nm, (b) 100-nm, (c) 200-nm and (d) 400-nm pore filter or by freeze-thaw treatment (e-l) of 3 to 17 cycles before extrusion through a 400-nm pore filter. The bin width of the size distributions is in 2 nm.

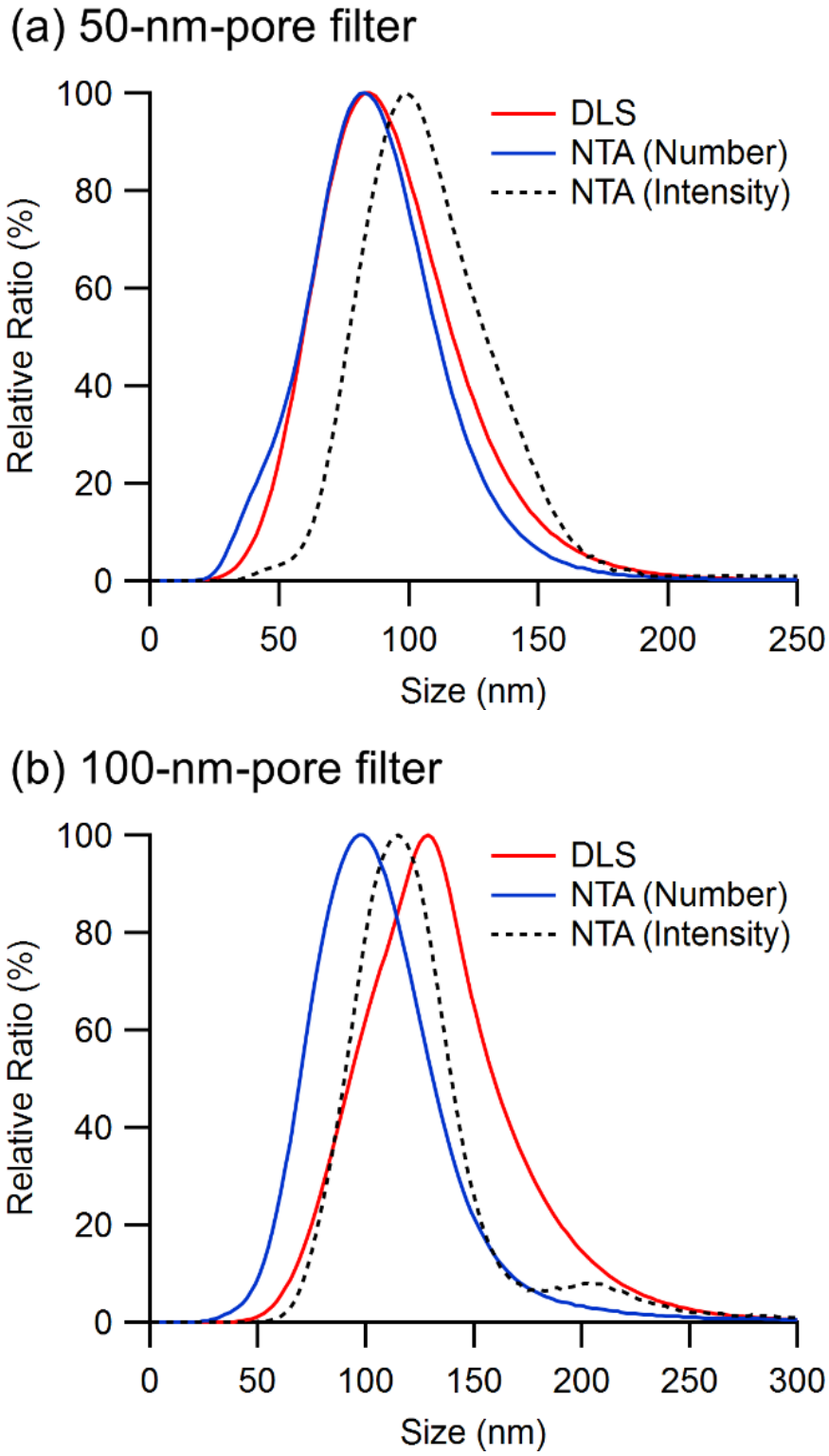
(a) 50-nm-pore filter
Relative Ratio (%)
Size (nm)
DLS
NTA (Number)
NTA (Intensity)
0
20
40
60
80
100
0
50
100
150
200
250
(b) 100-nm-pore filter
Relative Ratio (%)
Size (nm)
DLS
NTA (Number)
NTA (Intensity)
0
20
40
60
80
100
0
50
100
150
200
250
300

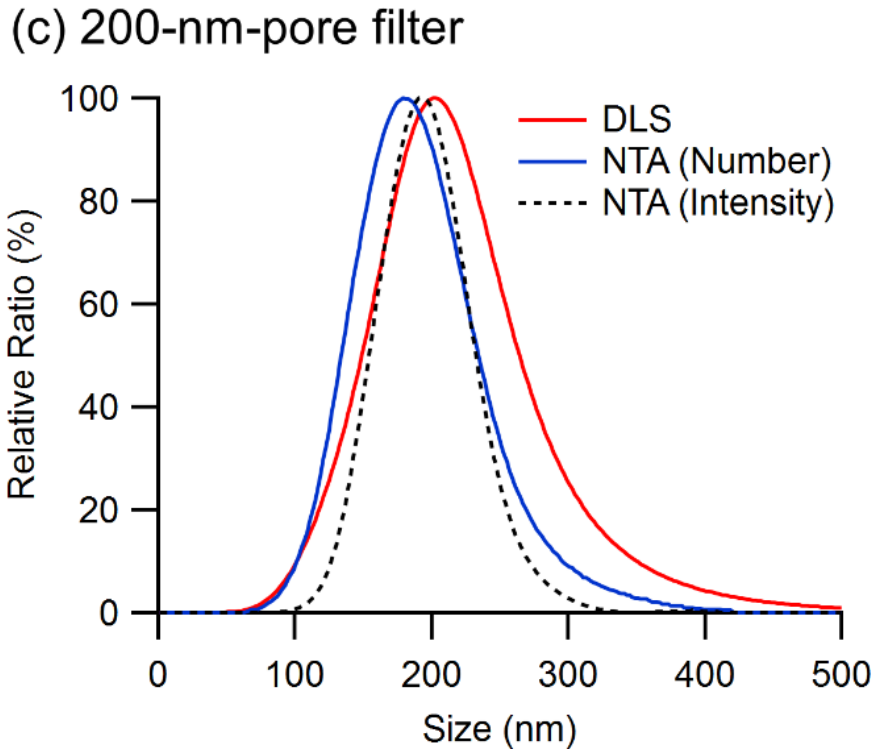
(c) 200-nm-pore filter
Relative Ratio (%)
100
80
60
40
20
0
0
100
200
300
400
500
Size (nm)
DLS
NTA (Number)
NTA (Intensity)

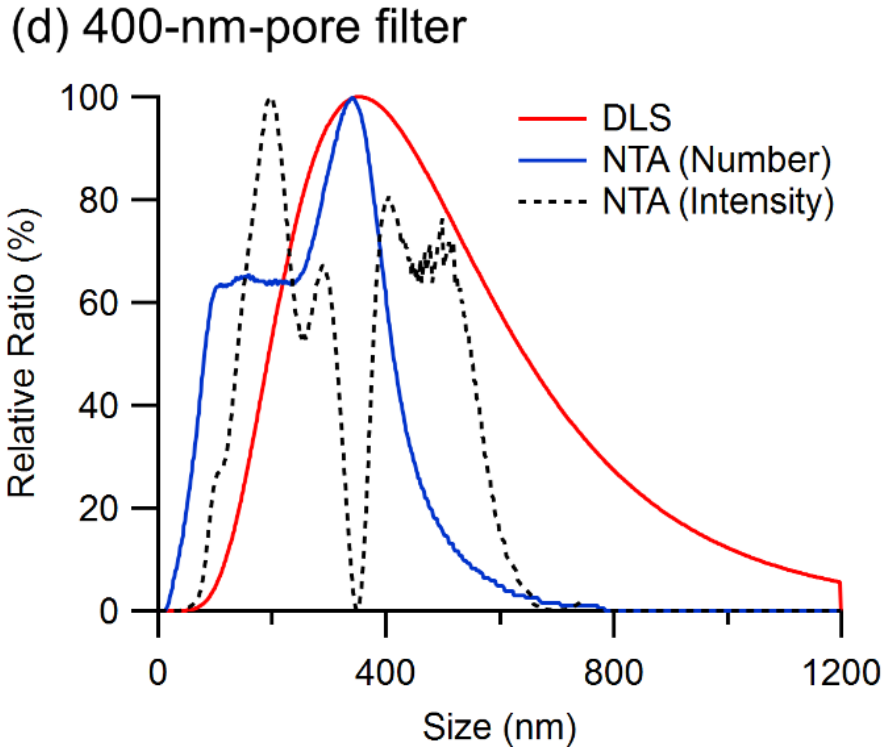
(d) 400-nm-pore filter
Relative Ratio (%)
100
80
60
40
20
0
0
400
800
1200
Size (nm)
DLS
NTA (Number)
NTA (Intensity)

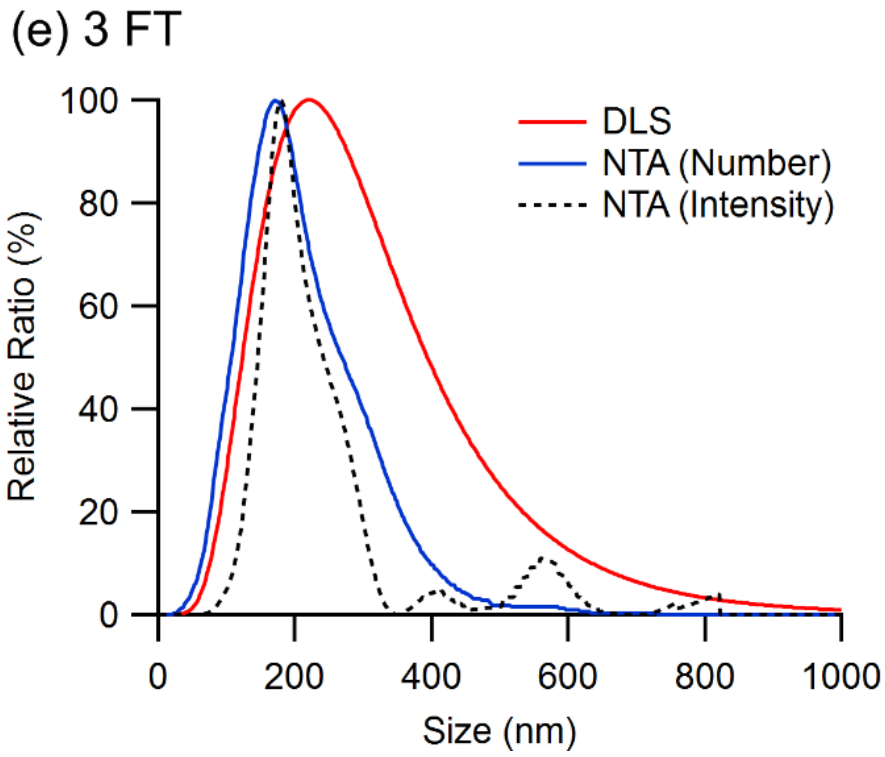
(e) 3 FT
Relative Ratio (%)
100
80
60
40
20
0
0
200
400
600
800
1000
Size (nm)
DLS
NTA (Number)
NTA (Intensity)

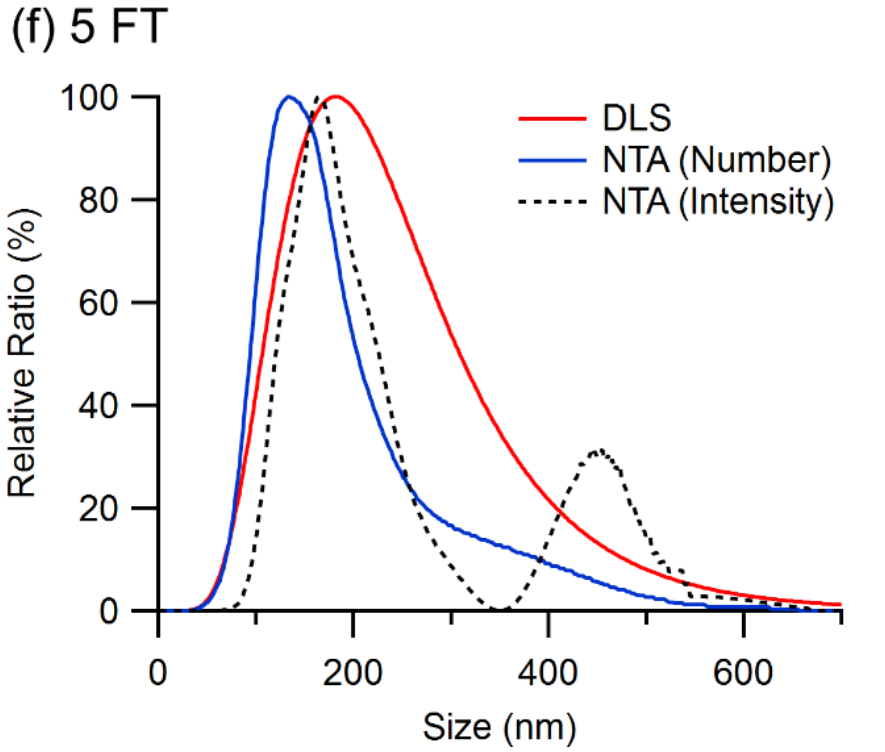
(f) 5 FT
Relative Ratio (%)
100
80
60
40
20
0
0
200
400
600
Size (nm)
DLS
NTA (Number)
NTA (Intensity)

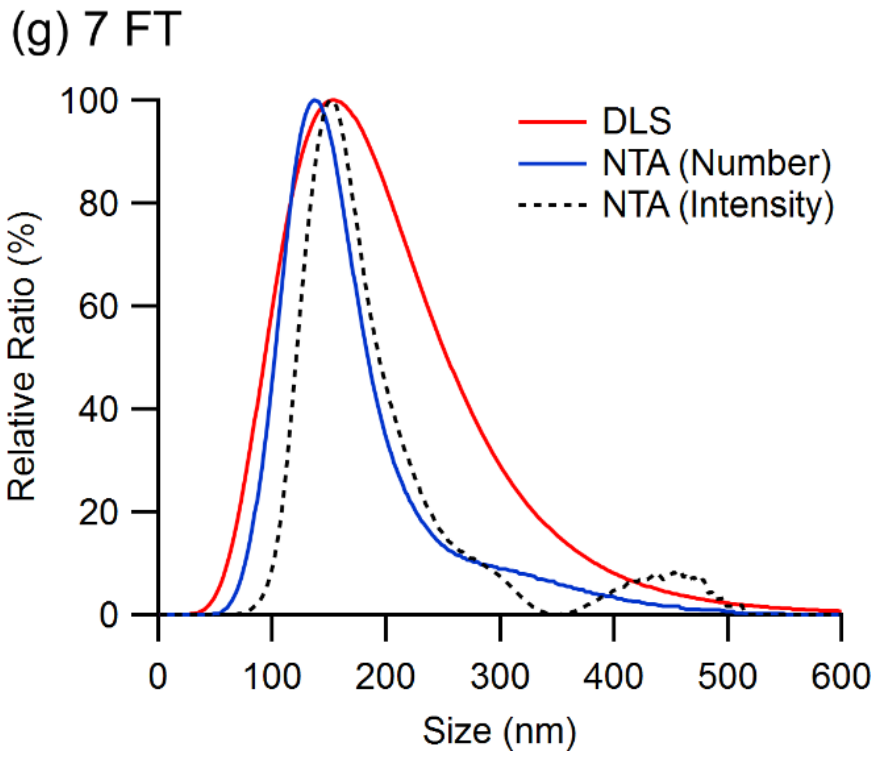
(g) 7 FT
Relative Ratio (%)
100
80
60
40
20
0
0
100
200
300
400
500
600
Size (nm)
DLS
NTA (Number)
NTA (Intensity)

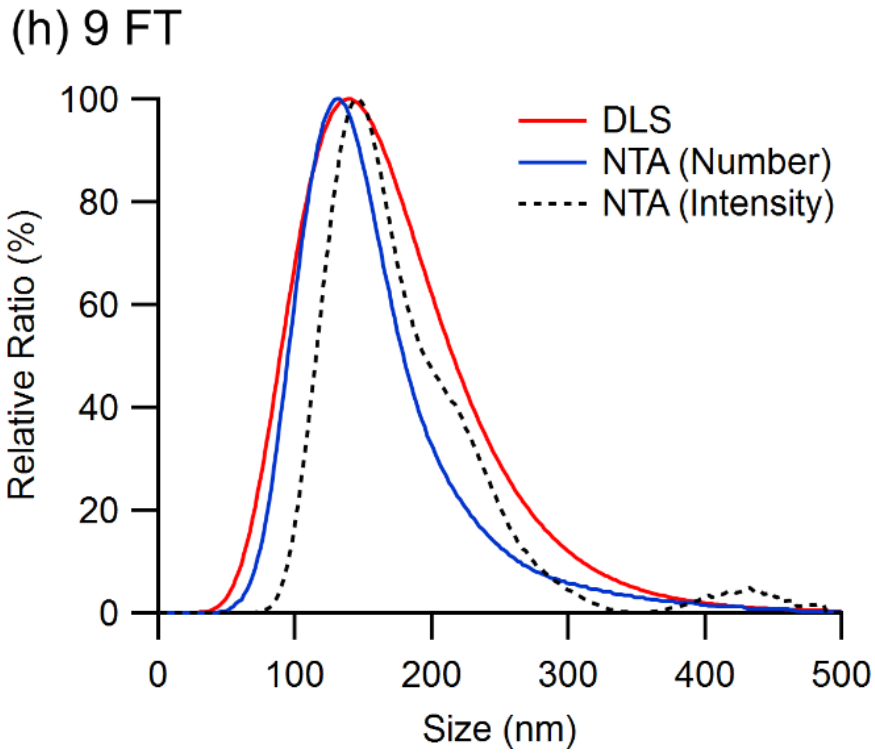
(h) 9 FT
Relative Ratio (%)
100
80
60
40
20
0
0
100
200
300
400
500
Size (nm)
DLS
NTA (Number)
NTA (Intensity)

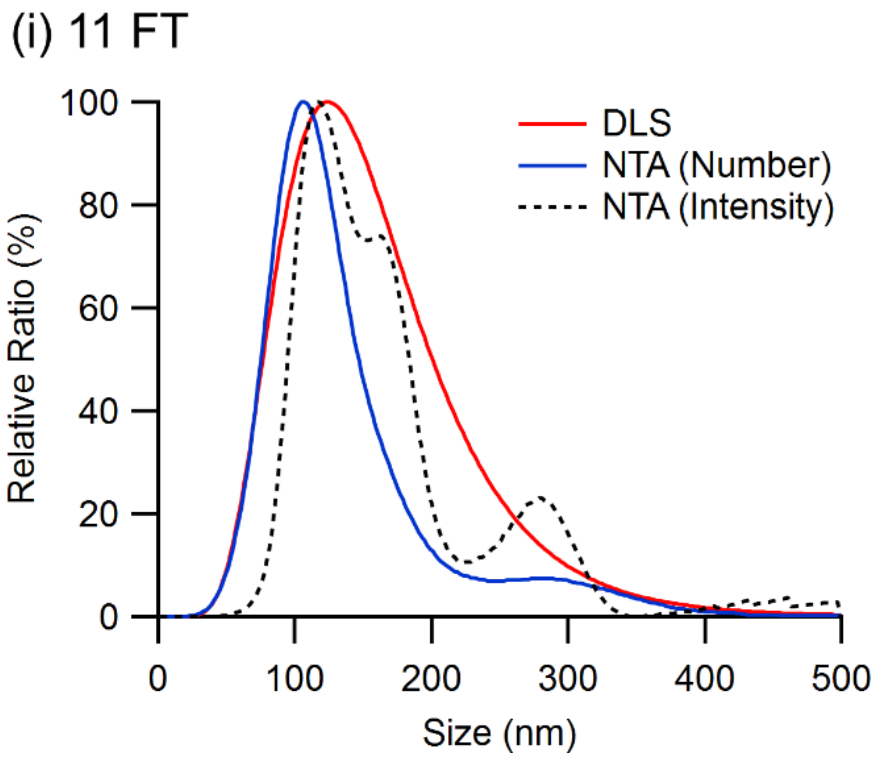
(i) 11 FT
Relative Ratio (%)
100
80
60
40
20
0
0
100
200
300
400
500
Size (nm)
DLS
NTA (Number)
NTA (Intensity)

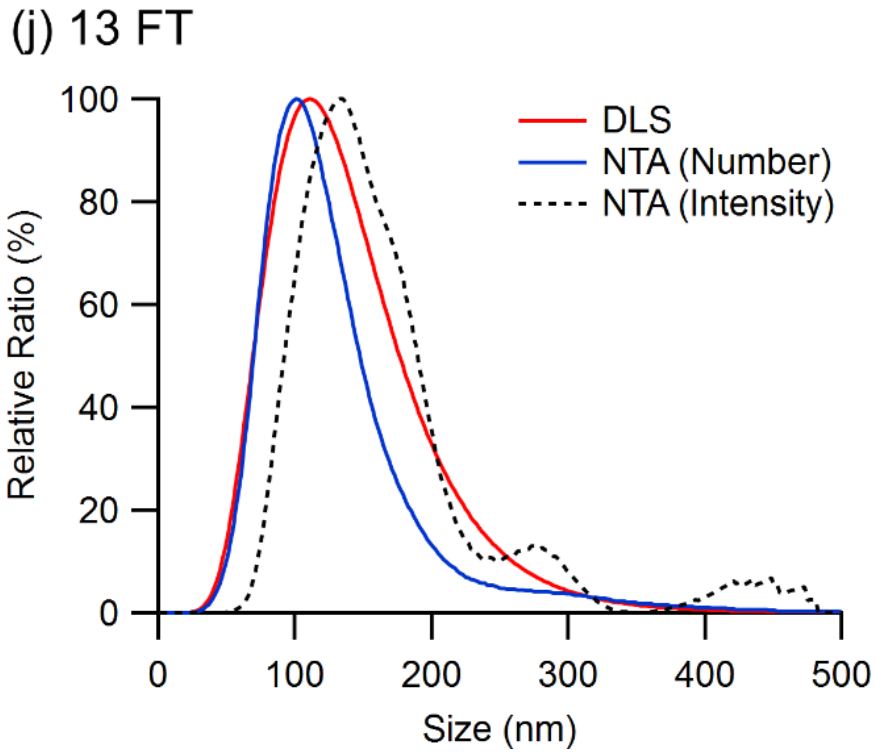
(j) 13 FT
Relative Ratio (%)
100
80
60
40
20
0
0
100
200
300
400
500
Size (nm)
DLS
NTA (Number)
NTA (Intensity)

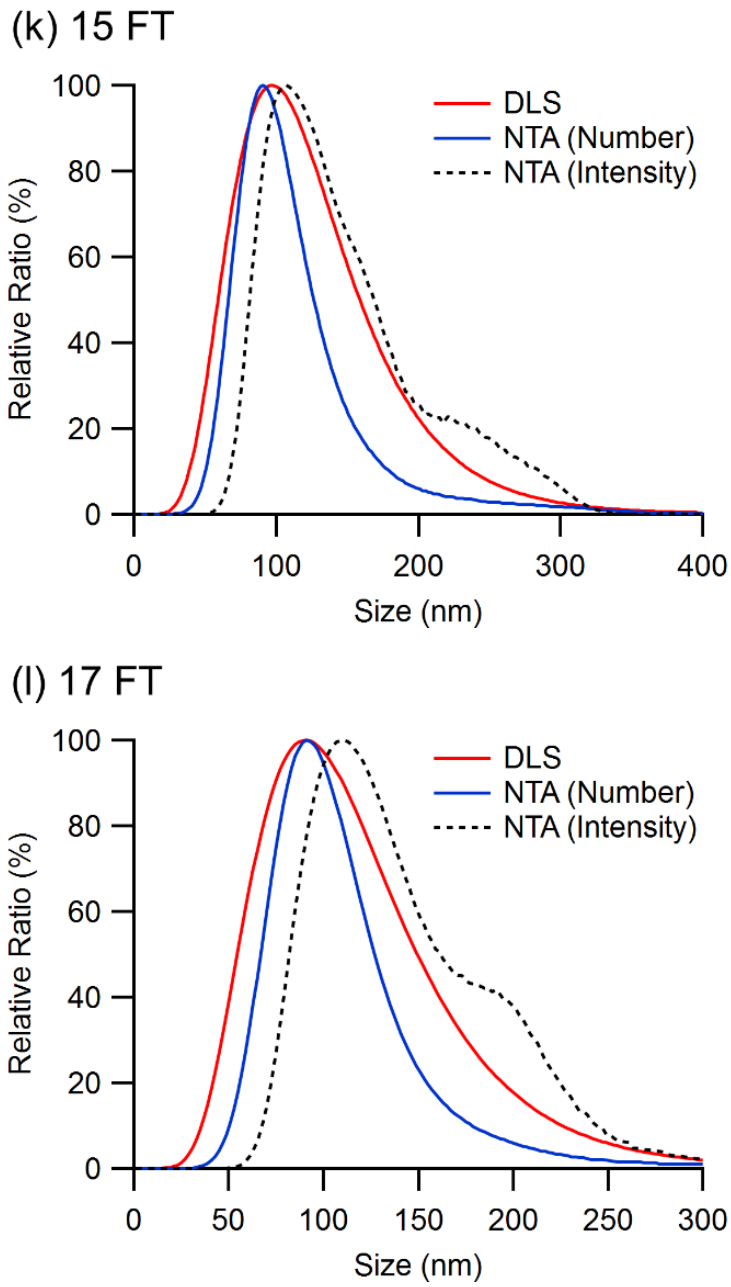

Figure 4.7 Size distribution of the POPC vesicle samples prepared in various polydispersity conditions measured by DLS and NTA. DLS results (solid red line) are from the cumulant method while NTA results (solid blue line) are acquired by applying the iterative method. For comparison, the size distribution of NTA is reconstructed into an intensity-weighted distribution (dotted black line) by introducing the thin-shell sphere model for the conversion. The vesicle samples were prepared by extrusion through (a) 50-nm, (b) 100-nm, (c) 200-nm and (d) 400-nm pore filters or by freeze-thaw treatment of (e-l) 3 to 17 cycles before extrusion through a 400-nm pore filter.

By applying the iterative method as the preferred method for the size distribution estimation of NTA measurements, the size distributions of the vesicle samples acquired by DLS and NTA are compared in Figure 4.7. A comparison of the distribution profiles shows that the size distribution of the vesicle samples is monomodal for most of the samples except V400 and the distribution from NTA is shifted toward smaller sizes than its corresponding distribution from DLS. This shift can be attributed to the different physical quantity that the two measurement techniques acquire, i.e., the intensity of scattered light and number of particles for DLS and NTA, respectively, indicating a larger shift for higher polydispersity [45, 48]. However, the shift (i.e., the difference in the mean sizes measured by DLS and NTA), is very small compared with the acquired PI and RV of the samples even after applying the iterative method for better size estimation of NTA.

Filipe et al. [52] proposed that the small shift can be explained by the lower detection limit of DLS, which detects small particles below 30 nm, which also explains the relatively high PI value measured by DLS. It expects a smaller RV for a size distribution acquired by NTA than the corresponding PI by DLS since NTA would neglect the small size range from the true size distribution and produce a narrower distribution. However, the results of FT11 and FT13 show that their respective RV from NTA is larger than their corresponding PI from DLS while the mean size of each sample measured by NTA and DLS is similar, which is contradictory to the expectation.

Theoretically, the small difference in the mean sizes measured by DLS and NTA can be due to the complex nature of the light scattering intensity in relation to the scattering form factor of the sample [48]. Therefore, the number-weighted size distribution acquired by NTA was reconstructed into an intensity-weighted distribution (as shown in Figure 4.7) by assuming an isotropic thin-shell hollow sphere model for the vesicle samples and introducing the RGD approximation to construct the form factor [48, 55, 71] The reconstruction revealed mean sizes of 102 ± 1, 118 ± 9, 191 ± 4 and 279 ± 46 nm and RVs of 0.065, 0.056, 0.033 and 0.271 for V50, V100, V200 and V400, respectively, and mean sizes of 209 ± 17, 201 ± 7, 173 ± 4, 165 ± 3, 147 ± 6, 148 ± 5,

131 ± 2 and 130 ± 3 nm and RVs of 0.116 ± 0.045, 0.169 ± 0.021, 0.090 ± 0.020, 0.076 ± 0.002, 0.113 ± 0.019, 0.128 ± 0.002, 0.110 ± 0.003 and 0.102 ± 0.013 for the vesicle samples treated with 3 to 17 FT cycles, respectively.

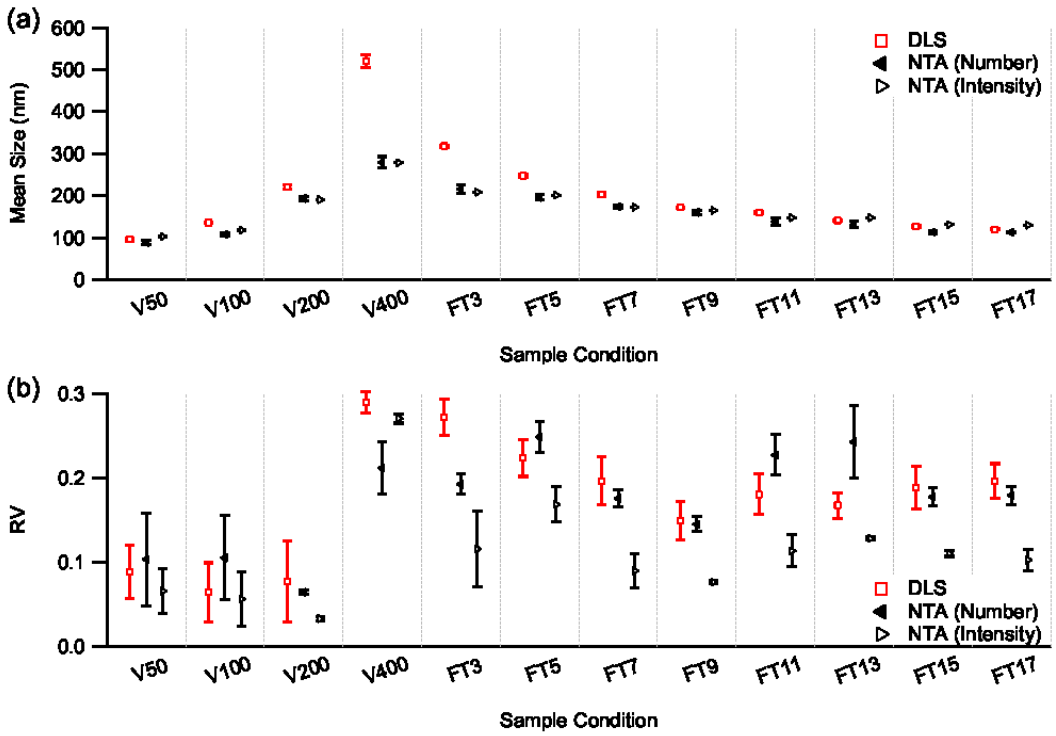

Figure 4.8 (a) Mean size and (b) relative variance of the POPC vesicle samples measured by NTA compared with DLS (open red square). NTA results were analyzed by the iterative method (solid black triangle) and reconstructed into an intensity-weighted distribution (open black triangle) using the thin-shell sphere model for the conversion.

Figure 4.8 compares the mean sizes and RVs of the original number-weighted and the converted intensity-weighted distributions from NTA with those from DLS. The mean sizes measured by NTA and those acquired from its reconstructed intensity-weighted size distribution are very close to each other. However, the RVs from the reconstructed NTA size distributions are significantly low for some samples, but it is questionable if those samples can be considered monodisperse based only on the reconstructed values. This result indicates that converting the NTA size distribution to an intensity-weighted distribution does not effectively mitigate the difference in the mean sizes observed by

DLS and NTA and that it is better to compare the measurements by DLS and NTA when the size distributions are expressed in their original weightings.

4.5 Conclusion

This chapter introduces and compares two particle size measurement techniques, DLS and NTA, for the size characterization of polydisperse macromolecular assemblies. While both techniques acquire size information by detecting the diffusion coefficient of the measured particles, they differ in the quantity of the size distribution they provide, i.e. number from NTA and intensity from DLS. Three size distribution estimation methods for NTA were tested to compare their performance using monomodal PS latex standards. The two MLE-based methods, i.e., the FTLA and iterative methods, produced results comparable to each other and in line with those from DLS while the direct conversion resulted in a larger variance, especially for small particles, due to the limitation of obtaining sufficiently long particle tracks. This result indicates that an MLE-based approach should be applied for the accurate measurement of small sized particles with NTA.

The two MLE-based size distribution estimation methods for NTA were further tested on measurements of polydisperse vesicle samples prepared in various polydispersities, which obtained the same mean sizes despite their different strategies to finding the optimal size distribution from the given track data. However, the calculated likelihood of the acquired size distributions obtained by the two methods indicated that FTLA sacrificed likelihood at the expense of a smoother size distribution, further suggesting that the iterative method is preferable for polydisperse samples.

The results for the vesicle samples obtained by NTA using the iterative method were then compared with those from DLS. The mean sizes were comparable except for those samples with a very high polydispersity index, i.e., V400 and FT3. However, the mean sizes of some samples, e.g., FT9 to FT17, measured by NTA were larger than or very close to those from DLS, which seems contradictory to the fact that the mean size from

an intensity-weighted size distribution is larger than that from its corresponding number-weighted size distribution. Although the low size detection limit of NTA was pointed out as a source of the contradiction by reducing the variance measured by NTA, it does not fully explain why the mean sizes of V50 were less different between DLS and NTA compared with V100 and V200 despite its higher PI value.

Additionally, the number-weighted size distribution of the vesicle samples from NTA was converted into an intensity-weighted distribution by assuming the thin-shell hollow sphere model with the RGD approximation to verify the influence of the different quantities that DLS and NTA produce. While the mean size given by NTA after conversion was very close to the value before conversion, the RV after the conversion was much reduced compared to that from DLS and NTA. Considering the nature of the vesicle samples, it is questionable whether the small relative variance after reconstruction is reliable. Therefore, the conversion of a number-weighted size distribution of NTA into an intensity-weighted one does not seem to effectively explain the difference in the mean sizes measured by DLS and NTA, and the size information from DLS and NTA is better compared in their original weightings.

References

[1] Shi, J., et al., Nanotechnology in drug delivery and tissue engineering: from discovery to applications. *Nano Lett*, 2010. **10**(9): p. 3223-30.

[2] Parveen, S., R. Misra, and S.K. Sahoo, Nanoparticles: a boon to drug delivery, therapeutics, diagnostics and imaging. *Nanomedicine*, 2012. **8**(2): p. 147-66.

[3] Blanco, E., H. Shen, and M. Ferrari, Principles of nanoparticle design for overcoming biological barriers to drug delivery. *Nat Biotechnol*, 2015. **33**(9): p. 941-51.

[4] Chang, H.I. and M.K. Yeh, Clinical development of liposome-based drugs: formulation, characterization, and therapeutic efficacy. *Int J Nanomedicine*, 2012. **7**: p. 49-60.

[5] Tan, M.L., P.F. Choong, and C.R. Dass, Recent developments in liposomes, microparticles and nanoparticles for protein and peptide drug delivery. *Peptides*, 2010. **31**(1): p. 184-93.

[6] Bamrungsap, S., et al., Nanotechnology in therapeutics: a focus on nanoparticles as a drug delivery system. *Nanomedicine (Lond)*, 2012. **7**(8): p. 1253-71.

[7] Warne, N.W., Development of high concentration protein biopharmaceuticals: the use of platform approaches in formulation development. *Eur J Pharm Biopharm*, 2011. **78**(2): p. 208-12.

[8] Tsuchikama, K. and Z. An, Antibody-drug conjugates: recent advances in conjugation and linker chemistries. *Protein Cell*, 2018. **9**(1): p. 33-46.

[9] Li, B.L., et al., Directing Assembly and Disassembly of 2D MoS2 Nanosheets with DNA for Drug Delivery. *ACS Appl Mater Interfaces*, 2017. **9**(18): p. 15286-15296.

[10] Komiyama, M., et al., Chemistry Can Make Strict and Fuzzy Controls for Bio-Systems: DNA Nanoarchitectonics and Cell-Macromolecular Nanoarchitectonics. *Bull Chem Soc Jpn*, 2017. **90**(9): p. 967-1004.

[11] Muller, R.H. and C.M. Keck, Challenges and solutions for the delivery of biotech drugs--a review of drug nanocrystal technology and lipid nanoparticles. *J Biotechnol*, 2004. **113**(1-3): p. 151-70.

[12] Brigger, I., C. Dubernet, and P. Couvreur, Nanoparticles in cancer therapy and diagnosis. *Adv Drug Deliv Rev*, 2012. **64**: p. 24-36.

[13] Barenholz, Y., Doxil ®, the first FDA-approved nano-drug: Lessons learned. *J Control Release*, 2012. **160**(2): p. 117-134.

[14] Cavalli, A., et al., Multi-target-directed ligands to combat neurodegenerative diseases. *J Med Chem*, 2008. **51**(3): p. 347-372.

[15] Sams-Dodd, F., Target-based drug discovery: is something wrong? *Drug Discov Today*, 2005. **10**(2): p. 139-147.

[16] Gregoriadis, G., Engineering liposomes for drug delivery: Progress and problems. *Trends Biotechnol*, 1995. **13**(12): p. 527-537.

[17] Rawat, M., et al., Nanocarriers: promising vehicle for bioactive drugs. *Biol Pharm Bull*, 2006. **29**(9): p. 1790-8.

[18] Al-Jamal, W.T. and K. Kostarelos, Liposomes: from a clinically established drug delivery system to a nanoparticle platform for theranostic nanomedicine. *Acc Chem Res*, 2011. **44**(10): p. 1094-104.

[19] Metselaar, J.M. and G. Storm, Liposomes in the treatment of inflammatory disorders.

Expert Opin Drug Deliv, 2005. **2**(3): p. 465-76.

[20] He, C.B., et al., Size-dependent absorption mechanism of polymeric nanoparticles for oral delivery of protein drugs. *Biomaterials*, 2012. **33**(33): p. 8569-8578.

[21] Banerjee, A., et al., Role of nanoparticle size, shape and surface chemistry in oral drug delivery. *J Control Release*, 2016. **238**: p. 176-185.

[22] Coradeghini, R., et al., Size-dependent toxicity and cell interaction mechanisms of gold nanoparticles on mouse fibroblasts. *Toxicol Lett*, 2013. **217**(3): p. 205-16.

[23] Braun, N.J., et al., Modification of the protein corona-nanoparticle complex by physiological factors. *Mater Sci Eng C Mater Biol Appl*, 2016. **64**: p. 34-42.

[24] Hama, S., et al., Overcoming the polyethylene glycol dilemma via pathological environment-sensitive change of the surface property of nanoparticles for cellular entry. *J Control Release*, 2015. **206**: p. 67-74.

[25] Natarajan, S.K. and S. Selvaraj, Mesoporous silica nanoparticles: importance of surface modifications and its role in drug delivery. *RSC Advances*, 2014. **4**(28): p. 14328-14334.

[26] Soliman, G.M., et al., Tailoring the efficacy of nimodipine drug delivery using nanocarriers based on A2B miktoarm star polymers. *Biomaterials*, 2010. **31**(32): p. 8382-92.

[27] Coelho, J.F., et al., Drug delivery systems: Advanced technologies potentially applicable in personalized treatments. *EPMA J*, 2010. **1**(1): p. 164-209.

[28] Love, W.G., et al., Specific accumulation of cholesterol-rich liposomes in the inflammatory tissue of rats with adjuvant arthritis. *Ann Rheum Dis*, 1990. **49**(8): p. 611-4.

[29] Hua, S. and S.Y. Wu, The use of lipid-based nanocarriers for targeted pain therapies. *Front Pharmacol*, 2013. **4**: p. 7.

[30] de Temmerman, P.J., et al., Size measurement uncertainties of near-monodisperse, near-spherical nanoparticles using transmission electron microscopy and particle-tracking analysis. *Journal of Nanoparticle Research*, 2014. **16**(10): p. 17.

[31] Troiber, C., et al., Comparison of four different particle sizing methods for siRNA polyplex characterization. *European Journal of Pharmaceutics and Biopharmaceutics*, 2013. **84**(2): p. 255-264.

[32] Fraunhofer, W., G. Winter, and C. Coester, Asymmetrical flow field-flow fractionation and multiangle light scattering for analysis of gelatin nanoparticle drug carrier systems. *Anal Chem*, 2004. **76**(7): p. 1909-20.

[33] Liu, J., J.D. Andya, and S.J. Shire, A critical review of analytical ultracentrifugation and field flow fractionation methods for measuring protein aggregation. *AAPS J*, 2006. **8**(3): p. E580-E589.

[34] Berne, B.J. and R. Pecora, *Dynamic light scattering: with applications to chemistry, biology, and physics*. Dover ed. 2000, Mineola, N.Y.: Dover Publications. vii, 376 pp.

[35] Maulucci, G., et al., Particle size distribution in DMPC vesicles solutions undergoing different sonication times. *Biophys J*, 2005. **88**(5): p. 3545-50.

[36] Merkus, H.G., *Particle size measurements: fundamentals, practice, quality*. Particle Technology Series. 2009, New York: Springer. xii, 533 pp.

[37] Sokolova, V., et al., Characterisation of exosomes derived from human cells by nanoparticle tracking analysis and scanning electron microscopy. *Colloids Surf B Biointerfaces*, 2011. **87**(1): p. 146-50.

[38] Anderson, W., et al., A comparative study of submicron particle sizing platforms: accuracy, precision and resolution analysis of polydisperse particle size distributions. *J Colloid Interface Sci*, 2013. **405**: p. 322-30.

[39] Bootz, A., et al., Comparison of scanning electron microscopy, dynamic light scattering and analytical ultracentrifugation for the sizing of poly(butyl cyanoacrylate) nanoparticles. *Eur J Pharm Biopharm*, 2004. **57**(2): p. 369-75.

[40] Striegel, A.M., Modern size-exclusion liquid chromatography : practice of gel permeation and gel filtration chromatography. 2nd ed. 2009: Hoboken, N.J.: Wiley.

[41] Yohannes, G., et al., Asymmetrical flow field-flow fractionation technique for separation and characterization of biopolymers and bioparticles. *J Chromatogr A*, 2011. **1218**(27): p. 4104-4116.

[42] Wyatt, P.J., Light scattering and the absolute characterization of macromolecules. *Anal Chim Acta*, 1993. **272**(1): p. 1-40.

[43] Podzimek, S., Light scattering, size exclusion chromatography, and asymmetric flow field flow fractionation : powerful tools for the characterization of polymers, proteins, and nanoparticles. 2011: Hoboken, N.J.: Wiley.

[44] van der Pol, E., et al., Innovation in detection of microparticles and exosomes. *J Thromb Haemost*, 2013. **11 Suppl 1**: p. 36-45.

[45] Hassan, P.A., S. Rana, and G. Verma, Making sense of Brownian motion: colloid characterization by dynamic light scattering. *Langmuir*, 2015. **31**(1): p. 3-12.

[46] Stetefeld, J., S.A. McKenna, and T.R. Patel, Dynamic light scattering: a practical guide and applications in biomedical sciences. *Biophysical Reviews*, 2016. **8**(4): p. 409-427.

[47] Boyd, R.D., S.K. Pichaimuthu, and A. Cuenat, New approach to inter-technique comparisons for nanoparticle size measurements: using atomic force microscopy, nanoparticle tracking analysis and dynamic light scattering. *Colloids and Surfaces A: Physicochemical and Engineering Aspects*, 2011. **387**(1-3): p. 35-42.

[48] Hallett, F.R., J. Watton, and P. Krygsman, Vesicle sizing: Number distributions by dynamic light scattering. *Biophys J*, 1991. **59**(2): p. 357-362.

[49] Bell, N.C., et al., Emerging techniques for submicrometer particle sizing applied to Stober silica. *Langmuir*, 2012. **28**(29): p. 10860-72.

[50] Amini, R., et al., Intertechnique comparisons for nanoparticle size measurements and shape distribution. *J Hazard Toxic Radioact Waste*, 2016. **20**(1): p. B4015004.

[51] Malloy, A. and B. Carr, NanoParticle tracking analysis - The Halo™ system. *Particle & Particle Systems Characterization*, 2006. **23**(2): p. 197-204.

[52] Filipe, V., A. Hawe, and W. Jiskoot, Critical evaluation of nanoparticle tracking analysis (NTA) by NanoSight for the measurement of nanoparticles and protein aggregates. *Pharmaceutical Research*, 2010. **27**(5): p. 796-810.

[53] James, A.E. and J.D. Driskell, Monitoring gold nanoparticle conjugation and analysis of biomolecular binding with nanoparticle tracking analysis (NTA) and dynamic light scattering (DLS). *Analyst*, 2013. **138**(4): p. 1212-8.

[54] Dragovic, R.A., et al., Sizing and phenotyping of cellular vesicles using nanoparticle tracking analysis. *Nanomedicine*, 2011. **7**(6): p. 780-8.

[55] Yang, D.T., et al., Evaluation of Nanoparticle Tracking for Characterization of Fibrillar Protein Aggregates. *AIChE J*, 2014. **60**(4): p. 1236-1244.

[56] Gross, J., et al., Nanoparticle tracking analysis of particle size and concentration detection in suspensions of polymer and protein samples: Influence of experimental

and data evaluation parameters. *European Journal of Pharmaceutics and Biopharmaceutics*, 2016. **104**: p. 30-41.

[57] Saveyn, H., et al., Accurate particle size distribution determination by nanoparticle tracking analysis based on 2-D Brownian dynamics simulation. *Journal of Colloid and Interface Science*, 2010. **352**(2): p. 593-600.

[58] Walker, J.G., Improved nano-particle tracking analysis. *Measurement Science and Technology*, 2012. **23**(6): p. 065605.

[59] Kestens, V., et al., Validation of a particle tracking analysis method for the size determination of nano- and microparticles. *Journal of Nanoparticle Research*, 2017. **19**(8): p. 271.

[60] *Particle size analysis: Dynamic light scattering (DLS)*, in *ISO 22412:2017*. 2017, International Standard Organization: Geneva, Switzerland.

[61] Koppel, D.E., Analysis of macromolecular polydispersity in intensity correlation spectroscopy: the method of cumulants. *J Chem Phys*, 1972. **57**(11): p. 4814-4820.

[62] Gardiner, C., et al., Extracellular vesicle sizing and enumeration by nanoparticle tracking analysis. *Journal of Extracellular Vesicles*, 2013. **2**.

[63] Lucy, L.B., Iterative technique for rectification of observed distributions. *Astronomical Journal*, 1974. **79**(6): p. 745-754.

[64] Veklerov, E. and J. Llacer, Stopping rule for the MLE algorithm based on statistical hypothesis testing. *IEEE Trans Med Imag*, 1987. **6**(4): p. 313-319.

[65] Hebert, T.J., Statistical stopping criteria for iterative maximum-likelihood reconstruction of emission images. *Phys Med Biol*, 1990. **35**(9): p. 1221-1232.

[66] Hanus, L.H. and H.J. Ploehn, Conversion of intensity-averaged photon correlation spectroscopy measurements to number-averaged particle size distributions. 1. Theoretical development. *Langmuir*, 1999. **15**(9): p. 3091-3100.

[67] Patty, P.J. and B.J. Frisken, Direct determination of the number-weighted mean radius and polydispersity from dynamic light-scattering data. *Appl Opt*, 2006. **45**(10): p. 2209-16.

[68] Pecora, R. and S.R. Aragon, Theory of light scattering from hollow spheres. *Chem Phys Lipids*, 1974. **13**(1): p. 1-10.

[69] Pencer, J. and F.R. Hallett, Effects of vesicle size and shape on static and dynamic

light scattering measurements. *Langmuir*, 2003. **19**(18): p. 7488-7497.

[70] Mayer, L.D., et al., Solute distributions and trapping efficiencies observed in freeze-thawed multilamellar vesicles. *Biochim Biophys Acta*, 1985. **817**(1): p. 193-6.

[71] Matsuzaki, K., et al., Optical characterization of liposomes by right angle light scattering and turbidity measurement. *Biochim Biophys Acta*, 2000. **1467**(1): p. 219-26.

Chapter 5*

Improved Size Determination by Nanoparticle Tracking Analysis: Influence of Recognition Radius

Nanoparticle Tracking Analysis is a size measurement technique that determines the size distribution of particles in suspension by tracking individual particles undergoing Brownian motion. A key element in the measurement analysis is the recognition radius, which distinguishes the individual, tracked particles from one another. However, by defining a finite radius, the displacement of tracked particles is effectively restricted, translating into an overestimation of particle size. A modified probability model that describes the restricted displacement of a tracked particle is introduced to achieve more accurate size distribution determination. Through virtual NTA measurement by computer simulations and real NTA experiments, the analytical performance of the modified displacement probability was tested in comparison to the conventional probability. Whereas the conventional displacement probability results in an overestimation of the particle size, the modified displacement probability mitigates the effect of the overestimation and provides more accurate mean size within an error of less than 6% the nominal size.

---

* This chapter is accepted as A. Kim, W. Bernt, and N.J. Cho. Improved Size Determination by Nanoparticle Tracking Analysis: Influence of Recognition Radius. *Analytical Chemistry* 91, 9508-9515 (2019). DOI: 10.1021/acs.analchem.9b00454.

5.1 Introduction

Dynamic light scattering (DLS) is a widely used technique to measure the size of suspended macromolecules and nanoparticles in liquid suspension [1-6]. Unlike other measurement techniques that often require sample preparation for sizing, DLS is a widely used technique for particle sizing because it has a label-free readout and measurements can be completed in a short amount of time [7-9]. However, DLS is also well known for its size-dependent sensitivity in determining particle size [8, 10-14]. By illuminating a sample in liquid with a laser beam and detecting the scattered light, DLS determines the size, or the hydrodynamic diameter, of the particles in the sample using its diffusion coefficient acquired from the autocorrelation of the scattered light [7, 8, 15]. Since the intensity of light scattered by a particle is approximately proportional to the square of the volume of the particle, the results of DLS often overestimate the size of polydisperse samples like macromolecules if the size distribution is wide [7, 8, 10].

Nanoparticle tracking analysis (NTA) is a recently developed technique that determines the particle size by measuring the diffusion coefficient of the particles in the sample as in DLS [16, 17]. While DLS detects the intensity of the scattered light to acquire the diffusion coefficient, NTA takes a series of two-dimensional images of the suspended particles in the liquid over time and measures the displacement of each particle from the images to convert into the diffusion coefficient [16, 18]. By tracking individual particles, NTA determines their respective diffusion coefficient and overcomes the size-dependent sensitivity that DLS has [18-20]. Since both DLS and NTA acquire the particle size using the diffusion coefficient by the Stokes-Einstein equation, the NTA is a complementary size measurement technique to DLS [21-24].

As the NTA technique is a relatively new technique, it is important to verify its operating performance to characterize nanoparticulate samples. Initial NTA studies focused on its validation in comparison to other measurement techniques, including DLS [18, 19, 21, 25]. Filipe et al. [18] used mono- and multi-modal nanoparticles to compare the accuracy and size resolution of NTA with those of DLS. They observed that NTA provided as consistent

results as DLS on monomodal nanoparticle samples and had a better size resolution than DLS on multi-modal nanoparticle samples, especially when there were a small number of very large particles in the samples.

Other studies investigated the accuracy of NTA regarding the track length or the number of frames over which a particle is tracked [19, 21, 25, 26]. As the uncertainty of the determined particle size by NTA is inversely proportional to the square root of the track length [19, 21, 27-29], they suggested a minimum track length to improve the deviation of the determined size distribution by NTA. Though screening tracks by the minimum track length improves the accuracy of the size determination by NTA, it is not always achievable to acquire tracks of sufficient length, especially when the particle concentration of a sample is high [25, 28, 29]. Recognizing that the track length acquired by NTA is finite, a few studies suggested improved size distribution determination methods based on the maximum likelihood estimation (MLE) principle [28, 29]. The methods try to find a size distribution that maximizes the likelihood of the acquired tracks by either an iterative approach [28] or a parameter optimization [29] assuming a certain size distribution form with adjustable parameters.

In the aforementioned studies, the authors assumed that the two-dimensional displacement of the tracked particles by NTA could be described by a Rayleigh distribution, the conventional distribution for Brownian motion in two dimensions. While the displacement described by the Rayleigh distribution allows unbounded displacements of a particle, meaning that the displacement of a particle can be infinite, the displacement of a tracked particle observed by NTA is bounded by the recognition radius, or the Max Jump Distance in the NTA software (version 3.0 and later) for Malvern Panalytical's NanoSight instruments, which determines the maximum displacement of a particle to be recognized as the same particle and rejects a longer displacement than the radius [25, 27]. This indicates that the measured displacement of particles by NTA is effectively reduced from its ideal displacement distribution, meaning that the measured size by NTA can be different from its true value due to the finite recognition radius [25, 30]. Van der Meeren et al. [25] investigated the effect of the recognition radius on NTA measurements using latex

nanoparticle samples and observed an overestimation of the measured size when using a small recognition radius. From this observation, they suggested that a recognition radius more than three times the diffusion length would be required for an accurate size determination since 99% of the observed displacements of the particles are within that range [25, 31]. However, they also found that such a requirement for a recognition radius is not always achievable since the inter-particle distance at higher particle concentration could effectively restrict the recognition radius. When the inter-particle distance is not sufficiently long with respect to the diffusion length of the particles, it could result in erroneous tracks where a neighboring particle is recognized as the tracked particle other than the tracked particle itself [25]. This necessitates the investigation on the influence of the recognition radius in determining the particle size in NTA measurements, especially when the recognition range is restricted and how to correct its effect to acquire more accurate results from NTA measurements.

Herein, a modified displacement probability is introduced so that it reflects the finite recognition radius for improved size distribution determination by NTA measurements. The modified probability was tested to mitigate the effect of the finite recognition radius in estimating the size distribution. The method is based on the iterative MLE approach suggested by Walker [28] and incorporates the modified probability into the likelihood calculation. To verify its feasibility, a series of computer simulations was made that generated particle tracks from virtual NTA measurements. With those tracks acquired from the simulation, the iterative MLE method was applied to determine a particle size distribution. Using the conventional and the modified displacement probabilities for the likelihood calculation of the iterative MLE method, the results from the two probabilities were compared. The comparison showed that the conventional probability overestimates the mean size of the size distribution if the recognition radius is short, in line with the theoretical calculation, whereas the mean size acquired with the modified probability is unaffected by the recognition radius and close to the nominal value. The results also showed that the conventional probability provides a very narrow size distribution on a small recognition radius even when the true size distribution is somewhat broad, while the modified probability overestimate the variance of the size distribution on the same small

recognition radius. From another simulation set with a bi-modal particle size distribution, it was also investigated if the two probabilities could resolve the two separated peaks from the determined size distribution and found that the modified probability works properly on a wider range of the recognition radius in resolving the two peaks than the conventional probability. In addition, the influence of the particle concentration was tested, showing that the variance of the determined size distribution increases and deviates from the nominal value as concentration increases. This deviation of the acquired relative variance appeared due to false tracks which tracked two different particles as the same particle over two successive images. The findings from the simulation were also confirmed by real NTA measurements.

5.2 Theory

NTA measures the size of nanoparticles in suspension by measuring the diffusion coefficient of individual particles and determines particle size based on the Stokes-Einstein equation [16, 18, 21]:

$$D = \frac{k_B T}{3\pi\eta d} \quad (5.1)$$

where D is the diffusion coefficient of a particle, k_B is the Boltzmann constant, T is the temperature, η is the viscosity of the medium and d is the hydrodynamic diameter of the particle. In NTA measurements, sequential images of the light scattered by suspended particles are recorded at fixed time intervals, providing the basis to determine the trajectories of individual particles which are known as tracks [16, 32]. The tracks, or the average squared displacement $\langle z \rangle$ of the tracks, are then related to the diffusion coefficient as expressed in Eq. 3.6.

When a particle is tracked, the two-dimensional position of the particle in an image frame is compared with that of the particles in the following frame. A particle in the following frame is assumed to be the same particle as in the previous frame if the distance between the two particles across the two successive frames is within an arbitrarily chosen distance, which is defined as the recognition radius [18, 25, 31]. This recognition process continues

for the subsequent image frames and forms a track of the particle until either no particle or two or more particles are found within the recognition radius in the following frame. The different recognition scenarios are outlined in Figure 5.1.

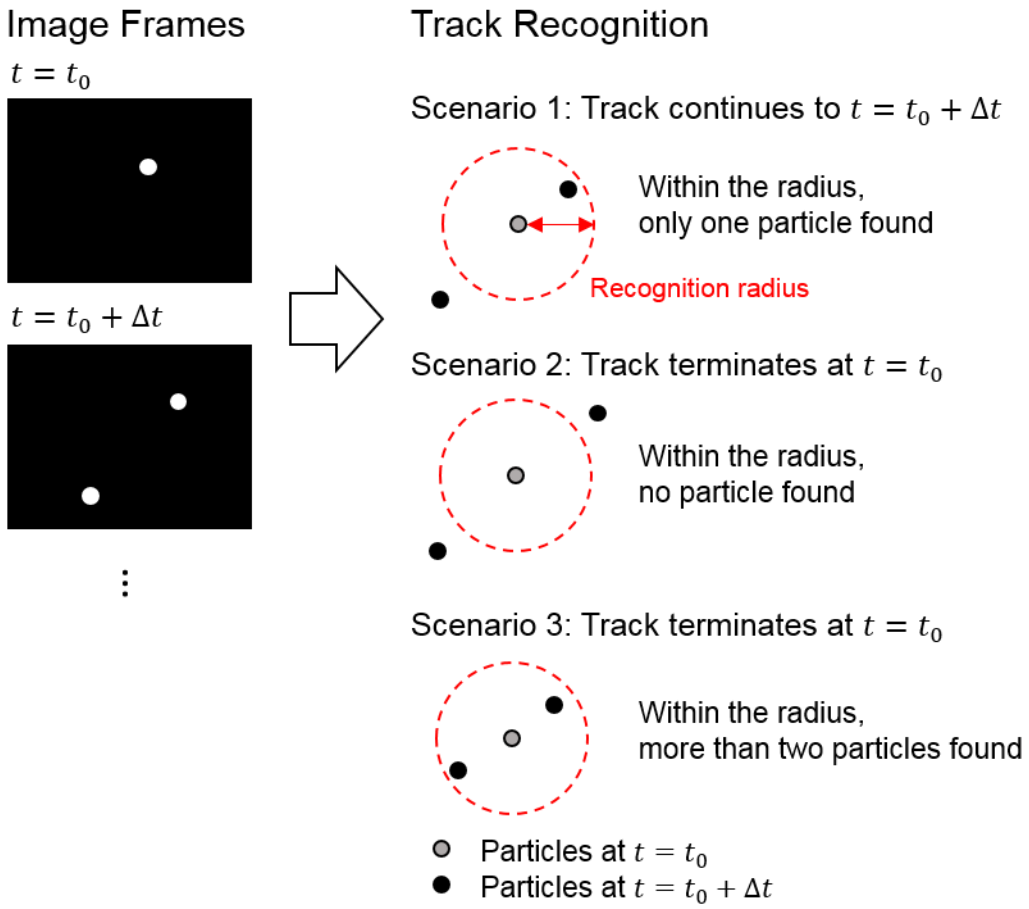

Figure 5.1 Illustrative description of the NTA tracking process. The particle locations at $t_0 + \Delta t$ are evaluated with respect to the particle locations at t_0 to identify particles' trajectory and construct a track. Scenario 1: Only one particle at $t_0 + \Delta t$ is found within the recognition radius from a particle at t_0, which identifies the two particles as the same particle, and the tracking process continues to $t_0 + \Delta t$. Scenario 2: No particle at $t_0 + \Delta t$ is found within the recognition radius, which terminates the tracking process at t_0. Scenario 3: More than two particles at $t_0 + \Delta t$ are found within the recognition range, which interferes and terminates the tracking process at t_0.

Mathematically, the displacement of each segment that comprises a track is described by the Brownian motion of the tracked particle, whose displacement probability $p(r)$ is described by the Rayleigh distribution [25, 28, 29]:

$$p(r) = \frac{r}{2D\Delta t} e^{-\frac{r^2}{4D\Delta t}} \quad (5.2)$$

where r is the two-dimensional displacement of a segment of the tracked particle. Since an estimation of the diffusion coefficient of a particle with a single segment of the particle displacement is prone to a stochastic error, a track consisting of a series of displacement segments is used for a more accurate estimation of the diffusion coefficient of a particle by taking the average squared displacement [19, 21, 27-29].

For a track consisting of K segments with its kth segment's displacement r_k (or its squared displacement $z_k = r_k^2$), the conventional distribution probability $P_K(z)$ of the average squared displacement z is known to follow a gamma distribution [28, 31]:

$$P_K(z) = \frac{(K/u^2)^K}{(K-1)!} z^{K-1} e^{-Kz/u^2} \quad (5.3)$$

where $z = \frac{1}{K}\sum_k z_k$ and $u = \sqrt{4D\Delta t}$, or the diffusion length of the particle on the given time interval Δt.

For the displacement distribution of a track consisting of K segments, it is expected that the mean $\langle z \rangle$ would be u^2 according to the following integration [28]:

$$\langle z \rangle = \int_0^\infty dz\, z P_K(z) = u^2 \quad (5.4)$$

by which the measured average squared displacement is related to the diffusion length u, and hence to the diffusion coefficient by the following formula [16, 18, 28, 29]:

$$d = \frac{4k_B T \Delta t}{3\pi\eta z} \quad (5.5)$$

It deserves the attention to the integration in Eq. 5.4 assumes that the displacement of the tracked particle is unbounded, although this assumption is invalid due to the recognition radius that is incorporated into the NTA tracking algorithm. Any displacement that goes

beyond the recognition radius terminates the tracking process, resulting in an exclusion of a probable long displacement from the displacement measurement [18, 25, 31]. As such, this exclusion would lead to an underestimated average squared displacement value that is affected by the recognition radius L as follows:

$$\langle z\rangle_{\text{Obs}} \cong \int_0^{L^2} dz\, zP_K(z) < \int_0^{\infty} dz\, zP_K(z) = u^2 \quad (5.6)$$

where $\langle z\rangle_{\text{Obs}}$ is the average squared displacement of a track taking into account the as-defined recognition radius. It can be assumed $\langle z\rangle_{\text{Obs}}$ is the same as the unbounded average squared displacement $\langle z\rangle$ if the recognition radius is sufficiently long such that the probability of the displacement beyond the range can be neglected. However, such a long recognition radius is not always viable as it may increase the chance that neighboring particles interfere with the tracking process of the tracked particle, resulting in an early termination of a track which introduces larger uncertainty in determining particle size [25, 30, 31]. Therefore, the influence of a finite recognition radius on $\langle z\rangle_{\text{Obs}}$ needs to be reflected in determining the diffusion length u, requiring a modified displacement probability $R_K(z)$ that considers the recognition radius.

For $K = 1$, the modified displacement probability $R_1(z)$ is given by a conditional probability under the condition that the displacement is within the recognition radius:

$$R_1(z) = \frac{P_1(z)}{\int_0^{L^2} dz\, P_1(z)} = \frac{1}{\alpha u^2} e^{-z/u^2} \;\; (0 \le z \le L^2) \quad (5.7)$$

where $\alpha = 1 - e^{-L^2/u^2}$. Since the probability $R_K(z)$ at the range of z greater than L^2 or less than 0 is negligible, the range of z between 0 and L^2 was described here. The modified displacement probability of a track with a segment length K ($K \ge 2$) can be acquired in recursive form, whose general form is described as follows:

$$R_{K,i}(z) = \frac{(L^2)^{K-1}}{(K-1)!} \frac{1}{\alpha^K (u^2)^K} K e^{-Kz/u^2} F_{K,i}(z) \quad (5.8)$$

$$F_{K,i}(z) = \sum_{j=0}^{[K/2]-1} \left\{ \begin{array}{l} f_{K,i,j} \cdot \left(\dfrac{K}{L^2} z - (i-1)\right)^{K-1-2j} \\ +(-1)^K \cdot f_{K,i-1,j} \cdot \left(i - \dfrac{K}{L^2} z\right)^{K-1-2j} \end{array} \right\} + h_{K,i} \quad (5.9)$$

where $R_{K,i}(z)$ denotes $R_K(z)$ for $\frac{i-1}{K}L^2 \le z < \frac{i}{K}L^2$, where i is a positive integer from 1 to K, and $[K/2]$ is the largest integer that is equal to or less than $\frac{K}{2}$. The coefficients, f's and h's, are given in a recursive manner. For an odd integer of K greater than 1,

$$f_{K,0,j} = 0 \quad \text{for } j = 0, 1, \dots, \frac{K-3}{2} \tag{5.10a}$$

$$f_{K,K,j} = 0 \quad \text{for } j = 0, 1, \dots, \frac{K-3}{2} \tag{5.10b}$$

$$f_{K,i,j} = \frac{f_{K-1,i,j} - f_{K-1,i-1,j}}{K-1-2j} \cdot (K-1) \qquad \text{for } i = 1, 2, \dots, K-1 \text{ and } j = 0, 1, \dots, \frac{K-3}{2} \tag{5.10c}$$

$$h_{K,i} = \sum_{j=0}^{\frac{K-3}{2}} \frac{2\, f_{K-1,i-1,j}}{K-1-2j} \cdot (K-1) \tag{5.10d}$$

$$h_{K,K} = 0 \tag{5.10e}$$

For an even integer of K,

$$f_{K,0,j} = 0 \quad \text{for } j = 0, 1, \dots, \frac{K}{2} - 1 \tag{5.11a}$$

$$f_{K,K,j} = 0 \quad \text{for } j = 0, 1, \dots, \frac{K}{2} - 1 \tag{5.11b}$$

$$f_{K,i,j} = (K-1) \times \begin{cases} \dfrac{f_{K-1,i,j} - f_{K-1,i-1,j}}{K-1-2j}, & j = 0, 1, \dots, \dfrac{K}{2} - 2 \quad \text{for } i = 1, 2, \dots, K-1 \\ h_{K-1,i}, & j = \dfrac{K}{2} - 1 \end{cases} \tag{5.11c, 5.11d}$$

$$h_{K,i} = 0 \tag{5.11e}$$

$$h_{K,K} = 0$$

The initial conditions at $K = 1$ are given as

$$F_{1,1}(z) = h_{1,1} \tag{5.12a}$$

$$f_{1,1,0} = 1 \tag{5.12b}$$

$$f_{1,0,0} = 0 \tag{5.12c}$$

$$h_{1,1} = 1 \tag{5.12d}$$

From the modified probability $R_K(z)$, the reduced mean of the average squared displacement due to the finite recognition radius can be calculated as well as the overestimation ratio of the particle size:

$$\langle z \rangle_{\text{Obs}} = \int_0^{L^2} dz\, z R_K(z) = u^2 - L^2 \left(\frac{1}{\alpha} - 1\right) \quad (5.13)$$

$$\frac{d_{\text{Obs}}}{d} = \frac{\langle z \rangle}{\langle z \rangle_{\text{Obs}}} = \frac{1}{1 - L^2/u^2 \left(\frac{1}{\alpha} - 1\right)} = 1 + \frac{L^2/u^2\, e^{-L^2/u^2}}{1 - e^{-L^2/u^2}(1 + L^2/u^2)} \quad (5.14)$$

The relation shows that the overestimation ratio of the particle size is more pronounced if the recognition radius L is small with respect to the diffusion length u of the tracked particle.

5.3 Materials and Methods

5.3.1 Materials

Two aliquots of concentrated (~10 wt%) polystyrene latex microspheres (51.6 ± 3 nm and 181.6 ± 9 nm) in liquid suspension were obtained from Colloidal Metrics Corporation (Mountain View, CA). These microspheres were diluted into 0.1-µm-filtered 10 mM KCl (potassium chloride) until the NanoSight provided a concentration of 1×10^9 particles/ml for each sample. These suspensions were then further diluted 1:10 into 0.1-µm-filtered 10 mM KCl to give a measured concentration of 1×10^8 particles/ml.

5.3.2 NTA Simulation

To test the conventional and modified displacement probabilities for the size distribution, Brownian motion of particles were simulated and tracked according to the NTA detection principle. For the particle placements and movements, a three-dimensional space was created with its width and height corresponding to the field-of-view of the CMOS camera, i.e., 640 and 480 pixels, respectively, with the pixel size set to 179 nm, and the depth to the focal depth of the objective lens, i.e. 7.16 µm [30, 32]. To allow fluctuations in the number of particles detected within the field-of-view over time, an additional space that extends in

each of the three dimensions was given. The extension in each direction was six times the diffusion length of the mean particle size of the simulations or at least 2 μm, and the boundary of the space was made periodic in each direction [33].

The number of generated particles was determined by the volume of the created space and the nominal particle concentration. For instance, the average number of particles observed in a frame is about 70 when the concentration is set to 1×10^9 particles/ml. The initial position of the generated particles was given randomly in the three-dimensional space, and the movement of each particle in each direction at the subsequent frames was randomly generated to follow a normal distribution with a standard deviation of $\sqrt{2D_i\Delta t}$,[34] where D_i is the diffusion coefficient of the ith particle and Δt is the time interval between the frames set as 30.74 milliseconds. The time duration of each simulation was 60 seconds, corresponding to 1952 frames including the initial frame. The simulation did not consider either the effect of measurement errors in determining the position of the particles or the drift in the solution [28].

For the recognition of tracks, the position of a particle generated by the simulation in one frame is evaluated with the position of the particles in the following frame. If the distance to the nearest particle in the following frame is less than an arbitrarily chosen recognition radius, the particle in the following frame is considered as the same particle in the previous frame and becomes a segment of the constructed track [31]. If either the distance to the nearest particle is larger than the recognition radius or the distance to the second nearest particle is less than the recognition radius, the particle in the previous frame is regarded as not present in the following frame, resulting in a termination of the track. Since this process evaluates only the distance for the track recognition, two different particles can be recognized as the same particle to produce an abnormal track [25].

5.3.3 Experimental Setup

The instrument used for the analysis was the Malvern NanoSight LM10 (Amesbury, UK) equipped with a 20× objective, a 405 nm 50 mW laser and a Scientific CMOS detector and

software version NTA 2.3 Beta 7. A syringe pump was utilized to flow the samples through the laser viewing module at a rate of 5 ± 2 μm/s. The video data for the NTA measurements were collected for 60 seconds, which was repeated three times for each sample. Acquired video data was processed by the NTA software version 3.1.46 to acquire tracks. During the process, the detection threshold was set to an optimal value depending on the nominal particle size and the concentration, while the value was used for the three runs of each sample condition. The recognition radius, or the max jump distance in the NTA software, varied from 6 to 30 pixels, corresponding to a range of 1.1 to 5.4 μm. The recognized tracks produced by the NTA software were used for the determination of the particle size distribution.

5.3.4 Method for Size Distribution Determination

NTA determines the size of tracked particles from their diffusion coefficient acquired from the average squared displacements of the tracks. A simple method to obtain the particle size distribution from the acquired tracks is to form a histogram of the particle sizes by directly converting the average squared displacements of the tracks using Eq. 5.4 [16, 18, 28, 29, 31]. However, the determined particle size by the direct conversion has an inherent stochastic uncertainty due to the nature of Brownian motion, which necessitates particles to be tracked over many frames to reduce the uncertainty which depends on the track length [21, 28, 29]. Since the availability of tracks with a long track length depends on the measurement conditions, an accurate size determination by the direct conversion is not always achievable even for very monodisperse samples [28, 29, 31, 35].

Other approaches based on the maximum likelihood estimation (MLE) principle have been suggested that find a size distribution that maximizes the likelihood of the obtained tracks [28, 29]. Among them, an iteration-based MLE method is chosen for this study that increases the likelihood at each iteration since it does not require prior knowledge about the particle size distribution for the iteration [28, 31, 35]. For a given displacement probability $P(z_m|n_m, d_b)$, where z_m and n_m are the average squared displacement and the track length of the mth track, respectively, and d_b is the particle size corresponding to the

bth bin number of the size distribution $f(d)$, the size distribution after the rth iteration $f^{(r)}(d)$ is given by following relation [28, 31]:

$$f^{(r+1)}(d_b) = f^{(r)}(d_b) \cdot \frac{1}{M} \sum_{m=1}^{M} \frac{P(z_m|n_m, d_b)}{\sum_{b=1}^{B} P(z_m|n_m, d_b) f(d_b) / \sum_{b=1}^{B} f(d_b)} \quad (5.15)$$

where M is the number of observed tracks.

In this study, both the conventional displacement probability $P_K(z)$ and the modified displacement probability $R_K(z)$ were used and compared for the size distribution determination. A uniform size distribution was used for the initial size distribution $f^{(0)}(d)$ for both probabilities [28, 36]. Regarding the termination criteria of the iteration, the chi-square statistic of the error between a histogram of the mean squared displacement and that calculated from the rth iteration solution was used, where the change in χ^2 becomes less than 1% of the value at the previous iteration [28, 31].

5.4 Results and Discussion

5.4.1 Simulated NTA Measurements

To evaluate the conventional and the modified displacement probabilities for the size distribution estimation, a simulated NTA measurement was generated with a model particle set with a uniform size of 100 nm and a concentration of 1×10^9 particles/ml. The result was then analyzed to acquire particle tracks at a recognition radius of 1, 1.5, 2 and 5 μm.

Figure 5.2(a) shows the distribution of the tracks by the track length. Among those recognized tracks, a total of 8310, 5329, 4616 and 3585 tracks whose track length is more than 4 were used for the size distribution determination for a recognition radius of 1, 1.5, 2 and 5 μm, respectively [29]. The acquired tracks were processed to recover a size distribution using the iteration-based MLE method with the conventional and the modified displacement probabilities as shown in Figure 5.3(a) and (b), respectively. When the recognition radius is 2 and 5 μm, the obtained mean size is close to the nominal size regardless of the employed probabilities. On the other hand, when the recognition radius is

short, i.e. 1 and 1.5 µm, respectively, the mean size determined with the conventional probability is 152 and 107 nm, or an overestimation by a factor of 1.52 and 1.07, which is close to an expected factor of 1.50 and 1.06 according to Eq. 5.14.

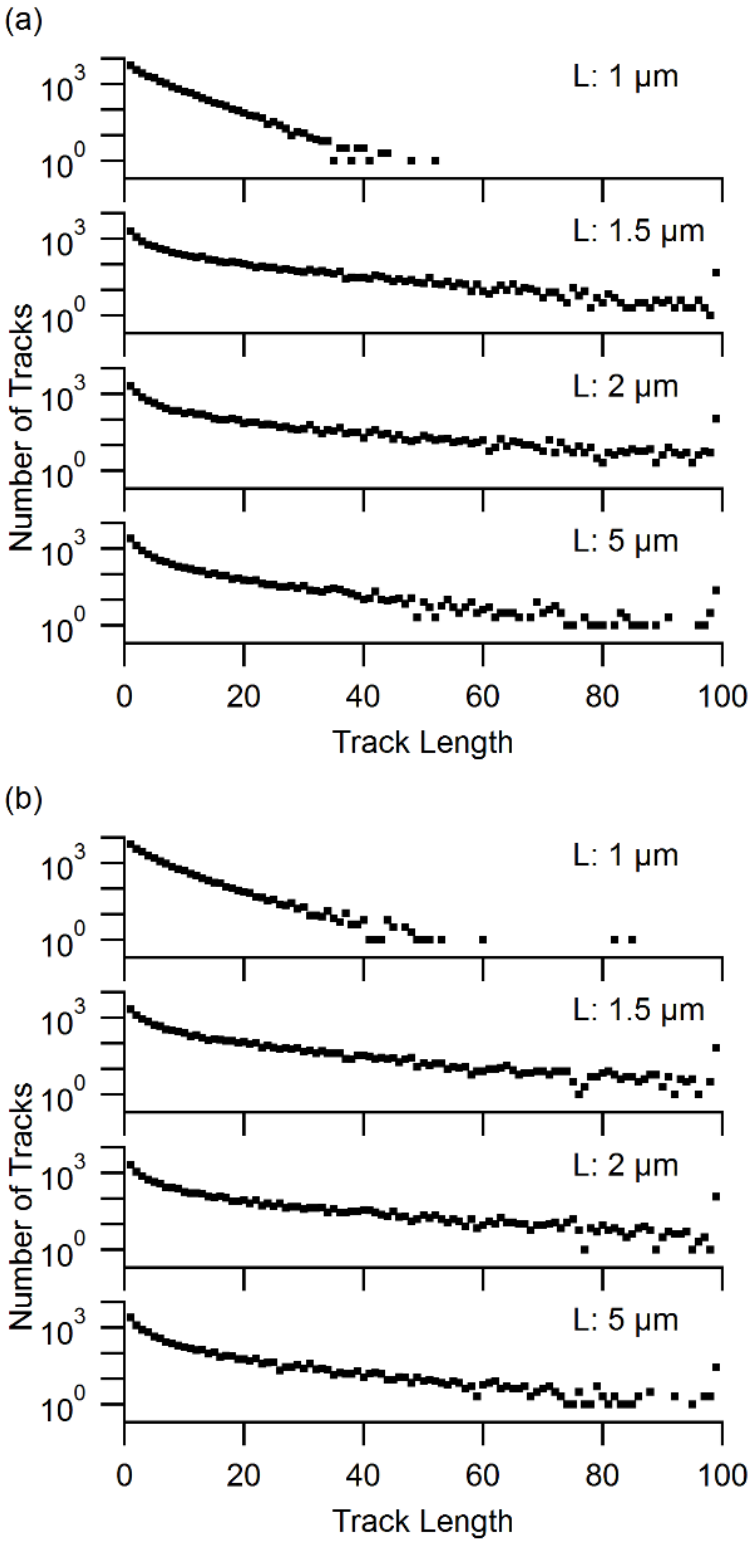

Figure 5.2 Results from computer simulations. The distribution of tracks used in Figures 5.3 and 5.4 at a recognition range of 1, 1.5, 2 and 5 µm. The tracks were acquired from the simulations used in (a) Figure 5.3, whose size is 100 nm at a concentration of 1×10^9 particles/ml, and in (b)

Figure 5.4, whose size distribution consists of an 'ideal' set of a normal distribution with a mean of 100 nm and and relative variance 0.05 at a concentration of 1×10^9 particles/ml. A total of 21605, 9855, 9078 and 8855 tracks were collected from the 100-nm-sized particles simulation, among which 8310, 5329, 4616 and 3585 tracks whose track length is more than 4 were chosen for the analysis at a recognition range of 1, 1.5, 2 and 5 μm, respectively. A total of 21420, 10270, 9123 and 8730 tracks were collected from the particles simulation of the normal distribution, among which 7677, 5357, 4607 and 3564 tracks whose track length is more than 4 were chosen for the analysis at a recognition range of 1, 1.5, 2 and 5 μm, respectively.

In contrast, the acquired mean size with the modified displacement probability is 102 nm and 100 nm at a recognition radius of 1 and 1.5 μm, respectively. It suggests that the overestimation of the mean size produced by the conventional probability can be mitigated by using the modified probability. However, relative variance or variance of the distribution divided by the square of its mean size, of 0.009 acquired with the conventional probability at a recognition radius of 1 μm is close to the nominal value, i.e., 0, while the modified probability gives 0.061 at the same recognition radius. This observation leads to an idea that the conventional probability is more adequate in analyzing a narrow size distribution despite its overestimation on the mean size since the overestimation is predictable and might be corrected by rescaling with the expected overestimation.

To verify if the conventional probability is useful in determining a size distribution on a short recognition radius despite the overestimation of the mean size, another NTA simulation was conducted with a model particle set whose size distribution follows a normal distribution. Its mean size and relative variance were chosen as 100 nm and 0.05, respectively, and the concentration was given as 1×10^9 particles/ml. In generating the particles for the simulation, the size of the particles was chosen to be 'ideally' distributed so that they comprise quantiles of a normal distribution with the given mean size and variance [29]. The simulated data was then recognized at a recognition radius of 1, 1.5, 2 and 5 μm, whose produced tracks are shown in Figure 5.2(b). Among those tracks, a total of 7677, 5357, 4607 and 3564 tracks whose track length is more than 4 were chosen and processed to determine a size distribution using the two displacement probabilities as shown in Figure 5.4.

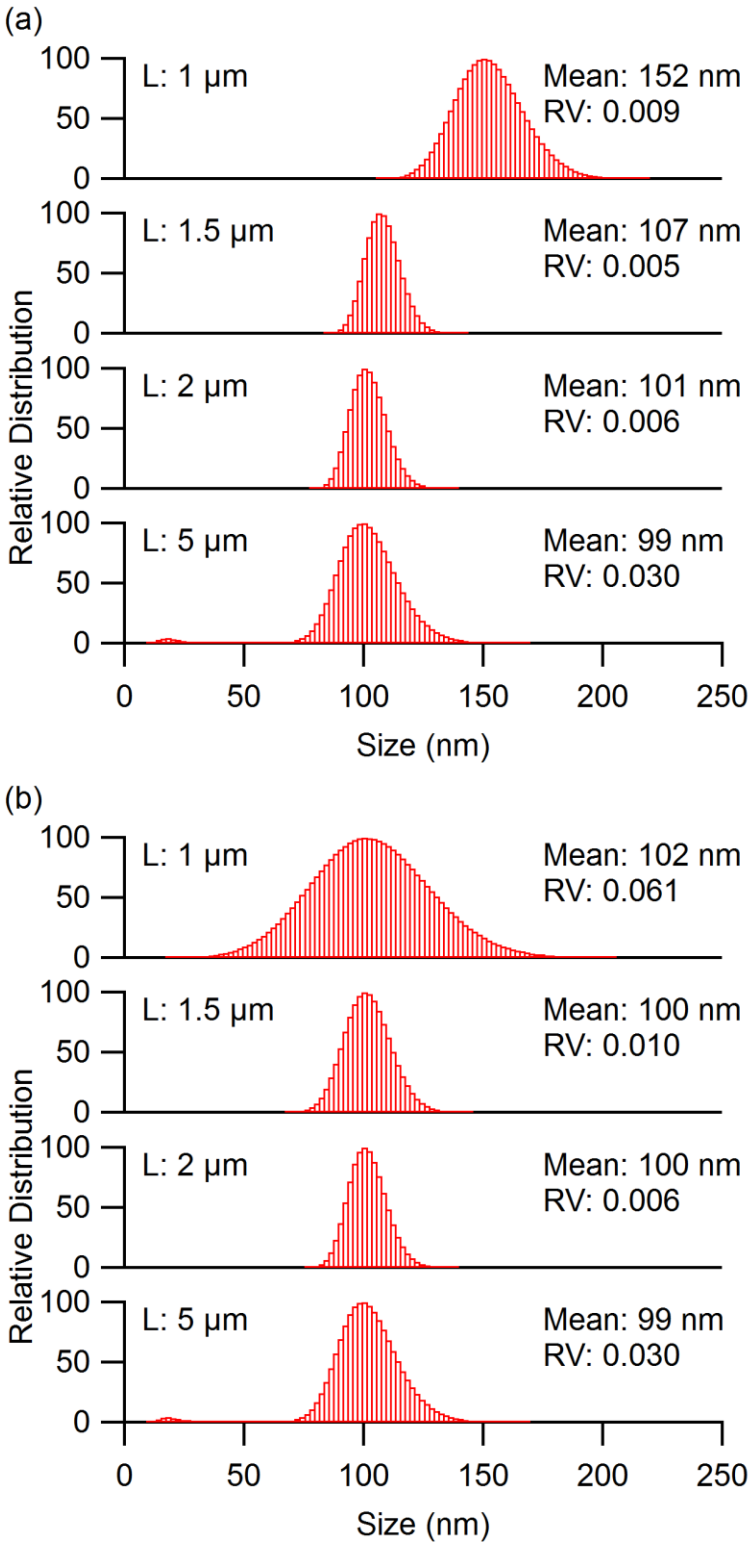

Figure 5.3 Simulated NTA measurements of ideally monodisperse, 100-nm diameter nanoparticles. Different recognition radius values, *L*, of 1, 1.5, 2 and 5 µm were tested based on a total of 8310, 5329, 4616 and 3585 tracks, respectively. Acquired tracks were processed to

determine the size distribution using the iteration-based MLE method with the (a) conventional displacement probability or (b) modified displacement probability. The nanoparticle concentration was 1×10^9 particles/ml. The computed mean diameter and relative variation (RV) for each size distribution are reported.

The results are similar to what observed in the previous simulation results. At a recognition radius of 2 and 5 μm, the obtained mean size regardless of the employed probability is close to the nominal mean size of 100 nm. When the recognition radius is short, i.e., 1 μm, the mean size determined with the conventional probability is overestimated by a factor of 1.54 in line with the expectation, while the mean size observed with the modified probability is 107 nm. However, relative variance acquired with the conventional probability at the recognition radius of 1 μm is 0.009. It is a significant underestimation compared to the nominal value of 0.05 and is the same as the value acquired from the previous simulation with a model particle set with a relative variance of 0. Whereas, relative variance acquired with the modified probability is 0.083, which is larger than the nominal value. This indicates that relative variance measured by NTA could mislead regardless of the employed displacement probability for the analysis if a small recognition radius is applied.

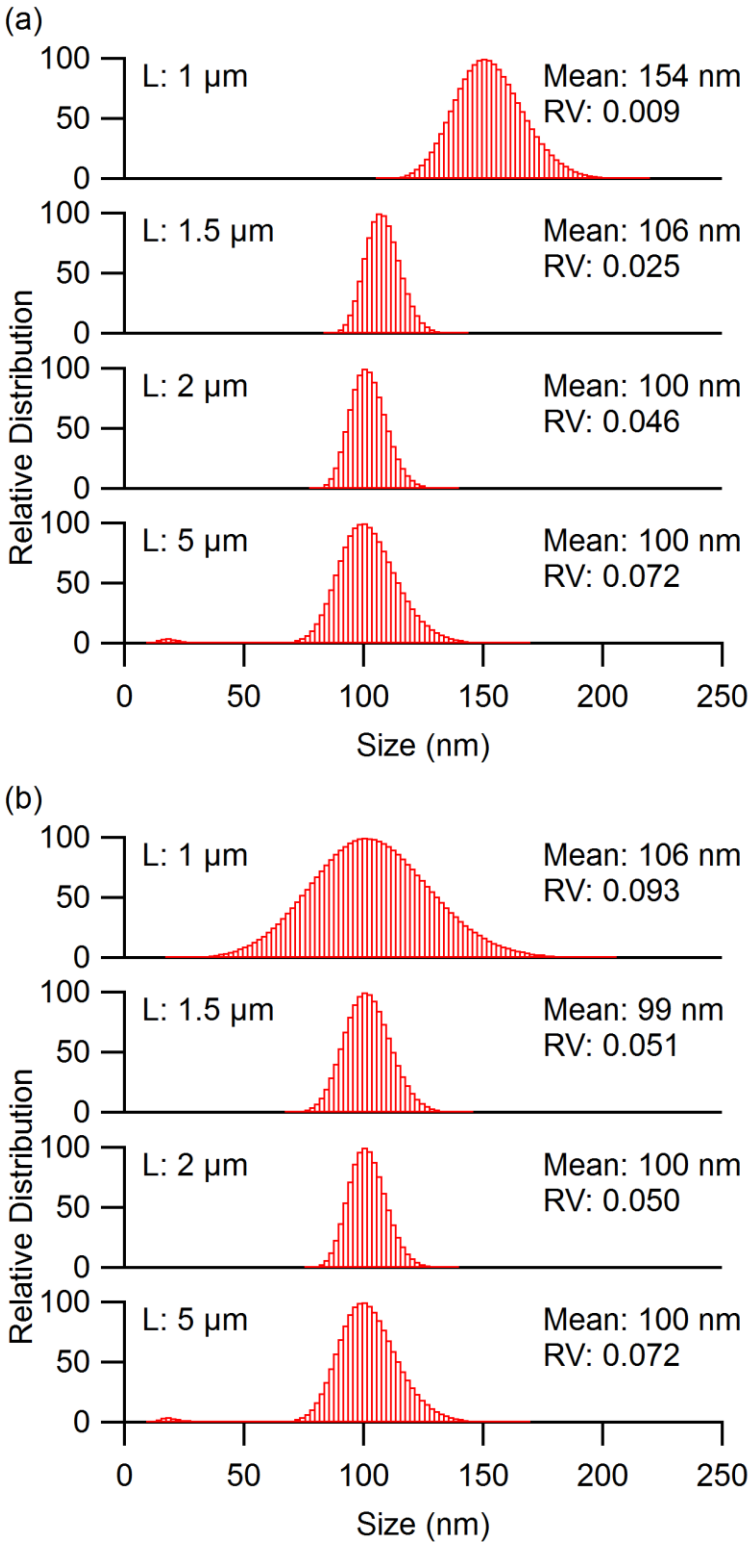

Figure 5.4 Simulated NTA measurements of 100 ± 5 nm diameter nanoparticles. Different recognition radius values, *L*, of 1, 1.5, 2 and 5 µm were tested based on a total of 7677, 5357, 4607 and 3564 tracks, respectively. Acquired tracks were processed to determine the size

distribution using the iteration-based MLE method with the (a) conventional displacement probability or (b) modified displacement probability. The nanoparticle concentration was 1×10^9 particles/ml. The computed mean diameter and relative variation (RV) for each size distribution are reported.

To extend the observation on the influence of the recognition radius and the displacement probabilities, a series of NTA simulations with model size distributions of various mean size and relative variance were conducted. Mean size of 20, 50, 100 and 200 nm and relative variance of 0, 0.01 and 0.05 were chosen for the model size distributions at a concentration of 1×10^9 particles/ml. Two types of particle size distribution were evaluated for each pair of mean size and relative variance: one from a bi-modal distribution and the other from a normal distribution. For a normal distribution, as described in the previous simulation, the size of particles was chosen to be 'ideally' distributed so that they comprise quantiles of a normal distribution with the given mean size and relative variance. For a bi-modal distribution, two sub-populations of an equal number with a size of 18 and 22 nm, and 15.5 and 24.5 nm for a mean size of 20 nm, 45 and 55 nm, and 39 and 61 nm for a mean size of 50 nm, 90 and 110 nm, and 78 and 122 nm for a mean size of 100 nm, and 180 and 220 nm, and 155 and 245 nm for a mean size of 200 nm were generated for relative variance of 0.01 and 0.05, respectively. For relative variance of 0, monomodal particles of 20, 50, 100 and 200 nm size were generated for a mean size of 20, 50, 100 and 200 nm, respectively. For each combination of mean size and relative variance, 25 sets of simulations were conducted. The simulated results were processed to construct tracks at a various recognition radius from 1 to 5 μm and analyzed to determine a size distribution with the two displacement probabilities.

Conventional Probability Modified Probability

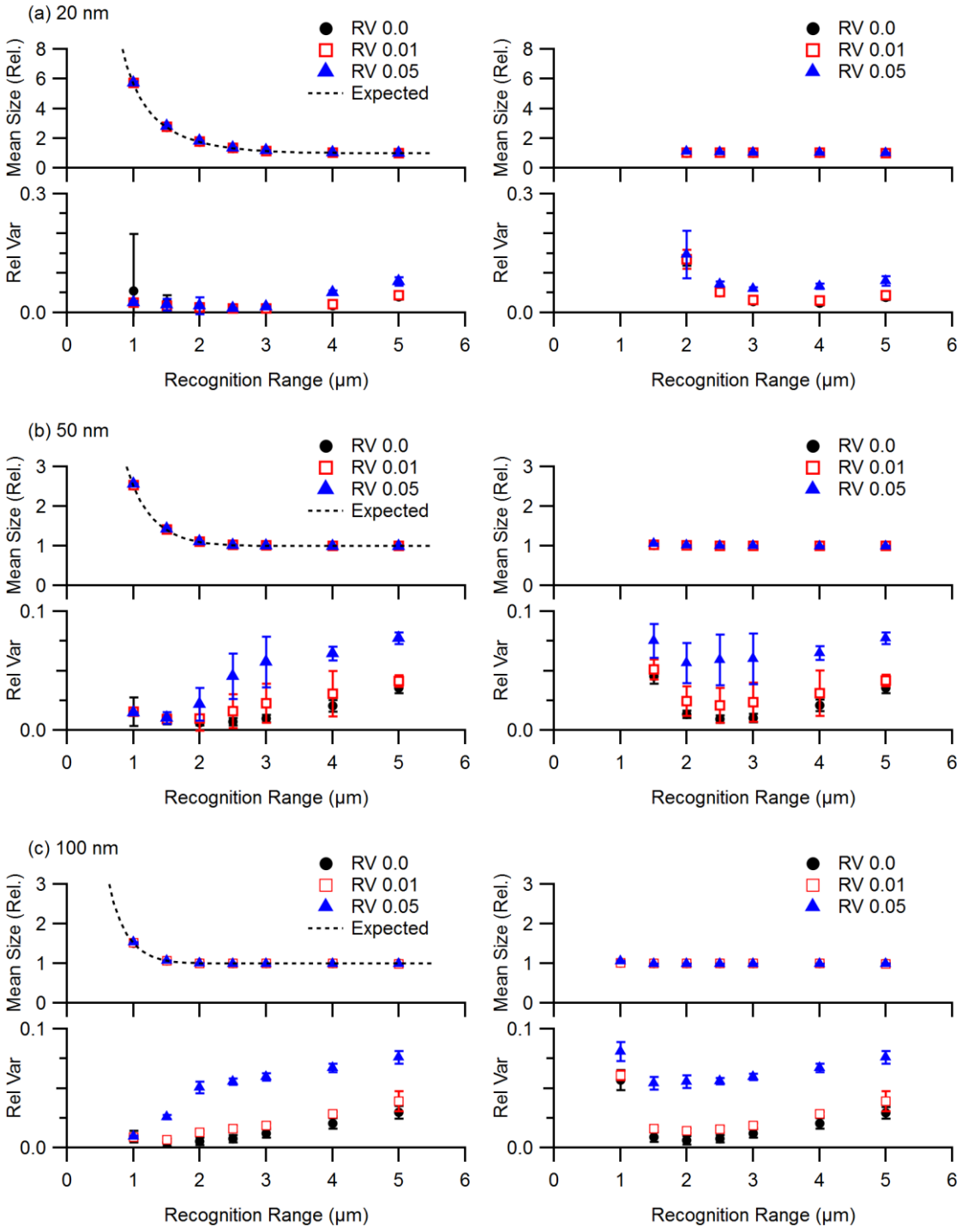

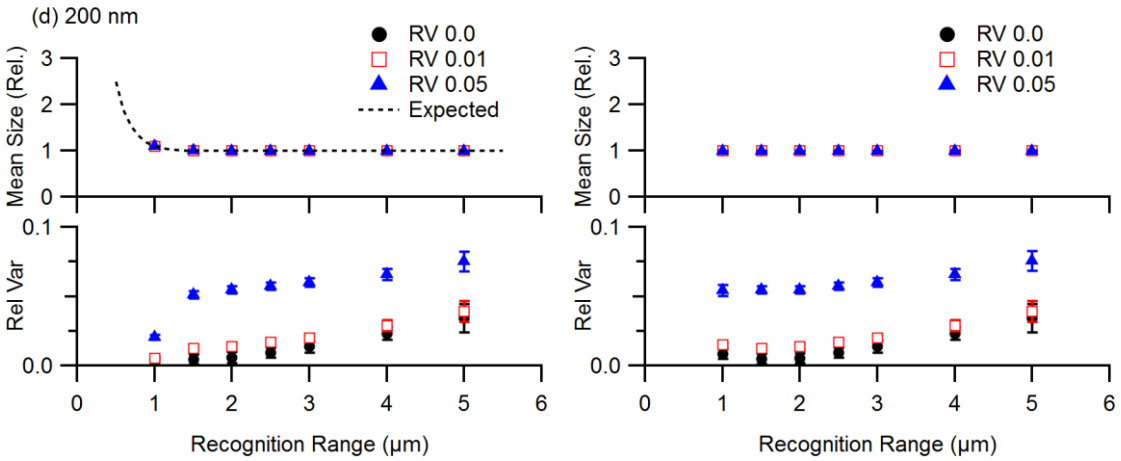

Figure 5.5 Results from a computer simulation. Mean size and relative variance of the size distributions determined from the simulated Brownian movements of particles, where the tracks of the particles are recognized at a various recognition radius from 1 to 5 μm. For each simulation, an 'ideal' set of particles whose size distribution follows a normal distribution of a mean size of (a) 20, (b) 50, (c) 100 and (d) 200 nm with relative variance of 0 (black circle), 0.01 (red open square) and 0.05 (blue triangle) at a concentration of 1×10^9 particles/ml was used. For each combination of a mean size and relative variance, 25 runs of simulated NTA measurements were produced. From the recognized tracks of the simulated measurements on a various recognition radius, the size distribution was estimated by the iterative MLE method with the conventional displacement probability (left) and the modified displacement probability (right). The acquired mean size is displayed with respect to the nominal mean size of the respective simulated particle sets. Dashed guidelines show the expected overestimated mean size due to the use of the conventional probability. Note that the size distributions on the simulations of a mean size condition of 20 and 50 nm estimated with the modified displacement probability do not converge well when the recognition radius is 1.5 and 1 μm, respectively, and their corresponding mean size and relative variance are not displayed in (a) and (b).

The mean size and relative variance determined from the simulations with a normal distribution and a bi-modal distribution are presented in Figures 5.5 and 5.6, respectively. The acquired mean size and relative variance from the two different types of size distribution are not different from each other. When the recognition radius is long enough, the acquired mean size with the conventional probability is the same as the respective nominal mean size of the simulation conditions regardless of the mean size and relative variance.

Conventional Probability

Modified Probability

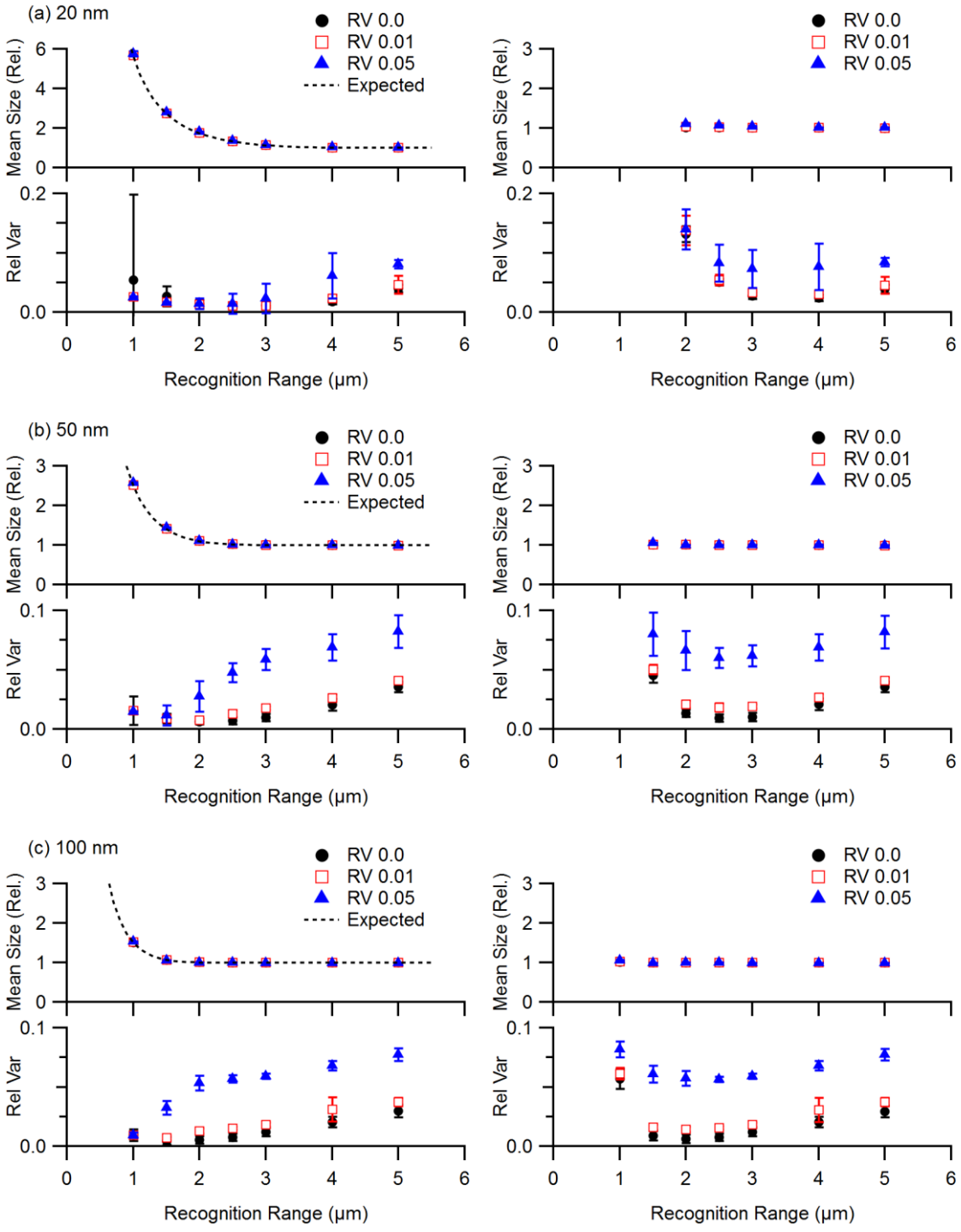

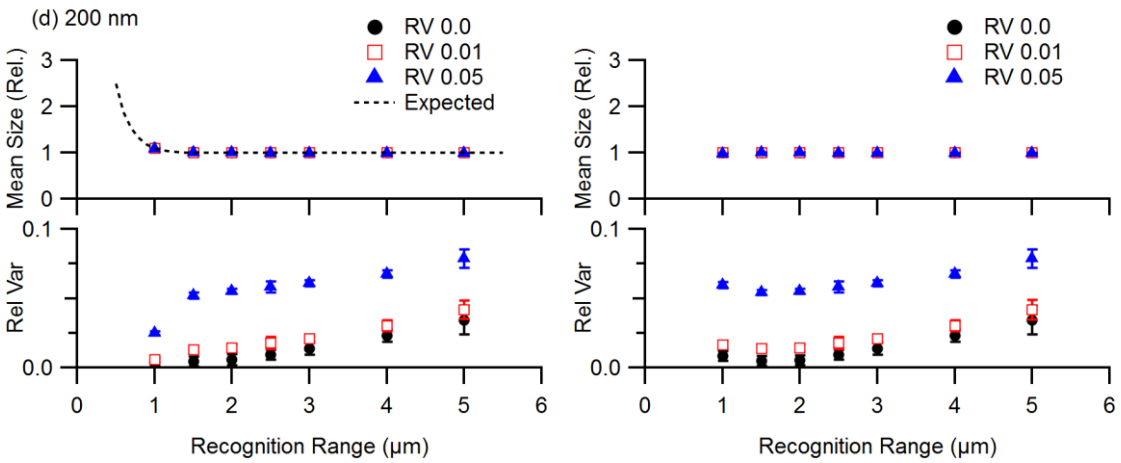

Figure 5.6 Results from a computer simulation. Mean size and relative variance of the size distributions determined from the simulated Brownian movements of particles, where the tracks of the particles are recognized at a various recognition range from 1 to 5 μm. For each simulation, a set of particles with a bi-modal distribution whose mean size is (a) 20, (b) 50, (c) 100 and (d) 200 nm with relative variance of 0 (black circle), 0.01 (red open square) and 0.05 (blue triangle) at a concentration of 1×10^9 particles/ml was used. The corresponding size pairs for 20-, 50-, 100- and 200-nm mean size are 18 and 22, 45 and 50, 90 and 110, and 180 and 220 nm, respectively, for relative variance of 0.01, and 15.5 and 24.5, 39 and 61, 78 and 122, and 155 and 245 nm, respectively, for relative variance of 0.05. For each combination of a mean size and relative variance, 25 runs of simulated NTA measurements were produced. From the recognized tracks of the simulated measurements on a various recognition range, the size distribution was estimated by the iterative MLE method with the conventional displacement probability (left) and the modified displacement probability (right). The acquired mean size is displayed with respect to the nominal mean size of the respective simulated particle sets. Dashed guidelines show the expected overestimated mean size due to the use of the conventional probability. Note that the estimated size distributions on the simulations with a mean size condition of 20 and 50 nm do not converge well when the recognition range is 1.5 and 1 μm, respectively, and their corresponding mean size and relative variance are not displayed in (a) and (b).

As the recognition radius decreases, the mean size acquired with the conventional probability increases and follows the expected overestimated mean size (dashed lines) regardless of the simulation condition. As expected, the overestimation of the mean size is more apparent on a smaller nominal mean size, i.e., the corresponding diffusion length is longer. On the contrary, the mean size acquired with the modified probability is in line with

their respective nominal mean size regardless of the nominal mean size and relative variance throughout a recognition radius of 1 to 5 μm, where the maximum deviation of the acquired mean size is less than 6% of the nominal value. Remarkably, on the condition with a mean size of 20 and 50 nm, the modified probability failed in obtaining a proper size distribution at a small recognition radius, e.g., 1 μm, and the corresponding mean size and relative variance are not displayed in Figures 5.5 and 5.6. Except in those cases, the comparison suggests that the modified probability provides a more accurate mean size for NTA measurements if the recognition radius is not long enough compared to the diffusion length of the particles in the sample.

On the other hand, relative variance acquired with the two probabilities shows a deviation from the nominal value when the recognition radius is very long, unlike what is observed on the mean size. With the conventional probability, at a long recognition radius, e.g., 5 μm, the obtained relative variance is significantly larger than the nominal relative variance regardless of the nominal mean size and relative variance. The same observation is found when the modified probability is used. In fact, when the recognition radius is 5 μm, a spurious peak is found at a small-size range of the acquired size distributions other than the major peak centered at the nominal mean size as observed in Figures 5.3 and 5.4. It is probable that the observed spurious peak contributes to the increased relative variance at the long recognition radius. Such spurious peaks can be produced due to false tracks made during the NTA track recognition, where two different particles are recognized as the same particle over two successive frames and form a false track which cannot be screened by the tracking principle of NTA [25]. This is obvious if the simulation results are processed again while those false tracks are excluded from the analysis. A total of 17, 11, 10 and 3 tracks at a recognition radius of 1, 1.5, 2 and 5 μm, respectively, were those false tracks included in the data used for the previous simulation of 100-nm size particles shown in Figure 5.2. A total of 18, 8, 11 and 25 false tracks were found from the data used for the simulation of a normal distribution with a mean size of 100 nm and relative variance of 0.05 shown in Figure 5.3, at a recognition radius of 1, 1.5, 2 and 5 μm, respectively. Figures 5.7 and 5.8 show the determined size distributions acquired from the screened tracks of the previous

simulations with a nominal relative variance of 0 and 0.05, respectively. From the acquired size distributions with the screened tracks, no spurious peak is found at a small-size range.

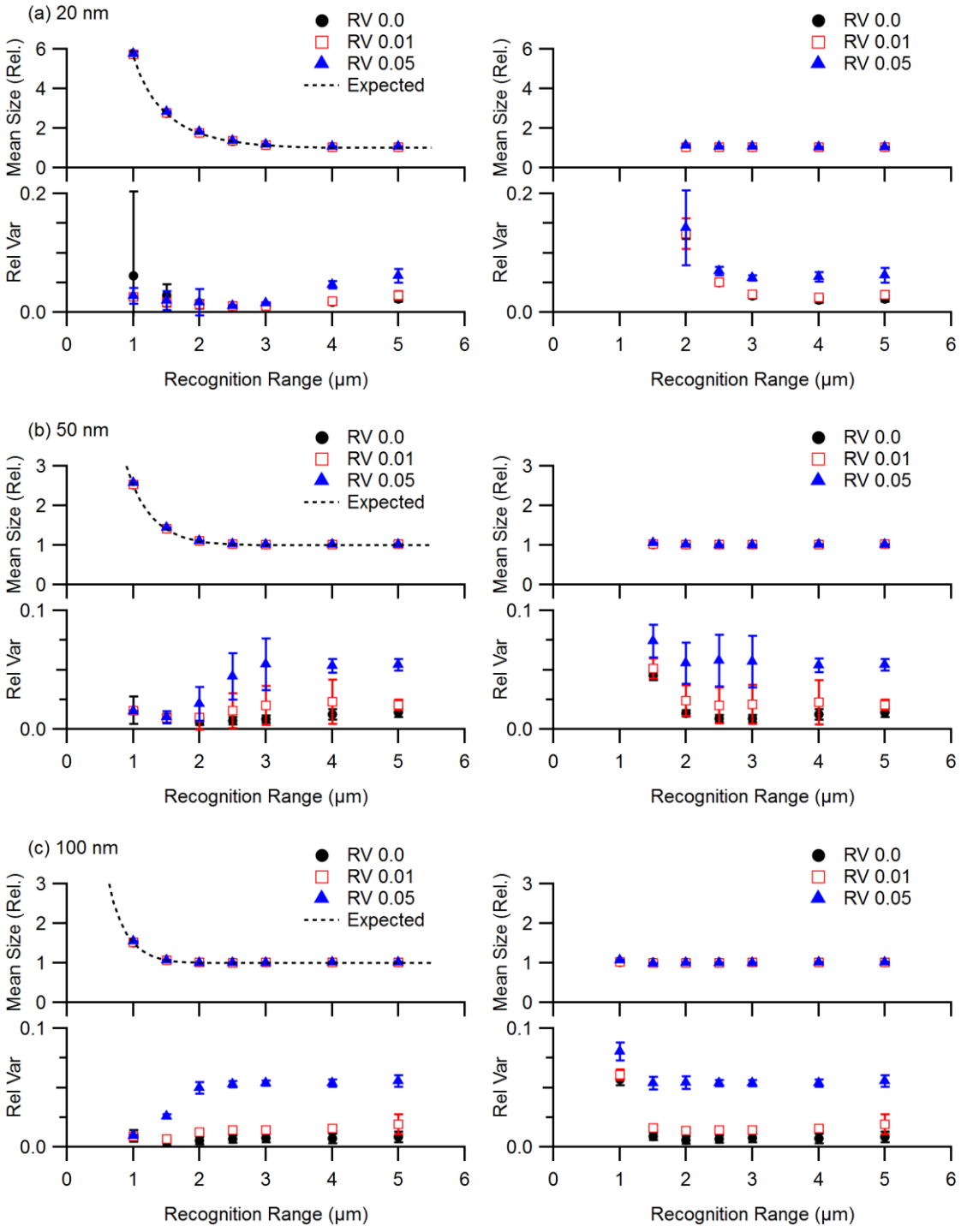

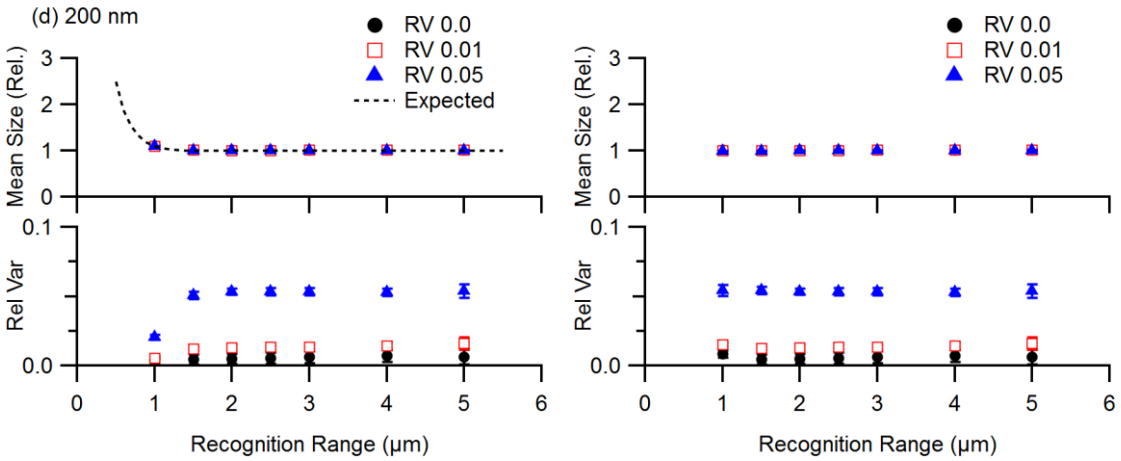

Figure 5.7 Reanalyzed results of the computer simulation shown in Figure 5.5. Mean size and relative variance of the size distributions determined from the simulated Brownian movements of particles, where those false tracks are excluded from the analysis. For each simulation, an 'ideal' set of particles whose size distribution follows a normal distribution of a mean size of (a) 20, (b) 50, (c) 100 and (d) 200 nm with relative variance of 0 (black circle), 0.01 (red open square) and 0.05 (blue triangle) at a concentration of 1×10^9 particles/ml was used. For each combination of a mean size and relative variance, 25 runs of simulated NTA measurements were produced. From the recognized tracks of the simulated measurements on a various recognition range, the size distribution was estimated by the iterative MLE method with the conventional displacement probability (left) and the modified displacement probability (right). The acquired mean size is displayed with respect to the nominal mean size of the respective simulated particle sets. Dashed guidelines show the expected overestimated mean size due to the use of the conventional probability. Note that the estimated size distributions on the simulations with a mean size condition of 20 and 50 nm do not converge well when the recognition range is 1.5 and 1 μm, respectively, and their corresponding mean size and relative variance is not displayed in (a) and (b).

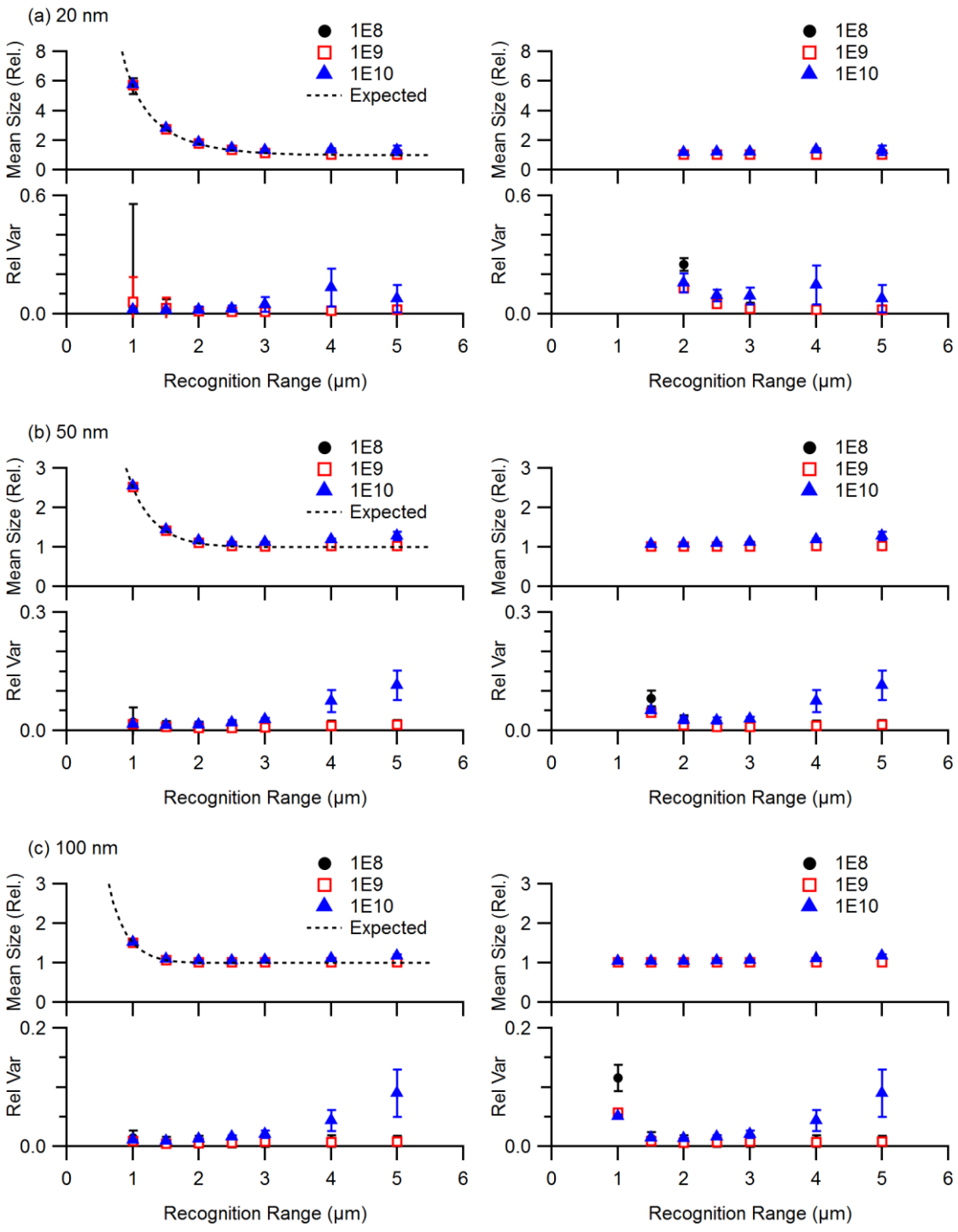
(a) 20 nm
(b) 50 nm
(c) 100 nm
1E8
1E9
1E10
Expected
Mean Size (Rel.)
Rel Var
Recognition Range (µm)

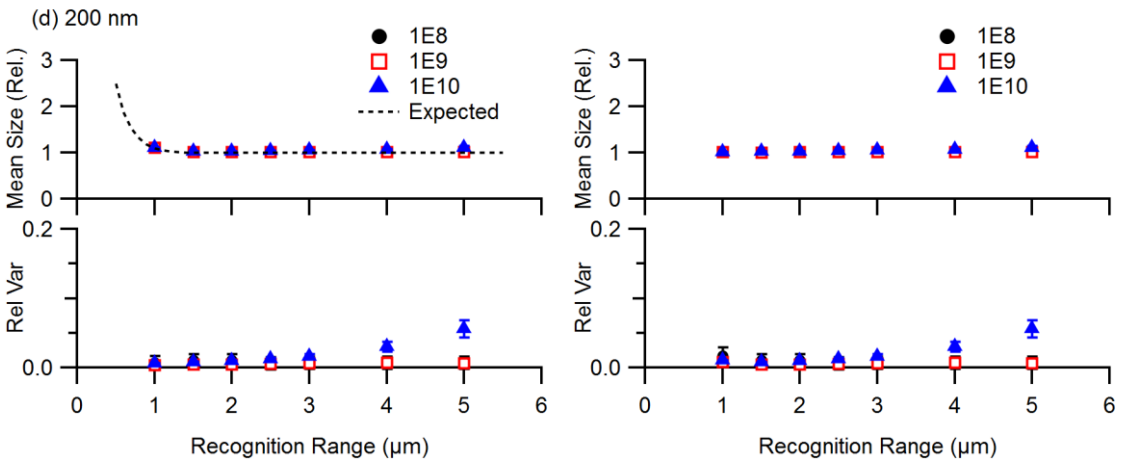

Figure 5.8 Reanalyzed results of the computer simulation shown in Figure 5.6. Mean size and relative variance of the size distributions determined from the simulated Brownian movements of particles, where those false tracks are excluded from the analysis. For each simulation, monomodal particles with a size of (a) 20, (b) 50, (c) 100, and (d) 200 nm at a concentration of 1×10^{8} (black circle), 1×10^{9} (red open square) and 1×10^{10} particles/ml (blue triangle) were generated. For each combination of mean size and concentration, 25 runs of simulated NTA measurements were produced. From the recognized tracks of the simulated measurements on a various recognition range, the size distribution was estimated by the iterative MLE method with the conventional displacement probability (left) and the modified displacement probability (right). The acquired mean size is displayed with respect to the nominal mean size of the respective simulated particle sets. Dashed guidelines show the expected overestimated mean size due to the use of the conventional probability. Note that the size distributions from the simulations of a mean size condition of 20 and 50 nm estimated by the modified displacement probability do not converge well when the recognition range is below 1.5 and 1 μm, respectively, and their corresponding relative variance is not displayed.

In addition, the relative variance acquired from the screened track data, regardless of the applied probability for the analysis, is very close to the nominal value at a long recognition radius. When the exclusion of false tracks is applied to the analysis of all the simulations used in Figure 5.5, it becomes more apparent that the increased relative variance at a long recognition radius results from the false tracks, as shown in Figure 5.7. This suggests that NTA analysis can be corrupted by false tracks if a long recognition radius is used for track recognition [25].

On a decreasing recognition radius, the obtained relative variance decreases gradually and approaches to their respective nominal values regardless of the displacement probability used for the analysis. This indicates that the false tracks can be reduced by decreasing the recognition radius. When the recognition radius gets even smaller, the determined relative variance starts to deviate from the nominal value to a very small value when analyzed with the conventional probability or to a very large value with the modified probability. Since both the probabilities do not provide a proper relative variance value on either a very long or very short recognition radius, it suggests that a proper recognition radius that avoids the two ends is required for accurate NTA analysis.

5.4.2 Size Resolution of NTA

As in Figure 5.5, relative variance of the size distributions acquired with the two displacement probabilities on a small recognition radius deviates from the nominal value. If the conventional displacement probability is used to determine a size distribution on a small recognition radius, it will result in a very small relative variance even for a particle set of broad size distribution. Therefore, it would not resolve two separated sub-populations of a size distribution from each other since the two peaks of the sub-populations would be merged into a very narrow one when analyzed with the conventional probability. On the other hand, the modified displacement probability on a small recognition radius would give larger relative variance than the nominal value and produce a broad peak even though a true size distribution is very narrow. These indicate that the size resolution of NTA achievable on a small recognition radius is limited.

To investigate and compare the size resolution of NTA depending on the employed probability and the recognition radius, the results from the previous simulations using a bi-modal size distribution, shown in Figure 5.6, were examined. The acquired size distributions from the simulations were evaluated if two separated peaks are observable from the determined size distributions on a various recognition radius. The condition of the investigated simulations is a mean size of 20, 50, 100 and 200 nm with a relative variance

of 0.05, where the nominal peaks are located at 15.5 and 24.5 nm, 39 and 61 nm, 78 and 122 nm, and 155 and 245 nm, respectively.

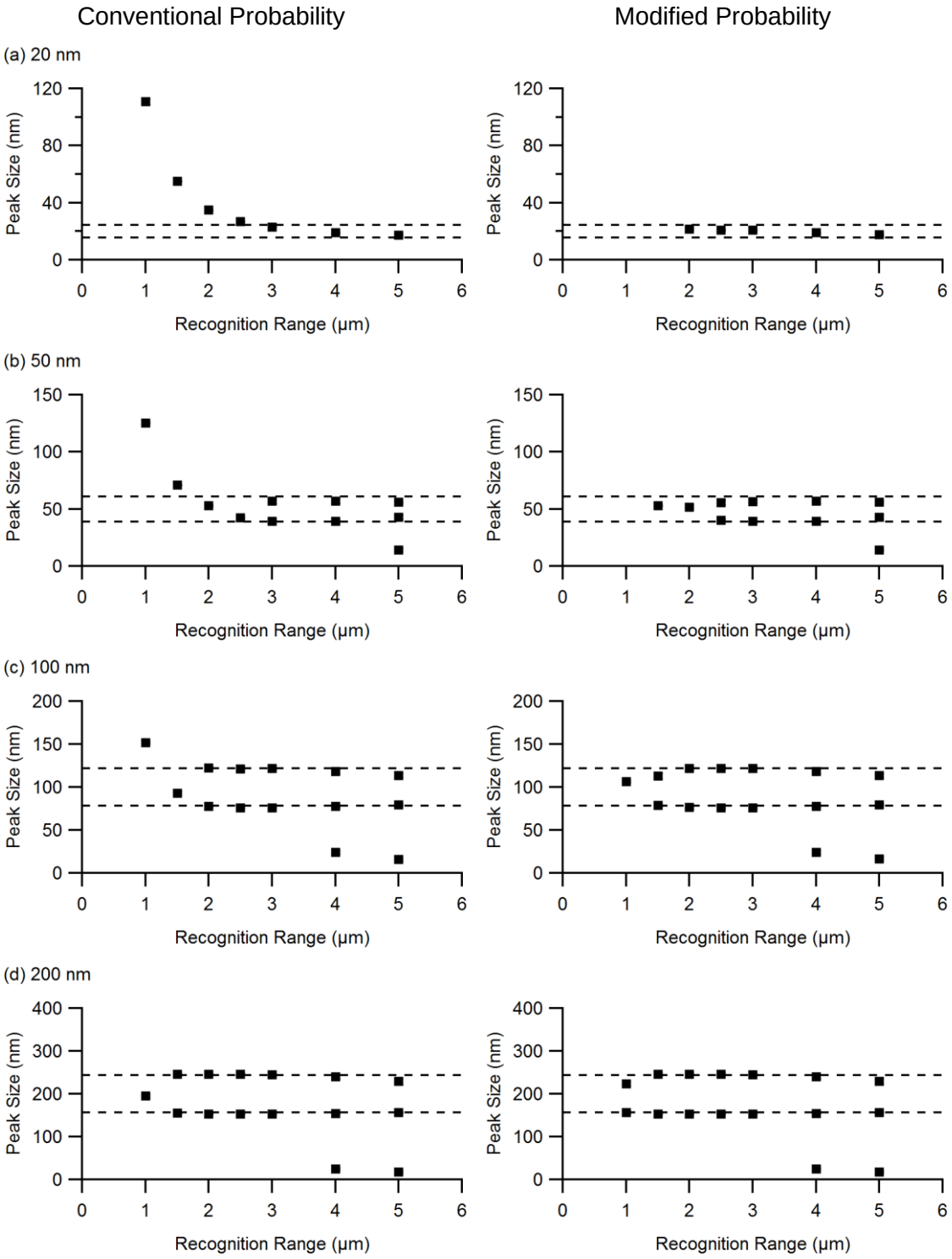

Figure 5.9 Results from a computer simulation. The position of the peaks identified from the size distributions determined from the simulated Brownian movements of particles, where the tracks of the particles are recognized at a various recognition radius from 1 to 5 μm. For each simulation, a set of particles with a bi-modal distribution whose mean size is (a) 20, (b) 50, (c) 100 and (d) 200 nm with relative variance of 0.05 at a concentration of 1×10^9 particles/ml was used. The corresponding position of the nominal peaks for a mean size of 20, 50, 100 and 200 nm are 16 and 25, 39 and 61, 78 and 122, and 155 and 245 nm, respectively. For each mean size condition, 25 runs of simulated NTA measurements were produced. From the recognized tracks of the simulated measurements on a various recognition radius, the size distribution was estimated by the iterative MLE method with the conventional displacement probability (left) and the modified displacement probability (right). Dashed guidelines show the respective nominal peak positions.

Figure 5.9 identifies the position of the peaks found from the results of the bi-modal size distribution simulations analyzed with the two probabilities on a various recognition radius from 1 to 5 μm. At a long recognition radius, where the recognition radius is long enough compared to the diffusion length, the two peaks are observable for the nominal mean size of 50, 100 and 200 nm. The identified positions agree well with their respective nominal peak positions regardless of the probabilities. A spurious peak at a small-size range is also observed for the three mean size conditions at a very long recognition radius, e.g., 5 μm. However, it is not possible to resolve the two separate peaks when the nominal mean size is 20 nm at the recognition radius regardless of the displacement probability as shown in Figure 5.9(a). On the other hand, only a single peak is identified for all the mean size conditions at a short recognition radius regardless of the displacement probability. This confirms that a short recognition radius limits the size resolution of NTA measurements and inhibits its proper size distribution determination. Remarkably, the modified probability allows a wider range for the recognition radius that could resolve the two separate peaks than the conventional probability does.

5.4.3 Influence of particle concentration

False tracks can undermine correct size distribution determination of NTA measurements. Since false tracks are created when two different particles are recognized as the same

particle, the probability of false track creation would depend on the concentration of particles as well as the recognition radius set for the analysis [25]. Furthermore, an increase of the particle concentration would lead to a higher probability of early termination of the particle tracking process since neighboring particles around the tracked particle would jump into the recognition radius and interrupt the tracking process more frequently [25]. This suggests that an increased particle concentration results in a poorer resolution of NTA size distribution determination along with the influence of the false tracks since the uncertainty of the determined size of a track are inversely proportional to the square root of its track length [19, 21, 27-29].

To identify the influence of the particle concentration in NTA size distribution determination, a series of NTA simulations with a model particle set with a uniform size of 20, 50, 100 and 200 nm at a various concentration of 1×10^{8}, 1×10^{9} and 1×10^{10} particles/ml was conducted. For each combination of the mean size and concentration, 25 sets of simulations were produced. The simulated results were processed to construct tracks at a various recognition radius from 1 to 5 μm and analyzed to determine a size distribution with the two displacement probabilities.

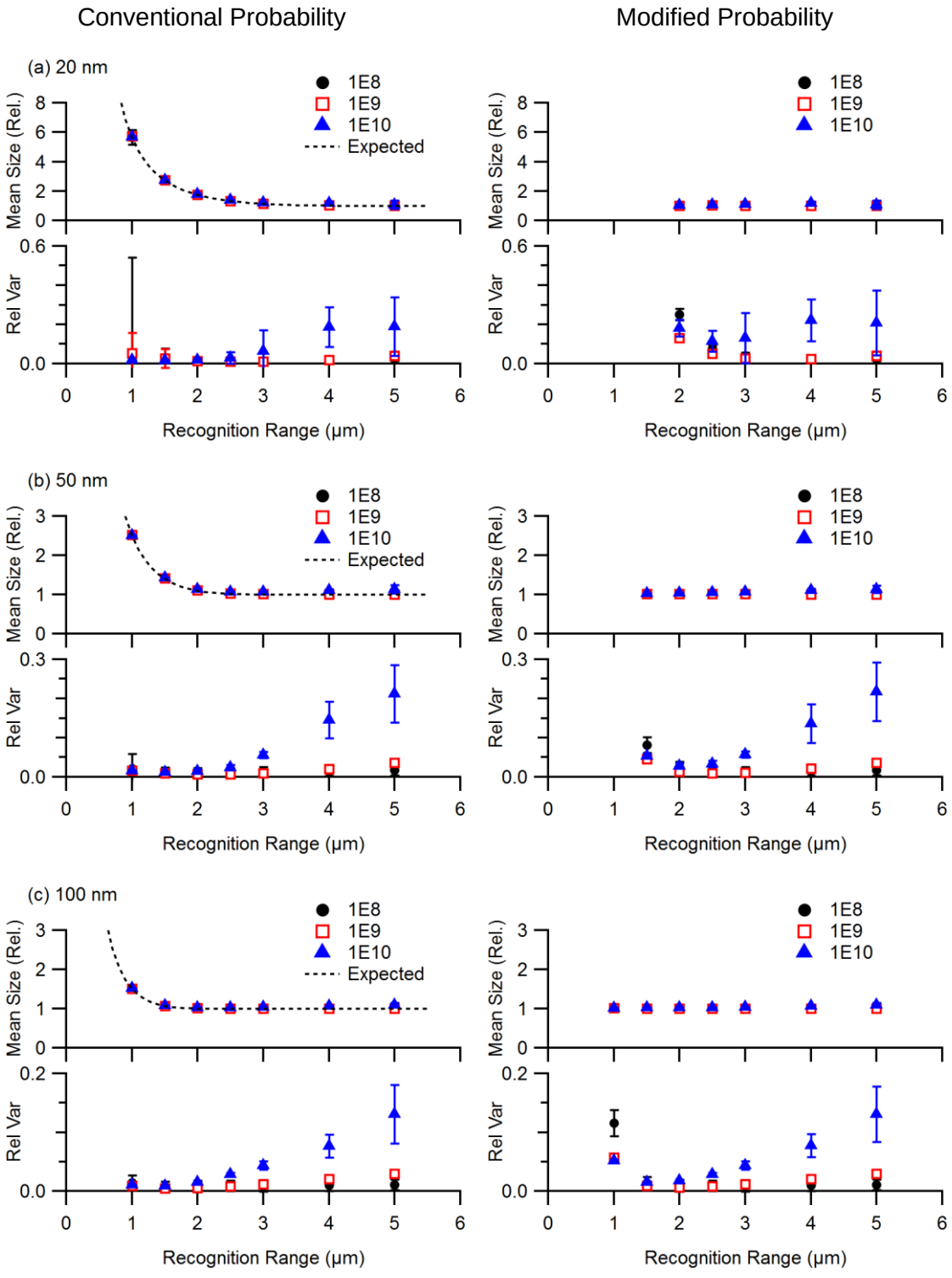
Conventional Probability
Modified Probability
(a) 20 nm
(b) 50 nm
(c) 100 nm
1E8
1E9
1E10
Expected
Mean Size (Rel.)
Rel Var
Recognition Range (µm)

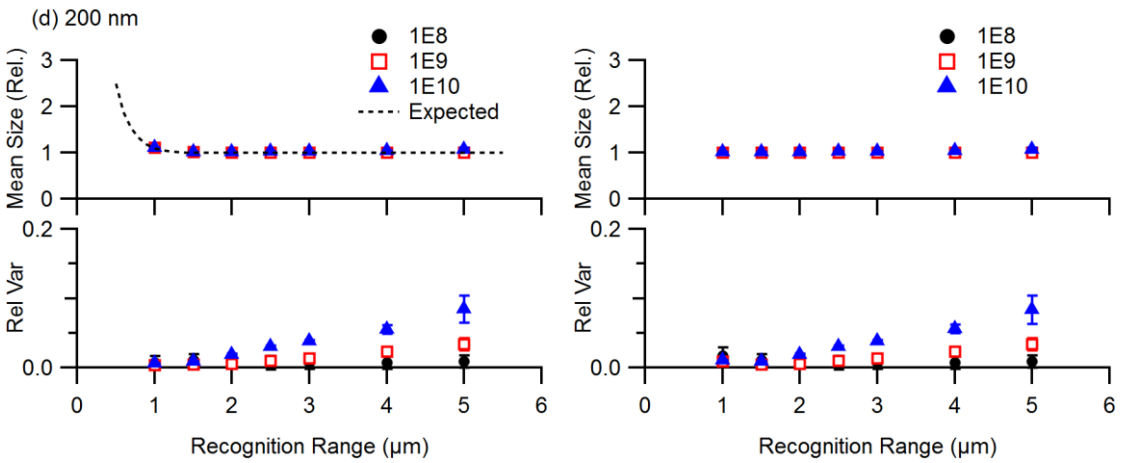

Figure 5.10 Results from a computer simulation. Mean size and relative variance of the size distributions determined from the simulated Brownian movements of particles, where the tracks of the particles are recognized at a various recognition radius from 1 to 5 μm. For each simulation, monomodal particles with a size of (a) 20, (b) 50, (c) 100, and (d) 200 nm at a concentration of 1×10^{8} (black circle), 1×10^{9} (red open square) and 1×10^{10} particles/ml (blue triangle) were generated. For each combination of mean size and concentration, 25 runs of simulated NTA measurements were produced. From the recognized tracks of the simulated measurements on a various recognition radius, the size distribution was estimated by the iterative MLE method with the conventional displacement probability (left) and the modified displacement probability (right). The acquired mean size is displayed with respect to the nominal mean size of the respective simulated particle sets. Dashed guidelines show the expected overestimated mean size due to the use of the conventional probability. Note that the size distributions from the simulations of a mean size condition of 20 and 50 nm estimated by the modified displacement probability do not converge well when the recognition radius is below 1.5 and 1 μm, respectively, and their corresponding relative variance is not displayed in (a) and (b).

Figure 5.10 compares the mean size and relative variance determined from the simulation results. The dependence of the mean size on the recognition radius shows the same results as what observed in the previous results regardless of the concentration condition. At a short recognition radius, the conventional probability provides an overestimated mean size and a very narrow size distribution, while the modified probability mitigates the overestimation in the mean size with a large relative variance. On the conditions of a small nominal mean size, i.e., 20 and 50 nm, the results acquired with the modified probability did not provide a proper size distribution at a small recognition radius, e.g., 1 μm and are

not displayed in Figure 5.10(a) and (b). At a long recognition radius, the mean size produced by the two probabilities is close to the nominal value regardless of the probabilities.

On the other hand, the relative variance of the acquired size distributions shows a significant dependence on the concentration condition. On a higher concentration, a larger value of relative variance of the determined size distributions is measured for all the nominal mean size conditions and the recognition radius. At a concentration of 1×10^{8} particles/ml, relative variance acquired at a recognition radius of 5 μm is 0.027 ± 0.021, 0.017 ± 0.012, 0.011 ± 0.003 and 0.009 ± 0.004 with the conventional probability and 0.028 ± 0.023, 0.017 ± 0.012, 0.011 ± 0.003 and 0.009 ± 0.004 with the modified probability for the mean size conditions of 20, 50, 100 and 200 nm, respectively. On an increased concentration of 1×10^{9} particles/ml, relative variance acquired at the same recognition radius of 5 μm is 0.040 ± 0.021, 0.036 ± 0.008, 0.030 ± 0.004 and 0.034 ± 0.009 with the conventional probability and 0.039 ± 0.020, 0.036 ± 0.008, 0.030 ± 0.003 and 0.034 ± 0.009 with the modified probability for the mean size conditions of 20, 50, 100 and 200 nm, respectively. On a concentration of 1×10^{10} particles/ml, relative variance of 0.190 ± 0.150, 0.212 ± 0.074, 0.130 ± 0.050 and 0.084 ± 0.020 with the conventional probability and of 0.208 ± 0.164, 0.217 ± 0.074, 0.130 ± 0.047 and 0.083 ± 0.021 with the modified probability was acquired for the mean size conditions of 20, 50, 100 and 200 nm, respectively, at the recognition radius of 5 μm. The observation indicates that the size distribution acquired with NTA has a broader distribution than the true distribution, where the degree of the broadening gets bigger on a higher particle concentration.

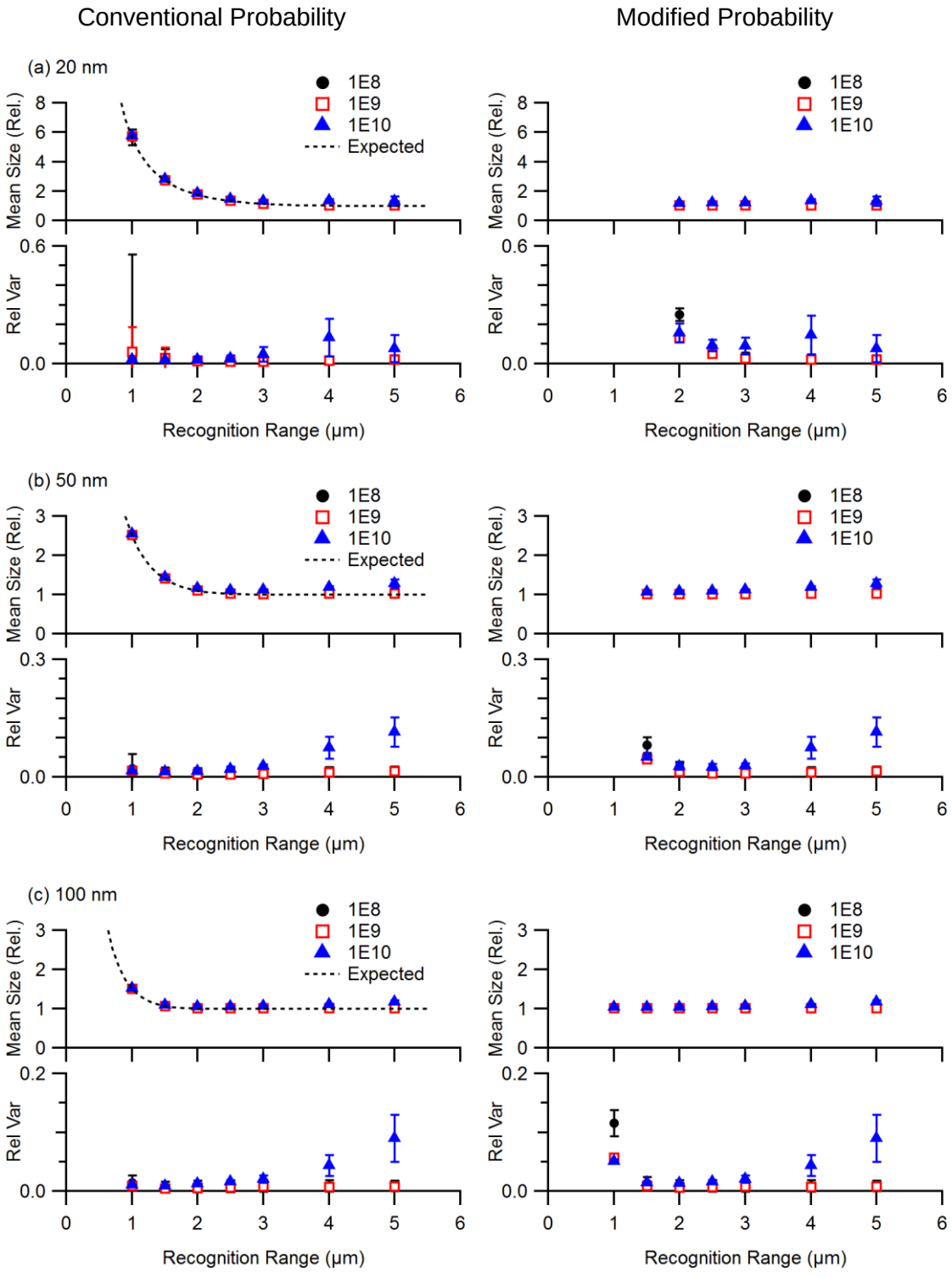
Conventional Probability
Modified Probability
(a) 20 nm
(b) 50 nm
(c) 100 nm
1E8
1E9
1E10
Expected
Mean Size (Rel.)
Rel Var
Recognition Range (µm)

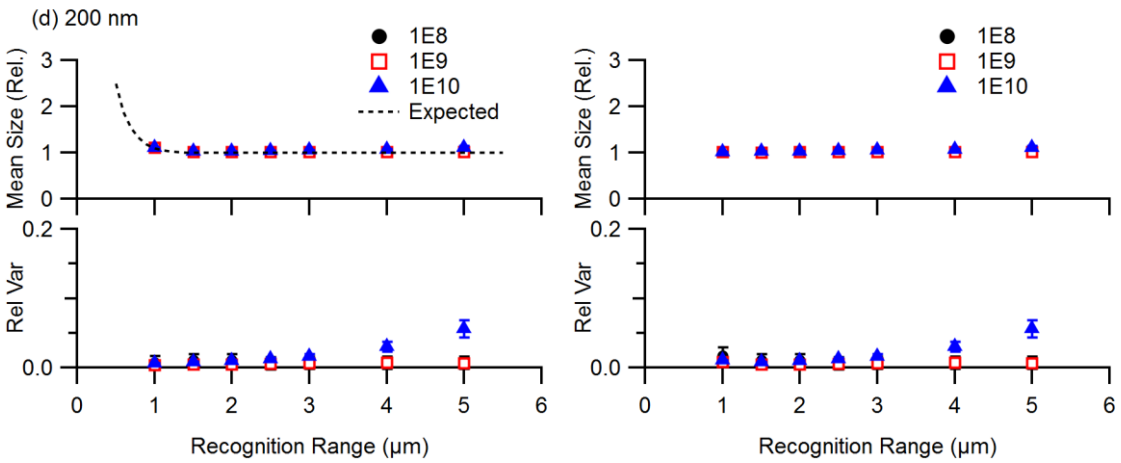

Figure 5.11 Reanalyzed results of the computer simulation shown in Figure 5.10. Mean size and relative variance of the size distributions determined from the simulated Brownian movements of particles, where those false tracks are excluded from the analysis. For each simulation, monomodal particles with a size of (a) 20, (b) 50, (c) 100, and (d) 200 nm at a concentration of 1×10^{8} (black circle), 1×10 (red open square) and 1×10^{10} particles/ml (blue triangle) were generated. For each combination of mean size and concentration, 25 runs of simulated NTA measurements were produced. From the recognized tracks of the simulated measurements on a various recognition range, the size distribution was estimated by the iterative MLE method with the conventional displacement probability (left) and the modified displacement probability (right). The acquired mean size is displayed with respect to the nominal mean size of the respective simulated particle sets. Dashed guidelines show the expected overestimated mean size due to the use of the conventional probability. Note that the size distributions from the simulations of a mean size condition of 20 and 50 nm estimated by the modified displacement probability do not converge well when the recognition range is below 1.5 and 1 μm, respectively, and their corresponding relative variance is not displayed.

As discussed earlier, the larger relative variance on a higher concentration condition could be due to an increased number of false tracks. To investigate the effect of false tracks, the simulation results were re-analyzed with those false tracks excluded from the analysis as presented in Figure 5.11. Overall, the two displacement probabilities provided very similar results to each other when evaluated at the recognition radius of 5 μm. If the false tracks are excluded from the analysis, relative variance of the determined size distributions for a mean size of 20, 50, 100 and 200 nm, respectively, is 0.024 ± 0.022, 0.015 ± 0.012, 0.009 ± 0.003 and 0.007 ± 0.002 at a concentration of 1×10^{8} particles/ml at the recognition radius

of 5 µm. The values are not much different from the results acquired with the false tracks included. Since the number of particles detected in the field-of-view is very small at the concentration level, i.e., approximately 7 particles, it is unlikely that the tracking process is corrupted by false tracks. At a concentration of 1×10^9 particles/ml, relative variance of 0.022 ± 0.020, 0.014 ± 0.008, 0.008 ± 0.001 and 0.006 ± 0.002 are acquired for a mean size of 20, 50, 100 and 200 nm, respectively, at the same recognition radius. The acquired values are very similar with their respectively corresponding relative variance measured at the concentration of 1×10^8 particles/ml, indicating that the larger relative variance at the concentration of 1×10^9 particles/ml is due to the false tracks.

At a concentration of 1×10^{10} particles/ml, on the other hand, 0.077 ± 0.069, 0.114 ± 0.038, 0.090 ± 0.040 and 0.056 ± 0.012 are given for relative variance of the determined size distribution for a mean size of 20, 50, 100 and 200 nm, respectively, at the same recognition radius of 5 µm when the false tracks were excluded. Although the acquired values are significantly smaller than those acquired with the false tracks included, meaning that the false tracks make the acquired size distribution much broader, the values are yet larger than their respectively corresponding values measured at the concentration of 1×10^8 and 1×10^9 particles/ml. It indicates that false tracks are not the only source of a broad size distribution determined by NTA at a very high concentration.

As discussed earlier, another supposed cause of such broad size distributions measured by NTA is an early termination of tracks due to an increased number of neighboring particles on a higher concentration. In fact, the average track length of the analyzed tracks at the concentration of 1×10^{10} particles/ml is 5.3, 5.9, 6.6 and 7.5 for the mean size conditions of 20, 50, 100 and 200 nm, respectively, at the recognition radius of 5 µm. Figure 5.12 reveals the average track length of the acquired tracks on various nominal mean size and concentration. On the other hand, the average track length is 13.5, 21.6, 29.9 and 38.6 at the concentration of 1×10^8 particles/ml and 9.0, 12.6, 16.7 and 22.2 at the concentration of 1×10^9 particles/ml for a mean size of 20, 50, 100 and 200 nm, respectively, at the recognition radius of 5 µm. The significant difference in the average track length depending

on the particle concentration suggests that the reduced average track length results in a broader size distribution on an increasing concentration.

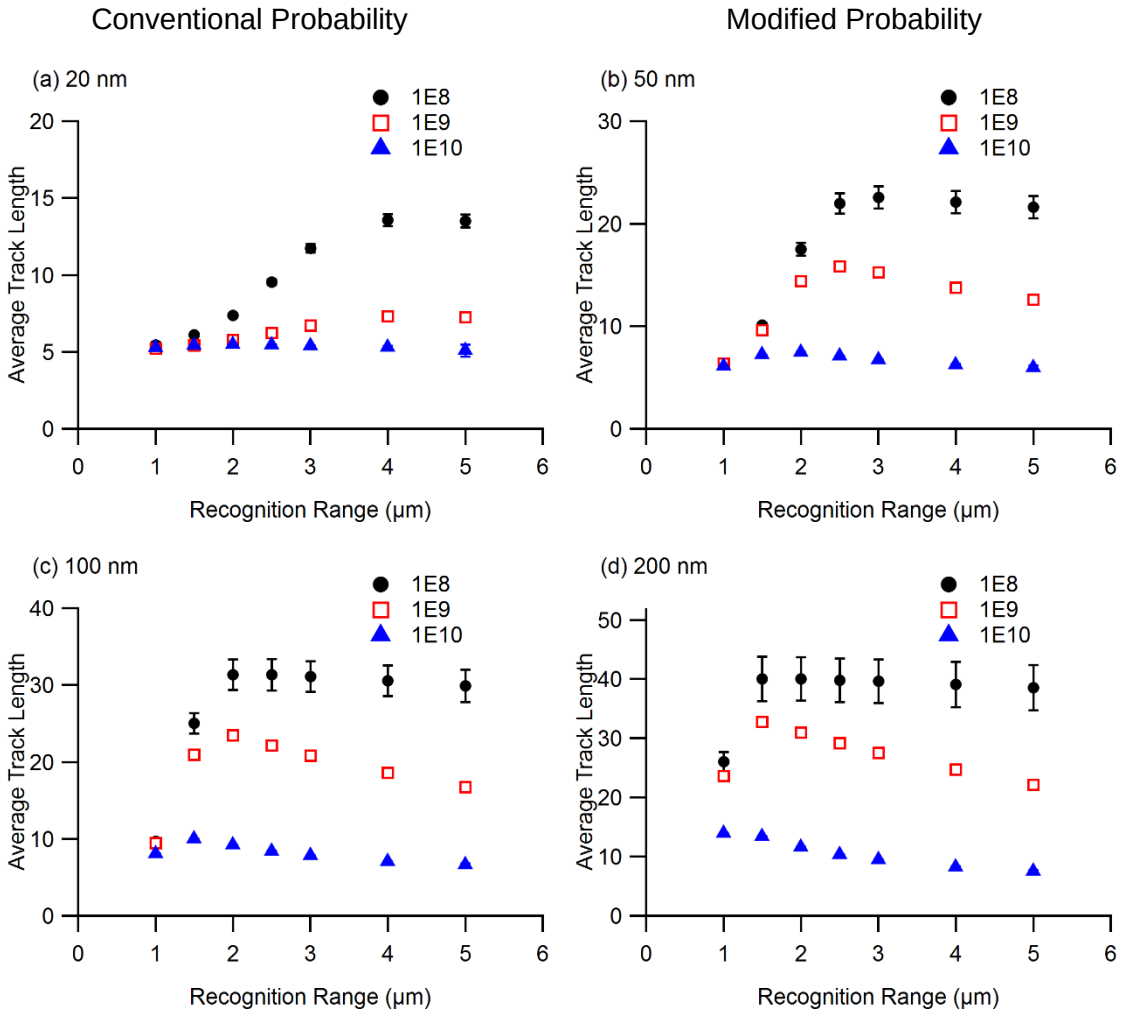

Figure 5.12 Results from a computer simulation. The average track length of the particles tracks used for the size distribution determination from the simulated Brownian movements of particles, where the tracks of the particles are recognized at a various recognition range from 1 to 5 μm. For each simulation, monomodal particles with a size of (a) 20, (b) 50, (c) 100, and (d) 200 nm at a concentration of 1×10^{8} (black circle), 1×10^{9} (red open square) and 1×10^{10} particles/ml (blue triangle) were generated. For each combination of mean size and concentration, 25 runs of simulated NTA measurements were produced.

From the observation, it could be expected that a narrower size distribution from NTA if the probability of the tracking termination is reduced and hence the average track length to be increased. At any given concentration condition, the probability of track termination is

related with the probability of the neighboring particles jumping into the recognition radius of the tracked particle, meaning that the termination probability would decrease if the recognition radius is reduced. This is obvious from Figure 5.10, where relative variance becomes smaller on a decreasing recognition radius regardless of the mean size and the concentration. The observation is supported by the average track length depending on the recognition radius as shown in Figure 5.12. This finding suggests that a smaller recognition radius would be preferred to acquire a narrower size distribution since it would result in a longer track length of the tracks used for NTA analysis.

5.4.4 PS nanoparticle standards

Having tested the conventional and the modified displacement probabilities on the simulated results, the two probabilities were applied to experimental NTA data. PS latex standards of a nominal mean size of 51.6 and 181.6 nm were measured at two different particle concentration conditions, namely 1×10^8 and 1×10^9 particles/ml. The particle tracks from NTA were constructed at a various recognition radius from 1.1 to 5.4 μm and processed with the conventional and the modified displacement probabilities. Figure 5.13 shows the results of NTA measurements on the PS latex standards. For the sample of a nominal mean size of 51.6 nm, as in Figure 5.13(a) and (b), the mean size obtained with the conventional probability is close to the nominal mean size at a recognition radius of 5.4 μm, where the mean size of 68 ± 5 and 54 ± 2 nm is determined for the 1×10^8 and 1×10^9 particles/ml concentrations, respectively. At this recognition radius, the mean size obtained with the modified probability is the same as that acquired with the conventional probability. Remarkably, the slight deviation of the acquired mean size from the nominal value seems due to the increased relative variance which would be described later. In fact, the modal value of the determined size distribution listed in Table 5.1 is very close to the nominal size for the two concentration conditions [32].

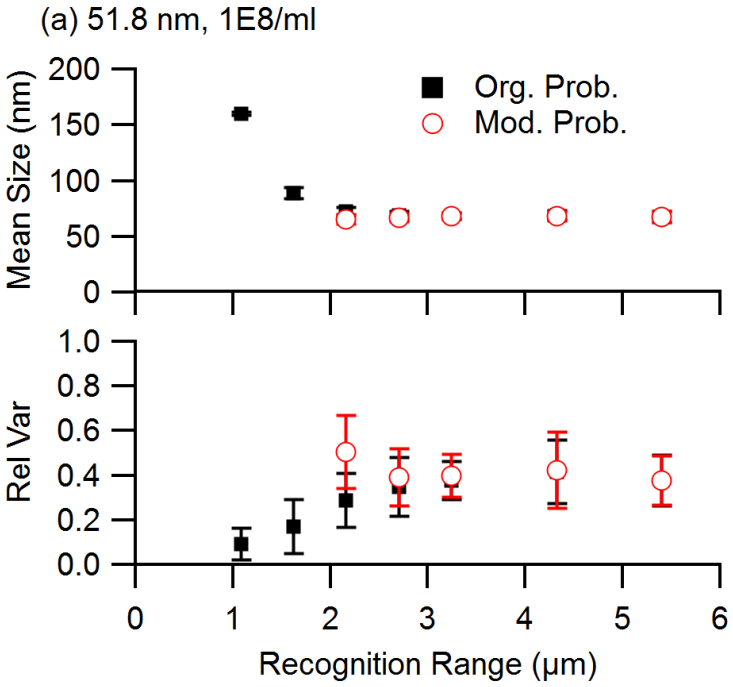
(a) 51.8 nm, 1E8/ml
Org. Prob.
Mod. Prob.
Mean Size (nm)
200
150
100
50
0
Rel Var
1.0
0.8
0.6
0.4
0.2
0.0
0
1
2
3
4
5
6
Recognition Range (µm)

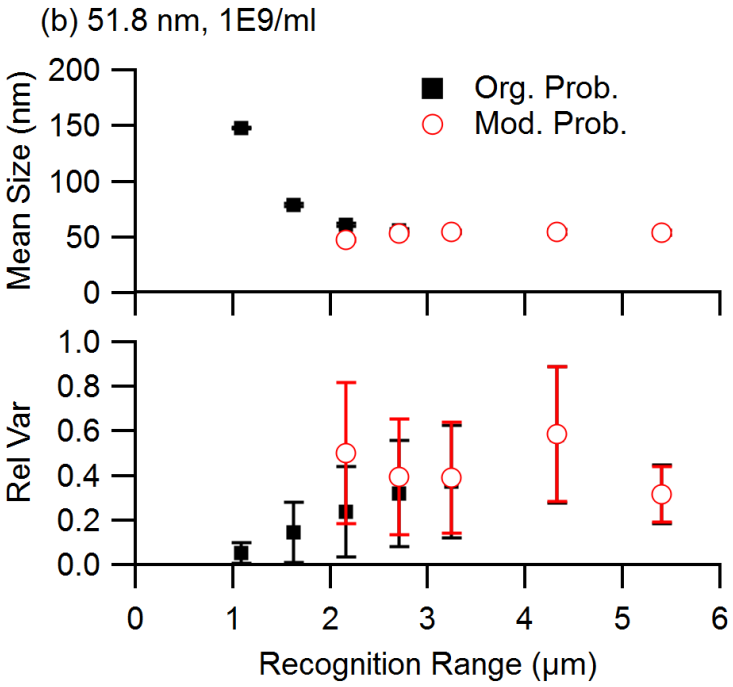
(b) 51.8 nm, 1E9/ml
Org. Prob.
Mod. Prob.
Mean Size (nm)
200
150
100
50
0
Rel Var
1.0
0.8
0.6
0.4
0.2
0.0
0
1
2
3
4
5
6
Recognition Range (µm)

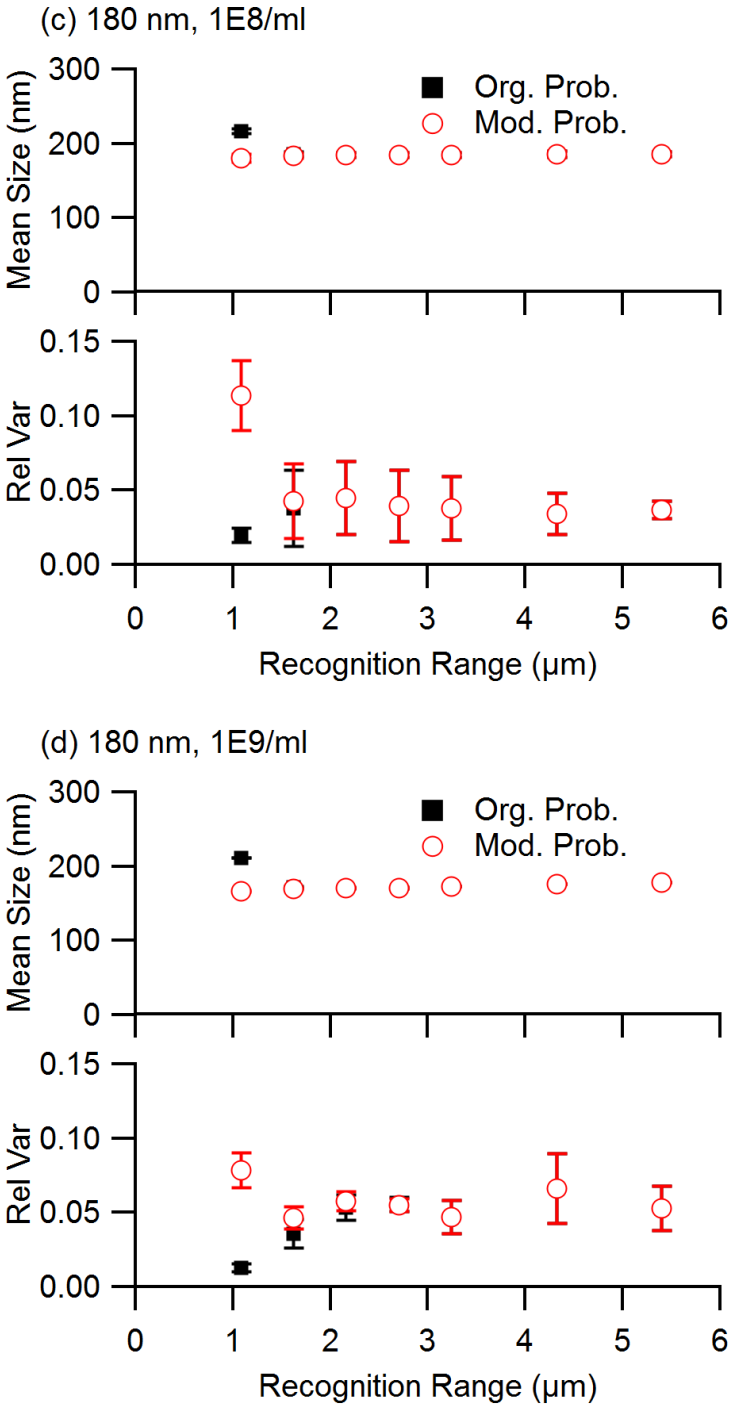

Figure 5.13 Mean size and relative variance of the size distributions determined from NTA measurements of PS latex nanoparticles with a nominal size of (a) 51.6 and (b) 181.6 nm using a various recognition radius from 1.1 to 5.4 µm at two different concentrations of 1×10^{8} (left) and 1×10^{9} particles/ml (right). Three runs of measurements were conducted for each combination of nominal sample size and concentration. From the tracks acquired from the NTA measurements at

a various recognition radius, the size distribution was estimated by the iterative estimation method with the conventional (black square) and the modified (red open circle) displacement probabilities. With the modified displacement probability, it was not possible to achieve a good convergence of the size estimation when the recognition radius is small, i.e. up to 1.6 μm for the 51.6-nm standard and not displayed in (a) and (b).

On a subsequent decrease of the recognition radius, the mean size acquired with the conventional probability gradually increases. At a recognition radius of 1.1 μm, the mean size determined for the 1×10^8 and 1×10^9 particles/ml concentrations with the conventional probability was 160 ± 1 and 148 ± 1 nm, respectively. On the other hand, the modified probability provides a consistent mean size value regardless of the recognition radius. However, it failed to acquire a proper size distribution on a very small recognition radius when the recognition radius is below 1.6 μm.

For the sample of a nominal mean size of 181.6 nm, as shown in Figure 5.13(c) and (d), the acquired mean size at a recognition radius of 5.4 μm is 186 ± 3 and 178 ± 1 nm for the 1×10^8 and 1×10^9 particles/ml concentrations, respectively, regardless of the displacement probability. On a decreasing recognition radius, the mean size shows the same trends as observed from the 51.6-nm standard.

Relative variance acquired with the two displacement probabilities is also in line with the observation from the simulated results. For the sample of a nominal mean size of 51.6 nm, relative variance at a recognition radius of 5.4 μm is 0.377 ± 0.112 and 0.316 ± 0.130 for the 1×10^8 and 1×10^9 particles/ml concentrations, respectively, when the conventional probability is used. The values acquired with the modified probability are the same as those from the conventional probability at the same recognition radius. On a decreasing recognition radius, the relative variance acquired with the conventional probability gradually decreases as is observed from the simulated results. At a recognition radius of 1.1 μm, relative variance is 0.092 ± 0.071 and 0.055 ± 0.047 for the 1×10^8 and 1×10^9 particles/ml concentrations, respectively.

Table 5.1 Mean size, modal size and relative variance of the size distributions determined from NTA measurements of PS latex nanoparticles with a nominal size of 51.6 and 181.6 nm using a various recognition range from 1.1 to 5.4 μm at two different concentrations of 1×10^8 and 1×10^9 particles/ml. Three runs of measurements were conducted for each combination of nominal sample size and concentration. From the tracks acquired from the NTA measurements at a various recognition range, the size distribution was estimated by the iterative estimation method with the conventional and the modified displacement probabilities.

Sample	Rec. Range (μm)	Conv Mean (nm)	Mode (nm)	Rel. Var.	Modi Mean (nm)	Mode (nm)	Rel. Var.
PS 51.6 nm	1.1	160 ± 1	148 ± 3	0.092 ± 0.070	58 ± 1	1 ± 0	2.242 ± 0.756
1×10^8 /ml	1.6	89 ± 5	78 ± 2	0.171 ± 0.120	55 ± 7	1 ± 0	0.872 ± 0.178
	2.2	73 ± 3	60 ± 1	0.289 ± 0.121	65 ± 4	51 ± 2	0.507 ± 0.163
	2.7	69 ± 3	55 ± 0	0.348 ± 0.131	67 ± 4	53 ± 0	0.390 ± 0.127
	3.2	68 ± 3	53 ± 2	0.377 ± 0.084	68 ± 3	53 ± 2	0.397 ± 0.097
	4.3	69 ± 4	52 ± 1	0.416 ± 0.142	68 ± 4	53 ± 2	0.422 ± 0.170
	5.4	68 ± 5	54 ± 2	0.377 ± 0.112	68 ± 5	54 ± 2	0.379 ± 0.112
PS 51.6 nm	1.1	148 ± 1	140 ± 1	0.045 ± 0.032	25 ± 1	1 ± 0	4.801 ± 1.664
1×10^9 /ml	1.6	79 ± 1	76 ± 1	0.115 ± 0.106	35 ± 2	1 ± 0	1.296 ± 0.502
	2.2	61 ± 1	57 ± 0	0.189 ± 0.151	48 ± 1	44 ± 1	0.434 ± 0.251
	2.7	57 ± 1	51 ± 0	0.264 ± 0.180	54 ± 1	48 ± 1	0.333 ± 0.204
	3.2	56 ± 1	49 ± 0	0.350 ± 0.175	56 ± 1	49 ± 0	0.369 ± 0.181
	4.3	56 ± 2	51 ± 2	0.466 ± 0.219	56 ± 2	51 ± 2	0.470 ± 0.221
	5.4	56 ± 2	51 ± 0	0.293 ± 0.104	58 ± 2	50 ± 1	0.333 ± 0.115
PS 181.6 nm	1.1	209 ± 1	206 ± 2	0.010 ± 0.001	170 ± 2	166 ± 3	0.075 ± 0.014
1×10^8 /ml	1.6	177 ± 1	175 ± 0	0.067 ± 0.048	175 ± 2	174 ± 1	0.072 ± 0.043
	2.2	177 ± 0	173 ± 0	0.090 ± 0.037	176 ± 0	173 ± 0	0.091 ± 0.037
	2.7	176 ± 0	173 ± 2	0.091 ± 0.039	176 ± 0	173 ± 2	0.091 ± 0.039
	3.2	176 ± 1	173 ± 0	0.069 ± 0.026	176 ± 1	173 ± 0	0.069 ± 0.026
	4.3	174 ± 1	175 ± 2	0.053 ± 0.022	174 ± 1	175 ± 2	0.053 ± 0.022
	5.4	174 ± 2	175 ± 2	0.045 ± 0.011	174 ± 2	175 ± 2	0.045 ± 0.011
PS 181.6 nm	1.1	207 ± 0	204 ± 1	0.014 ± 0.004	160 ± 1	158 ± 1	0.080 ± 0.015
1×10^9 /ml	1.6	164 ± 1	163 ± 2	0.045 ± 0.008	159 ± 1	161 ± 2	0.060 ± 0.009
	2.2	158 ± 1	164 ± 1	0.061 ± 0.012	158 ± 1	164 ± 1	0.064 ± 0.012
	2.7	161 ± 1	166 ± 1	0.082 ± 0.023	161 ± 1	166 ± 1	0.085 ± 0.022
	3.2	165 ± 1	166 ± 1	0.074 ± 0.009	165 ± 0	166 ± 1	0.074 ± 0.010
	4.3	171 ± 0	167 ± 2	0.056 ± 0.011	171 ± 0	167 ± 2	0.056 ± 0.011
	5.4	174 ± 0	168 ± 2	0.053 ± 0.009	174 ± 0	168 ± 2	0.053 ± 0.009

Relative variance acquired with the modified probability has the same value acquired with the conventional probability on a subsequent decrease of the recognition radius from 5.4 μm. When the recognition radius becomes even smaller, relative variance acquired with the modified probability shows a value different from that acquired with the conventional probability and started to increase. At a recognition radius of 2.2 μm, relative variance acquired with the modified probability is 0.507 ± 0.163 and 0.503 ± 0.318 for the 1×10^{8} and 1×10^{9} particles/ml concentrations, respectively, whereas the corresponding value acquired with the conventional probability is 0.289 ± 0.121 and 0.239 ± 0.202. Remarkably, the modified probability fails to acquire a proper size distribution on a small recognition radius below 1.6 μm and gives a huge relative variance. Figure 5.14 presents the acquired size distributions of each sample at a various recognition radius.

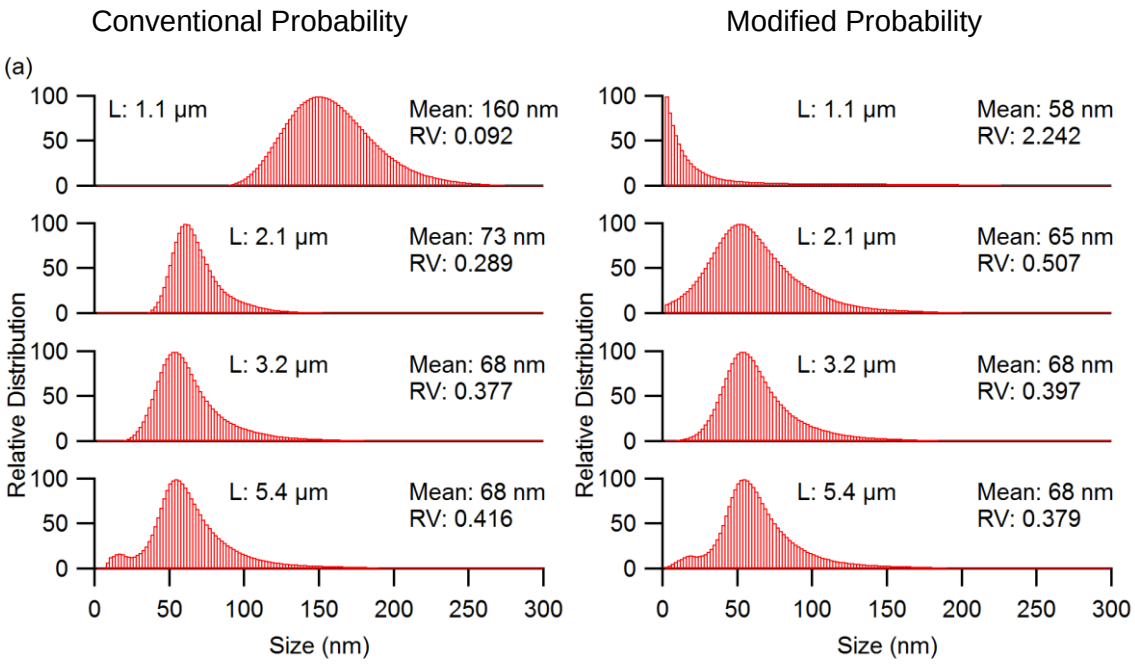

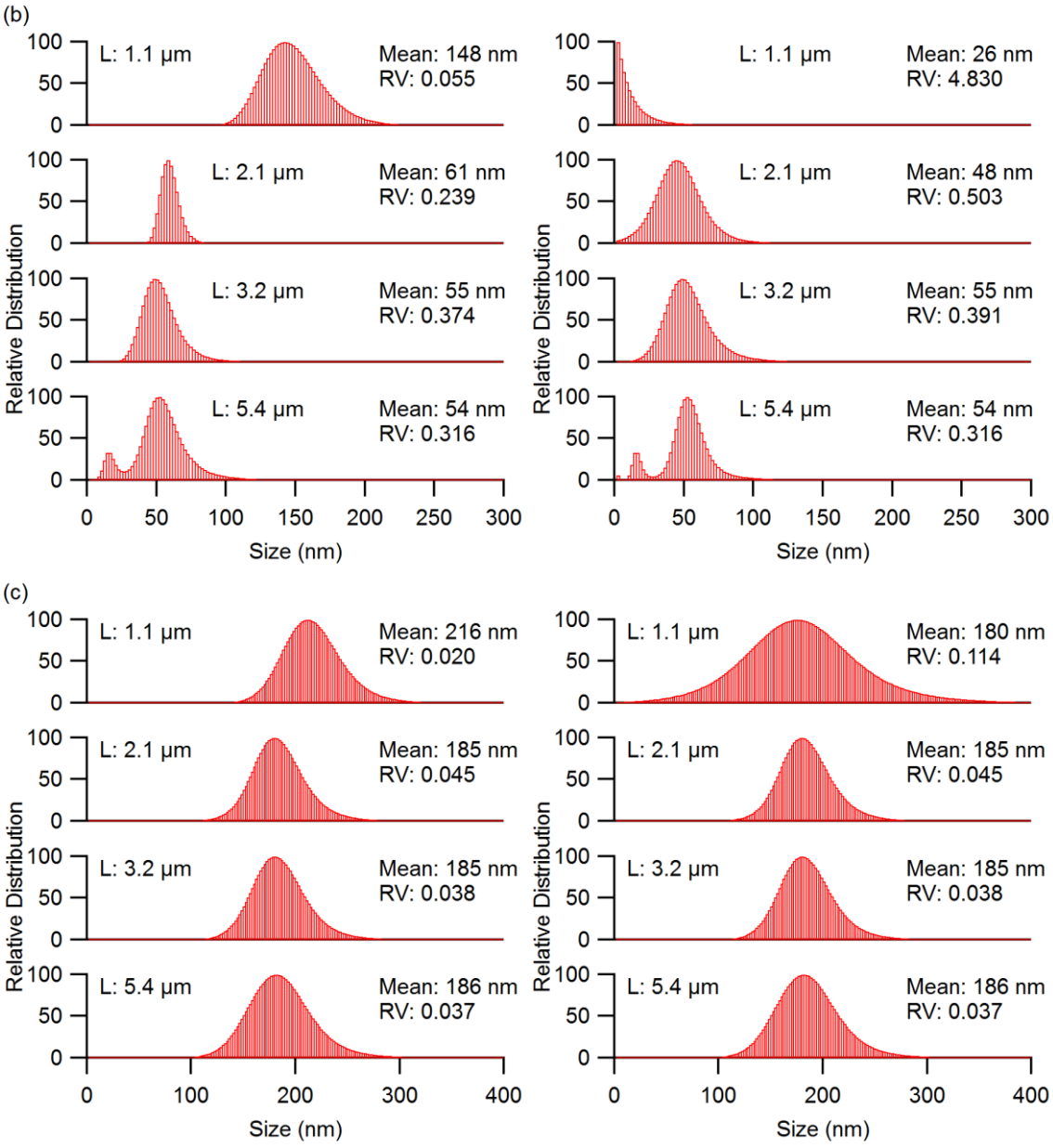
(b)
L: 1.1 µm
Mean: 148 nm
RV: 0.055
L: 2.1 µm
Mean: 61 nm
RV: 0.239
L: 3.2 µm
Mean: 55 nm
RV: 0.374
L: 5.4 µm
Mean: 54 nm
RV: 0.316
L: 1.1 µm
Mean: 26 nm
RV: 4.830
L: 2.1 µm
Mean: 48 nm
RV: 0.503
L: 3.2 µm
Mean: 55 nm
RV: 0.391
L: 5.4 µm
Mean: 54 nm
RV: 0.316
Relative Distribution
Size (nm)
(c)
L: 1.1 µm
Mean: 216 nm
RV: 0.020
L: 2.1 µm
Mean: 185 nm
RV: 0.045
L: 3.2 µm
Mean: 185 nm
RV: 0.038
L: 5.4 µm
Mean: 186 nm
RV: 0.037
L: 1.1 µm
Mean: 180 nm
RV: 0.114
L: 2.1 µm
Mean: 185 nm
RV: 0.045
L: 3.2 µm
Mean: 185 nm
RV: 0.038
L: 5.4 µm
Mean: 186 nm
RV: 0.037
Relative Distribution
Size (nm)

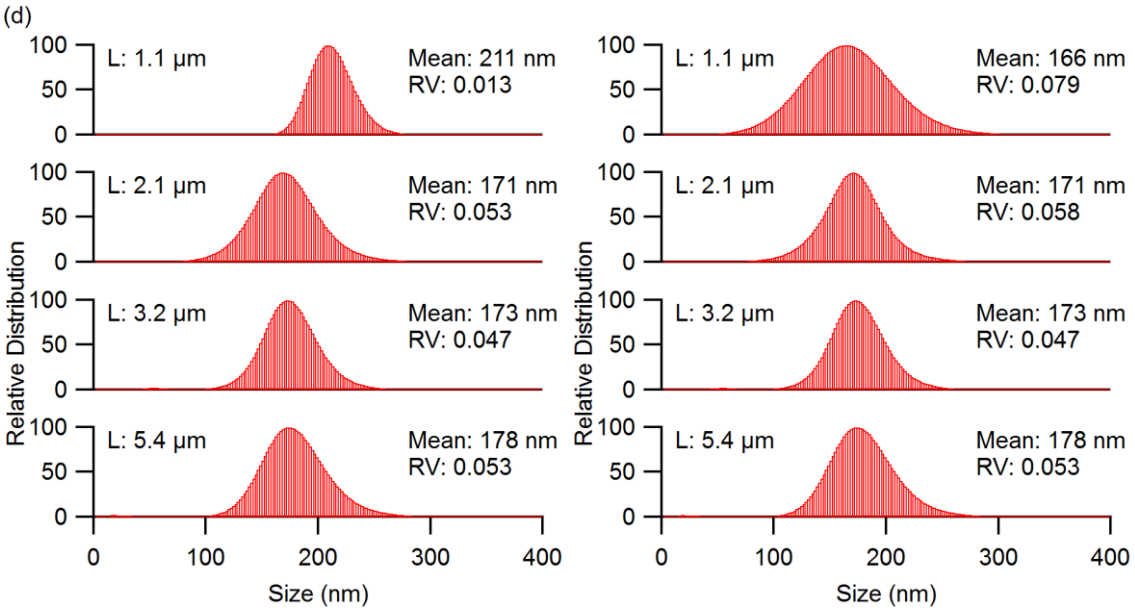

Figure 5.14 Size distributions determined from NTA measurements of PS latex nanoparticles with a nominal size of (a, b) 51.6 and (c, d) 181.6 nm at a recognition range *L* from 1.1 to 5.4 µm. For each nominal size, two different concentration levels, (a, c) 1×10^9 and (b, d) 1×10^8 particles/ml, were prepared for each particle size. Three runs of measurements were conducted for each combination of nominal sample size and concentration, where the distributions above are the average of the three runs each. The size distributions are estimated with the conventional displacement probability (left) and the modified displacement probability (right) on the tracks recognized at a various recognition range from 1.1 µm (top) to 5.4 µm (bottom). Those tracks with a minimum track length of 5 was used for the analysis. The bin width of the size distributions is 2 nm, and each distribution is normalized with respect to its respective maximum. With the modified displacement probability, it was not possible to achieve a good convergence of the size estimation on the 51.6-nm standard at a recognition range of 1.1 µm.

For the sample of a nominal mean size of 181.6 nm, relative variance acquired at a recognition radius of 5.4 µm is 0.037 ± 0.006 and 0.053 ± 0.015 for the 1×10^8 and 1×10^9 particles/ml concentrations, respectively, regardless of the displacement probability used. As was seen from the smaller 51.6-nm sample, relative variance acquired with the conventional probability decreases on a decreasing recognition radius. Relative variance acquired with the modified probability shows the same behavior as was seen in the 51.6-nm standard, where it has the same value to that acquired with the conventional probability

on a subsequent decrease from 5.4 μm and starts to deviate from their respectively corresponding value from the conventional probability on a very small recognition radius.

Regarding large relative variance observed at a long recognition radius, the simulation results attributed it to the false tracks, where two different particles are recognized as the same particle. Indeed, the size distribution of the 51.6-nm standard acquired at a recognition radius of 5.4 μm, presented in Figure 5.14(a), shows a spurious peak as seen in the simulation results. However, the relative variance of the 51.6-nm standard is much larger compared to the value observed from the simulation results. This seems due to false identification of particles, increasing the probability of false tracking [26, 27, 37, 38]. Since the scattered light from the 51.6-nm particles is not strong enough to be well distinguished from the background noise and artifacts could be identified as particles, it might introduce more false tracks. As a larger particle scatters stronger light and is easier to be distinguished from the background, less false tracks and smaller relative variance can be expected on larger particles. On the 181.6-nm standard, relative variance of the size distribution acquired at a long recognition radius is significantly smaller than that observed from the 51.6-nm standard. This indicates that the size distribution of smaller particles analyzed by NTA could have more uncertainty due to their weak scattering power that introduces more false tracks. The comparison of the two displacement probabilities on the real NTA measurements confirms the observations from the simulated results and suggests that the modified displacement probability is useful in determining a particle size distribution by NTA especially in the conditions where the recognition radius should be restricted.

5.5 Conclusion

An improved method was suggested for determining the size distribution of NTA based on the MLE approach that takes the recognition radius into account. By considering the recognition radius used for particle tracking in NTA, a modified displacement probability was introduced for the likelihood calculation of the MLE method. Simulated NTA measurements were conducted to test the conventional and the modified displacement probabilities for the likelihood calculation in determining the size distribution, finding that

the conventional probability results in an overestimation in the mean size determination on a short recognition radius whereas the estimated mean size with the modified probability is not affected by the recognition radius.

On the other hand, both the conventional and the modified displacement probabilities failed to acquire a proper value compared to the nominal value on a short recognition radius. On a short recognition radius, relative variance acquired with the conventional probability was measured to have a value that is very close to zero regardless of the nominal relative variance while the modified probability gave a value larger than the nominal value. On a very long recognition radius, the size distributions determined with both probabilities have larger relative variance than expected. At a low concentration of 1×10^8 and 1×10^9 particles/ml, the high relative variance is due to the false tracks that result in a spurious peak in the acquired size distributions. At a higher concentration of 1×10^{10} particles/ml, an early termination of particles tracks results in an increase on relative variance in addition to the false tracks since an increased probability of interrupting neighboring particles inhibits a proper size distribution determination. This implies that a smaller recognition radius is more effective in obtaining an accurate size distribution from NTA measurements and that the modified displacement probability is more suited for the NTA analysis since it provides a better resolution at a small recognition radius. The results obtained from the PS nanoparticle standards were consistent with the observations from the simulations.

References

[1] Dong, C., et al., Size-dependent activity and selectivity of carbon dioxide photocatalytic reduction over platinum nanoparticles. *Nature Communications*, 2018. **9**(1): p. 1252.

[2] Peng, R., et al., Size effect of Pt nanoparticles on the catalytic oxidation of toluene over Pt/CeO2 catalysts. *Applied Catalysis, B: Environmental*, 2018. **220**: p. 462-470.

[3] Sneed, B.T., A.P. Young, and C.-K. Tsung, Building up strain in colloidal metal nanoparticle catalysts. *Nanoscale*, 2015. **7**(29): p. 12248-12265.

[4] Stark, W.J., et al., Industrial applications of nanoparticles. *Chemical Society Reviews*,

2015. **44**(16): p. 5793-5805.

[5] Sun, J.-K., et al., Toward homogenization of heterogeneous metal nanoparticle catalysts with enhanced catalytic performance: soluble porous organic cage as a stabilizer and homogenizer. *Journal of the American Chemical Society*, 2015. **137**(22): p. 7063-7066.

[6] Wang, C., et al., Highly efficient transition metal nanoparticle catalysts in aqueous solutions. *Angewandte Chemie*, 2016. **128**(9): p. 3143-3147.

[7] Berne, B.J. and R. Pecora, *Dynamic light scattering: with applications to chemistry, biology, and physics*. Dover ed. 2000, Mineola, N.Y.: Dover Publications. vii, 376 pp.

[8] Pecora, R., Dynamic light scattering: applications of photon correlation spectroscopy. 2013: Springer Science & Business Media.

[9] Merkus, H.G., *Particle size measurements: fundamentals, practice, quality*. Particle Technology Series. 2009, New York: Springer. xii, 533 pp.

[10] Hassan, P.A., S. Rana, and G. Verma, Making sense of Brownian motion: colloid characterization by dynamic light scattering. *Langmuir*, 2015. **31**(1): p. 3-12.

[11] Chu, B., Laser light scattering: basic principles and practice. 2007: Courier Corporation.

[12] Ferré-D'Amaré, A.R. and S.K. Burley, Use of dynamic light scattering to assess crystallizability of macromolecules and macromolecular assemblies. *Structure*, 1994. **2**(5): p. 357-359.

[13] Elofsson, U.M., P. Dejmek, and M.A. Paulsson, Heat-induced aggregation of β-lactoglobulin studied by dynamic light scattering. *International Dairy Journal*, 1996. **6**(4): p. 343-357.

[14] Hawe, A., et al., Taylor dispersion analysis compared to dynamic light scattering for the size analysis of therapeutic peptides and proteins and their aggregates. *Pharmaceutical Research*, 2011. **28**(9): p. 2302-2310.

[15] 22412:2008, I., Particle size analysis -- Dynamic light scattering (DLS). 2008.

[16] Malloy, A. and B. Carr, NanoParticle tracking analysis - The Halo™ system. *Particle & Particle Systems Characterization*, 2006. **23**(2): p. 197-204.

[17] Bob Carr, P.H., Andrew Malloy, Philip Nelson, Matthew Wright, Jonathan Smith, Applications of nanoparticle tracking analysis in nanoparticle research - a mini-review.

European Journal of Parenteral & Pharmaceutical Sciences, 2009. **14**: p. 35-40.

[18] Filipe, V., A. Hawe, and W. Jiskoot, Critical evaluation of nanoparticle tracking analysis (NTA) by NanoSight for the measurement of nanoparticles and protein aggregates. *Pharmaceutical Research*, 2010. **27**(5): p. 796-810.

[19] Bell, N.C., et al., Emerging techniques for submicrometer particle sizing applied to Stober silica. *Langmuir*, 2012. **28**(29): p. 10860-72.

[20] James, A.E. and J.D. Driskell, Monitoring gold nanoparticle conjugation and analysis of biomolecular binding with nanoparticle tracking analysis (NTA) and dynamic light scattering (DLS). *Analyst*, 2013. **138**(4): p. 1212-8.

[21] Boyd, R.D., S.K. Pichaimuthu, and A. Cuenat, New approach to inter-technique comparisons for nanoparticle size measurements: using atomic force microscopy, nanoparticle tracking analysis and dynamic light scattering. *Colloids and Surfaces A: Physicochemical and Engineering Aspects*, 2011. **387**(1-3): p. 35-42.

[22] Troiber, C., et al., Comparison of four different particle sizing methods for siRNA polyplex characterization. *European Journal of Pharmaceutics and Biopharmaceutics*, 2013. **84**(2): p. 255-264.

[23] Tran Le, T., et al., Determination of heat-induced effects on the particle size distribution of casein micelles by dynamic light scattering and nanoparticle tracking analysis. *International Dairy Journal*, 2008. **18**(12): p. 1090-1096.

[24] Panchal, J., et al., Analyzing subvisible particles in protein drug products: a comparison of dynamic light scattering (DLS) and resonant mass measurement (RMM). *AAPS Journal*, 2014. **16**(3): p. 440-51.

[25] Van Der Meeren, P., M. Kasinos, and H. Saveyn, Relevance of two-dimensional brownian motion dynamics in applying nanoparticle tracking analysis, in Methods in Molecular Biology. 2012. p. 525-534.

[26] Gardiner, C., et al., Extracellular vesicle sizing and enumeration by nanoparticle tracking analysis. *Journal of Extracellular Vesicles*, 2013. **2**.

[27] Gross, J., et al., Nanoparticle tracking analysis of particle size and concentration detection in suspensions of polymer and protein samples: Influence of experimental and data evaluation parameters. *European Journal of Pharmaceutics and Biopharmaceutics*, 2016. **104**: p. 30-41.

[28] Walker, J.G., Improved nano-particle tracking analysis. *Measurement Science and Technology*, 2012. **23**(6): p. 065605.

[29] Saveyn, H., et al., Accurate particle size distribution determination by nanoparticle tracking analysis based on 2-D Brownian dynamics simulation. *Journal of Colloid and Interface Science*, 2010. **352**(2): p. 593-600.

[30] Zhou, C., et al., Characterization of Nanoparticle Tracking Analysis for Quantification and Sizing of Submicron Particles of Therapeutic Proteins. *Journal of Pharmaceutical Sciences*, 2015. **104**(8): p. 2441-2450.

[31] Wagner, T., H.G. Lipinski, and M. Wiemann, Dark field nanoparticle tracking analysis for size characterization of plasmonic and non-plasmonic particles. *Journal of Nanoparticle Research*, 2014. **16**: p. 2419.

[32] Hole, P., et al., Interlaboratory comparison of size measurements on nanoparticles using nanoparticle tracking analysis (NTA). *Journal of Nanoparticle Research*, 2013. **15**: p. 2101.

[33] Ladd, A.J., Short-time motion of colloidal particles: Numerical simulation via a fluctuating lattice-Boltzmann equation. *Physical Review Letters*, 1993. **70**(9): p. 1339.

[34] Michalet, X., Mean square displacement analysis of single-particle trajectories with localization error: Brownian motion in an isotropic medium. *Physical Review E: Statistical Physics, Plasmas, Fluids, and Related Interdisciplinary Topics*, 2010. **82**(4): p. 041914.

[35] Kestens, V., et al., Validation of a particle tracking analysis method for the size determination of nano- and microparticles. *Journal of Nanoparticle Research*, 2017. **19**(8): p. 271.

[36] Lucy, L.B., Iterative technique for rectification of observed distributions. *Astronomical Journal*, 1974. **79**(6): p. 745-754.

[37] Bai, K., et al., Interference from Proteins and Surfactants on Particle Size Distributions Measured by Nanoparticle Tracking Analysis (NTA). *Pharmaceutical Research*, 2017. **34**(4): p. 800-808.

[38] de Temmerman, P.J., et al., Size measurement uncertainties of near-monodisperse, near-spherical nanoparticles using transmission electron microscopy and particle-tracking analysis. *Journal of Nanoparticle Research*, 2014. **16**(10): p. 17.

Chapter 6

Discussion and Future Work

This chapter summarizes key findings obtained in the thesis and interprets the meaning of the findings in the analysis of DLS and NTA for characterization of polydisperse biological samples. Based on the findings, it also presents future work to improve the analysis methods for NTA by introducing biased particle detection.

6.1 General Discussion

In this thesis, two size measurement techniques, DLS and NTA, were evaluated and compared for the size characterization of polydisperse biological samples. Since the two techniques determine the particle size by measuring the diffusion coefficient, the major part of the objective was to verify how the different quantities used to express the amount of particles by the two techniques are compared. The evaluation also extended to the investigation of the influence of parameters used in NTA. In particular, the influence of the recognition radius that is used to track particles in NTA was investigated using simulations while changing the conditions. The simulations provided an ideal situation for NTA measurement, where the particle size and the concentration were varied. The simulation results were also confirmed by real experiments.

Comparison of DLS and NTA on polydisperse samples

Chapter 4 introduced and compared two particle size measurement techniques, DLS and NTA, for the size characterization of polydisperse macromolecular assemblies. While both techniques acquire size information by detecting the diffusion coefficient of the measured particles, they differ in the quantity of the size distribution they provide, i.e. number from NTA and intensity from DLS. Three size distribution estimation methods for NTA were tested to compare their performance using monomodal PS latex standards. The two MLE-based methods, i.e., the FTLA and iterative methods, produced results comparable to each other and in line with those from DLS while the direct conversion resulted in a larger variance, especially for small particles, due to the limitation of obtaining sufficiently long particle tracks. This result indicated that an MLE-based approach should be applied for accurate measurements of small sized particles with NTA.

The two MLE-based size distribution estimation methods for NTA were further tested on measurements of polydisperse vesicle samples prepared in a various polydispersity, which obtained the same mean sizes despite their different strategies to finding the optimal size distribution from the given track data. However, the calculated likelihood of the acquired

size distributions obtained by the two methods indicated that FTLA sacrificed likelihood at the expense of a smoother size distribution, further suggesting that the iterative method is preferable for polydisperse samples.

The results for the vesicle samples obtained by NTA using the iterative method were then compared with those from DLS. The mean sizes were comparable except for those samples with a very high polydispersity index. However, the mean sizes of some samples measured by NTA were larger than or very close to those from DLS, which seems contradictory to the fact that the mean size from an intensity-weighted size distribution is larger than that from its corresponding number-weighted size distribution. Although the low size detection limit of NTA was pointed out as a source of the contradiction by reducing the variance measured by NTA, it did not fully explain the reason.

Additionally, the number-weighted size distribution of the vesicle samples from NTA was converted into an intensity-weighted distribution by assuming the thin-shell hollow sphere model with the RGD approximation to verify the influence of the different quantities that DLS and NTA produce. While the mean size given by NTA after conversion was very close to the value before conversion, the RV after the conversion was much reduced compared to that from DLS and NTA. Considering the nature of the vesicle samples, it is questionable whether the small relative variance after reconstruction is reliable. Therefore, the conversion of a number-weighted size distribution of NTA into an intensity-weighted one does not seem to effectively explain the difference in the mean sizes measured by DLS and NTA, and the size information from DLS and NTA is better compared in their original weightings.

Influence of the recognition radius in NTA

In Chapter 5, an improved method was suggested for determining the size distribution of NTA based on the MLE approach that took the recognition radius into account. By considering the recognition radius used for particle tracking in NTA, a modified displacement probability was introduced for the likelihood calculation of the MLE method.

Simulated NTA measurements were conducted to test the conventional and the modified displacement probabilities for the likelihood calculation in determining the size distribution, finding that the conventional probability results in an overestimation in the mean size determination on a short recognition radius whereas the estimated mean size with the modified probability is not affected by the recognition radius.

On the other hand, both the conventional and the modified displacement probabilities failed to acquire a proper value compared to the nominal value on a short recognition radius. On a short recognition radius, relative variance acquired with the conventional probability was measured to have a value that was very close to zero regardless of the nominal relative variance while the modified probability gave a value larger than the nominal value. On a very long recognition radius, the size distributions determined with both probabilities have larger relative variance than expected. At a low concentration, the high relative variance was due to the false tracks that result in a spurious peak in the acquired size distributions. At a higher concentration, an early termination of particles tracks resulted in an increase on relative variance in addition to the false tracks since an increased probability of interrupting neighboring particles inhibited a proper size distribution determination. This implies that a smaller recognition radius is more effective in obtaining an accurate size distribution from NTA measurements and that the modified displacement probability is more suited for the NTA analysis since it provides a better resolution at a small recognition radius. The results obtained from the PS nanoparticle standards were consistent with the observations from the simulations.

6.2 Future Outlook

While the size distribution from NTA measurements is determined from the acquired tracks, the determination process assumes the tracks reflect the true particle size distribution of the sample. However, the detection and tracking process of the particles in real NTA measurements can be influenced by many factors [1-6].

Some of those factors are introduced due to the detection principle of NTA, while others are originated from either the physical nature or the instrument configuration of NTA. The former factors are logical consequences of the principle, which are predictable and can be corrected by theoretical approaches [7, 8]. For instance, the chance of a particle to be tracked in the next image frame depends on the diffusion scale of the particle which is related with its size. It means that a small particle is less tracked compared to a larger particle, i.e. the track length of tracks from small particles tends to be shorter. Consequently, tracks from small particles would be more rejected from the size distribution analysis if a minimum track length is applied for the screening process of the tracks to reduce stochastic uncertainty [9]. As a result, the tracks acquired from a polydisperse sample contain more of those tracks from larger particles than from smaller particles. Since the chance of the track termination can be expressed with a gamma distribution, it can be incorporated into the size distribution estimation to reflect the different probability of the track termination.

On the other hand, the latter factors depend on the experimental conditions of NTA measurements such as sample characteristics, illuminating laser, focal depth of the objective lens and so on, which requires calibrations to reflect the conditions onto the analysis [2, 10]. For example, NTA identifies the position of particles from captured 2D video images by finding the local maxima of the intensity of the pixels in the images. Since the intensity of the light scattered by a particle is approximately proportional to the square of the particle volume, a larger particle can obscure the presence of neighboring smaller particles, making smaller particles hidden or less detected. The effect may vary depending on sample characteristics as well as the optical configuration, making it very difficult to describe in an analytical manner to incorporate into the size distribution analysis.

Finally, a few factors will be discussed to improve the size distribution estimation of NTA measurements.

Size-Dependent Tracking of Particles

For a particle detected in a frame to be tracked in the following frame, i.e. two particles across two successive frames are identified as the same particle, three conditions should be met:

(a) the particle to be tracked in the preceding frame has no neighboring particle within the recognition range of the particle,

(b) the particle is found within the recognition range at the following frame, and

(c) no other particle is found within the recognition range at the following frame [2].

Each criterion can be translated into a condition for the probabilistic description.

(a) The probability that no other particle is found within the recognition range of a tracked particle is acquired by using the distribution of the distance to the nearest particle.

(b) The probability of a particle in the preceding frame to be found within the recognition range at the following frame is a combination of two conditions. One is that the particle in the preceding frame should be detected in the following frame, i.e. it does not go out of the detection volume that the instrumentation is able to observe. The other is that the particle should not move out of the recognition range in the following frame.

(c) The probability that no particle but the tracked particle is found within the recognition range is given from a time evolution of the distance distribution used in (a), where the time evolution is described by the Brownian motion of the neighboring particles.

To describe the probability of the neighboring particles around the tracked particle appeared in the conditions (a) and (c), the probabilistic distribution $v(r)$ of the distance to the nearest particle can be used, which is expressed by a Rayleigh distribution whose scale parameter is $1/\sqrt{2n_A\pi}$, where n_A is the areal particle density given by the product of the particle concentration and the focal depth of the objective lens. Considering the condition (b) is independent from the other conditions, the probability is given as an integral form

$$P = \left(1 - e^{-L^2/u^2}\right)\left(1 - \frac{u}{\sqrt{\pi}H}\right)\int_L^\infty dr \int_L^\infty dr'\, \nu(r) T(r \to r'; \bar{u}) \quad (6.1)$$

where L is the recognition radius, u is the diffusion scale of the tracked particle, H is the height of the detection volume of NTA, $\bar{u}$ is the representative diffusion scale of the neighboring particles and $T(r \to r'; \bar{u})$ is the radial diffusion of the neighboring particle from r to r'.

$$T(r \to r'; \bar{u}) = \int_0^\infty dx\, f(x) T\left(r \to r'; u(x)\right) \quad (6.2)$$

where $f(x)$ is the normalized particle size distribution of the measured sample which satisfies

$$\int_0^\infty dx\, f(x) = 1 \quad (6.3)$$

However, the probability above does not consider the history of tracked particle. That is, the probabilistic distribution $\nu(r)$ of the distance to the neighboring particles takes a different form depending on the track length and, as a result, the probability also has a dependence on the track length. To properly describe the probability, it is required to find the distribution $\nu_k(r)$ for a tracked particle with a track length k and its relation with its following distribution $\nu_{k+1}(r)$, which can be acquired from the above integrational form for the probability tracked in the following frame,

$$\nu_{k+1}(R) = \int_L^\infty dr \int_L^\infty dr'\, \nu_k(r)\left(1 - e^{-L^2/u^2}\right) \times \left(1 - \frac{u}{\sqrt{\pi}H}\left((K+1)^{\frac{1}{4}} - K^{\frac{1}{4}}\right)\right) T(r \to r'; \bar{u}) T(r' \to R; u) \quad (6.4)$$

where the term $T(r' \to R; u)$ is introduced to reflect the position change of the tracked particle at the next frame.

Noticeably, the second condition of the tracked particle that does not go out of the recognition radius in the vertical direction, is expressed by a conditional probability, where the particle is within the detection volume for k consecutive times and goes out of the volume at the next frame.

Tracks with a track length k is generated when a particle track is terminated after tracked k times, the number of tracks with a track length k is given by

$$N_k = \int_0^\infty dr v_k(r) - \int_0^\infty dr v_{k+1}(r) \quad (6.5)$$

The factor N_k explains the amount, or the survival ratio, of a tracked particle with a track length k, and can be incorporated with the displacement probability of tracked particles for better estimation of NTA size distribution analysis.

References

[1] Filipe, V., A. Hawe, and W. Jiskoot, Critical evaluation of nanoparticle tracking analysis (NTA) by NanoSight for the measurement of nanoparticles and protein aggregates. *Pharmaceutical Research*, 2010. **27**(5): p. 796-810.

[2] Maguire, C.M., et al., Benchmark of Nanoparticle Tracking Analysis on Measuring Nanoparticle Sizing and Concentration. *Journal of Micro and Nano-Manufacturing*, 2017. **5**(4): p. 10.

[3] Tong, M., et al., Flow speed alters the apparent size and concentration of particles measured using NanoSight nanoparticle tracking analysis. *Placenta*, 2016. **38**: p. 29-32.

[4] Zhou, C., et al., Characterization of Nanoparticle Tracking Analysis for Quantification and Sizing of Submicron Particles of Therapeutic Proteins. *Journal of Pharmaceutical Sciences*, 2015. **104**(8): p. 2441-2450.

[5] Krueger, A.B., P. Carnell, and J.F. Carpenter, Characterization of factors affecting nanoparticle tracking analysis results with synthetic and protein nanoparticles. *Journal of pharmaceutical sciences*, 2016. **105**(4): p. 1434-1443.

[6] Defante, A.P., et al., Using image attributes to assure accurate particle size and count using nanoparticle tracking analysis. *Journal of pharmaceutical sciences*, 2018. **107**(5): p. 1383-1391.

[7] Saveyn, H., et al., Accurate particle size distribution determination by nanoparticle

tracking analysis based on 2-D Brownian dynamics simulation. *Journal of Colloid and Interface Science*, 2010. **352**(2): p. 593-600.

[8] Walker, J.G., Improved nano-particle tracking analysis. *Measurement Science and Technology*, 2012. **23**(6): p. 065605.

[9] Van Der Meeren, P., M. Kasinos, and H. Saveyn, Relevance of two-dimensional brownian motion dynamics in applying nanoparticle tracking analysis, in Methods in Molecular Biology. 2012. p. 525-534.

[10] Hole, P., et al., Interlaboratory comparison of size measurements on nanoparticles using nanoparticle tracking analysis (NTA). *Journal of Nanoparticle Research*, 2013. **15**: p. 2101.